

# COSMOLOGICAL IMPLICATIONS OF FIELD SPACE GEOMETRY

MARIOS BOUNAKIS

Thesis submitted for the degree of  
Doctor of Philosophy



*School of Mathematics, Statistics & Physics  
Newcastle University  
Newcastle upon Tyne  
United Kingdom*

**February 2021**



Life is not an easy matter... You cannot live through it without falling into frustration and cynicism unless you have before you a great idea which raises you above personal misery, above weakness, above all kinds of perfidy and baseness.

-Leon Trotsky, Diary in Exile, 1935

“There is nothing like looking, if you want to find something. You certainly usually find something, if you look, but it is not always quite the something you were after.”

-J.R.R. Tolkien, The Hobbit, or There and Back Again, 1937

## Declaration

I, the author, hereby declare that the contents of this thesis are my own work, except where specific reference is made to the work of others, and that they have not been submitted, partially or in whole, for any other degree or qualification in this, or any other university. The methodologies and results presented in this dissertation are original and based on the research conducted at the School of Mathematics, Statistics and Physics, Newcastle University, from September 2016 to February 2021, under the supervision of Prof. Ian G. Moss and Dr. Gerasimos Rigopoulos. The materials included, here, contain nothing which is the outcome of work done in collaboration with others, except as described below.

- Chapter 2 is based on the publication [1], prepared under the supervision of Dr. Gerasimos Rigopoulos. My contribution to this work was extensive and included the systematic development of the Feynman rules presented, as well as the diagrammatic expansion of the Langevin equation solutions. Furthermore, I performed the analytical computations of the illustrative N-point functions, independently, and obtained their associated diagrams, while actively contributing to the preparation of the manuscript.
- Chapter 3 is based on the publication [2], prepared under the supervision of Prof. Ian G. Moss, during the first year of my studies. My contribution revolved around the analytical computation of the covariant effective action operators, their diagonalisation, and the subsequent derivation of the Gravity-scalar beta-functions.
- Chapter 4 is based on the publication [3], prepared with guidance from both Prof. Ian G. Moss and Dr. Gerasimos Rigopoulos. The theoretical framework was, partially, provided by the supervisory team, but the entirety of the calculations, results, and diagrams are my own. The preparation and corrections of the manuscript were also, largely, carried out independently.

After the completion of the original papers and the review of the examination committee, several clarifications and extensions have been added and are, hereafter, included in this thesis.

## Acknowledgements

The fact that a single name appears on the cover does not do justice to the people whose devotion and dedication played a vital role in the long and arduous process of performing the work presented here, as well as the preparation of this dissertation.

The debt to my supervisory team, Professor Ian G. Moss and Dr. Gerasimos Rigopoulos can never be repaid. Their unwavering support, insightful guidance, and inspiring discussions will forever be treasured. The breadth of their knowledge, only surpassed by their inquisitive nature and manifest patience has fuelled my passion and motivated me through the everyday struggles associated with postgraduate research. Special thanks are extended to Professor Ian G. Moss and his wife, Olga, for welcoming me to their home on several occasions and organising the, always eagerly anticipated, Big Bang Barbeque.

Besides my supervisors, I would like to take the opportunity to thank and praise Matthias Neubert and Sacha Davidson for organising the CVIII session of the École de Physique des Houches, held in July 2017. My participation in this summer school has been one of the most thought-provoking and enriching, yet immensely enjoyable, periods in my student life. I am, also, grateful to Dr. Christian Steinwachs for intriguing discussions during, and after, my short visit to Freiburg.

Sincere thanks is extended to the examination committee, Dr. Paul McFadden and Prof. Arttu Rajantie for their detailed review of this thesis, the stimulating discussion during my defence, and the corrections they suggested.

Furthermore, I would like to thank my officemates and friends Horacio Guerra Ocampo, Joseph Reid, Matina Trachana, Dimitris Chiotis, Aida Gjoka, Francesca Fedele, Sophie Harbisher, Stephen Mason, Ashley Luke Wareham Wilkins, Clarissa Jade Barratt, Francesca Caloro, Kate Brown, Thomas Bland, Dora Koukaki, Maritina Markopoulou, and Evgenios Kakariadis.

Finally, and most importantly, I would like to express my most sincere and heartfelt gratitude to my family. Their generous, unfaltering, and unconditional emotional support deeply honours and humbles me. They have been the driving force behind the initiation and completion of my higher studies. This work is much theirs as it is mine.



# Abstract

One of the most fascinating aspects of recent endeavours in theoretical cosmology has been the investigation of the quantum effects of scalar fields in field-spaces with non-trivial geometries, in the early universe. The objective of this thesis is the presentation of a series of original research topics that result from such considerations.

The first part of this work explores an extension to Starobinsky's model of stochastic inflation. The functional integral describing the stochastic dynamics of a spectator field during inflation is reviewed. Comparisons are drawn between the diagrammatic expansion resulting from action and the one obtained directly from a perturbative solution of the corresponding Langevin equation. The Feynman rules for computing arbitrary temporal  $n$ -point functions are stated and illustrative computations are presented. The role played by the functional Jacobian determinant in the path integral is given increased attention. Multiplicative noise is also briefly considered; allowing the field to contribute to the expansion rate introduces additional vertices and exciting insights on the dependence of observable results on the discretization prescription are motivated.

The second part presents a covariant under field redefinitions Effective Field Theory proposed towards the resolution of the existing tension of conformal frame dependence. We are motivated by the meta-stability of the Higgs vacuum which, in the early universe, can lead to complications. It is shown, here, that the effective Higgs potential at large field values can be derived in a way that is independent of the choice of conformal frame for the space-time metric, resulting in unambiguous answers to questions about physical observables (eg. vacuum stability). This approach leads to new relations for the evolution of the coupling coefficients with the energy scale and motivates improved limits on the allowed values of the Higgs-curvature coupling.

The third part investigates the dynamics of a multifield inflation model with curved field-space. Abandoning the assumption of a single inflaton, which is both unphysical and not motivated by higher energy theories, results in the introduction of a scalar multiplet, with non-trivial kinetic terms. The recently proposed and topical Hyperinflation model is reviewed and a concise treatment of the evolution of the background and the quantum perturbations is introduced. Thus, bounds for the cosmological observables are established and comparisons with experimental data are drawn, resulting in restrictions in the admissible values of the field-space curvature parameter.

# Contents

<b>I</b>	<b>Introduction</b>	<b>1</b>
<b>1</b>	<b>Introduction to Cosmology and Inflation</b>	<b>2</b>
1.1	Preface . . . . .	2
1.2	Introduction to Cosmology . . . . .	3
1.2.1	Cosmological Fundamentals . . . . .	3
1.2.2	Shortcomings of Big Bang Cosmology . . . . .	6
1.3	Introduction to Inflation . . . . .	6
1.3.1	Inflationary Fundamentals . . . . .	6
1.3.2	Fundamentals of Cosmological Perturbation Theory . . . . .	8
1.3.3	Infrared Divergence in de Sitter . . . . .	11
1.3.4	Beyond Minimally-Coupled Slow-Roll Inflation . . . . .	13
<b>II</b>	<b>Topics in Inflationary Scalar Quantum Field Theory with Curved Field Space</b>	<b>14</b>
<b>2</b>	<b>Feynman Rules for Stochastic Inflationary Correlators</b>	<b>15</b>
2.1	Overview of the Chapter . . . . .	15
2.2	Stochastic Inflation: Classical System encompassing Quantum Behaviour . . . . .	16
2.3	Novel Diagrammatic Methods for Cosmological Stochastic Inflation . . . . .	17
2.3.1	From the Curved Spacetime QFT to the Langevin Equation . . . . .	17
2.3.2	From the Langevin to the Fokker-Planck Equation . . . . .	20
2.3.3	From Fokker-Planck to Schrödinger . . . . .	23
2.4	The Stochastic Path Integral Formulation . . . . .	24
2.5	Feynman Rules from the Path Integral . . . . .	27
2.5.1	Partition Function . . . . .	30
2.5.2	Two-Point Function . . . . .	30
2.5.3	Four-Point Function . . . . .	36
2.6	Stochastic Diagrams from the Langevin Equation in Pure de Sitter . . . . .	40
2.6.1	Diagrammatic Computation of the Two-Point Function . . . . .	42
2.6.2	Diagrammatic Computation of the Four-Point Function . . . . .	47
2.7	Backreaction Contributions to the Two-Point Correlators . . . . .	51



2.8	Conclusion and Motivation for Further Work . . . . .	53
<b>3</b>	<b>Covariant One-Loop Gravitational Corrections to the Effective Higgs Potential in de Sitter</b>	<b>55</b>
3.1	Overview of the Chapter . . . . .	55
3.2	Introduction . . . . .	55
3.3	Covariant Effective Actions . . . . .	59
3.3.1	Field Space Generalities . . . . .	59
3.3.2	Effective Action Generalities . . . . .	61
3.3.3	Construction of the Effective Action . . . . .	62
3.3.4	Fixing the Gauge . . . . .	65
3.4	The Gravity-Higgs Effective Field Theory . . . . .	67
3.4.1	Jordan Frame Lagrangian . . . . .	67
3.4.2	Conformal Transformation to the Einstein Frame . . . . .	68
3.5	Expansions of the Gravity-Higgs Action . . . . .	69
3.5.1	First Order Variations . . . . .	71
3.5.2	Second Order Variations . . . . .	71
3.5.3	Vilkovisky-DeWitt Corrections . . . . .	73
3.6	Gravity-Higgs Mode Expansions . . . . .	74
3.6.1	Covariant Gravity-Scalar Model . . . . .	74
3.6.2	Orthonormal Harmonic Basis Expansion . . . . .	75
3.7	Gravity-Higgs $\beta$ -functions . . . . .	78
3.8	Gauge Bosons, Goldstone Modes and Fermions . . . . .	80
3.9	The Gravity-Scalar Running Couplings . . . . .	83
3.10	Conclusion and Motivation for Further Work . . . . .	86
<b>4</b>	<b>Observational Constraints on Hyperinflation</b>	<b>87</b>
4.1	Overview of the Chapter . . . . .	87
4.2	The Motivation for Multifield Inflation . . . . .	87
4.2.1	Hyperinflation . . . . .	88
4.3	Model Description and Background Field Considerations . . . . .	88
4.3.1	Fundamentals . . . . .	88
4.3.2	Background Field and Linear Stability in de Sitter . . . . .	91
4.4	Linear Perturbations . . . . .	93
4.4.1	Linear Perturbation Analysis . . . . .	94
4.4.2	Local Orthogonal Basis . . . . .	94
4.4.3	Adiabatic and Isocurvature Perturbation Power Spectra . . . . .	96
4.5	Conclusion and Motivation for Further Work . . . . .	101

<b>III</b>	<b>Conclusion</b>	<b>102</b>
5	Summary & Motivation for Future Work	103
<b>IV</b>	<b>Appendix</b>	<b>115</b>
<b>A</b>	<b>Schrödinger-like Probability Equation</b>	<b>116</b>
<b>B</b>	<b>Field space Geometry</b>	<b>118</b>
	B.1 Covariant Background Field Expansion . . . . .	118
	B.2 The NLSM Perturbation Equation of Motion . . . . .	119
	B.2.1 The Vilkovisky-deWitt Term . . . . .	120
	B.2.2 Perturbation Equation of Motion . . . . .	120
<b>C</b>	<b>Zeta-function Evaluation</b>	<b>122</b>
<b>D</b>	<b>Stochastic Noise Kernel for Hyperinflation</b>	<b>127</b>
	D.1 Noise Kernel for the Heaviside Coarse-Graining Window . . . . .	127
	D.2 Noise Kernel for the Chintz Coarse-Graining Window . . . . .	129

## List of Figures

3.1	Running couplings $\lambda$ , $\lambda_6$ , and $\mu_{\text{eff}}^2$ . . . . .	84
3.2	The effective Higgs potential plotted as a function of the Higgs field. . . . .	85
4.1	Phase diagram of the background field in hyperbolic field-space. . . . .	91
4.2	Phase diagrams of the hyperbolic solution for various values of the potential gradient . . . . .	93
4.3	Evolution into the homogeneous hyperbolic solution. . . . .	93
4.4	Temporal evolution of the adiabatic and isocurvature modes in hyperbolic- field-space . . . . .	97
4.5	Evolution of the linearised field perturbations . . . . .	98
4.6	The adiabatic and entropic power spectra . . . . .	98
4.7	The adiabatic spectral index, as a function on field-space curvature . . . . .	99
D.1	Temporal evolution of the noise kernel components, after horizon exit . . . . .	131

## List of Tables

2.1	Feynman rules for the free-field two point function, the retarded propagator, and the ghost propagator . . . . .	28
2.2	Feynman rules for the vertices of a spectator field in de Sitter and the determinant-originating ghost . . . . .	29
2.3	Feynman rules for the vertices induced by multiplicative noise . . . . .	29
2.4	Feynman diagrams contributing to the one-loop four-point function including F-propagator loops . . . . .	37
2.5	Feynman diagrams contributing to the one-loop four-point function including G-propagator loops . . . . .	38
2.6	Graphical representation of the solutions of the stochastic differential equations . . . . .	41
2.7	Graphical representation of the contributing terms to the 2-point function, up to $O(\lambda)$ . . . . .	43
2.8	Graphical representation of the $\langle \phi_{(1)}(\omega)\phi_{(1)}(\omega') \rangle$ terms contributing to the expectation value of the two-point correlator, at $\mathcal{O}(\lambda^2)$ . . . . .	44
2.9	Graphical representation of the $\langle \phi_{(2)}(\omega)\phi_{(0)}(\omega') \rangle$ and $\langle \phi_{(0)}(\omega)\phi_{(2)}(\omega') \rangle$ terms contributing to the expectation value of the two-point correlator, at $\mathcal{O}(\lambda^2)$ . . . . .	45
2.10	Horizontal topology ‘tree’ diagrams contributing to the one-loop four-point function including F-propagator loops . . . . .	49
2.11	Vertical topology ‘tree’ diagrams contributing to the one-loop four-point function including F-propagator loops . . . . .	49
3.1	Table of index notations . . . . .	60
3.2	$\beta$ -functions for the curvature coupling and the mass of a gravity coupled scalar field . . . . .	79
3.3	$\beta$ -functions for the quartic self-coupling $\lambda$ and the sixth order self-coupling $\lambda_6$ of a gravity coupled scalar . . . . .	80
3.4	W and Z vector boson contributions to the $\beta$ -functions for the curvature coupling and the mass of a gravity coupled scalar . . . . .	82
3.5	W and Z vector boson contributions to the $\beta$ -functions for the quartic, $\lambda$ , and sixth order, $\lambda_6$ , scalar self-couplings of a gravity coupled scalar field . . . . .	82
C.1	Numerical values for Laplace-like operator eigenvalues . . . . .	124

# Part I

## Introduction

# Chapter 1. Introduction to Cosmology and Inflation

## 1.1 Preface

The quantum properties of scalar fields play a central role in modern cosmological investigations. From the theoretical prediction [4–8] and subsequent experimental observation [9, 10] of the Higgs field, to the seminal work on inflation [11–13] scalar fields have been shown to be cornerstones in the contemporary interplay between particle physics and cosmology. In this thesis we investigate various quantum effects of scalar fields in the early universe, with increased attention to the role played by non-trivial kinetic terms, giving rise to a curved field space.

In the first chapter we aim to offer a concise overview of the fundamentals of the Cosmological Standard Model, and its shortcomings, present the resolution proposed by the inflationary scenario and review the fundamentals of cosmological perturbation theory.

In the second chapter, we focus on the low-energy limit of a minimally-coupled, light scalar field in de Sitter. The breakdown of standard perturbative methods, resulting from infrared divergences, motivates the use of alternative techniques for the computation of arbitrary temporal  $n$ -point functions. Utilising the technology of stochastic inflation we produce Feynman Rules for Stochastic Inflationary Correlators [1], perform illustrative computations that improve the accuracy of the expectation values of two-point and four-point functions, and manifestly show the equivalence between the diagrammatic and path-integral solutions to all orders. Finally, we briefly consider the case of backreaction.

In the third chapter we shift our attention to the high-energy behaviour of a spectator scalar field in de Sitter. We treat General Relativity as an Effective Field Theory of quantum gravity and introduce an effective action that is covariant under field transformations. This approach allows us to treat the ultra-violet divergences and obtain, unambiguously, the covariant 1-loop Gravitational Corrections to Higgs Potentials [2]. Hence, we present new relations for the evolution of the coupling coefficients with the energy scale and motivate improved limits on the allowed values of the Higgs-curvature coupling.

In the fourth chapter, we abandon the assumption of single-field, slow-roll inflation and examine a model of multifield inflation. The dynamics of the inflaton field, which is taken to evolve in a 2-dimensional hyperbolic field space, and its perturbations are investigated and tight Observational Constraints on Hyperinflation [3] potentials are established.

Lastly, we conclude this thesis by summarising our results and offering some remarks and directions for potential future work.

## 1.2 Introduction to Cosmology

Cosmogony is a topic whose importance can only be surpassed by its antiquity. The great successes of the past century, from General Relativity and the (Cosmological) Standard Model to Quantum Field Theory and Inflation have widened our horizons and given us glimpses of the primordial universe. This short introduction does not aim to paint the entire picture of our understanding of the primordial forces that brought our universe into being, but rather put the original research presented in the following chapters in context. For a truly detailed and thorough exposition to the physics of the early universe, the interested reader is referred to [14–19] and references therein.

### 1.2.1 Cosmological Fundamentals

This subsection reviews the basics of the Cosmological Standard Model and its shortcomings. A more detailed exposition on the topic can be found in any textbook or lecture note series [16, 17, 20].

#### FLRW Metric

Observational evidence from surveys of the Cosmic Microwave Background suggests that the observable universe appears, on large scales, isotropic [21] and homogeneous [22], respecting translational and rotational invariance. Adopting such an assumption motivates the definition of the Friedman-Lemaître-Robertson-Walker (FLRW) space-time metric with line element,

$$ds^2 = -dt^2 + a^2(t) \left[ \frac{dr^2}{1 - kr^2} + r^2 (d\theta^2 + \sin^2 \theta d\phi^2) \right], \quad (1.1)$$

where  $a$  is the cosmic scale factor,  $t$  is the cosmic time,  $\{r, \phi, \theta\}$  are the comoving polar coordinates describing the 3-dimensional spatial hypersurface and  $k$  is the curvature parameter, taking negative, zero and positive values for a hyperbolic, Euclidean and elliptic space, respectively. Physical distances are given by  $R(t) = a(t)r$ . An important quantity for the description of an expanding space is the Hubble parameter  $H$ :

$$H \equiv \frac{\dot{a}}{a}, \quad (1.2)$$

that obtains a positive value for an expanding and a negative value for a collapsing universe. Here and in the rest of the thesis (unless explicitly stated), we utilise natural units, setting  $c = \hbar = 1$ . Hence, the Hubble parameter sets the characteristic time-scale  $t \approx H^{-1}$  and length-scale  $d \approx H^{-1}$  in the homogeneous universe. Causal cosmological processes taking place in this expanding background should occur in time intervals a lot smaller than a Hubble time and over spatial distances a lot smaller than a Hubble length.

## Horizons

Depending on the sign of the line element, the separation of two events in the FLRW space-time is characterised as time-like, when  $ds^2 < 0$ , light-like, when  $ds^2 = 0$  or space-like, when  $ds^2 > 0$ . Defining conformal time as

$$\eta = \int \frac{dt}{a(t)}, \quad (1.3)$$

the radial propagation of light is given, using (1.1), by

$$ds^2 = a^2(\eta) (-d\eta^2 + dl^2). \quad (1.4)$$

This, readily motivates the definition of the comoving particle horizon: *The maximal comoving distance traversed by light between an initial time  $t_i$  and some later time  $t$ .*

$$l_{P.H}(\eta) = \eta - \eta_i = \int_{t_i}^t \frac{dt'}{a(t')}, \quad (1.5)$$

with  $t_i$  often taken to be the initial singularity  $t_i = 0$ .

Rescaling, one obtains the physical horizon  $d_H(t) \equiv a(t) l_{P.H}(t)$  which has a manifestly physical meaning: Since light has not had the time to traverse a distance larger than  $d_H(t)$ , events separated by such a distance have never been in causal contact. Furthermore, the comoving particle horizon of an expanding universe, that follows the description of the traditional Big Bang scenario, is always increasing. Hence, regions that are contemporarily causally connected may have been independent in the past, which comes in contrast with the observed homogeneity and isotropy. We will return to this when we discuss the shortcomings of the Cosmological Standard Model.

## Dynamics

The content of the universe defines the dynamics of the scale factor  $a(t)$ . Starting from the Einstein field equations, with  $M_{Pl}$  being the Planck mass  $M_{Pl}^2 = (8\pi G)^{-1}$

$$G_{\mu\nu} \equiv R_{\mu\nu} - \frac{1}{2}g_{\mu\nu}R = M_{Pl}^{-2} T_{\mu\nu}, \quad (1.6)$$

where  $R_{\mu\nu}$  and  $R$  are the Ricci tensor and scalar, respectively.

The matter content of the universe can be described by a perfect cosmological fluid with energy momentum tensor

$$T_{\mu\nu} = (\rho + p) u_\mu u_\nu + p g_{\mu\nu}, \quad (1.7)$$

where  $\rho$  is the energy density,  $p$  the isotropic pressure and  $u_\mu$  the unit timelike four-velocity of the fluid, as measured by a comoving observer in a local inertial frame.



Thus, the Einstein field equations (1.6), can be re-written as the Friedmann equations:

$$\begin{aligned} H^2(t) &= \frac{1}{3M_p^2} \rho - \frac{k}{a^2(t)}, \\ \dot{H} + H^2 &= \frac{\ddot{a}}{a} = -\frac{1}{6M_p^2} (\rho + 3p), \end{aligned} \tag{1.8}$$

with  $\dot{a}$  and  $\ddot{a}$  signifying the first and second derivatives of the scale factor with respect to cosmic time  $t$ . These can be combined to give the continuity equation:

$$\frac{d\rho}{dt} + 3H(\rho + p) = 0. \tag{1.9}$$

Defining the equation of state parameter  $w \equiv p/\rho$ , which takes values depending on the type of fluid of interest ( $w = \{0, 1/3, -1\}$  for dust, radiation and the cosmological constant respectively) and integrating (1.9), leads to

$$\rho \propto a^{-3(1+w)}. \tag{1.10}$$

Hence, the scale factor's dependence on time, for  $w \neq -1$ , is

$$a(t) \propto t^{\frac{2}{3}(1+w)}, \tag{1.11}$$

and for the particular case of the cosmological constant,  $w = -1$ ,

$$a(t) \propto e^{Ht}. \tag{1.12}$$

Substituting the various components' temporal dependence in (1.8), the Friedman equation becomes

$$H^2(t) = \frac{1}{3M_{Pl}^2} \left[ \rho_r(t_0) \frac{a^4(t_0)}{a^4(t)} + \rho_m(t_0) \frac{a^3(t_0)}{a^3(t)} + \rho_v(t_0) \right] - \frac{k}{a^2(t)} \tag{1.13}$$

with the subscripts referring to radiation, dust (non-relativistic matter) and vacuum energy, respectively. It is evident that if  $\rho_v \neq 0$  and  $k \leq 0$ , the vacuum energy density will dominate irrespective of the initial values of the radiation, matter and vacuum energy densities. Contemporary observational evidence [23] indicates that our universe has a curvature parameter  $k \rightarrow 0$ , while currently being vacuum energy dominated. This era was preceded by a period of matter domination which followed after the initial radiation dominated state. The effect of the decoupling of photons from matter, in this early stage in the universe's history, left a thermal relic propagating in a transparent universe and is being observed as the Cosmic Microwave Background.

### 1.2.2 Shortcomings of Big Bang Cosmology

Despite the success of the FLRW metric and the Friedmann equation in describing the dynamics of the early universe, there are numerous problems that require addressing. In short, according to the Cosmological Standard Model, our universe could not have been such that could foster life to observe it, unless it originally was very homogeneous, but not too much and very spatially flat, but not completely. These very precise initial conditions constitute the *horizon* and *flatness* problems.

## 1.3 Introduction to Inflation

In the early 1980's a series of works [11–13] proposed *Inflation*, a period of exponential expansion, driven by a scalar field appropriately named *inflaton*, which resolves a series of initial condition problems that the Big Bang scenario posed.

### 1.3.1 Inflationary Fundamentals

Re-writing (1.5) as a function of the scale factor, with the initial time being the singularity  $t_s \rightarrow 0$

$$\eta = \int_{\ln a(t_s)}^{\ln a(t)} d[\ln a(t')] \frac{1}{a(t')H[a(t')]} \quad (1.14)$$

we observe that despite two events separated by distances greater than  $1/(aH)$  being in no causal contact today, it is possible that they had been in causal contact in the early universe if the comoving Hubble radius  $1/(aH)$  was much larger, then; addressing the horizon problem. Furthermore, re-writing the Friedmann equation (1.8) for a non-flat universe as

$$\left|1 - \frac{\rho}{3H^2 M_{Pl}^2}\right| = \frac{1}{a^2 H^2}, \quad (1.15)$$

it is evident that the shrinking of the comoving Hubble radius, dynamically resolves the flatness problem. This condition implies, further, an accelerated expansion,

$$\frac{d}{dt} (aH)^{-1} = -\frac{\ddot{a}}{(aH)^2}. \quad (1.16)$$

From the second Friedmann equation (1.8), defining  $\epsilon \equiv -\dot{H}/H^2$ ,

$$\frac{\ddot{a}}{a} = H^2(1 - \epsilon) = -\frac{1}{6M_p^2}(\rho + 3p) \quad (1.17)$$

acceleration is shown to correspond to the condition  $\epsilon < 1$ , as well as  $p < -\frac{1}{3}\rho$ . In Einstein Gravity, the conditions of a shrinking comoving Hubble radius, an accelerated expansion and negative pressure are satisfied by a universe dominated by a nearly constant (vacuum) energy density. Alternatively, this role can be played by the potential of a scalar field.

In the simplest versions of inflationary models, the dynamics of these fields, which are

minimally coupled to gravity, are expressed by the action:

$$S = \int d^4x \sqrt{-g} \left[ \frac{1}{2\kappa^2} R - \frac{1}{2} g^{\mu\nu} \partial_\mu \phi \partial_\nu \phi - V(\phi) \right], \quad (1.18)$$

with  $\kappa^2 = M_{Pl}^{-2} = 8\pi G$ ,  $R$  is the Ricci scalar and  $V(\phi)$  includes all self-interaction terms. The action (1.18) can be split into the Einstein-Hilbert part

$$S_{EH} = \int d^4x \sqrt{-g} \frac{R}{2\kappa^2} \quad (1.19)$$

and the scalar field part

$$S_\phi = - \int d^4x \sqrt{-g} \left[ \frac{1}{2} g^{\mu\nu} \partial_\mu \phi \partial_\nu \phi + V(\phi) \right]. \quad (1.20)$$

The equation of motion for the homogeneous part of the inflaton is

$$\ddot{\phi} + 3H\dot{\phi} + V_{,\phi} = 0, \quad (1.21)$$

and the energy-momentum tensor is given by

$$T_{\mu\nu}^\phi \equiv \frac{2}{\sqrt{-g}} \frac{\delta S_\phi}{\delta g^{\mu\nu}} = \partial_\mu \phi \partial_\nu \phi - g_{\mu\nu} \left[ \frac{\partial^\rho \partial_\rho \phi}{2} + V(\phi) \right]. \quad (1.22)$$

The dynamics of the FLRW geometry are given by

$$H^2 = \frac{1}{3} \left( \frac{1}{2} \dot{\phi}^2 + V(\phi) \right) \quad (1.23)$$

and assuming spatial homogeneity for the inflaton, the equation of state becomes

$$w_\phi = \frac{p_\phi}{\rho_\phi} = \frac{\dot{\phi}^2 - 2V(\phi)}{\dot{\phi}^2 + 2V(\phi)}. \quad (1.24)$$

For the aforementioned conditions of negative pressure,  $w_\phi < 0$ , and accelerated expansion,  $w_\phi < -1/3$ , to hold, the potential energy needs to dominate over the kinetic term  $\dot{\phi}^2 \ll V(\phi)$ . In order for the inflationary epoch to be sustained for long enough - so that the comoving Hubble horizon shrinks adequately - the second time derivative must be comparatively negligible,  $\ddot{\phi} \ll |3H\dot{\phi}|, |V_{,\phi}|$ . This is encoded in the definition of the parameter

$$\eta_H = - \frac{\ddot{\phi}}{H\dot{\phi}}. \quad (1.25)$$

Both parameters,  $\epsilon_H$  defined above (1.17) and  $\eta_H$ , can be expressed in relation to the scalar field potential  $V(\phi)$ :

$$\epsilon_V(\phi) \equiv \frac{M_{Pl}^2}{2} \left( \frac{V_{,\phi}}{V} \right)^2, \quad (1.26)$$

and

$$|\eta_V|(\phi) \equiv M_{Pl}^2 \left( \frac{V_{,\phi\phi}}{V} \right). \quad (1.27)$$

The smallness of these parameters ensures that the universe undergoes a phase of accelerated expansion,  $\epsilon \ll 1$ , for long-enough time,  $|\eta| \ll 1$ . Under these conditions, the field will “roll” slowly enough toward the minimum of its potential until these “slow-roll” conditions (1.26) and (1.27) are violated [13].

The "slow-roll" regime,

$$\dot{\phi} \ll V(\phi) \quad \text{and} \quad \ddot{\phi} \ll |3H\dot{\phi}|, |V_{,\phi}|, \quad (1.28)$$

is then defined by the Hubble parameter being near-constant,

$$H^2 \approx \frac{V(\phi)}{3} \approx \text{constant} \quad (1.29)$$

the field velocity being given by

$$\dot{\phi} \approx -\frac{V_{,\phi}}{3H} \quad (1.30)$$

and the scale factor evolving, in de Sitter-like fashion, exponentially with time,  $a(t) \sim e^{Ht}$ .

### 1.3.2 Fundamentals of Cosmological Perturbation Theory

The Inflationary scenario, further to resolving the aforementioned problems of the Hot Big Bang Model, provides a natural explanation for the observable CMB anisotropies and the large-scale structure of the universe. Abandoning the assumption of homogeneity and isotropy results in examining the vacuum fluctuations of the inflaton and metric fields, which are predicted to manifest a near scale-invariant power spectrum, in direct agreement with observational results [24]. In order to briefly present the key features of cosmological perturbation theory, we begin by expanding the metric about the FLRW line element (1.1), in conformal time  $\eta$

$$ds^2 = a^2(\eta) \left\{ - (1 + 2A) d\eta^2 + 2\partial_i B dx^i d\eta + [(1 - 2\psi) \delta_{ij} + 2\partial_i \partial_j E] dx^i dx^j \right\} \quad (1.31)$$

with  $a$  being the scale factor and  $A, B, \psi$ , and  $E$  representing scalar fluctuations. The lapse function  $A$ , specifically, represents the fluctuation in the proper time interval with respect to the coordinate time interval.

Perturbing the inflaton around a homogeneous background  $\phi \rightarrow \phi + \delta\phi$ , substituting into the Klein-Gordon equation (1.21), and utilising the Einstein field equations (1.6), results in the equation of motion for the inflaton perturbation  $\delta\phi$ , to linear order in perturbation theory, in Fourier space [25, 26]:

$$\delta\ddot{\phi}_{\mathbf{k}} + 3H\delta\dot{\phi}_{\mathbf{k}} + \left( \frac{k^2}{a^2} + V_{,\phi\phi} \right) \delta\phi_{\mathbf{k}} = -2V_{,\phi} A_{\mathbf{k}} + \dot{\phi} \left[ \dot{A}_{\mathbf{k}} + 3\dot{\psi}_{\mathbf{k}} + \frac{k^2}{a^2} \left( a^2 \dot{E}_{\mathbf{k}} - a B_{\mathbf{k}} \right) \right], \quad (1.32)$$

for a given comoving wavenumber  $k$ , with overdots signifying derivatives with respect to cosmic time  $t$ .

The energy and momentum components of the (perturbed) Einstein field equations pose constraints on the metric perturbations appearing on the right-hand side of (1.32), resulting in

$$3H \left( \dot{\psi}_{\mathbf{k}} + H A_{\mathbf{k}} \right) + \frac{k^2}{a^2} \left[ \psi_{\mathbf{k}} + H \left( a^2 \dot{E}_{\mathbf{k}} - a B_{\mathbf{k}} \right) \right] = -\frac{1}{2M_{Pl}^2} \left[ \dot{\phi} \left( \delta\dot{\phi}_{\mathbf{k}} - \dot{\phi} A_{\mathbf{k}} \right) + V_{,\phi} \delta\phi_{\mathbf{k}} \right]$$

$$\dot{\psi} + H A_{\mathbf{k}} = \frac{\dot{\phi}}{2M_{Pl}^2} \delta\phi_{\mathbf{k}}.$$
(1.33)

The equation of motion for the perturbations (1.32) can be significantly simplified by the introduction of the Sasaki-Mukhanov variable [27],

$$Q_{\mathbf{k}} = \delta\phi_{\mathbf{k}} + \frac{\dot{\phi}}{H} \psi_{\mathbf{k}},$$
(1.34)

and the elimination of the metric perturbations, using (1.33):

$$\ddot{Q}_{\mathbf{k}} + 3H\dot{Q}_{\mathbf{k}} + \left[ \frac{k^2}{a^2} + V_{,\phi\phi} - \frac{1}{a^3 M_{Pl}^2} \partial_t \left( \frac{a^3}{H} \dot{\phi}^2 \right) \right] Q_{\mathbf{k}} = 0.$$
(1.35)

Redefining the field variable as  $v_{\mathbf{k}} = a Q_{\mathbf{k}}$ , in the spatially flat gauge  $\psi = 0$ , this equation takes the simpler form

$$v_{\mathbf{k}}'' + \left( k^2 - \frac{z''}{z} \right) v_{\mathbf{k}} = 0,$$
(1.36)

where primes denote derivatives with respect to conformal time  $\eta$ , as in (1.3), and we have defined the variable  $z$  as,

$$z^2 \equiv 2\epsilon M_{Pl}^2 a^2.$$
(1.37)

For the purpose of introducing the basic concepts relevant to this thesis, we focus, here, on solutions of the Sasaki-Mukhanov equation (1.36) for a test field in de Sitter,  $\epsilon \rightarrow 0$ , leading to the further simplification,

$$v_{\mathbf{k}}'' + \left( k^2 - \frac{2}{\eta} \right) v_{\mathbf{k}} = 0.$$
(1.38)

We start by promoting the field  $v$  and its conjugate momentum  $v'$  to quantum operators

$$\hat{v} = \int \frac{d^3\mathbf{k}}{2\pi^3} \left[ v_{\mathbf{k}}(\eta) \hat{a}_{\mathbf{k}} e^{i\mathbf{k}\cdot\mathbf{x}} + v_{\mathbf{k}}^*(\eta) \hat{a}_{\mathbf{k}}^\dagger e^{-i\mathbf{k}\cdot\mathbf{x}} \right]$$
(1.39)

and normalising them by demanding that

$$\langle v_{\mathbf{k}}, v_{\mathbf{k}} \rangle \equiv \frac{i}{\hbar} (v_{\mathbf{k}}^* v_{\mathbf{k}}' - v_{\mathbf{k}}'^* v_{\mathbf{k}}) = 1$$
(1.40)

with the creation and annihilation operators satisfying canonical commutation relations

$$\left[ \hat{a}_{\mathbf{k}}, \hat{a}_{\mathbf{k}'}^\dagger \right] = (2\pi)^3 \delta(\mathbf{k} - \mathbf{k}'). \quad (1.41)$$

### Bunch-Davies Vacuum and Mode Functions

A vacuum state must be chosen for the fluctuations, so that the action of the annihilation operator on it, annihilates the wave-function  $\hat{a}_{\mathbf{k}}|0\rangle = 0$ . This is customarily taken to be the Minkowski vacuum of a comoving observer in the far past  $\eta \rightarrow -\infty$ , or alternatively for  $k \gg aH$ . The Mukhanov equation (1.36), then, becomes the equation of motion of a simple harmonic oscillator

$$v_k'' + k^2 v_k = 0, \quad (1.42)$$

resulting in the initial condition

$$\lim_{k \gg aH} v_k = \frac{e^{-ik\eta}}{\sqrt{2k}}. \quad (1.43)$$

Returning to (1.38) we can see that an exact solution is given by

$$v_k = \alpha \frac{e^{-ik\eta}}{\sqrt{2k}} \left( 1 - \frac{i}{k\eta} \right) + \beta \frac{e^{ik\eta}}{\sqrt{2k}} \left( 1 + \frac{i}{k\eta} \right). \quad (1.44)$$

Utilising (1.40) and imposing (1.43), the values of the arbitrary parameters  $\alpha$  and  $\beta$  are fixed, leading to the Bunch-Davies mode functions

$$v_k = \frac{e^{-ik\eta}}{\sqrt{2k}} \left( 1 - \frac{i}{k\eta} \right). \quad (1.45)$$

### Power Spectra and Observables

These definitions permit the determination of the power spectrum of the *comoving curvature perturbation*,  $\mathcal{R} = \frac{H}{\dot{\phi}} \frac{v}{a} = \frac{H}{\dot{\phi}} \delta\phi$ , at the time of the mode's horizon crossing  $k = a(t_*) H(t_*)$ , as

$$\begin{aligned} \langle \mathcal{R}_{\mathbf{k}} \mathcal{R}_{\mathbf{k}'} \rangle &= \left( \frac{H_*}{\dot{\phi}_*} \right)^2 \langle \delta\phi_{\mathbf{k}} \delta\phi_{\mathbf{k}'} \rangle \\ &= \delta(\mathbf{k} + \mathbf{k}') \frac{2\pi^2}{k^3} \left( \frac{H_*}{\dot{\phi}_*} \right)^2 \left( \frac{H_*}{2\pi} \right)^2 \\ &= \delta(\mathbf{k} + \mathbf{k}') \frac{2\pi^2}{k^3} \Delta_{\mathcal{R}}^2(k), \end{aligned} \quad (1.46)$$

where we introduced the dimensionless power spectrum  $\Delta_{\mathcal{R}}^2(k)$  and denoted the ensemble average of quantum fluctuations as  $\langle \dots \rangle$ . This last quantity has proven vital for the connection between inflationary models and observational results, as it probes the depen-

dence of scalar quantum fluctuations to the wavelength scale, through the *scalar spectral index*

$$n_s - 1 \equiv \frac{d \ln \Delta_s^2}{d \ln k}, \quad (1.47)$$

with scale invariance corresponding to the value  $n_s = 1$ . A similar treatment of the tensor fluctuations of the Einstein-Hilbert action straightforwardly leads, see [17], to the realisation that each polarization mode obeys an equation of motion identical to that of the scalar fluctuation. Hence, the dimensionless power spectrum for the tensor fluctuation can be shown to be given by

$$\Delta_t^2(k) = 2 \Delta_h^2(k) = \frac{2}{M_{Pl}^2} \left( \frac{H_*}{\pi} \right)^2. \quad (1.48)$$

It is customary to normalise the tensor fluctuations to the amplitude of scalar fluctuations through the *tensor-to-scalar ratio*

$$r \equiv \frac{\Delta_t^2(k)}{\Delta_s^2(k)}, \quad (1.49)$$

which acts as a direct measure of the energy scale of the inflationary era, since with the measured value of  $\Delta_s^2 \sim 10^{-9}$ ,

$$V^{1/4} \sim \left( \frac{r}{0.01} \right)^{1/4} \cdot 10^{16} \text{ GeV}. \quad (1.50)$$

Among the simplest inflationary models would be one driven by a light ( $m \sim 10^{-5} M_{Pl}$ ), minimally coupled to gravity, scalar field with a quadratic potential ( $V = 1/2 m^2 \phi^2$ ), in de Sitter space. This model provides predictions for the tensor-to-scalar ratio and the spectral index, evaluated at CMB scales  $N_{CMB} \sim 60$  e-folds, of  $n_s \approx 0.96$  and  $r \approx 0.1$ , respectively, bringing it in fascinating agreement with the latest results from the Planck collaboration [28], which determine the observed scalar spectral index value  $n_s = 0.9649 \pm 0.0042$  at 68% CL and the tensor-to-scalar ratio being bounded from above, as  $r < 0.056$ .

### 1.3.3 Infrared Divergence in de Sitter

Despite the clarity that the single-field, slow-roll inflationary scenario boasts, it is not without issues. The exponential expansion that resolves the problems of the hot big bang scenario results in the whole spectrum red-shifting rapidly. Given long enough time almost all the higher modes of the inflaton will accumulate upon the zero mode, leading to infrared divergences. To see this explicitly, assume a massless minimally-coupled test scalar field in de Sitter and decompose it into spatial and temporal parts:

$$\phi(\mathbf{x}, \tau) = \int \frac{d^3 k}{(2\pi)^3} \left[ a_{\mathbf{k}} e^{i\mathbf{k}\cdot\mathbf{x}} \phi_{\mathbf{k}}(\tau) + a_{\mathbf{k}}^\dagger e^{-i\mathbf{k}\cdot\mathbf{x}} \phi_{\mathbf{k}}^*(\tau) \right], \quad (1.51)$$

where we have introduced a new time variable  $\tau \equiv \int^t dt'/a^3(t')$  which greatly simplifies the wave equation. Here  $a_{\mathbf{k}}$  and  $a_{\mathbf{k}}^\dagger$  are the annihilation and creation operators respectively,

as in(1.41). The mode amplitude function  $\phi_k(\tau)$  satisfies the equation of motion (1.21), which with respect to  $\tau$  takes the form

$$\phi_{k,\tau\tau}(\tau) + k^2 a^4 \phi_k(\tau) = 0. \quad (1.52)$$

Hence, the mode function in D spacetime dimensions and as a function of cosmic time  $t$  is [29]

$$\phi_k(t) = a^{-\left(\frac{D-1}{2}\right)} \sqrt{\frac{\pi}{4(1-\epsilon)H}} \mathcal{H}_\nu^{(1)}\left(\frac{-k}{(1-\epsilon)Ha}\right). \quad (1.53)$$

Here  $\nu = \frac{D-1-\epsilon}{2(1-\epsilon)}$  and  $\mathcal{H}_\nu^{(1)}(z)$  is the Hankel function of the first kind. In de Sitter space,  $\epsilon = 0$ , and in the small  $|\mathbf{k}|$  limit, where

$$\mathcal{H}_\nu^{(1)}(z) \approx -\mathcal{H}_\nu^{(2)}(z) \approx -\frac{i}{\pi} \Gamma(\nu) \left(\frac{z}{2}\right)^{-\nu} \quad (1.54)$$

the two-point correlation function,

$$\langle \phi(\mathbf{x}, t) \phi(\mathbf{x}', t') \rangle = \int \frac{d^3 k}{(2\pi)^3} e^{i\mathbf{k}\cdot(\mathbf{x}-\mathbf{x}')} \phi_k(t) \phi_k^*(t'), \quad (1.55)$$

can be seen to diverge in the infrared limit in four space-time dimensions. To see this, one may start from the mode amplitude two-point function

$$\phi_k(t) \phi_k^*(t') \xrightarrow{k \rightarrow 0} \frac{4^{|\nu|} (1-\epsilon)^{2|\nu|} \Gamma^2(|\nu|)}{4\pi(1-\epsilon) [H a^{D-1} H' a'^{D-1}]^{1/2}} \left[ \frac{H a H' a'}{k^2} \right]^{|\nu|} (1 + O(k^2)) \quad (1.56)$$

and observe that the leading term exhibits a  $k$ -dependence of  $k^{-2|\nu|}$ . Therefore, the two-point correlation function evolves proportionally to

$$\langle \phi(\mathbf{x}, \tau) \phi(\mathbf{x}', t') \rangle \propto \int dk e^{i\mathbf{k}\cdot(\mathbf{x}-\mathbf{x}')} k^{2-2|\nu|} (1 + O(k^2)). \quad (1.57)$$

It is evident that, in the case of a massless scalar in four-dimensional de Sitter  $|\nu| = \frac{3}{2}$ , equation (1.57) is logarithmically divergent. For a massive scalar, in de Sitter, for which  $\nu = \sqrt{\left(\frac{D-1}{2}\right)^2 - \left(\frac{M}{H}\right)^2}$  [30], one can Taylor expand (1.56) around  $M^2/H^2 \ll 1$ , to obtain

$$\lim_{t \rightarrow t'} \phi_k(t) \phi_k^*(t') \propto \frac{H^2}{k^3} \left[ 1 + \frac{M^2}{H^2} \log\left(\frac{k}{Ha}\right) \right], \quad (1.58)$$

which, at late enough times  $\frac{k}{Ha} \leq e^{-\frac{H^2}{M^2}}$ , is unsuitable for a perturbative treatment [31].

Furthermore, in the case of a massive scalar field with a quartic self-interaction potential  $V(\phi) \propto \lambda \phi^4$ , the perturbative expansion parameter, which will be shown to be  $\lambda H^4/m^4$ , leads to a break-down of perturbation theory for sufficiently small mass  $m^2 \leq \sqrt{\lambda} H^2$ , irrespective of the smallness of the self-interaction coupling constant,  $\lambda$ . We will present new methods for treating these divergences and computing N-point correlators for a light, minimally coupled inflaton in de Sitter (and beyond) in Chapter 2.



### 1.3.4 Beyond Minimally-Coupled Slow-Roll Inflation

There are various ways that the minimally-coupled slow-roll regime can be generalised, by abandoning the assumptions that characterise it.

- **Non-minimal coupling to gravity:** The simple single-field slow-roll action (1.18) is characterised by the lack of direct coupling between the inflaton field and the metric (minimal coupling). In general, the theory can be generalised with the inclusion of more involved terms (non-minimal coupling) between the inflaton and the graviton, see for example the review [32], however, using a field redefinition, non-minimally coupled theories can be written as minimally coupled ones. This process is not without its own problems and ambiguities, especially in relation to the potential metastability of the electroweak vacuum, in models in which the Higgs is either the inflaton or a spectator field in de Sitter.

#### Ultraviolet divergence in de Sitter-Higgs Vacuum Metastability

Einstein's General Relativity is well-known to be non-renormalisable [33–35] and exhibits divergences in the UV limit, rendering standard perturbative QFT methods ineffective for the description of the behaviour of fields during the inflationary era. Assuming that the Standard Model of particle physics is reliable at high energies can result in our vacuum being a long-lived metastable state. The Higgs potential barrier that surrounds the local minimum, depends strongly on the effective Higgs mass at high energies, and it is important that gravitational corrections are taken into account. In the inflationary energy range, General Relativity can be treated as an 'Effective Field Theory' of gravity. Assuming that inflation is driven by a weakly interacting inflaton field, we examine the effect that gravitational corrections have on the effective Higgs potential in Chapter 3.

- **Multifield Inflation** The assumption that inflation is driven by a single scalar field, despite leading successfully to agreements with observations, is not well-motivated by high-energy theories. Both the search for non-Gaussian signatures [36] and signs of isocurvature mode contribution in the CMB [28], as well as - more recently- developments in string cosmology [37–39] have motivated research towards inflationary models with multiple fields [40, 41]. Abandoning the single-inflaton ansatz, allows for the introduction of non-trivial kinetic terms, which can be encoded as the metric of the internal field space. In such models, the end of inflation can be delayed by this geometry, permitting steep potentials. The background dynamics and quantum perturbations of such a model are explored in Chapter 4.

## Part II

# Topics in Inflationary Scalar Quantum Field Theory with Curved Field Space

## Chapter 2. Feynman Rules for Stochastic Inflationary Correlators

### 2.1 Overview of the Chapter

In this chapter, we are focusing on the IR behaviour of a light, minimally coupled scalar field in an inflationary background.

We begin with a short introduction to the motivation behind the Stochastic Inflation formalism and an exposition of the literature that presents the methodology's success in encapsulating the long-wavelength behaviour of scalar fields in a curved spacetime, simplicity, and effectiveness (as compared to the full QFT computation) in quantitatively producing correlation functions, in agreement with perturbative techniques, and making predictions beyond perturbation theory.

Furthermore, we introduce the core elements of the formalism, demonstrating the methodology that permits the reduction of the IR dynamics of the full quantum system to a one-dimensional, quasi-classical Langevin equation. After obtaining the Fokker-Planck equation associated with the latter and showcasing its resemblance to the Schrödinger equation, we elaborate on the functional integral formulation of the stochastic dynamics of a spectator field during inflation, comparing its diagrammatic expansion to that obtained directly from a perturbative solution of the corresponding Langevin equation. We state Feynman rules for computing arbitrary temporal  $n$ -point functions and perform some illustrative computations for a light scalar ( $m \ll H_0$ ) subjected to quartic self-interaction  $\lambda \phi^4$ , paying attention to the role played by a functional Jacobian determinant in the path integral. We proceed to consider the case of backreaction, when the field contributes to the expansion parameter making the stochastic noise multiplicative and adding additional diagrams to the Feynman rules.

We close by noting challenges of the stochastic approach in providing results beyond the leading order, when gravity is consistently included. This modification would not only induce a backreaction,  $H \rightarrow H(\phi)$ , but also result in a state-dependent window function, altering the equation of motion. The use of mathematically equivalent prescriptions for the determination of the sequence of the operation of the stochastic and potential forces on the system (Ito, Stratonovich or arbitrary  $0 \leq \alpha \leq 1$  prescription) appear to lead to different results for physical quantities (statistical averages, correlators, etc.) - see [42] and references therein. The consistent inclusion of gravity requires either a prescription-invariant formalism, or the determination of a unique prescription, motivated by either a first principles computation or through other, independent of the system, techniques.

## 2.2 Stochastic Inflation: Classical System encompassing Quantum Behaviour

Inflation [11–13] has been shown to not only solve the zero-order problems of the Hot Big Bang scenario, but also provide a simple mechanism for the generation of the observable Large Scale Structure by placing a scalar field  $\phi$  in a (quasi-) de Sitter spacetime characterised by the Hubble rate  $H$ . Performing the mode expansion of the scalar field one readily observes a conceptual difference in the dynamical interaction between the long- and short-wavelength modes: whereas the equations of motion for the short-wavelength (UV) modes receive minimal adjustment (as compared to those in Minkowski spacetime) due to the existence of the background geometry, the long-wavelength (IR) modes will have their dynamics significantly affected. From a mathematical point of view, in the IR limit, a logarithmic divergence arises, pointing to the emergence of phenomena that require the employment of non-perturbative methods. From a physical point of view, the long-wavelength behaviour of quantum fields during inflation directly affects the physical processes in the post-inflationary era, from when observational data are taken, determining the values of the measured cosmological parameters. It is evident, hence, that the IR behaviour of scalar fields during inflation is well-worth examining.

A substantial amount of work has been carried out since Mukhanov and Chibisov [43] pointed out the dramatical enhancement that inflation has on the quantum effects of massless, minimally coupled scalars. Pioneers in the field have pointed out several methods to treat the interesting IR effects in curved spacetimes (for some excellent reviews the interested reader is encouraged to see [44, 45] and references therein) and have showcased the significant simplification that the technology of Stochastic Inflation offers, in calculating the leading order IR behaviour, in direct agreement with the full Quantum Field Theoretic treatment [31, 46–49] as well as presenting the opportunity to go beyond perturbation theory and obtain non-perturbative results [50].

It has been shown manifestly [49], to all loop orders, that the stochastic correlation functions produced from a QFT calculation, truncated to leading IR order, agree with the stochastic correlation functions found by Starobinsky [51] and Starobinsky and Yokoyama [52]. Recently, various new methodologies have been developed for the computation of scalar correlation functions in de Sitter, including the direct QFT approach (using the Schwinger-Dyson equations) [53, 54] and the spectral expansion at the level of the Fokker-Planck eigenvalue equation [55], extended beyond slow-roll [56], and applied in a  $1/N$  expansion for  $O(N)$ -symmetric systems [57, 58]. Lastly, we remark the novel approach on the description of the equilibrium state and the out-of-equilibrium dynamics of scalar fields in the static patch of de Sitter [59, 60], which offers intriguing insights to the effect that the presence of the cosmological horizon has on the thermalisation process, from the perspective of an inertial observer.

## 2.3 Novel Diagrammatic Methods for Cosmological Stochastic Inflation

### 2.3.1 From the Curved Spacetime QFT to the Langevin Equation

Following the work of [51, 52, 61], let us consider a minimally coupled, massive real scalar field  $\Phi$ , subjected to a potential  $V(\Phi)$  in a homogeneous and isotropic inflationary universe with a spatially flat metric,

$$ds^2 = -dt^2 + a^2(t) dx^2 = a^2(\tau) [-d\tau^2 + d\mathbf{x}^2], \quad (2.1)$$

with  $t$  and  $\tau$  denoting the cosmic and conformal times respectively and  $a(t)$  the scale factor. The Klein-Gordon equation, in de Sitter, is given by

$$\partial_t^2 \Phi + 3H \partial_t \Phi - \frac{\nabla^2}{a^2(t)} \Phi + V_{,\Phi} = 0, \quad (2.2)$$

with  $V_{,\Phi} = \partial_{\Phi} V(\phi)$  and  $H = \frac{\dot{a}(t)}{a(t)}$  the Hubble parameter, where the dot indicates a derivative with respect to the cosmic time  $t$ . In the ‘‘slow-roll’’ regime (1.28), in which the scalar field rolls down a flat potential, the evolution of the scalar is slower than the characteristic time  $H^{-1}$ , so the second time derivative can be omitted,

$$3H \partial_t \Phi - a^{-2}(t) \nabla^2 \Phi + V_{,\Phi} = 0. \quad (2.3)$$

Starobinsky’s [51] fascinating insight was to use the horizon length  $l \approx \tau$  as a measure in order to split the scalar field  $\Phi(x, t)$  into a short- and long-wavelength modes,

$$\Phi(x, t) = \phi(x, t) + q(x, t), \quad (2.4)$$

by introducing a coarse-graining window function  $W_k(t)$ , which defines the short-wavelength modes:

$$\begin{aligned} q(\mathbf{x}, t) &= \int \frac{d^3 k}{(2\pi)^3} W_k(t) \xi(\mathbf{x}, t) \\ &= \int \frac{d^3 k}{(2\pi)^3} W_k(t) \left[ U_k(t) a_{\mathbf{k}} e^{-i\mathbf{k}\cdot\mathbf{x}} + U^\dagger(t) a_{\mathbf{k}}^\dagger e^{i\mathbf{k}\cdot\mathbf{x}} \right], \end{aligned} \quad (2.5)$$

where  $a_{\mathbf{k}}$  and  $a_{\mathbf{k}}^\dagger$ , the annihilation and creation operators respectively, with canonical commutation relation  $[a_{\mathbf{k}}, a_{\mathbf{k}'}^\dagger] = (2\pi)^3 \delta(\mathbf{k} - \mathbf{k}')$ .

Utilising the split (2.4) and expanding the potential gradient around the perturbation  $q$  as  $V_{,\phi}(\phi + q) = V_{,\phi}(\phi) + \frac{dV_{,\phi}}{d\phi} q$  the Klein Gordon equation (2.3) becomes:

$$3H \partial_t \phi - a^{-2} \nabla^2 \phi + \partial_\phi V = - \left[ 3H \partial_t - a^{-2} \nabla^2 + V_{,\phi\phi} \right] q(\mathbf{x}, t). \quad (2.6)$$

Remembering that  $\xi$  is the perturbation field, which satisfies

$$\left[ 3 H \partial_t - a^{-2} \nabla^2 + V_{,\phi\phi} \right] \xi(\mathbf{x}, t) = 0, \quad (2.7)$$

identically, and focusing on the behaviour of the very long-wavelength modes  $\phi$ , for which  $|\mathbf{k}| \rightarrow 0$ , it is evident that the contribution of the gradient on the left hand side of (2.6) can be neglected. Thus, we obtain a first-order, non-linear equation:

$$\begin{aligned} \partial_t \phi + \frac{1}{3H} V_{,\phi} &= -\frac{1}{3H} \left[ 3 H \partial_t - a^{-2} \nabla^2 + V_{,\phi\phi} \right] q(\mathbf{x}, t) \\ &= -\int \frac{d^3 k}{(2\pi)^3} \partial_t W_k(t) \xi(\mathbf{x}, t) \\ &\equiv \Xi(\mathbf{x}, t), \end{aligned} \quad (2.8)$$

where, in the second line, we used the fact that the Klein-Gordon operator annihilates  $\xi(\mathbf{x}, t)$  (2.7) and the fact that the window function is purely time-dependent.

Making the simplest choice for the window function, that of a Heaviside function  $\Theta[|\mathbf{k}| - \epsilon a H]$ , makes the notion of the short-wavelength modes manifest: They are those with wavenumber  $|\mathbf{k}| > \epsilon a H$ , where  $\epsilon$  is a small constant.

With this choice for the Window function, (2.8) simplifies substantially, since

$$\partial_t \Theta(|\mathbf{k}| - \epsilon a H) = \epsilon a(t) H^2 \delta(|\mathbf{k}| - \epsilon a(t) H), \quad (2.9)$$

resulting in a concrete definition of the noise term,

$$\Xi(\mathbf{x}, t) = \frac{\epsilon a(t) H^2}{(2\pi)^3} \int d^3 k \delta(|\mathbf{k}| - \epsilon a H) \left[ a_{\mathbf{k}} U_k e^{-i\mathbf{k}\cdot\mathbf{x}} + a_{\mathbf{k}}^\dagger U_k^\dagger e^{i\mathbf{k}\cdot\mathbf{x}} \right], \quad (2.10)$$

with  $U_k$ , as in (2.5). These mode functions assume a set of normalised solutions, in four spacetime dimensions [29],

$$U_k(t) = \alpha^{-\frac{3}{2}} \frac{\sqrt{\pi}}{2} \mathcal{H}_\nu^{(1)}(|\mathbf{k}| \tau) H^{-1/2}, \quad (2.11)$$

where  $\mathcal{H}_\nu^{(1)}$  is the Hankel function of the first kind, with subscript  $\nu = \sqrt{9/4 - m^2/H^2}$ . For light scalar fields,  $\nu \approx 3/2$ , the mode function takes the much simpler form

$$U_k(t) = \frac{iH}{\sqrt{2|\mathbf{k}|}} \left( \tau - \frac{i}{|\mathbf{k}|} \right) e^{-i|\mathbf{k}|\tau}. \quad (2.12)$$

Let us pause for a moment here and appreciate (2.8). It is true that both the short- and long-wavelength modes have, formally, a quantum-mechanical operator nature, in the sense that their commutators with their respective derivatives are non-trivial. At late times, though, the commutator of the coarse-grained long-wavelength mode vanishes

$$[\phi(\mathbf{x}, t), \pi(\mathbf{x}, t)] = i \rightarrow \left[ \phi(\mathbf{x}, t), \dot{\phi}(\mathbf{x}, t) \right] = i a^{-3}(t) \approx 0. \quad (2.13)$$

Furthremore, as it was stated in [52] and explicitly manifested in [50], introducing an auxiliary field  $\varphi$ , whose mode function only includes the leading infrared contribution of (2.12)

$$U_k^\varphi \approx \frac{H}{\sqrt{2|\mathbf{k}|^3}}, \quad (2.14)$$

and replacing the scalar quantum field variable  $\phi$  with it, results in obtaining the same leading order behaviour as the QFT treatment, in the IR limit. Hence, one can use the technology for obtaining the equation of motion (and the probability distribution function in the next section) for the long-wavelength field (2.8), and, in essence, treat the resulting equation quasi-classically. This is due to the fact that in the mode expansion of this auxiliary field,

$$\varphi(\mathbf{x}, t) \equiv \int \frac{d^3k}{(2\pi)^3} \Theta[\epsilon a(t)H - |\mathbf{k}|] \frac{H}{\sqrt{2|\mathbf{k}|^3}} \left[ e^{i\mathbf{k}\cdot\mathbf{x}} a_{\mathbf{k}} + e^{-i\mathbf{k}\cdot\mathbf{x}} a_{\mathbf{k}}^\dagger \right], \quad (2.15)$$

– unlike a usual quantum field – there is a common multiplicative factor that accompanies the creation and annihilation operators, resulting in their time dependence being identical. Thus, the commutator of this auxiliary field and its time derivative vanishes,

$$[\varphi(\mathbf{x}, t), \dot{\varphi}(\mathbf{x}, t)] = 0, \quad (2.16)$$

reflecting the late-time behaviour of the long-wavelength modes (2.13). It is exactly this property, namely the commutativity of the auxiliary field variable and its derivative, that permits one to treat (2.8) as a quasi-classical equation for the long-wavelength modes, in de Sitter; quasi- because the creation and annihilation operators  $a_{\mathbf{k}}$  and  $a_{\mathbf{k}}^\dagger$  can take random values. This classically commuting, random variable is often referred to as “stochastic”.

Therefore, it follows that the long-wavelength modes obey (2.8) which is an inhomogeneous Klein-Gordon equation, where the force term, physically, can be interpreted as being due to the jitter caused by the quantum fluctuations of the perturbations of the background field (short-wavelength modes) crossing the horizon and giving the long-wavelength modes a stochastic “kick”.

We return to (2.10) to find the correlation of the noise term:

$$\begin{aligned} \langle \Xi(t_1) \cdot \Xi(t_2) \rangle &= \int d^3\mathbf{x} d^3\mathbf{x}' \delta(\mathbf{x} - \mathbf{x}') \langle \Xi(\mathbf{x}', t_1), \Xi(\mathbf{x}', t_2) \rangle \\ &= \epsilon \alpha(t) H^2 \epsilon \alpha(t') H^2 \int d^3\mathbf{x} \frac{d^3k}{(2\pi)^3} \frac{d^3k'}{(2\pi)^3} \delta[|\mathbf{k}| - \epsilon a(t) H] \delta[|\mathbf{k}'| - \epsilon a(t') H] \\ &\quad \left\{ \langle a_{\mathbf{k}} a_{\mathbf{k}'}^\dagger \rangle \frac{H^2}{\sqrt{4k^3 k'^3}} e^{-i\mathbf{x}\cdot(\mathbf{k}-\mathbf{k}')} + \langle a_{\mathbf{k}}^\dagger a_{\mathbf{k}'} \rangle \frac{H^2}{\sqrt{4k^3 k'^3}} e^{-i\mathbf{x}\cdot(\mathbf{k}-\mathbf{k}')} \right\} \\ &= \frac{H^3}{4\pi^2} [1 + 2n(|\mathbf{k}|)] \delta(t - t'), \end{aligned} \quad (2.17)$$

where  $\langle a_{\mathbf{k}}^\dagger a_{\mathbf{k}'} \rangle = (2\pi^3) \delta(\mathbf{k} - \mathbf{k}') n(|\mathbf{k}|)$  is the number operator and in the second to last line we used the identity  $\delta[f(x)] = \frac{1}{\|f'(x)\|_{x_0}} \delta(x)$  to manifest the explicit time-dependence of the delta function.

For a Bunch-Davies Vacuum [62],  $n(|k|) = 0$ , so the noise is  $\delta$ -correlated in time

$$\langle \Xi(t_1) \cdot \Xi(t_2) \rangle = \frac{H^3}{4\pi^2} \delta(t - t'). \quad (2.18)$$

### 2.3.2 From the Langevin to the Fokker-Planck Equation

As was established in the previous subsection, the IR dynamics of a scalar field in (quasi-)de Sitter, coarse grained over patches of physical size  $\Delta r \sim 1/H$  are described by the stochastic (slow-roll) dynamical equation,

$$\dot{\phi} + \frac{V'}{3H} = \hbar^{1/2} \mathcal{A}[\phi(t)] \xi(t), \quad (2.19)$$

where a prime denotes a derivative with respect to  $\phi$ ,  $\mathcal{A}$  satisfies

$$\mathcal{A}^2 = \frac{H^3}{4\pi^2}, \quad (2.20)$$

and  $\xi(t)$  is a Gaussian stochastic force term whose histories are weighted by a Gaussian probability distribution functional such that, for any functional  $F[\xi(t)]$ , the average over realisations of  $\xi(t)$  is given by ( $N$  is a normalization constant)

$$\langle F[\xi(t)] \rangle = N \int \mathcal{D}\xi F[\xi] e^{-\frac{1}{2} \int dt \xi(t)^2}, \quad (2.21)$$

implying  $\delta$ -correlation for the stochastic force,

$$\langle \xi(t) \xi(t') \rangle = \delta(t - t'). \quad (2.22)$$

In contrast to the introductory discussion 2.3.1, in the rest of this chapter we will keep  $c = 1$  but retain  $\hbar$  so as to explicitly keep track of terms related to stochastic fluctuations which are ultimately related to the quantum behaviour of the short-wavelength modes during inflation<sup>1</sup>. In what follows we will study two cases: Initially we will treat  $H$  as a constant, which results in the stochastic noise amplitude being independent of the field variable, making the noise “additive”, and  $\phi$  is a spectator field in de Sitter. This approach has been partially developed in previous publications [48, 49]. Followingly, we study the field backreacting on the spacetime, making the ansatz that (2.19) holds true, with the minimal alteration that the noise amplitude becomes field-dependent through  $H \rightarrow H(\phi)$ ,

<sup>1</sup>The units of various relevant quantities are therefore  $[\phi] = [\text{mass}]^{1/2}[\text{time}]^{-1/2}$ ,  $[\mathcal{A}] = [\text{time}]^{-3/2}$ ,  $[\xi] = [\text{time}]^{-1/2}$ ,  $[V] = [\text{mass}][\text{time}]^{-3}$  and  $[\hbar] = [\text{mass}][\text{time}]$ .



making the noise “multiplicative”. Hence, we assume slow roll such that

$$H^2 \simeq \frac{8\pi G}{3} V(\phi), \quad (2.23)$$

with de Sitter space given by the limit  $V(\phi) \rightarrow V_0$ .

Following the work of [63], any one dimensional stochastic equation of the form

$$\partial_t x = f(x) + g(x) \xi(t), \quad (2.24)$$

driven by a stochastic force  $\xi(t)$ , with drift  $f(x)$ , and diffusion coefficient  $D(x) = \frac{1}{2} g^2(x)$ , can be associated with a Fokker-Planck equation, which describes the evolution of the probability density function  $P(x, t)$  of the variable  $x(t)$ , given by

$$\partial_t P(x, t) = \partial_x [-f(x) - \Theta(0)g(x)g'(x)] P(x, t) + \partial_x^2 [D(x)P(x, t)]. \quad (2.25)$$

The introduction of the Heaviside function  $\Theta(t)$  follows, mathematically, from the fact that the stochastic noise  $\xi(t)$  is not a continuous function, but rather consists of a series of  $\delta$ -function “kicks” of random sign, and the resulting ambiguity associated with the computation of the integral

$$\mathcal{J}(t, \delta t) = \lim_{\delta t \rightarrow 0} \int_t^{t+\delta t} ds g[x(s)] \xi(s), \quad (2.26)$$

which is addressed by the generalised definition

$$\mathcal{J}_\Theta(t, \delta t) = g[x(t) + \Theta(0)\delta x] \int_t^{t+\delta t} ds \xi(s) \quad (2.27)$$

and reduces to the Ito, Stratonovich and isothermal conventions for  $\Theta(0) = \{0, \frac{1}{2}, 1\}$ , respectively.

Physically, the Heaviside function describes the sense in which the multiplicative noise amplitude  $g[x(s)]$  is to be evaluated: before, after or at some mid-point time relative to the effect of the stochastic “kick” that  $\xi(s)$  has on the system.

For our Langevin equation (2.19)  $f(\phi) = -\frac{V'}{3H}$  and  $g(\phi) = \hbar^{1/2} \mathcal{A}[\phi(t)]$  and the corresponding Fokker-Planck equation

$$\partial_t P(\phi, t) = \partial_\phi \left[ \frac{V'}{3H} + \frac{1}{2} (1 - \Theta(0)) [\hbar \mathcal{A}^2]' + \frac{1}{2} \hbar \mathcal{A}^2 \partial_\phi \right] P(\phi, t). \quad (2.28)$$

We give here a quick formal derivation as in [64], recalling that we are assuming the Stratonovich convention  $\Theta(0) = \frac{1}{2}$  in order to freely apply the normal rules of calculus. For a derivation in a general convention see [63].

Consider an arbitrary function  $\mathcal{F}(\phi_\xi)$  of the stochastic field  $\phi[\xi(t)] \equiv \phi_\xi(t)$ , where the subscript indicates that  $\phi_\xi$  is a solution to the Langevin equation for a particular noise

history  $\xi(t)$ , and therefore a functional of it. Its average over different noise histories is

$$\langle \mathcal{F}[\phi_\xi(t)] \rangle = \int \mathcal{D}\xi \mathcal{F}[\phi_\xi(t)] e^{-\frac{1}{2} \int dt \xi(t)^2} = \int d\phi \mathcal{F}(\phi) P(\phi, t). \quad (2.29)$$

In the first equation we write the expectation value of  $\mathcal{F}$  as an explicit average over the noise histories  $\xi$  while in the second we encode all  $\xi$ -dependence in a time dependent probability distribution  $P(\phi, t)$ , which gives the probability that the arbitrary field  $\phi$  takes the value associated with the solution of the Langevin equation with noise  $\xi(t)$ , at time  $t$ . Utilising the Langevin equation we have

$$\frac{d}{dt} \langle \mathcal{F}[\phi_\xi(t)] \rangle = \left\langle \frac{\delta \mathcal{F}}{\delta \phi_\xi} \left( -\frac{V'}{3H} + \hbar^{1/2} \mathcal{A} \xi \right) \right\rangle. \quad (2.30)$$

The term on the left-hand side can be written in terms of the probability distribution  $P(\phi, t)$  as

$$\frac{d}{dt} \langle \mathcal{F}[\phi(t)] \rangle = \int d\phi \mathcal{F}[\phi] \frac{\partial P}{\partial t}. \quad (2.31)$$

The first term on the right-hand side is easy to deal with:

$$\left\langle \frac{\delta \mathcal{F}}{\delta \phi_\xi} f \right\rangle = \int d\phi \frac{\delta \mathcal{F}}{\delta \phi} f P = - \int d\phi \mathcal{F} \frac{\partial}{\partial \phi} (f P). \quad (2.32)$$

To address the last term we use

$$\begin{aligned} 0 &= \int \mathcal{D}\xi \frac{\delta}{\delta \xi} \left( \frac{\delta \mathcal{F}}{\partial \phi_\xi} \mathcal{A} e^{-\frac{1}{2} \int dt \xi(t)^2} \right) \Rightarrow \\ \left\langle \frac{\delta \mathcal{F}}{\delta \phi_\xi} \mathcal{A} \xi \right\rangle &= \int \mathcal{D}\xi \frac{\partial}{\partial \phi_\xi} \left( \frac{\delta \mathcal{F}}{\partial \phi_\xi} \mathcal{A} \right) \frac{\delta \phi_\xi}{\delta \xi} e^{-\frac{1}{2} \int dt \xi(t)^2} \Rightarrow \\ \left\langle \frac{\delta \mathcal{F}}{\delta \phi_\xi} \mathcal{A} \xi \right\rangle &= \left\langle \frac{\partial}{\partial \phi_\xi} \left( \frac{\delta \mathcal{F}}{\partial \phi_\xi} \mathcal{A} \right) \frac{\delta \phi_\xi}{\delta \xi} \right\rangle, \end{aligned} \quad (2.33)$$

where the first line is the statement of the functional total derivative lemma, the second is the action of the differential operator on the argument, and in the last we used (2.29).

In (2.33) we encountered the term  $\frac{\delta \phi_\xi(t)}{\delta \xi(t)}$ , which still needs to be determined. The solution to the Langevin equation can be formally written as

$$\phi_\xi(t) = \phi_\xi(t_0) + \int_{t_0}^{\infty} \Theta(t - \tau) [f(\phi_\xi(\tau)) + \hbar^{1/2} \mathcal{A}[\phi(\tau)] \xi(\tau)] d\tau, \quad (2.34)$$

from which we obtain that the variation to the stochastic field value at time  $t$  resulting from the variation of the noise at a time  $t'$ , with  $\delta t = t - t' > 0$ , is

$$\frac{\delta \phi_\xi(t)}{\delta \xi(t')} \left\{ 1 - \delta t \Theta(t - t') [f'(t) + \xi(t) \hbar^{1/2} \mathcal{A}'[\phi(t)]] \right\} = \hbar^{1/2} \mathcal{A}[\phi(t)] \Theta(t - t'). \quad (2.35)$$

In the coincident limit  $\delta t \rightarrow 0$ , (2.35) reduces to

$$\frac{\delta\phi_\xi(t)}{\delta\xi(t)} = \hbar^{1/2} \mathcal{A}[\phi(t)] \Theta(0). \quad (2.36)$$

Substituting this relation in the last line of (2.33), integrating by parts twice, and utilising (2.29) we obtain

$$\left\langle \frac{\delta\mathcal{F}}{\delta\phi_\xi} \mathcal{A}\xi \right\rangle = \int d\phi \mathcal{F} \frac{\partial}{\partial\phi} \left[ \mathcal{A} \frac{\partial}{\partial\phi} (\hbar^{1/2} \mathcal{A}[\phi(t)] \Theta(0) P) \right]. \quad (2.37)$$

Putting everything together and noting that  $\mathcal{F}$  is arbitrary we arrive at

$$\frac{\partial P(\phi, t)}{\partial t} = \frac{\partial}{\partial\phi} \left[ \frac{V'}{3H} + \Theta(0) \hbar \mathcal{A} \frac{\partial}{\partial\phi} \mathcal{A} \right] P(\phi, t). \quad (2.38)$$

It is evident that Eqs.(2.28) and (2.38) are identical, but only when the Stratonovich convention  $\Theta(0) = 1/2$  is assumed, which was to be expected as normal rules of calculus were used to produce this Fokker-Planck equation.

The equilibrium solution reads

$$\begin{aligned} P_{\text{eq}}(\phi) &= \mathcal{N} e^{-2 \int \left( \frac{V'}{3H\hbar\mathcal{A}^2} + \frac{1-\Theta(0)}{2} \frac{(\mathcal{A}^2)'}{\mathcal{A}^2} \right) d\phi} \\ &= \mathcal{N} \mathcal{A}^{-1} e^{-2 \int d\phi \frac{V'}{3H\hbar\mathcal{A}^2}}, \end{aligned} \quad (2.39)$$

where  $\mathcal{N}$  is a normalization constant and in the second line we have used the Stratonovich convention  $\Theta(0) = 1/2$ .

### 2.3.3 From Fokker-Planck to Schrödinger

In this section, we transform the Fokker-Planck equation obtained above (2.28) to a Schrödinger-like equation (for a detailed derivation the interested reader is directed to Appendix A). To do so, we redefine the probability as:

$$P(\phi, t) \equiv f(\phi) \tilde{P}(\phi, t), \quad (2.40)$$

where the proportionality function  $f(\phi)$  is given by

$$\begin{aligned} f(\phi) &= \mathcal{N}' e^{-\int \left( \frac{V'}{3H\hbar\mathcal{A}^2} + \frac{2-\Theta(0)}{2} \frac{(\mathcal{A}^2)'}{\mathcal{A}^2} \right) d\phi} \\ &= \mathcal{M} \mathcal{A}^{-1} P_{\text{eq}}^{\frac{1}{2}}, \end{aligned} \quad (2.41)$$

with  $\mathcal{M}$  being an irrelevant constant (since we only care about ratios of the function  $f$  to itself and its derivatives).

Applying the redefinition (2.40) in (2.28), leads to a Wick-rotated ( $t \rightarrow -it$ ) Schrödinger-

like equation:

$$\dot{\tilde{P}}(\phi, t) = \hat{\mathcal{H}} \tilde{P}(\phi, t), \quad (2.42)$$

with Hamiltonian

$$\hat{\mathcal{H}} \equiv U(\phi) + \frac{1}{2} \hbar \mathcal{A}^2 \partial_\phi^2, \quad (2.43)$$

which can be associated with the Euclidean action

$$-S_{Schr}^{Eucl} = - \int dt \left[ \frac{\dot{\phi}^2}{2 \hbar \mathcal{A}^2} - U(\phi) \right]. \quad (2.44)$$

For the simple case of additive noise, where  $H$  is constant and all derivatives of  $H(\phi)$  and  $\mathcal{A}$  vanish, the resulting potential has the form:

$$-U(\phi) = -\frac{1}{2} \frac{V''}{3H} + \frac{1}{2} \left( \frac{V'}{3H} \right)^2 \frac{1}{\hbar \mathcal{A}^2}. \quad (2.45)$$

As it is shown in Appendix A, the general case  $H = H(\phi)$  is a lot more complicated.

## 2.4 The Stochastic Path Integral Formulation

In the previous section, we established the correspondence between the Fokker-Planck and Schrödinger equations, obtained the path integral formulation associated with the latter and showed in Appendix A, after expanding the full potential (A.6) for the case of multiplicative noise, that the resulting expression for the action is extremely involved.

Instead of using the Euclidean action (A.8), we follow here a different approach, which revolves around the introduction of an auxiliary scalar field  $\psi$ . This permits us to utilise the familiar machinery of the path integral formulation of quantum mechanics [65] to obtain solutions for the evolution of the probability distribution function  $\tilde{P}(\phi, t)$  associated with the scalar field and described by the original Langevin equation (2.19), with the inclusion of multiplicative noise.

In order to compute the expectation values of functions,  $\mathcal{O}[\phi(t_i)]$ , of the scalar field variable  $\phi(t_i)$  at times  $t_i$ , on solutions  $\phi_\xi$  of the stochastic equation (2.19) we can use the functional generalisation of the identity

$$\delta(x - x_0) = \delta(f(x)) \|f'(x)|_{x_0}\|, \quad (2.46)$$

where  $x_0$  is the solution to  $f(x) = 0$ , and write

$$\begin{aligned} \langle \mathcal{O}[\phi(t_i)] \rangle &= \int \mathcal{D}\xi \mathcal{D}\phi \mathcal{O}[\phi(t_i)] \delta[\phi - \phi_\xi] e^{-\frac{1}{2} \int dt \xi(t)^2} \\ &= \int \mathcal{D}\xi \mathcal{D}\phi \mathcal{O}[\phi(t_i)] \delta \left[ \dot{\phi} + \frac{V'}{3H} - \hbar^{1/2} \mathcal{A}[\phi(t)] \xi(t) \right] \mathcal{J}[\phi] e^{-\frac{1}{2} \int dt \xi(t)^2}. \end{aligned} \quad (2.47)$$

The resulting Jacobian determinant is

$$\begin{aligned}\mathcal{J}[\phi] &= \text{Det} \left[ \frac{\delta}{\delta\phi} \left( \dot{\phi} + \frac{V'}{3H} - \hbar^{1/2} \mathcal{A} \xi \right) \right]_{\phi=\phi_\xi} \\ &= \text{Det} \left[ \left( \frac{d}{dt} \delta(t-t') + \left( \frac{V'}{3H} \right)' - \hbar^{1/2} \mathcal{A}' \xi \right) \right]_{\phi=\phi_\xi},\end{aligned}\quad (2.48)$$

with  $\mathcal{A}' \equiv \partial\mathcal{A}/\partial\phi$ . An interesting point that should be noted here is that in (2.48) the derivative is taken with respect to the scalar field variable  $\phi$  and is then evaluated for the particular field configuration  $\phi = \phi_\xi$ . Then, the delta functional ensures that the scalar field variable is set to the particular solution of the Langevin equation, for all such solutions, hence the subscript is redundant and henceforth omitted.

The delta functional can be expressed via a functional Fourier integral as

$$\delta \left[ \dot{\phi} + \frac{V'}{3H} - \hbar^{1/2} \mathcal{A}[\phi(t)] \xi(t) \right] = \int \mathcal{D}\psi e^{i \int dt \psi \left( \dot{\phi} + \frac{V'}{3H} - \hbar^{1/2} \mathcal{A}[\phi(t)] \xi(t) \right)}. \quad (2.49)$$

A convenient way to express the determinant  $\mathcal{J}[\phi]$  is via the use of anti-commuting fields  $\bar{c}$  and  $c$ , as

$$\mathcal{J}[\phi] = \int \mathcal{D}c \mathcal{D}\bar{c} e^{\int dt \bar{c} \left( \frac{d}{dt} + \left( \frac{V'}{3H} \right)' - \hbar^{1/2} \mathcal{A}' \xi \right) c}. \quad (2.50)$$

We can then perform the Gaussian integral over  $\xi$ , which leaves us with

$$\langle \mathcal{O}[\phi(t_i)] \rangle = \int \mathcal{D}\psi \mathcal{D}\phi \mathcal{D}c \mathcal{D}\bar{c} \mathcal{O}[\phi(t_i)] e^{-S}, \quad (2.51)$$

with the action given by

$$S = \int dt \left[ \frac{1}{2} \hbar \mathcal{A}^2 \psi^2 - i\psi \left( \frac{d\phi}{dt} + \frac{V'}{3H} \right) + \bar{c} \left( \frac{d}{dt} + \left( \frac{V'}{3H} \right)' - i\psi \hbar \mathcal{A} \mathcal{A}' \right) c \right], \quad (2.52)$$

and where we have used the anti-commutativity of  $\bar{c}$  and  $c$  to remove one of the resulting terms containing  $\bar{c}c\bar{c} = 0$ . Furthermore, assuming the slow roll relation (2.23), the stochastic action becomes

$$S = \int dt \left[ \frac{1}{2} \hbar \mathcal{A}^2 \psi^2 - i\psi \left( \frac{d\phi}{dt} + \frac{(\sqrt{V})'}{(6\pi G)^{1/2}} \right) + \bar{c} \left( \frac{d}{dt} + \frac{(\sqrt{V})''}{(6\pi G)^{1/2}} - i\psi \hbar \mathcal{A} \mathcal{A}' \right) c \right]. \quad (2.53)$$

Adding source currents

$$S \rightarrow S - iJ\psi - J^a\phi - \bar{J}_c c - \bar{c} J_{\bar{c}}, \quad (2.54)$$

where  $\bar{J}_c$  and  $J_{\bar{c}}$  are Grassmann valued, one obtains a generating functional  $Z[J, J^a, \bar{J}_c, J_{\bar{c}}]$ , which, when appropriately differentiated, provides the expectation values for the fields. We remark on the importance (which will be manifest in section 2.5.1) of the fact that,

from (2.47) for  $\mathcal{O}[\phi] \rightarrow 1$ ,

$$Z[J, 0, 0, 0] = 1. \quad (2.55)$$

In the following sections, we will take the potential to have the form

$$V(\phi) = V_0 + V_{(\phi)} = V_0 + \frac{1}{2} \frac{m^2}{\hbar^2} \phi^2 + V_{\text{int}}, \quad (2.56)$$

such that, utilising (1.29), one obtains

$$H^2 = H_0^2 + \frac{8\pi G}{6} \frac{m^2}{\hbar^2} \phi^2 + \frac{8\pi G}{3} V_{\text{int}}. \quad (2.57)$$

When we discuss Feynman rules we will choose, for concreteness, a quartic interaction potential

$$V_{\text{int}} = \frac{1}{4!} \frac{\lambda}{\hbar} \phi^4. \quad (2.58)$$

The slow-roll condition (1.27), along with observational constraints for the field perturbations, place bounds to the permissible values of the scalar field mass and the self-interaction coupling [51],

$$\frac{m^2}{\hbar^2} \lesssim \frac{H_0^2}{20} \quad \frac{\lambda}{\hbar} \lesssim 10^{-12}, \quad (2.59)$$

motivating a hierarchy for the terms in the potential

$$V_0 \gg \frac{m^2}{\hbar^2} \phi^2 \gg \frac{\lambda}{\hbar} \phi^4. \quad (2.60)$$

Hence, the conditions of the field being "light",  $V'' < H^2$ , and subdominant compared to the background,  $V_{(\phi)} < V_0$ , are met. The implications of these bounds to the temporal range of applicability of our approach will be explored at the end of the following section.

## 2.5 Feynman Rules from the Path Integral

In this section, we derive Feynman rules directly from the path integral with action (2.53), including a weak backreaction on the expansion rate  $H = H(\phi)$  corresponding to multiplicative noise in the Langevin equation. Starting from (2.53) and keeping the leading order terms in the dimensionless quantity  $\chi \equiv \hbar G H_0^2 / 2\pi$  (which is  $H_0^2 / (2\pi M_p^2)$  in units where  $\hbar = 1$ ), the action in the exponent in the path integral (2.51) becomes

$$S = \frac{1}{2} \int \frac{d\omega}{2\pi} \left\{ \begin{aligned} & \left( \begin{array}{cc} \tilde{\phi}(-\omega) & \tilde{\psi}(-\omega) \end{array} \right) \begin{pmatrix} 0 & -\omega - i\eta\hbar \\ +\omega - i\eta\hbar & \frac{\hbar H_0^3}{4\pi^2} \end{pmatrix} \begin{pmatrix} \tilde{\phi}(\omega) \\ \tilde{\psi}(\omega) \end{pmatrix} \\ & + \tilde{c}(-\omega) (i\omega + \eta\hbar) \tilde{c}(\omega) \end{aligned} \right\} + S_{\text{int}}, \quad (2.61)$$

where we integrated by parts to make the kinetic term symmetric, went to Fourier space

$$\phi(t) = \int_{-\infty}^{+\infty} \frac{d\omega}{2\pi} \tilde{\phi}(\omega) e^{i\omega t}, \quad (2.62)$$

and defined  $\eta\hbar = \frac{m^2}{3\hbar^2 H_0}$ , which has dimensions of inverse time.  $S_{\text{int}}$  contains the interactions

$$S_{\text{int}} = \int dt \left\{ \begin{aligned} & -i \left[ \frac{\lambda}{18\hbar H_0} \right] \psi \phi^3 - \left[ \frac{\lambda}{6\hbar H_0} \right] \bar{c} \phi^2 c \\ & + \left[ \chi \frac{m^2}{2\hbar^2 H_0} \right] \phi^2 \psi^2 + \left[ \chi \frac{\lambda}{4!\hbar H_0} \right] \phi^4 \psi^2 + \\ & - \left[ i \chi \frac{m^2}{\hbar^2 H_0} \right] \bar{c} \psi \phi c - \left[ i \chi \frac{\lambda}{3!\hbar H_0} \right] \bar{c} \psi \phi^3 c + \dots \end{aligned} \right\}. \quad (2.63)$$

The first line in (2.63) contains terms arising, in de Sitter, due to self interaction of  $\phi$  while the second and third lines are the leading order gravitational terms, due to the field's backreaction on the spacetime geometry, with the ellipsis denoting terms of  $\mathcal{O}(\chi^2)$  or suppressed by further factors of  $\frac{m^2}{H_0^2}$  and  $\lambda$ .

We define  $\delta(\Sigma\omega_i) \equiv 2\pi \delta(\Sigma\omega_i)$  and remark that the quadratic term of (2.61) involves the matrix

$$\mathbf{A}_{\omega'\omega} = \begin{pmatrix} 0 & \omega' - i\eta\hbar \\ -\omega' - i\eta\hbar & \frac{\hbar H_0^3}{4\pi^2} \end{pmatrix} \delta(\omega' + \omega) \quad (2.64)$$

whose inverse, defined through

$$\int \frac{d\omega}{2\pi} \mathbf{A}_{\omega'\omega} \cdot \mathbf{A}_{\omega\omega''}^{-1} = \mathbf{1} \times \delta(\omega' - \omega''), \quad (2.65)$$

leads to the two point functions of the free scalar fields

$$\begin{aligned} \begin{pmatrix} \langle \phi(\omega')\phi(\omega) \rangle & \langle \phi(\omega')\psi(\omega) \rangle \\ \langle \psi(\omega')\phi(\omega) \rangle & \langle \psi(\omega')\psi(\omega) \rangle \end{pmatrix} &= \begin{pmatrix} \frac{\hbar H_0^3}{4\pi^2(\eta\hbar^2+\omega^2)} & \frac{i}{\eta\hbar+i\omega'} \\ \frac{i}{\eta\hbar+i\omega} & 0 \end{pmatrix} \delta(\omega' + \omega) \\ &\equiv \begin{pmatrix} F(\omega) & G(\omega') \\ G(\omega) & 0 \end{pmatrix} \delta(\omega' + \omega). \end{aligned} \quad (2.66)$$

Similarly, for the ghosts, we obtain

$$\langle \tilde{c}(\omega')\tilde{c}(\omega) \rangle = \frac{1}{\eta\hbar + i\omega} \delta(\omega' + \omega). \quad (2.67)$$

$F(\omega)$  is the Fourier transform of the free field two-point function

$$\langle \phi(t)\phi(t') \rangle = \int \frac{d\omega}{2\pi} F(\omega) e^{i\omega(t-t')} = \frac{\hbar H_0^3}{8\pi^2 \eta\hbar} e^{-\eta|t-t'|}, \quad (2.68)$$

whereas the  $\phi - \psi$  correlator corresponds to the retarded Green function

$$\langle \phi(t)\psi(t') \rangle = \int \frac{d\omega}{2\pi} G(\omega) e^{i\omega(t-t')} = \Theta(t-t') e^{-\eta(t-t')}. \quad (2.69)$$

Obviously, setting  $\omega \rightarrow -\omega$ , or exchanging  $t \leftrightarrow t'$ , gives the advanced Green function. Note that the  $\psi$  field always sits at an earlier time than  $\phi$  in the correlators, imbuing them with a directionality, unlike the  $F(t, t')$  correlator which is symmetric in  $t$  and  $t'$ . The ghost correlator also has a natural directionality and is simply related to the retarded propagator  $\mathcal{G}(\omega) = -iG(\omega)$ . As we will see, it serves to maintain the normalization of the generating functional (2.55). Finally, note that from (2.69),  $\Theta(0) = \frac{1}{2}$  and hence our formalism implicitly imposes the Stratonovich convention for the stochastic process.

With the propagators described above and the interactions presented in (2.63), one is led to a diagrammatic expansion for arbitrary temporal correlators  $\langle \phi(t_1) \dots \phi(t_n) \rangle$  dictated by the following Feynman rules:

- Diagrams are constructed using the **propagators** below



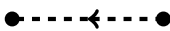
$F(\omega)$	$\frac{H_0^3 \hbar}{4\pi^2(\eta\hbar^2+\omega^2)}$	
$G(\omega)$	$\frac{i}{(\eta\hbar+i\omega)}$	
$\mathcal{G}(\omega)$	$\frac{1}{(\eta\hbar+i\omega)}$	

Table 2.1: Feynman rules for the free-field two point function  $F(\omega)$ , the retarded propagator  $G(\omega)$ , and the ghost propagator  $\mathcal{G}(\omega)$ .

Each line is associated with a frequency  $\omega$  running along it. The directionality associated with  $G$  is indicated by the wiggly-straight line with the two ends corresponding to the  $\psi$  and  $\phi$  fields respectively. If  $\omega$  runs from the wiggly to the straight



end, it is counted as positive, whereas it is counted as  $-\omega$  if it runs from the straight to the wiggly end. Alternatively, in configuration space the wiggly end corresponds to the earlier time. In ghost lines, the arrow, flowing from  $c$  to  $\bar{c}$ , also indicates the time direction and the sense in which a frequency associated to the line is counted as positive.

- These propagators are joined together with **vertices**. In the case of a spectator scalar subjected to a potential  $V(\phi) = (\lambda/4! \hbar) \phi^4$ , in de Sitter, the vertices are given in Table 2.2.

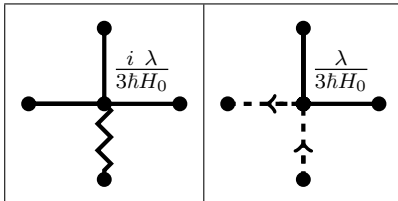


Table 2.2: Feynman rules for the vertices of a spectator field in de Sitter with quartic self-interaction and the ghost resulting from the Jacobian determinant.

Note that for a  $\phi^n$  interaction there would be  $n - 1$  straight legs in the left diagram and  $n - 2$  straight legs in the ghost diagram with the appropriate vertex factor. There are also additional “gravitational vertices” stemming from the  $\phi$ -dependence of the noise amplitude (multiplicative noise) in (2.53), shown in Table 2.3:

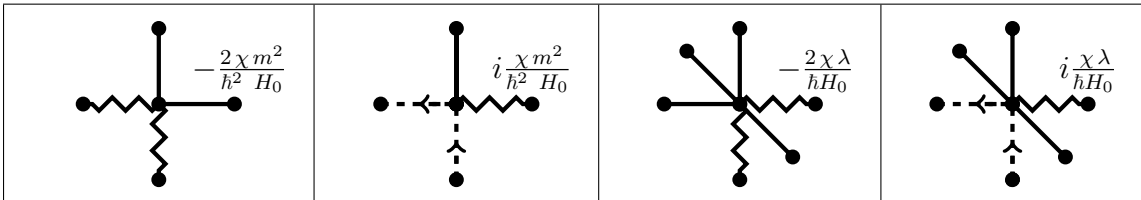


Table 2.3: Feynman rules for the vertices induced by multiplicative noise.

- **Frequency conservation** applies at each vertex.
- Running inside **each closed loop** is a frequency  $\sigma$  which is integrated over with  $\int \frac{d\sigma}{2\pi}$ .
- All **external points** at times  $t_i$  come with a straight leg



which attaches to a vertex on either a straight or a wiggly leg, creating the associated  $F$  or  $G$  propagator.

- Each external line connecting to  $t_i$  carries a frequency  $\omega_i$ . It is counted as  $+\omega_i$  if it exits the diagram and  $-\omega_i$  if it enters the diagram. The overall direction of frequency flow is conventional. In addition to their  $F$  or  $G$  factors, **external lines** also carry an  $e^{\pm i\omega_i t_i}$  factor.

- **Total frequency** is conserved across the whole diagram and external frequencies are integrated over with  $\int \frac{d\omega}{2\pi}$ .
- Diagrams should be divided by their **symmetry factor**.

We now apply these rules to perform a few illustrative computations of correlation functions by constructing the corresponding diagrams. We will focus here on the spectator field case and will utilise the extra vertices to compute some of their contributions in section 2.7.

### 2.5.1 Partition Function

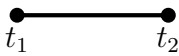
In the absence of external currents  $J_\psi$ ,  $\bar{J}_c$  and  $J_{\bar{c}}$ , the generating functional is unity by construction, see (2.55). Therefore, all vacuum bubbles must vanish. Indeed, this is achieved by cancellations from the ghost loops. The partition function is expanded as:

$$Z = 1 + \text{[diagram 1]} + \text{[diagram 2]} + \text{[diagram 3]} + \text{[diagram 4]} + \text{[diagram 5]} + \text{[diagram 6]} + \dots \quad (2.70)$$

One should note that the bubble stemming from the  $\phi^3\psi$  interaction (first bubble above), cancels the one from the  $\bar{c}\phi^2c$  (second bubble above). The other four order  $\lambda$  bubbles shown stem from multiplicative noise, when  $H = H(\phi)$ , and also cancel due to ghost loops: the  $\bar{c}\phi\psi c$  bubble cancels the one from  $\phi^2\psi^2$  (third and fourth bubble above) and the  $\psi^2\phi^4$  bubble cancelling the one from  $\bar{c}\psi\phi^3c$  (fifth and sixth bubble above). The symmetry factors for  $\phi^2\psi^2$ ,  $\psi^2\phi^4$  and  $\bar{c}\psi\phi^3c$  are  $\frac{1}{2}$ ,  $\frac{1}{2}$  and  $\frac{1}{4}$ , respectively. This diagrammatic cancellation persists to all orders and is a consequence of the inclusion of the determinant  $\mathcal{J}[\phi]$ , expressed in terms of ghost fields, which ensures the correct normalization of the delta functional. More precisely, the cancellations are due to the fact that  $\mathcal{G}(\omega) = -iG(\omega)$ , the symmetry factors of the diagrams and the corresponding factors of  $i$  in the vertices.

### 2.5.2 Two-Point Function

The tree-level contribution to the 2-point function  $\langle\phi(t_1)\phi(t_2)\rangle$ ,



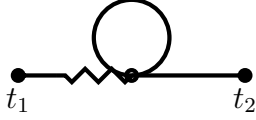
is simply an F-type propagator. Applying the rules and choosing the frequency to run from right to left and defining  $\sigma \equiv \frac{\omega}{\eta}$ , we get:

$$\langle \phi(t_1)\phi(t_2) \rangle^{(0)} = F(t_1, t_2) = \left[ \frac{\hbar \mathcal{A}^2}{\eta \hbar} \right] \int \frac{d\sigma}{2\pi} \frac{e^{i\eta\sigma(t_1-t_2)}}{(1+\sigma^2)} = \frac{\hbar H_0^3}{8\pi^2 \eta \hbar} e^{-\eta \hbar |t_1-t_2|}, \quad (2.71)$$

a well known result [52].

To first order in  $\lambda$ , the contributing Feynmann diagrams are:

### The Left Seagull



$$A = -\frac{1}{2} \frac{\lambda H_0^5 \hbar}{24 \cdot 4\pi^4 \eta \hbar} \int \frac{d\omega}{2\pi} \frac{e^{i\omega(t_1-t_2)}}{(\eta \hbar + i\omega)(\eta \hbar^2 + \omega^2)}, \quad (2.72)$$

where the frequency was taken to run from right to left and the symmetry factor is  $\frac{1}{2}$ .

### The Right Seagull



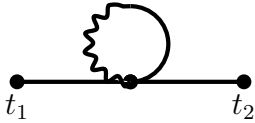
$$B = -\frac{1}{2} \frac{\lambda H_0^5 \hbar}{24 \cdot 4\pi^4 \eta \hbar} \int \frac{d\omega}{2\pi} \frac{e^{i\omega(t_1-t_2)}}{(\eta \hbar^2 + \omega^2)(\eta \hbar - i\omega)}, \quad (2.73)$$

where the assumptions made above, have been applied. Together they give

$$A + B = -\frac{\lambda H_0^5 \hbar}{24\pi^4} \frac{\hbar}{4} \int \frac{d\omega}{2\pi} \frac{e^{i\omega(t_1-t_2)}}{(\eta \hbar^2 + \omega^2)^2}, \quad (2.74)$$

which is symmetric in  $t_1 \leftrightarrow t_2$ .

Two more diagrams can be formed at order  $\lambda$  with the existing vertices, one including a closed  $G$  propagator line



$$C = \frac{-\lambda H_0^5 \hbar}{24 \pi^4} \frac{\hbar}{2} \int \frac{d\omega}{2\pi} \frac{e^{i\omega(t_1-t_2)}}{(\eta \hbar^2 + \omega^2)^2} \Theta(0) \quad (2.75)$$

and the ghost-loop diagram



$$G = \frac{\lambda H_0^5 \hbar}{24 \pi^4} \frac{\hbar}{2} \int \frac{d\omega}{2\pi} \frac{e^{i\omega(t_1-t_2)}}{(\eta \hbar^2 + \omega^2)^2} \Theta(0), \quad (2.76)$$

where  $\Theta(0) = \frac{1}{2}$  with the ghost loop acting to precisely cancel the retarded propagator loop, as expected.<sup>2</sup>

<sup>2</sup>This is true for any assignment of a value for  $\Theta(0)$ , not only for  $\Theta(0) = 1/2$ , as our formalism implies here, reflecting the fact that for additive noise,  $H = H_0$ , results are independent of the stochastic discretization prescription: Stratonovich, Ito or otherwise.

Then, the first order in  $\lambda$  contribution to the two point function is given by:

$$\begin{aligned}\langle\phi(t_1)\phi(t_2)\rangle^{(1)} &= \frac{\hbar\mathcal{A}^2}{\eta\hbar} \left[-\frac{\lambda}{3\hbar H_0}\right] \left[\frac{\hbar\mathcal{A}^2}{2\eta\hbar^2}\right] \int \frac{d\sigma}{2\pi} \frac{e^{i\eta\sigma(t_1-t_2)}}{(1+\sigma^2)^2} \\ &= \frac{\hbar\mathcal{A}^2}{\eta\hbar} \left[-\frac{\lambda}{3\hbar H_0}\right] \left[\frac{\hbar\mathcal{A}^2}{2\eta\hbar^2}\right] \frac{1}{4} (1+\eta|\Delta t|) e^{-\eta|\Delta t|},\end{aligned}\quad (2.77)$$

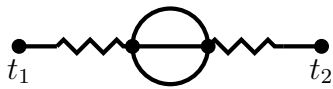
where  $\Delta t = t_1 - t_2$ .

### NNLO de Sitter contributions

To second order in  $\lambda$ , there are 3 distinct topologies of connected Feynman diagrams: Sunsets, Seagulls and Cacti.

#### The Symmetric Sunset

Taking frequency  $\omega$  to run through the diagram from right to left and noting that the diagram's symmetry factor is  $\frac{1}{6}$ , we have



$$\begin{aligned}\mathcal{SS} &= \frac{1}{6} \left(i\frac{\lambda}{3H_0\hbar}\right)^2 \int \frac{d\omega}{2\pi} \frac{e^{i\omega(t_1-t_2)} i^2}{(\eta\hbar - i\omega)(\eta\hbar + i\omega)} \mathcal{I}_{SS}(\omega) \\ &= \frac{\lambda^2 H_0^7 \hbar}{9\eta\hbar^2 (8\pi^2)^3} \int \frac{d\omega}{2\pi} \frac{e^{i\omega(t_1-t_2)} (\eta\hbar^2 + \omega^2)}{(\eta\hbar^2 + \omega^2)^2 [(3\eta\hbar)^2 + \omega^2]},\end{aligned}\quad (2.78)$$


where the  $\mathcal{I}_{SS}(\omega)$  factor involves integrations from the two loops.

$$\mathcal{I}_{SS}(\omega) = \left(\frac{H_0^3 \hbar}{4\pi^2}\right)^3 \int \frac{d\sigma d\rho}{2\pi 2\pi} \frac{1}{(\eta\hbar^2 + \sigma^2)(\eta\hbar^2 + \rho^2)(\eta\hbar^2 + (\sigma + \rho + \omega)^2)}, \quad (2.79)$$

with  $\sigma$  running clockwise in the upper loop and  $\rho$  running anti-clockwise in the lower.

#### The Left Sunset

With frequency running, again, from right to left and including the symmetry factor  $\frac{1}{2}$ , we have



$$\begin{aligned}\mathcal{LS} &= \frac{1}{2} \left(i\frac{\lambda}{3H_0\hbar}\right)^2 \left(\frac{H_0^3 \hbar}{4\pi^2}\right) \int \frac{d\omega}{2\pi} \frac{e^{i\omega(t_1-t_2)} i \mathcal{I}_{LS}(\omega)}{(\eta\hbar^2 + \omega^2)(\eta\hbar + i\omega)} \\ &= \frac{\lambda^2 H_0^7 \hbar}{9\eta\hbar^2 (8\pi^2)^3} \int \frac{d\omega}{2\pi} \frac{e^{i\omega(t_1-t_2)} (\eta\hbar - i\omega)(3\eta\hbar - i\omega)}{(\eta\hbar^2 + \omega^2)^2 [(3\eta\hbar)^2 + \omega^2]},\end{aligned}\quad (2.80)$$

where the loop integral, now, is given by

$$\mathcal{I}_{LS}(\omega) = \left(\frac{H_0^3 \hbar}{4\pi^2}\right)^2 \int \frac{d\rho d\sigma}{2\pi 2\pi} \frac{i}{(\eta\hbar^2 + \sigma^2)(\eta\hbar^2 + \rho^2)(\eta\hbar + i(\sigma + \rho + \omega))}, \quad (2.81)$$

with  $\sigma$  and  $\rho$  running in the loops as above.

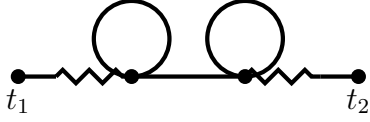
**The Right Sunset**


$$\begin{aligned}
 \mathcal{RS} &= \frac{1}{2} \left( i \frac{\lambda}{3H_0 \hbar} \right)^2 \left( \frac{H_0^3 \hbar}{4\pi^2} \right) \int \frac{d\omega}{2\pi} \frac{e^{i\omega(t_1-t_2)} i \mathcal{I}_{\mathcal{RS}}(\omega)}{(\eta \hbar^2 + \omega^2) (\eta \hbar - i\omega)} \\
 &= \frac{\lambda^2 H_0^7 \hbar}{9\eta \hbar^2 (8\pi^2)^3} \int \frac{d\omega}{2\pi} \frac{e^{i\omega(t_1-t_2)} (\eta \hbar + i\omega)(3\eta \hbar + i\omega)}{(\eta \hbar^2 + \omega^2)^2 [(3\eta \hbar)^2 + \omega^2]}
 \end{aligned} \tag{2.82}$$

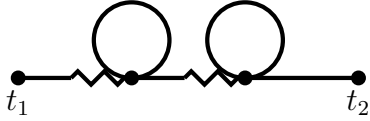
where, as above,

$$\mathcal{I}_{\mathcal{RS}}(\omega) = \left( \frac{H_0^3 \hbar}{4\pi^2} \right)^2 \int \frac{d\rho d\sigma}{2\pi 2\pi} \frac{i}{(\eta \hbar^2 + \sigma^2) (\eta \hbar^2 + \rho^2) (\eta \hbar - i(\sigma + \rho + \omega))}. \tag{2.83}$$

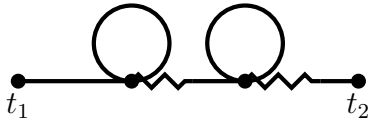
We note the minus signs in the frequencies that enter the propagators, resulting from their flow from the straight to the wiggly ends of the lines.

**The Symmetric Double Seagulls**


$$\begin{aligned}
 \mathcal{SDS} &= \frac{1}{4} \left( i \frac{\lambda}{3H_0 \hbar} \right)^2 \left( \frac{1}{2\eta \hbar} \frac{H_0^3 \hbar}{4\pi^2} \right)^2 \int \frac{d\omega}{2\pi} \frac{e^{i\omega(t_1-t_2)} \frac{H_0^3 \hbar}{4\pi^2} i^2}{(\eta \hbar^2 + \omega^2)^2} \\
 &= \frac{1}{4} \frac{2\lambda^2 H_0^7 \hbar}{9\eta \hbar^2 (8\pi^2)^3} \int \frac{d\omega}{2\pi} \frac{e^{i\omega(t_1-t_2)}}{(\eta \hbar^2 + \omega^2)^2}
 \end{aligned} \tag{2.84}$$

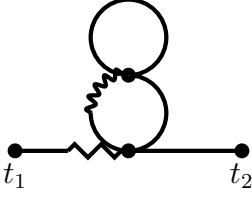
**The Left Double Seagulls**


$$\begin{aligned}
 \mathcal{LDS} &= \frac{1}{4} \left( i \frac{\lambda}{3H_0 \hbar} \right)^2 \left( \frac{1}{2\eta \hbar} \frac{H_0^3 \hbar}{4\pi^2} \right)^2 \int \frac{d\omega}{2\pi} \frac{e^{i\omega(t_1-t_2)} \frac{H_0^3 \hbar}{4\pi^2} i^2}{(\eta \hbar + i\omega)^2 (\eta \hbar^2 + \omega^2)} \\
 &= \frac{1}{4} \frac{2\lambda^2 H_0^7 \hbar}{9\eta \hbar^2 (8\pi^2)^3} \int \frac{d\omega}{2\pi} \frac{e^{i\omega(t_1-t_2)}}{(\eta \hbar^2 + \omega^2) (\eta \hbar + i\omega)^2}
 \end{aligned} \tag{2.85}$$

**The Right Double Seagulls**


$$\begin{aligned}
 \mathcal{RDS} &= \frac{1}{4} \left( i \frac{\lambda}{3H_0 \hbar} \right)^2 \left( \frac{1}{2\eta \hbar} \frac{H_0^3 \hbar}{4\pi^2} \right)^2 \int \frac{d\omega}{2\pi} \frac{e^{i\omega(t_1-t_2)} \frac{H_0^3 \hbar}{4\pi^2} i^2}{(\eta \hbar - i\omega)^2 (\eta \hbar^2 + \omega^2)} \\
 &= \frac{1}{4} \frac{2\lambda^2 H_0^7 \hbar}{9\eta \hbar^2 (8\pi^2)^3} \int \frac{d\omega}{2\pi} \frac{e^{i\omega(t_1-t_2)}}{(\eta \hbar^2 + \omega^2) (\eta \hbar - i\omega)^2}
 \end{aligned} \tag{2.86}$$

### The Left Cactus



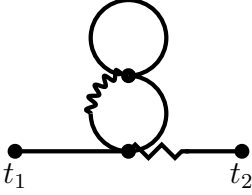
$$\begin{aligned} \mathcal{L}\mathcal{C} &= \frac{1}{2} \left( i \frac{\lambda}{3H_0\hbar} \right)^2 \mathcal{I}_{\mathcal{L}\mathcal{C}} \int \frac{d\omega}{2\pi} \frac{e^{i\omega(t_1-t_2)} i \frac{H_0^3\hbar}{4\pi^2}}{(\eta\hbar + i\omega)(\eta\hbar^2 + \omega^2)} \\ &= \frac{1}{2} \frac{\lambda^2 H_0^7 \hbar}{9\eta\hbar^3 (8\pi^2)^3} \int \frac{d\omega}{2\pi} \frac{e^{i\omega(t_1-t_2)} (\eta\hbar - i\omega)}{(\eta\hbar^2 + \omega^2)^2} \end{aligned} \quad (2.87)$$

where,

$$\mathcal{I}_{\mathcal{L}\mathcal{C}} = \frac{1}{2\eta\hbar} \frac{H_0^3\hbar}{4\pi^2} \int \frac{d\sigma}{2\pi} \frac{i \frac{H_0^3\hbar}{4\pi^2}}{(\eta\hbar + i\sigma)(\eta\hbar^2 + \sigma^2)}, \quad (2.88)$$

is the  $\omega$ -independent factor stemming from the loop integrations.

### The Right Cactus



$$\begin{aligned} \mathcal{R}\mathcal{C} &= \frac{1}{2} \left( i \frac{\lambda}{3H_0\hbar} \right)^2 \mathcal{I}_{\mathcal{R}\mathcal{C}} \int \frac{d\omega}{2\pi} \frac{e^{i\omega(t_1-t_2)} \frac{H_0^3\hbar}{4\pi^2} i}{(\eta\hbar^2 + \omega^2)(\eta\hbar - i\omega)} \\ &= \frac{1}{2} \frac{\lambda^2 H_0^7 \hbar}{9\eta\hbar^3 (8\pi^2)^3} \int \frac{d\omega}{2\pi} \frac{e^{i\omega(t_1-t_2)} (\eta\hbar + i\omega)}{(\eta\hbar^2 + \omega^2)^2} \end{aligned} \quad (2.89)$$

with  $\mathcal{I}_{\mathcal{R}\mathcal{C}} = \mathcal{I}_{\mathcal{L}\mathcal{C}}$ . This concludes the topologically different connected 2-point diagrams, to second order in  $\lambda$ .

Cacti involving a closed  $G$  loop at their top are cancelled by the corresponding closed ghost loops. Hence, adding up the  $\mathcal{O}(\lambda^2)$  contributions to the two-point function

$$\begin{aligned} \langle \phi(t)\phi(t') \rangle^{(2)} &= \frac{\hbar \mathcal{A}^2}{2\eta\hbar} \left[ -\frac{\lambda}{3\hbar H_0} \right]^2 \left[ \frac{\mathcal{A}^2 \hbar}{2\eta\hbar^2} \right]^2 \int \frac{d\sigma}{2\pi} \frac{e^{i\eta\sigma(t_1-t_2)}}{(1+\sigma^2)^2} \frac{1}{2} \left[ -1 + \frac{4}{1+\sigma^2} + \frac{32}{9+\sigma^2} \right] \\ &= \frac{\hbar \mathcal{A}^2}{2\eta\hbar} Q^2 \frac{1}{24} [(3\eta\hbar^2 |\Delta t|^2 + 18\eta\hbar |\Delta t| + 15) e^{-\eta\hbar |\Delta t|} + e^{-3\eta\hbar |\Delta t|}], \end{aligned} \quad (2.90)$$

where  $Q = \left[ -\frac{\lambda}{3\hbar H_0} \right] \cdot \left[ \frac{\hbar \mathcal{A}^2}{2\eta\hbar^2} \right]$  is the expansion parameter.

It is clear from these results that, for temporal correlators, the relevant expansion parameter is  $|Q| \equiv \frac{\lambda \mathcal{A}^2}{6\eta\hbar^2 H_0}$ , as noted in [48, 55, 66], and is a reasonable expansion parameter so long that  $|Q| \ll 1$  or  $\frac{m^2}{\hbar^2} \gg \sqrt{\lambda} H^2$ . This condition is well within the bounds placed by the slow-roll approximation,  $m^2/\hbar^2 \ll H^2$ , see (2.59). The aforementioned results (2.71), (2.77) and (2.90) agree with, at the coincident limit  $|\Delta t| \rightarrow 0$ , and generalise the results of [48]. It is easy to see that, for large temporal separation, the dominant term at each order in the perturbative expansion depends on the combination  $Q \eta\hbar \Delta t$ . This indicates a breakdown of this approximation for  $|\Delta t| > \frac{1}{Q\eta\hbar}$ . Nevertheless, this restriction is irrelevant in this context, since fields separated by a physical time interval  $|\Delta t| > \frac{1}{\eta\hbar}$  become -essentially- uncorrelated, due to the exponential  $e^{-\eta\hbar |\Delta t|}$  [48].

Resumming the two-point correlation function, up to second order in the expansion parameter, leads to an intriguing comparison between our approach and the spectral expansion method [55], in the limit  $|Q| \ll 1$ . We start by defining  $Z \equiv \frac{\hbar \mathcal{A}^2}{2\eta\hbar}$  and rearranging the sum of (2.71), (2.77) and (2.90):

$$\begin{aligned} \langle \phi(t)\phi(t') \rangle_{\text{sum}} &= Z e^{-\eta\hbar|\Delta t|} \left[ 1 + \frac{Q\eta\hbar|\Delta t|}{2} + \frac{1}{2} \left( \frac{Q\eta\hbar|\Delta t|}{2} \right)^2 + \dots \right] \\ &+ Z e^{-\eta\hbar|\Delta t|} \frac{Q}{2} \left[ 1 + \frac{5}{2} \left( \frac{Q^2}{2} \right) + \dots \right] \\ &+ Z e^{-\eta\hbar|\Delta t|} \left( \frac{Q}{2} \right)^2 3\eta\hbar|\Delta t| + \frac{1}{6} Z \left( \frac{Q}{2} \right)^2 e^{-3\eta\hbar|\Delta t|} \end{aligned} \quad (2.91)$$

with dots indicating higher order terms expected to appear when higher order in  $\lambda$  corrections to the two-point function are summed. Focusing on the first line of (2.91), we readily recognise the first terms of the exponential  $e^{-\frac{|Q|\eta\hbar|\Delta t|}{2}}$ . The coefficient  $|Q|\eta\hbar/2$  is the first order in  $Q$  correction to the lowest non-trivial eigenfunction of the spectral expansion method [55]. The last term manifests the dependence of the expansion on the third eigenvalue (to zeroth-order), verifying through an independent computation that, as expected, only the odd eigenvalues contribute to the two-point function due to the  $\phi \rightarrow -\phi$  symmetry of our potential.

Lastly, the prefactor  $Z$  introduced above is in exact agreement with the one obtained through the spectral expansion method, solidifying our confidence in the approach adopted in this work.

It is worth noting that, by utilising de Sitter invariance, the temporal correlator can provide the spatial 2-point function  $\langle \phi(\mathbf{r}_1)\phi(\mathbf{r}_2) \rangle$ , a quantity of more direct observational interest, by replacing [48, 52, 55, 67]

$$\eta\hbar|\Delta t| \rightarrow 2\frac{\eta\hbar}{H} \ln(aH|\mathbf{r}_1 - \mathbf{r}_2|) \quad (2.92)$$

in the expressions (2.77) and (2.90), where  $t$  is some arbitrary time of interest. This applies when equilibrium has been reached, an assumption implicit in all presented computations.

### 2.5.3 Four-Point Function

The Feynman rules can easily be applied to compute any higher point function at arbitrary times. For illustration we compute here the tree-level and one-loop connected 4-point functions, the latter of which are given by ‘‘candy’’ diagrams. The existence of  $F$  and  $G$  lines introduces different topologies that contribute to the final result.

#### Tree-Level Contribution to the Four-point Function

Utilising the Feynman rules of Tables 2.1 and 2.2, and assigning incoming frequencies  $\omega_1$  and  $\omega_3$  to the  $F$  and  $G$  lines attached to  $t_1$  and  $t_3$ , respectively, and outgoing frequencies  $\omega_2$  and  $\omega_4$  to the  $F$  lines connected to  $t_2$  and  $t_4$  one obtains for the  $\mathcal{O}(\lambda^1)$  four-point function:

$$\begin{aligned}
 \mathcal{P}_3 &= \frac{i \lambda}{3\hbar H_0} \int \frac{d\omega_1 d\omega_2 d\omega_3 d\omega_4}{(2\pi)^4} \frac{e^{-i\omega_1 t_1 + i\omega_2 t_2 - i\omega_3 t_3 + i\omega_4 t_4} \left(\frac{H_0^3 \hbar}{4\pi^2}\right)^3 i}{(\eta\hbar^2 + \omega_1^2) (\eta\hbar^2 + \omega_2^2) (\eta\hbar - i\omega_3)(\eta\hbar^2 + \omega_4^2)} \\
 &\quad \cdot \delta(\omega_1 + \omega_3 - \omega_2 - \omega_4) \\
 &= -\frac{\lambda}{3\hbar H_0} \left(\frac{\hbar H_0^3}{4\pi^2}\right)^3 \int \frac{\prod_i d\omega_i}{(2\pi)^4} \frac{e^{-i\omega_1 t_1 + i\omega_2 t_2 - i\omega_3 t_3 + i\omega_4 t_4} (\eta\hbar + i\omega_3)}{\prod_i (\eta\hbar^2 + \omega_i^2)} \\
 &\quad \cdot \delta(\omega_1 + \omega_3 - \omega_2 - \omega_4).
 \end{aligned}
 \tag{2.93}$$

The total tree-level contribution to the four-point function can be obtained trivially by shifting the position of the retarded propagator to the other three options, and summing. The terms linear to  $\omega$  in the numerator vanish due to the  $\delta$ -function. Hence, one obtains:

$$\begin{aligned}
 \mathcal{P}_{\text{total}} &= -\frac{4\lambda\eta\hbar}{3\hbar H_0} \left(\frac{H_0^3 \hbar}{4\pi^2}\right)^{-1} \int \frac{\prod_i d\omega_i}{(2\pi)^4} \prod_i F(\omega_i) e^{i\Sigma(\omega_i t_i)} \delta(\Sigma\omega_i) \\
 &= 8 \left[\frac{\hbar \mathcal{A}^2}{\eta\hbar}\right]^2 \left[-\frac{\lambda}{3\hbar H_0}\right] \left[\frac{\hbar \mathcal{A}^2}{2\eta\hbar^2}\right] \int \frac{\prod_i d\sigma_i}{(2\pi)^4} \prod_i \frac{1}{1 + \sigma_i^2} \cdot \delta(\Sigma\sigma_i) e^{i(\eta\hbar \Sigma\sigma_i t_i)} \tag{2.94} \\
 &= 8 [2Z]^2 [Q] \int \frac{\prod_i d\sigma_i}{(2\pi)^4} \prod_i \frac{1}{1 + \sigma_i^2} \cdot \delta(\Sigma\sigma_i) e^{i(\eta\hbar \Sigma\sigma_i t_i)},
 \end{aligned}$$

with  $Z$  defined above (2.91) and  $Q$ , the expansion parameter, defined underneath (2.90)

#### One Loop $F$ - Candies

For the first set of diagrams we choose to connect  $t_1$  to  $t_3$  without having to go through the loop. There are four such diagrams, differing in the distribution of external  $F$  and  $G$  lines, shown below. For each diagram the symmetry factor is  $1/2$  due to the internal  $F$  propagators.



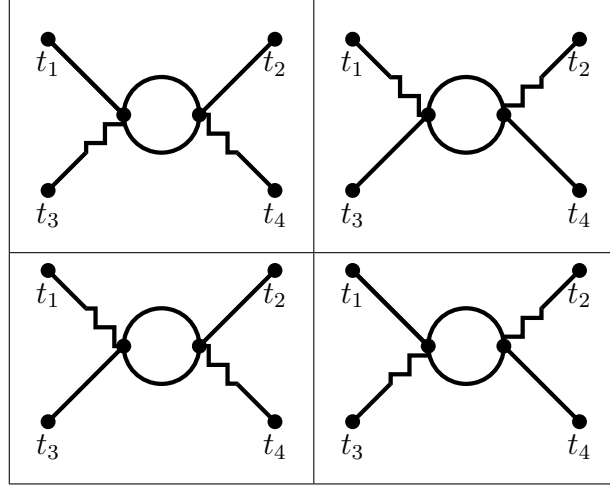


Table 2.4: The Feynman diagrams contributing to the one-loop four-point function including F-propagator loops.

Focusing on the upper left diagram, we assign incoming frequencies  $\omega_1$  and  $\omega_3$  to the  $F$  and  $G$  lines attached to  $t_1$  and  $t_3$ , respectively, and outgoing frequencies  $\omega_2$  and  $\omega_4$  to the  $F$  and  $G$  lines connected to  $t_2$  and  $t_4$ , while we assign frequency  $\sigma$  to run counter-clockwise in the loop. Applying the rules we have for this “candy” diagram

$$\begin{aligned}
 \mathcal{F}_{\mathcal{C}_1} &= \frac{1}{2} \left( \frac{i\lambda}{3\hbar H_0} \right)^2 \int \frac{d\omega_1 d\omega_2 d\omega_3 d\omega_4}{(2\pi)^4} \frac{e^{-i\omega_1 t_1 + i\omega_2 t_2 - i\omega_3 t_3 + i\omega_4 t_4} \left( \frac{H_0^3 \hbar}{4\pi^2} \right)^2 i^2}{(\eta\hbar^2 + \omega_1^2) (\eta\hbar^2 + \omega_2^2) (\eta\hbar - i\omega_3)(\eta\hbar + i\omega_4)} \\
 &\quad \cdot \mathcal{I}_{\mathcal{F}_{\mathcal{C}_1}}(\omega_1, \omega_3) \delta(\omega_2 + \omega_4 - \omega_1 - \omega_3) \\
 &= \frac{1}{2} \left( \frac{i\lambda}{3\hbar H_0} \right)^2 \int \frac{d\omega_1 d\omega_2 d\omega_3 d\omega_4}{(2\pi)^4} \frac{e^{-i\omega_1 t_1 + i\omega_2 t_2 - i\omega_3 t_3 + i\omega_4 t_4} \left( \frac{H_0^3 \hbar}{4\pi^2} \right)^2 i^2 (\eta\hbar + i\omega_3)(\eta\hbar - i\omega_4)}{(\eta\hbar^2 + \omega_1^2) (\eta\hbar^2 + \omega_2^2) (\eta\hbar^2 + \omega_3^2)(\eta\hbar^2 + \omega_4^2)} \\
 &\quad \cdot \mathcal{I}_{\mathcal{F}_{\mathcal{C}_1}}(\omega_1, \omega_3) \delta(\omega_2 + \omega_4 - \omega_1 - \omega_3),
 \end{aligned} \tag{2.95}$$

where the loop integral is

$$\begin{aligned}
 \mathcal{I}_{\mathcal{F}_{\mathcal{C}_1}}(\omega_1, \omega_3) &= \left( \frac{H_0^3 \hbar}{4\pi^2} \right)^2 \int \frac{d\sigma}{2\pi} \frac{1}{(\eta\hbar^2 + \sigma^2) (\eta\hbar^2 + (\omega_1 + \omega_3 + \sigma)^2)} \\
 &= \left( \frac{H_0^3 \hbar}{4\pi^2} \right)^2 \frac{1}{\eta\hbar} \frac{1}{4\eta\hbar^2 + (\omega_1 + \omega_3)^2}.
 \end{aligned} \tag{2.96}$$

The other three diagrams are obtained by shifting the placement of the  $G$  lines. It is easy to see that the top right diagram ( $\mathcal{F}_{\mathcal{C}_2}$ ) is obtained by replacing  $(\eta\hbar + i\omega_3)(\eta\hbar - i\omega_4) \rightarrow (\eta\hbar + i\omega_1)(\eta\hbar - i\omega_2)$  in the numerator of (2.95), the bottom left ( $\mathcal{F}_{\mathcal{C}_3}$ ) by  $(\eta\hbar + i\omega_3) \rightarrow (\eta\hbar + i\omega_1)$  and the bottom right ( $\mathcal{F}_{\mathcal{C}_4}$ ) by  $(\eta\hbar - i\omega_4) \rightarrow (\eta\hbar - i\omega_2)$ . Remarkably, adding up all the diagrams results in cancellations, leading to

$$\sum_i \mathcal{FC}_i(t_1, t_2, t_3, t_4) = \frac{1}{2\eta\hbar} \left( \frac{\lambda}{3\hbar H_0} \right)^2 \int \frac{\prod_i d\omega_i}{(2\pi)^4} \prod_i F(\omega_i) e^{i\Sigma(\omega_i t_i)} \delta(\Sigma\omega_i), \quad (2.97)$$

where we redefined the signs of all the frequencies, which is possible since  $F(\omega)$  is even.

The other two possibilities, connecting  $t_1$  to  $t_2$  or  $t_1$  to  $t_4$  without going through the loop, give an identical result and therefore the sum of all F-Candy diagrams contributes

$$\mathcal{FC}(t_1, t_2, t_3, t_4) = \frac{3}{2\eta\hbar} \left( \frac{\lambda}{3\hbar H_0} \right)^2 \int \frac{\prod_i d\omega_i}{(2\pi)^4} \prod_i F(\omega_i) e^{i\Sigma(\omega_i t_i)} \delta(\Sigma\omega_i). \quad (2.98)$$

### One Loop $G$ -Candies

The other set of contributing one-loop diagrams consists of  $G$ -candies, in which one of the internal loop propagators is of  $G$ -type. We choose the external times to be connected as seen below,

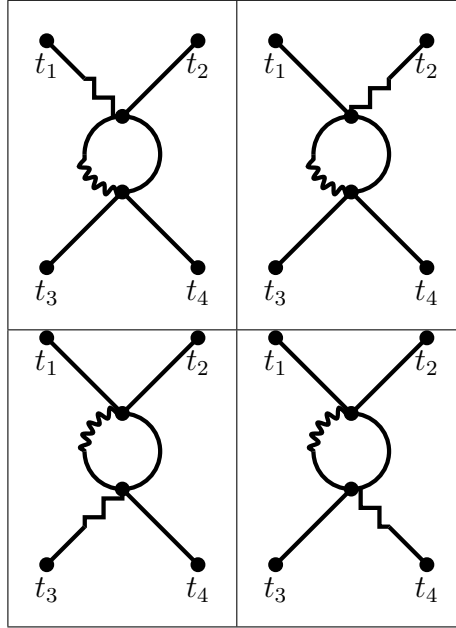


Table 2.5: The Feynman diagrams contributing to the one-loop four-point function including  $G$ -propagator loops.

and compute the top left diagram of this group. Assigning incoming frequencies  $\omega_1$  and  $\omega_3$  (to  $t_1$  and  $t_3$  respectively), outgoing  $\omega_2$  and  $\omega_4$  (to  $t_2$  and  $t_4$ ), frequency  $\sigma$  running counter-clockwise in the loop, and noting that the symmetry factor is, now, unity (no possible exchange of  $F$ -lines in the loop), we have

$$\mathcal{GC}_1 = \frac{1}{2\eta\hbar} \left[ \frac{\lambda}{3\hbar H_0} \right]^2 \int \frac{d\omega_1 d\omega_2 d\omega_3 d\omega_4}{(2\pi)^4} e^{-i\omega_1 t_1 + i\omega_2 t_2 - i\omega_3 t_3 + i\omega_4 t_4} \frac{\eta\hbar + i\omega_1}{(2\eta\hbar) - i(\omega_1 - \omega_2)} \cdot F(\omega_1) F(\omega_2) F(\omega_3) F(\omega_4) \delta(-\omega_1 + \omega_2 - \omega_3 + \omega_4), \quad (2.99)$$

where we directly included the loop integral

$$\mathcal{I}_{GC_1} = \int \frac{d\sigma}{2\pi} \frac{i}{(\eta\hbar - i(\sigma + \omega_1 - \omega_2))} \frac{\frac{H_0^3 \hbar}{4\pi^2}}{\eta\hbar^2 + \sigma^2}. \quad (2.100)$$

The other 3 diagrams are obtained by performing the appropriate permutations, as above, leading to a total of

$$\begin{aligned} \sum_i \mathcal{G} &= \frac{1}{2\eta\hbar} \left[ \frac{\lambda}{3\hbar H_0} \right]^2 \int \frac{\prod_i d\omega_i}{(2\pi)^4} e^{i(-\omega_1 t_1 + \omega_2 t_2 - \omega_3 t_3 + \omega_4 t_4)} \prod_i F(\omega_i) \delta(-\omega_1 + \omega_2 - \omega_3 + \omega_4) \\ &\cdot \left[ \frac{\eta\hbar + i\omega_1}{(2\eta\hbar) + i(\omega_1 - \omega_2)} + \frac{\eta\hbar - i\omega_2}{(2\eta\hbar) + i(\omega_1 - \omega_2)} + \frac{\eta\hbar + i\omega_3}{(2\eta\hbar) - i(\omega_1 - \omega_2)} + \frac{\eta\hbar - i\omega_4}{(2\eta\hbar) - i(\omega_1 - \omega_2)} \right] \\ &= \frac{1}{\eta\hbar} \left[ \frac{\lambda}{3\hbar H_0} \right]^2 \int \frac{\prod_i d\omega_i}{(2\pi)^4} e^{i(\sum \omega_i t_i)} \prod_i F(\omega_i) \delta(\sum \omega_i), \end{aligned} \quad (2.101)$$

where in the last equation, the relevant transformations ( $\omega_i \rightarrow -\omega_i, i = 1, 2$ ) have been performed. As in the case of  $F$ -candies, the other two possibilities, i.e. connecting  $t_1$  to  $t_2$  or  $t_1$  to  $t_4$  without going through the loop, give an identical result and therefore all  $G$ -Candy diagrams contribute

$$\mathcal{GC}(t_1, t_2, t_3, t_4) = \frac{3}{\eta\hbar} \left( \frac{\lambda}{3\hbar H_0} \right)^2 \int \frac{\prod_i d\omega_i}{(2\pi)^4} \prod_i F(\omega_i) e^{i\sum(\omega_i t_i)} \delta(\sum \omega_i). \quad (2.102)$$

Finally, adding the sums of  $F$ - and  $G$ -candies results in:

$$\begin{aligned} \mathcal{Z}(t_1, t_2, t_3, t_4) &= \frac{9}{2\eta\hbar} \left( \frac{\lambda}{3\hbar H_0} \right)^2 \int \frac{\prod_i d\omega_i}{(2\pi)^4} \cdot \delta(\sum \omega_i) e^{i(\sum \omega_i t_i)} \prod_i F(\omega_i) \\ &= 18 \left[ \frac{\hbar \mathcal{A}^2}{\eta\hbar} \right]^2 \left[ -\frac{\lambda}{3\hbar H_0} \right]^2 \left[ \frac{\mathcal{A}^2 \hbar}{2\eta\hbar^2} \right]^2 \int \frac{\prod_i d\sigma_i}{(2\pi)^4} \prod_i \frac{1}{1 + \sigma_i^2} \cdot \delta(\sum \sigma_i) e^{i(\eta\hbar \sum \sigma_i t_i)}. \end{aligned} \quad (2.103)$$

From the expressions (2.71),(2.77) (2.90),(2.94) and (2.103), we can infer the general form of the contribution to the  $N$ -point function, up to the  $m$ -th order in  $\lambda$ , formulated as a conjectured diagram (C.D.):

$$\text{C.D.}(t_1, t_2, \dots) = \mathcal{N} \left[ \frac{\hbar \mathcal{A}^2}{\eta\hbar} \right]^{\frac{N}{2}} Q^m \int \frac{\prod_i d\sigma_i}{(2\pi)^N} \prod_i f(\sigma) \cdot \delta(\sum \sigma_i) e^{i(\eta\hbar \sum \sigma_i t_i)}, \quad (2.104)$$

where  $\mathcal{N}$  is a constant resulting from the loop integrals and  $f(\sigma)$  is a function of the dimensional parameter  $\sigma \equiv \frac{\omega}{\eta\hbar}$  which depends on the diagram topology. Ultimately, the expansion parameter is  $|Q| \equiv \frac{\lambda \mathcal{A}^2}{6\eta\hbar^2 H_0}$ , consistent with our 2-point function observations.

## 2.6 Stochastic Diagrams from the Langevin Equation in Pure de Sitter

In this section, we compute the 2-point and 4-point functions to order  $\lambda^2$  directly from the Langevin equation for the potential (2.56). We demonstrate how this perturbative solution can be represented graphically as ‘tree’ diagrams and manifestly show that they are identical to those obtained in section 2.5. Nevertheless, this graphical representation requires a non-insignificant amount of labour, compared to the direct application of the Feynman rules stated previously. Therefore, this section not only validates the previous computations, but also demonstrates the efficiency of using the Feynman rules stated in section 2.5 compared to working with the direct solution of the Langevin equation.

We start by rewriting (2.19), as

$$\dot{\phi} + \eta\hbar\phi + \frac{\lambda}{6 \cdot 3\hbar H_0} \phi^3 = \hbar^{1/2} \mathcal{A} \xi(t), \quad (2.105)$$

where, for simplicity, we ignore in this section any dependence of  $\mathcal{A}$  on  $\phi$ . Expanding the solution  $\phi(t) = \phi_{(0)} + \phi_{(1)} + \phi_{(2)} + \dots$  to different orders in  $\lambda$  and, accordingly, splitting the Langevin equation (2.105) into different orders results in:

$$\dot{\phi}_{(0)} + \eta\hbar\phi_{(0)} = \hbar^{1/2} \mathcal{A} \xi(t) \quad (2.106)$$

$$\dot{\phi}_{(1)} + \eta\hbar\phi_{(1)} + \frac{\lambda}{6 \cdot 3\hbar H_0} \phi_{(0)}^3 = 0 \quad (2.107)$$

$$\dot{\phi}_{(2)} + \eta\hbar\phi_{(2)} + \frac{\lambda}{6 \cdot 3\hbar H_0} (3\phi_{(0)}^2 \phi_{(1)}) = 0 \quad (2.108)$$

⋮

By defining the Fourier transform as in (2.62), we directly obtain in Fourier space and to order  $O(\lambda^0)$

$$\phi_{(0)}(\omega) = \frac{1}{\eta\hbar + i\omega} \hbar^{1/2} \mathcal{A} \xi(\omega) \equiv G^R(\omega) \hbar^{1/2} \mathcal{A} \xi(\omega). \quad (2.109)$$

Fourier transforming the cubic term in (2.107),

$$\phi_{(0)}^3(t) = \int \frac{d\omega d\omega' d\omega''}{(2\pi)^3} \phi_{(0)}(\omega) \phi_{(0)}(\omega') \phi_{(0)}(\omega'') e^{i(\omega+\omega'+\omega'')t}, \quad (2.110)$$

the first order equation reads, in Fourier space,

$$\begin{aligned} & (\eta\hbar + i\omega) \phi_{(1)}(\omega) \\ &= - \frac{\lambda}{6 \cdot 3\hbar H_0} \int \frac{d\omega_1 d\omega_2 d\omega_3}{(2\pi)^3} \delta(\omega_1 + \omega_2 + \omega_3 - \omega) \phi_{(0)}(\omega_1) \phi_{(0)}(\omega_2) \phi_{(0)}(\omega_3) \\ &= - \frac{\lambda \left( \hbar^{\frac{1}{2}} \mathcal{A} \right)^3}{6 \cdot 3\hbar H_0} \int \frac{d\omega_1 d\omega_2 d\omega_3}{(2\pi)^3} \delta(\omega_1 + \omega_2 + \omega_3 - \omega) \\ & \quad G^R(\omega_1) \xi(\omega_1) G^R(\omega_2) \xi(\omega_2) G^R(\omega_3) \xi(\omega_3) \end{aligned} \quad (2.111)$$

and therefore the  $O(\lambda^1)$  solution is straightforwardly obtained, as

$$\phi_{(1)}(\omega) = -\frac{\lambda (\hbar^{1/2} \mathcal{A})^3}{6 \cdot 3\hbar H_0} G^R(\omega) \int \frac{d\omega_1 d\omega_2 d\omega_3}{(2\pi)^3} \delta(\omega_1 + \omega_2 + \omega_3 - \omega) \cdot G^R(\omega_1)\xi(\omega_1) G^R(\omega_2)\xi(\omega_2) G^R(\omega_3)\xi(\omega_3). \quad (2.112)$$

Likewise, the  $O(\lambda^2)$  solution reads

$$\begin{aligned} \phi_{(2)}(\omega) &= \frac{\lambda^2 (\hbar^{1/2} \mathcal{A})^5}{12\hbar^2 \cdot 9H_0^2} G^R(\omega) \\ &\cdot \int \frac{d\omega_1 d\omega_2 d\omega_3 d\omega'_1 d\omega'_2 d\omega'_3}{(2\pi)^6} \delta(\omega_1 + \omega_2 + \omega_3 - \omega'_3) \delta(\omega'_1 + \omega'_2 + \omega'_3 - \omega) \\ &\cdot G^R(\omega'_1)\xi(\omega'_1) G^R(\omega'_2)\xi(\omega'_2) G^R(\omega'_3) G^R(\omega_1)\xi(\omega_1) G^R(\omega_2)\xi(\omega_2) G^R(\omega_3)\xi(\omega_3). \end{aligned} \quad (2.113)$$

These results can be represented in a graphical way as ‘tree’ graphs, as in Table 2.6.

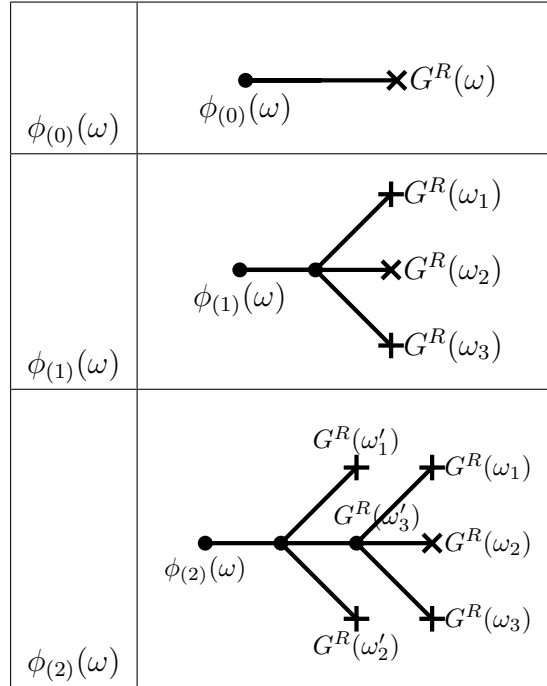


Table 2.6: Graphical representation of the solutions of the stochastic differential equations, up to  $O(\lambda^2)$ . Crosses represent  $\xi$  sources while lines stand for retarded propagators  $G^R$ , which evolve the sources to build up the field or, equivalently, its Fourier transform at frequency  $\omega$ . Note that different crosses can be thought of as injecting different frequencies in the tree and each vertex conserves the total frequency flowing in and out of it. Higher orders can be obtained similarly, as increasingly complex “trees”.

### 2.6.1 Diagrammatic Computation of the Two-Point Function

Let us, now, look again at the two-point function  $\langle \phi(\omega)\phi(\omega') \rangle$  and expand it, as above, up to 2nd order in  $\lambda$ .

$$\begin{aligned}
 \langle \phi(\omega)\phi(\omega') \rangle &= \langle (\phi_{(0)}(\omega) + \phi_{(1)}(\omega) + \phi_{(2)}(\omega) + \dots) (\phi_{(0)}(\omega') + \phi_{(1)}(\omega') + \phi_{(2)}(\omega') + \dots) \rangle \\
 &= \langle \phi_{(0)}(\omega)\phi_{(0)}(\omega') \rangle \\
 &\quad + \langle \phi_{(0)}(\omega)\phi_{(1)}(\omega') \rangle + \langle \phi_{(1)}(\omega)\phi_{(0)}(\omega') \rangle \\
 &\quad + \langle \phi_{(0)}(\omega)\phi_{(2)}(\omega') \rangle + \langle \phi_{(2)}(\omega)\phi_{(0)}(\omega') \rangle + \langle \phi_{(1)}(\omega)\phi_{(1)}(\omega') \rangle + \dots
 \end{aligned} \tag{2.114}$$

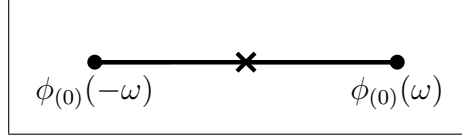
Substituting from (2.109), the 0th order, in  $\lambda$ , correlator is given as

$$\langle \phi_{(0)}(\omega)\phi_{(0)}(\omega') \rangle = \frac{\hbar H_0^3}{4\pi^2} \frac{1}{\eta\hbar^2 + \omega^2} \delta(\omega + \omega'), \tag{2.115}$$

where the Fourier transform of  $\xi$  and (2.22) have been used to obtain

$$\langle \xi(\omega)\xi(\omega') \rangle = \delta(\omega + \omega'). \tag{2.116}$$

The operation of taking the expectation value on the product of noise terms can be graphically represented as



i.e. to obtain correlators two crosses can be joined together producing an  $F$ -line with frequency  $\omega$  flowing across it.

#### $O(\lambda)$ Contributions

For the  $O(\lambda^1)$  contribution to the correlator, we have

$$\begin{aligned}
 \langle \phi_{(0)}(t)\phi_{(1)}(t') \rangle &= \int \frac{d\omega d\omega'}{(2\pi)^2} e^{i(\omega t + \omega' t')} \langle \phi_{(0)}(\omega)\phi_{(1)}(\omega') \rangle \\
 &= \left( \frac{\hbar H_0^3}{4\pi^2} \right)^2 \int \frac{d\omega_1 d\omega_2 d\omega_3 d\omega d\omega'}{(2\pi)^5} e^{i(\omega t + \omega' t')} \left( -\frac{\lambda}{6\hbar \cdot 3H_0} G^R(\omega) G^R(\omega') \right) \\
 &\quad \cdot \left\{ \langle \xi(\omega)\xi(\omega_1) \rangle \langle \xi(\omega_2)\xi(\omega_3) \rangle \right. \\
 &\quad \quad + \langle \xi(\omega)\xi(\omega_2) \rangle \langle \xi(\omega_1)\xi(\omega_3) \rangle \\
 &\quad \quad \left. + \langle \xi(\omega)\xi(\omega_3) \rangle \langle \xi(\omega_1)\xi(\omega_2) \rangle \right\} \\
 &\quad \cdot G^R(\omega_1)G^R(\omega_2)G^R(\omega_3) \delta(\omega_1 + \omega_2 + \omega_3 - \omega'),
 \end{aligned} \tag{2.117}$$

where Wick's theorem was used to expand  $\langle \xi(\omega)\xi(\omega_1)\xi(\omega_2)\xi(\omega_3) \rangle$ . This leads to

$$\langle \phi_{(0)}(t)\phi_{(1)}(t') \rangle = -\frac{\lambda H_0^5 \hbar}{(8\pi^2)^2 3\eta\hbar} \int \frac{d\omega}{2\pi} \frac{1}{\eta^2 + \omega^2} \frac{1}{\eta - i\omega} e^{i\omega(t-t')}, \quad (2.118)$$

and the Fourier space correction to the two-point function is

$$\Delta(\omega) = -\frac{\lambda H_0^5 \hbar}{(8\pi^2)^2 3\eta\hbar} \frac{1}{\eta^2 + \omega^2} \frac{1}{\eta - i\omega}. \quad (2.119)$$

In order to obtain the term,  $\langle \phi_{(0)}(t'), \phi_{(1)}(t) \rangle$ , one may observe that changing  $t \leftrightarrow t'$  (or equivalently,  $\omega \leftrightarrow \omega'$ ) in equation (2.117), results in the expression in question,

$$\langle \phi_{(0)}(t'), \phi_{(1)}(t) \rangle = -\frac{\lambda H_0^5 \hbar}{(8\pi^2)^2 3\eta\hbar} \int \frac{d\omega}{2\pi} \frac{1}{\eta^2 + \omega^2} \frac{1}{\eta + i\omega} e^{i\omega(t-t')}. \quad (2.120)$$

Hence, in Fourier space,

$$\Delta'(\omega) = -\frac{\lambda H_0^5 \hbar}{(8\pi^2)^2 3\eta\hbar} \frac{1}{\eta^2 + \omega^2} \frac{1}{\eta + i\omega}. \quad (2.121)$$

Finally, adding (2.119) and (2.121) results in the  $O(\lambda)$  contribution to the two-point function

$$F_1(\omega) = -\frac{2\lambda H_0^5 \hbar}{3\eta\hbar (8\pi^2)^2 [\eta^2 + \omega^2]^2}, \quad (2.122)$$

which, as expected, is exactly equivalent to (2.77). This result can be obtained graphically by joining all the crosses in the "trees" representing  $\phi_{(0)}$  and  $\phi_{(1)}$ , depicted in Table 2.7,

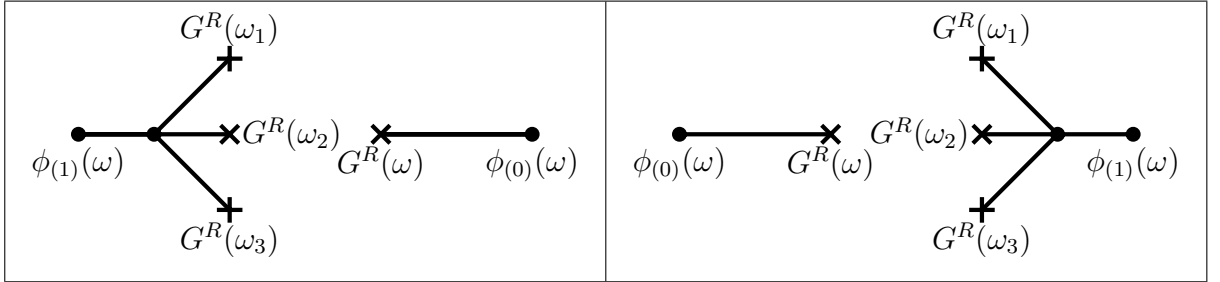
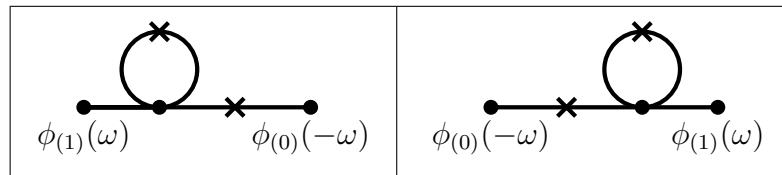


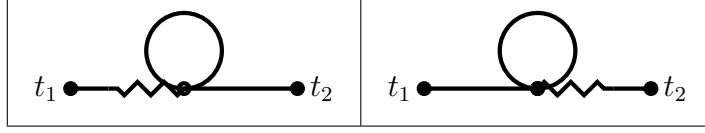
Table 2.7: Graphical representation of the contributing terms to the 2-point function, up to  $O(\lambda)$ .

as seen below



One can easily see that the resulting diagrams are equivalent to those obtained in section 2.5, directly using the Feynman rules by noting that a crossed line in this formalism equates to a straight  $F$ -line and a straight line here equates to a straight-jagged line in

the path integral formalism.



This correspondence is true to all orders and for all such diagrams.

### $O(\lambda^2)$ Contributions

The terms that contribute to  $O(\lambda^2)$  can be seen in (2.114) to be  $\langle \phi_{(0)}(\omega)\phi_{(2)}(\omega') \rangle$ ,  $\langle \phi_{(2)}(\omega)\phi_{(0)}(\omega') \rangle$  and  $\langle \phi_{(1)}(\omega)\phi_{(1)}(\omega') \rangle$ . Having calculated  $\phi_{(0)}(\omega), \phi_{(1)}(\omega)$  and  $\phi_{(2)}(\omega)$  in (2.109), (2.112) and (2.113) respectively, we determine the NNLO correction to the two-point function as follows:

$$\begin{aligned}
 \langle \phi_{(1)}(\omega)\phi_{(1)}(\omega') \rangle &= \frac{\lambda^2}{(6\hbar \cdot 3H_0^2)} \left( \frac{\hbar H_0^3}{4\pi^2} \right)^3 G^R(\omega)G^R(\omega') \\
 &\cdot \int \frac{d\omega_1 d\omega_2 d\omega_3}{(2\pi)^6} \delta(\omega_1 + \omega_2 + \omega_3 - \omega) \delta(\omega'_1 + \omega'_2 + \omega'_3 - \omega') \\
 &\cdot G^R(\omega_1)G^R(\omega_2)G^R(\omega_3)G^R(\omega'_1)G^R(\omega'_2)G^R(\omega'_3) \\
 &\cdot \langle \xi(\omega_1) \cdot \xi(\omega_2) \cdot \xi(\omega_3) \cdot \xi(\omega'_1) \cdot \xi(\omega'_2) \cdot \xi(\omega'_3) \rangle.
 \end{aligned} \tag{2.123}$$

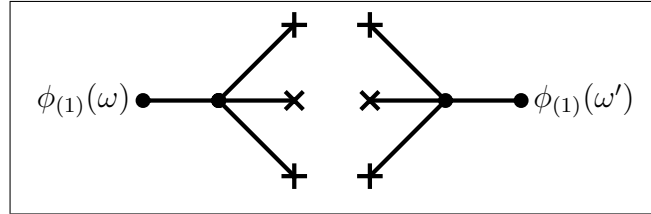
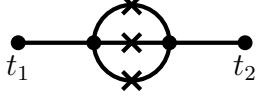


Table 2.8: Graphical representation of the  $\langle \phi_{(1)}(\omega)\phi_{(1)}(\omega') \rangle$  terms contributing to the expectation value of the two-point correlator, at 2-loop order.

Using Wick's theorem, it is evident that there are 15 terms of different pairs in  $\langle \tilde{\xi}(\omega_1) \cdot \tilde{\xi}(\omega_2) \cdot \xi(\omega_3) \cdot \xi(\omega'_1) \cdot \xi(\omega'_2) \cdot \xi(\omega'_3) \rangle$ . The diagrammatic presentation of those (or alternatively, the symmetries of the integrals and the delta functions) demonstrates that there are only two topologically inequivalent ways for these 15 terms to be organised: 6 "Symmetric Sunset" diagrams and 9 "Symmetric Double Seagull" diagrams.

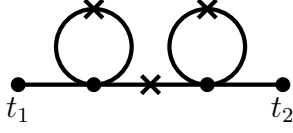


## The Symmetric Sunset



$$\begin{aligned}
 \mathcal{SS} &= 6 \left( \frac{\lambda}{6\hbar \cdot 3H_0} \right)^2 \left( \frac{\hbar H_0^3}{4\pi^2} \right)^3 G^R(\omega) G^R(\omega') \int \frac{\prod_{i=1}^3 d\omega_i d\omega'_i}{(2\pi)^6} \\
 &\cdot \delta(\omega_1 + \omega_2 + \omega_3 - \omega) \delta(\omega'_1 + \omega'_2 + \omega'_3 - \omega') \\
 &\cdot G^R(\omega_1) G^R(\omega_2) G^R(\omega_3) G^R(\omega'_1) G^R(\omega'_2) G^R(\omega'_3) \\
 &\cdot \delta(\omega_1 + \omega'_1) \delta(\omega_2 + \omega'_2) \delta(\omega_3 + \omega'_3) \\
 &= \frac{\lambda^2 H_0^7 \hbar}{9\eta \hbar^2 (8\pi^2)^3 (\eta \hbar^2 + \omega^2) [(3\eta \hbar)^2 + \omega^2]}, \tag{2.124}
 \end{aligned}$$

## The Symmetric Double Seagull



$$\begin{aligned}
 \mathcal{SS} &= 9 \left( \frac{\lambda}{6\hbar \cdot 3H_0} \right)^2 \left( \frac{\hbar H_0^3}{4\pi^2} \right)^3 G^R(\omega) G^R(\omega') \int \frac{\prod_{i=1}^3 d\omega_i d\omega'_i}{(2\pi)^6} \\
 &\cdot \delta(\omega_1 + \omega_2 + \omega_3 - \omega) \delta(\omega'_1 + \omega'_2 + \omega'_3 - \omega') \\
 &\cdot G^R(\omega_1) G^R(\omega_2) G^R(\omega_3) G^R(\omega'_1) G^R(\omega'_2) G^R(\omega'_3) \\
 &\cdot \delta(\omega_1 + \omega_2) \delta(\omega_3 + \omega'_3) \delta(\omega'_1 + \omega'_2) \\
 &= \frac{\lambda^2 H_0^7 \hbar}{18\eta \hbar^2 (8\pi^2)^3 (\eta \hbar^2 + \omega^2)^2}, \tag{2.125}
 \end{aligned}$$

in exact agreement with (2.78) and (2.84).

Furthermore, there are two more second-order in  $\lambda$  contributions:

$$\begin{aligned}
 \langle \phi_{(2)}(\omega') \phi_{(0)}(\omega) \rangle &= G^R(\omega') \left[ \frac{\lambda^2}{12\hbar^2 \cdot 3H_0^2} \right] \left[ \frac{\hbar H_0^3}{4\pi^2} \right]^3 G^R(\omega) \\
 &\cdot \int \frac{\prod_{i=1}^3 d\omega_i d\omega'_i}{2\pi^6} \delta(\omega_1 + \omega_2 + \omega_3 - \omega'_3) \delta(\omega'_1 + \omega'_2 + \omega'_3 - \omega) \tag{2.126} \\
 &\cdot G^R(\omega_1) G^R(\omega_2) G^R(\omega_3) G^R(\omega'_1) G^R(\omega'_2) G^R(\omega'_3)
 \end{aligned}$$

and its  $\omega \rightarrow \omega'$  symmetric.

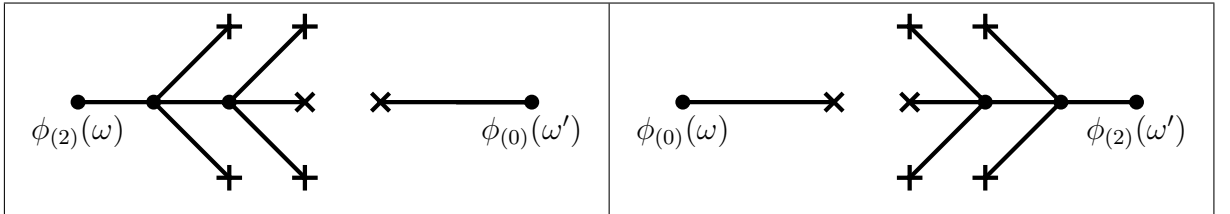
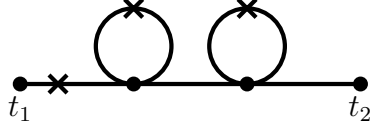


Table 2.9: Graphical representation of the  $\langle \phi_{(2)}(\omega) \phi_{(0)}(\omega') \rangle$  and  $\langle \phi_{(0)}(\omega) \phi_{(2)}(\omega') \rangle$  terms contributing to the expectation value of the two-point correlator, at 2-loop order.

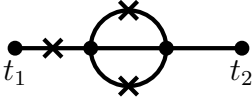
The 15 different ways which  $\langle \tilde{\xi}(\omega_1) \cdot \tilde{\xi}(\omega_2) \cdot \xi(\omega_3) \cdot \xi(\omega'_1) \cdot \xi(\omega'_2) \cdot \xi(\omega'_3) \rangle$  can be expanded out into, split (2.126) into 3 topologically different diagrams: 3 "Right Double Seagulls", 6 "Right Sunset" and 6 "Right Cactus" diagrams (and the corresponding "Left" ones for the  $\omega \rightarrow \omega'$  symmetric).

## The Right Double Seagulls



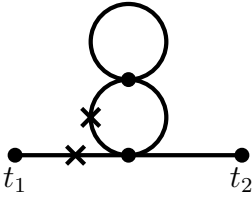
$$\begin{aligned}
 \mathcal{RDS} &= 3 \cdot \frac{2\lambda^2 \hbar H_0^7}{27 \cdot (8\pi^2)^3} G^R(\omega) G^R(\omega') \int \frac{\prod_{i=1}^3 d\omega_i d\omega'_i}{(2\pi)^6} \\
 &\quad \cdot \delta(\omega_1 + \omega_2 + \omega_3 - \omega'_2) \delta(\omega'_1 + \omega'_2 + \omega'_3 - \omega') \\
 &\quad \cdot G^R(\omega_1) G^R(\omega_2) G^R(\omega_3) G^R(\omega'_1) G^R(\omega'_2) G^R(\omega'_3) \\
 &\quad \cdot \delta(\omega'_1 + \omega'_3) \delta(\omega_1 + \omega_3) \delta(\omega_2 + \omega) \\
 &= \frac{1}{4} \frac{2\lambda^2 H_0^7 \hbar}{9\eta \hbar^2 (8\pi^2)^3} \frac{1}{(\eta \hbar^2 + \omega^2) (\eta \hbar - i\omega) (\eta \hbar - i\omega)} \\
 &\hspace{15em} (2.127)
 \end{aligned}$$

## The Right Sunset



$$\begin{aligned}
 \mathcal{RS} &= 6 \cdot \frac{2\lambda^2 \hbar H_0^7}{27 \cdot (8\pi^2)^3} G^R(\omega) G^R(\omega') \int \frac{\prod_{i=1}^3 d\omega_i d\omega'_i}{(2\pi)^6} \\
 &\quad \cdot \delta\left(\sum_{i=1}^3 \omega_i - \omega'_2\right) \delta\left(\sum_{i=1}^3 \omega'_i - \omega'\right) \\
 &\quad \cdot \prod_{i=1}^3 G^R(\omega_i) G^R(\omega'_i) \delta(\omega'_1 + \omega'_3) \delta(\omega_1 + \omega_3) \delta(\omega_2 + \omega) \\
 &= \frac{\lambda^2 H_0^7 \hbar}{9\eta \hbar^2 (8\pi^2)^3} \frac{(\eta \hbar + i\omega)(3\eta \hbar + i\omega)}{(\eta \hbar^2 + \omega^2)^2 [(3\eta \hbar)^2 + \omega^2]} \\
 &\hspace{15em} (2.128)
 \end{aligned}$$

## The Right Cactus



$$\begin{aligned}
 \mathcal{RC} &= 6 \cdot \frac{2\lambda^2 \hbar H_0^7}{27 \cdot (8\pi^2)^3} G^R(\omega) G^R(\omega') \int \frac{\prod_{i=1}^3 d\omega_i d\omega'_i}{(2\pi)^6} \\
 &\quad \cdot \delta\left(\sum_{i=1}^3 \omega_i - \omega'_2\right) \delta\left(\sum_{i=1}^3 \omega'_i - \omega'\right) \\
 &\quad \cdot \prod_{i=1}^3 G^R(\omega_i) G^R(\omega'_i) \delta(\omega + \omega'_3) \delta(\omega_2 + \omega_3) \delta(\omega'_1 + \omega_1) \\
 &= \frac{\lambda^2 H_0^7 \hbar}{18\eta \hbar^3 (8\pi^2)^3} \frac{(\eta \hbar + i\omega)}{(\eta \hbar^2 + \omega^2)^2} \\
 &\hspace{15em} (2.129)
 \end{aligned}$$

All are, of course, in direct one-to-one agreement with their path-integral counterparts (2.82), (2.86) and (2.89). It is obvious to see, taking  $\omega \rightarrow -\omega$  (or equivalently, exchanging  $t_1$  with  $t_2$ ), that the time-symmetric diagrams (2.80), (2.85) and (2.87) are, again, in one-to-one agreement with their diagrammatic counterparts.

### 2.6.2 Diagrammatic Computation of the Four-Point Function

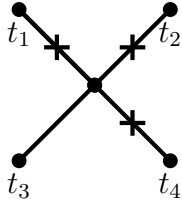
The same principles that led to the computation of the two-point function to tree-level (2.115), one-loop (2.122), and two-loop order (2.124) - (2.129) can be applied for the computation of the four-point function. Again, it is shown that there is a one-to-one correspondence between the two approaches.

#### Tree-Level Contribution to the Four-point Function

The tree-level contribution to the four-point function is given by :

$$\begin{aligned} \langle \phi(t_1)\phi(t_2)\phi(t_3)\phi(t_4) \rangle^{O(\lambda^2)} &= \langle \phi_1(t_1)\phi_0(t_2)\phi_0(t_3)\phi_0(t_4) \rangle + \langle \phi_0(t_1)\phi_1(t_2)\phi_0(t_3)\phi_0(t_4) \rangle \\ &+ \langle \phi_0(t_1)\phi_0(t_2)\phi_1(t_3)\phi_0(t_4) \rangle + \langle \phi_0(t_1)\phi_0(t_2)\phi_0(t_3)\phi_1(t_4) \rangle. \end{aligned} \quad (2.130)$$

We start by computing  $\langle \phi_0(t_1)\phi_0(t_2)\phi_1(t_3)\phi_0(t_4) \rangle$  and obtain the other three by symmetry.



$$\begin{aligned} &= 6 \int \frac{\prod_{i=1}^4 d\omega_i \prod_{j=1}^3 d\omega'_j}{(2\pi)^7} \cdot \left( -\frac{\lambda}{6 \cdot 3\hbar H_0} \right) (\mathcal{A}^2)^3 e^{i(\sum \omega_i t_i)} \\ &\quad \delta(\omega_1 + \omega'_1) \delta(\omega_2 + \omega'_2) \delta(\omega_4 + \omega'_3) \delta(\omega'_1 + \omega'_2 + \omega'_3 - \omega_3) \\ &\quad G^R(\omega_1) G^R(\omega_2) G^R(\omega_3) G^R(\omega_4) \cdot G^R(\omega'_1) G^R(\omega'_2) G^R(\omega'_3) \\ &= -\frac{\lambda}{3\hbar H_0} \left( \frac{\hbar H_0^3}{4\pi^2} \right)^3 \int \frac{\prod_{i=1}^4 d\omega_i}{(2\pi)^4} \frac{(\eta\hbar - i\omega_3) \cdot \delta(\sum_i \omega_i)}{\prod_{i=1}^4 (\eta\hbar^2 + \omega_i^2)} e^{i\sum \omega_i t_i}. \end{aligned} \quad (2.131)$$

We note the factor of 6 stemming from the Wick contractions of the stochastic noise terms (diagrammatically, each anchored external time with associated frequency  $\omega_1, \omega_2$  and  $\omega_3$ , respectively, can be connected with each of the three prongs  $\omega'_1, \omega'_2$  and  $\omega'_3$ , giving rise to a factor of 3; the other two prongs left have two different possible configurations, leading to the quoted multiplicative factor). Furthermore, after performing the substitutions  $t_1 \rightarrow -t_1$  and  $t_3 \rightarrow -t_3$  (so that the diagrammatic expansion is in agreement with the Feynman rules stated underneath Table 2.2), the aforementioned result is in agreement with the path integral result (2.93) and therefore (due to the symmetry of the integrals and the overall  $\delta$ -function) the total tree-level contribution of the diagrammatic approach is shown to agree with (2.94).

#### Diagrammatic $\mathcal{O}(\lambda^2)$ Contribution to the Four-Point Function

The one-loop ( $\mathcal{O}(\lambda^2)$ ) correction to the four-point vertex can, also, be calculated directly from the solutions of the stochastic differential equations. The one-loop four-point function can be expanded as follows:

$$\begin{aligned}
 \langle \phi(t_1)\phi(t_2)\phi(t_3)\phi(t_4) \rangle^{O(\lambda^2)} &= \langle \phi_0(t_1)\phi_0(t_2)\phi_1(t_3)\phi_1(t_4) \rangle + \langle \phi_1(t_1)\phi_1(t_2)\phi_0(t_3)\phi_0(t_4) \rangle \\
 &+ \langle \phi_0(t_1)\phi_1(t_2)\phi_1(t_3)\phi_0(t_4) \rangle + \langle \phi_1(t_1)\phi_0(t_2)\phi_0(t_3)\phi_1(t_4) \rangle \\
 &+ \langle \phi_1(t_1)\phi_0(t_2)\phi_1(t_3)\phi_0(t_4) \rangle + \langle \phi_0(t_1)\phi_1(t_2)\phi_0(t_3)\phi_1(t_4) \rangle \\
 &+ \langle \phi_2(t_1)\phi_0(t_2)\phi_0(t_3)\phi_0(t_4) \rangle + \langle \phi_0(t_1)\phi_2(t_2)\phi_0(t_3)\phi_0(t_4) \rangle \\
 &+ \langle \phi_0(t_1)\phi_0(t_2)\phi_2(t_3)\phi_0(t_4) \rangle + \langle \phi_0(t_1)\phi_0(t_2)\phi_0(t_3)\phi_2(t_4) \rangle.
 \end{aligned} \tag{2.132}$$

We note that these contributions can be grouped, depending on their correspondence to topologically different diagrams. The terms in the first, second and third line will be shown to represent  $F$ -Candies and those in the last two, as  $G$ -Candies. The final results, as expected, are shown to be identical to the computations of section (2.5.3).

### One Loop $F$ -Candies

The diagrams containing an  $F$ -loop can be separated depending on their topology in "Horizontal", "Vertical" and "Knotted" Candies. We explicitly show the calculation of the first type and present the result of the computation of the rest.

In order to calculate the first term of (2.132),  $\langle \phi_0(t_1)\phi_0(t_2)\phi_1(t_3)\phi_1(t_4) \rangle$ , we anchor the incoming particles as states  $\frac{1}{3}$  and the outgoing as  $\frac{2}{4}$ :

$$\begin{aligned}
 \langle \phi_0(t_1)\phi_0(t_2)\phi_1(t_3)\phi_1(t_4) \rangle &= 18 \int \frac{d\omega_1 d\omega_2 d\omega_3 d\omega_4 d\omega'_1 d\omega'_2 d\omega'_3 d\tilde{\omega}_1 d\tilde{\omega}_2 d\tilde{\omega}_3}{(2\pi)^{10}} \\
 &\cdot \left( \frac{\lambda}{18 H_0 \hbar} \right)^2 \left( \frac{H_0^3 \hbar}{4\pi^2} \right)^4 e^{i(\omega_i t_i)} \not\phi(\omega_1 + \omega'_1) \not\phi(\tilde{\omega}_2 + \omega'_2) \\
 &\cdot \not\phi(\tilde{\omega}_3 + \omega'_3) \not\phi(\tilde{\omega}_1 + \omega_2) \not\phi(\omega'_1 + \omega'_2 + \omega'_3 - \omega_3) \\
 &\cdot \not\phi(\tilde{\omega}_1 + \tilde{\omega}_2 + \tilde{\omega}_3 - \omega_4) G^R(\omega_1) G^R(\omega_2) G^R(\omega_3) G^R(\omega_4) \\
 &\cdot G^R(\omega'_1) G^R(\omega'_2) G^R(\omega'_3) G^R(\tilde{\omega}_1) G^R(\tilde{\omega}_2) G^R(\tilde{\omega}_3) \\
 &= 18 \left( \frac{\lambda}{18 H_0 \hbar} \right)^2 \left( \frac{H_0^3 \hbar}{4\pi^2} \right)^4 \int \frac{d\omega_1 d\omega_2 d\omega_3 d\omega_4}{(2\pi)^4} \frac{e^{i(\sum \omega_i t_i)}}{(2\eta\hbar)^2 + (\omega_1 + \omega_3)^2} \\
 &\cdot G^R(\omega_1) G^R(-\omega_1) G^R(\omega_2) G^R(-\omega_2) G^R(\omega_3) G^R(\omega_4) \not\phi(\sum \omega_i).
 \end{aligned} \tag{2.133}$$

The origin of the factor of 18 comes from the topologically equivalent Wick contractions: There are 3 distinct choices for  $t_1$  to be linked to any of the three prongs of  $t_3$  and the same holds for  $t_2$  and  $t_4$  (resulting in a factor of 9). The two left over prongs of each of  $t_3$  and  $t_4$  can form a loop in two different ways (resulting in a multiplicative factor of 2). Hence, there are 18 different Wick contractions of the eight  $\xi$ s that preserve the structure of the external times as described earlier. The last line of (2.133) reproduces the path integral result (2.95).

Performing the following permutations ( $1 \leftrightarrow 3, 2 \leftrightarrow 4$ ), ( $1 \leftrightarrow 3$ ), ( $2 \leftrightarrow 4$ ) and adding the individual diagram contributions, results in:

$$\begin{aligned}
 & \langle \phi_0(t_1)\phi_0(t_2)\phi_1(t_3)\phi_1(t_4) \rangle + \langle \phi_1(t_1)\phi_1(t_2)\phi_0(t_3)\phi_0(t_4) \rangle \\
 & \langle \phi_1(t_1)\phi_0(t_2)\phi_0(t_3)\phi_1(t_4) \rangle + \langle \phi_0(t_1)\phi_1(t_2)\phi_1(t_3)\phi_0(t_4) \rangle \\
 & = \frac{1}{2\eta\hbar} \left[ \frac{\lambda}{3\hbar H_0} \right]^2 \int \frac{d\omega_1 d\omega_2 d\omega_3 d\omega_4}{(2\pi)^4} \prod_i F(\omega_i) e^{i\Sigma(\omega_i t_i)} \delta(\Sigma\omega_i),
 \end{aligned} \tag{2.134}$$

in exact agreement with the path integral method result (2.97).

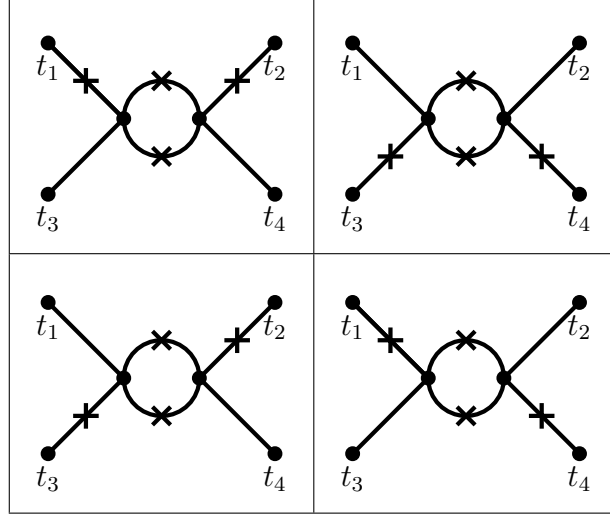


Table 2.10: The ‘tree’ diagrams contributing to the one-loop four-point function including F-propagator loops, with "horizontal" topology.

Furthermore, choosing to connect one of the prongs of the  $\phi_{(1)}(t_1)$  with  $\phi_0(t_2)$  results in the formation of the "vertical candy" diagrams, depicted in Table 2.11. Similarly to the "horizontal candy" diagrams, the sum of the four vertical ones, leads to:

$$\sum_i \mathcal{V}_i = \frac{1}{2\eta\hbar} \left[ \frac{\lambda}{3\hbar H_0} \right]^2 \int \frac{d\omega_1 d\omega_2 d\omega_3 d\omega_4}{(2\pi)^4} \prod_i F(\omega_i) e^{i\Sigma(\omega_i t_i)} \delta(\Sigma\omega_i). \tag{2.135}$$

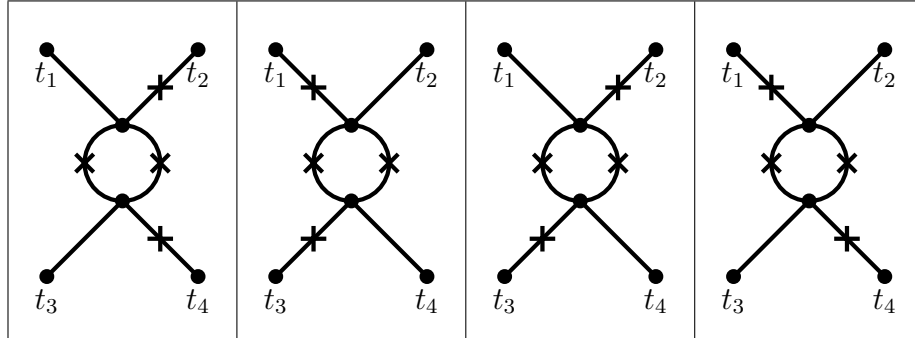


Table 2.11: The ‘tree’ diagrams contributing to the one-loop four-point function, including F-propagator loops, with "vertical" topology.

Lastly, the knotted candies give

$$\sum_i K_i = \frac{1}{2\eta\hbar} \left[ \frac{\lambda}{3\hbar H_0} \right]^2 \int \frac{d\omega_1 d\omega_2 d\omega_3 d\omega_4}{(2\pi)^4} \prod_i F(\omega_i) e^{i\Sigma(\omega_i t_i)} \delta(\Sigma\omega_i). \quad (2.136)$$

Ultimately, adding up all the contributions we obtain for the sum of the F-Candies:

$$\sum_i \mathcal{F}_i = \frac{3}{2\eta\hbar} \left[ \frac{\lambda}{3\hbar H_0} \right]^2 \int \frac{d\omega_1 d\omega_2 d\omega_3 d\omega_4}{(2\pi)^4} \prod_i F(\omega_i) e^{i\Sigma(\omega_i t_i)} \delta(\Sigma\omega_i). \quad (2.137)$$

### One Loop- $G$ Candies

The four last contributions in (2.132) form a different type of correction to the four-point vertex. Here, one of the three prongs of the  $\phi_2(t)$  closes in with one of three  $\phi_0(t)$  prongs. This will lead to diagrams in which one of the internal loop propagators is  $F$  and one that is  $G$  in the language of section 2.5.

Starting with  $\mathbb{A} \equiv \langle \phi_2(t_1)\phi_0(t_2)\phi_0(t_3)\phi_0(t_4) \rangle$ ,

$$\begin{aligned} \mathbb{A} &= 36 \cdot 3 \left( \frac{\lambda}{18 H_0 \hbar} \right)^2 \left( \frac{H_0^3 \hbar}{4\pi^2} \right)^4 \int \frac{\prod_{i=1}^4 d\omega_i \prod_{i=1}^3 d\omega'_i \prod_{i=1}^3 d\tilde{\omega}_i}{(2\pi)^{10}} e^{i(\Sigma\omega_i t_i)} \\ &\quad \cdot \delta(\omega'_1 + \tilde{\omega}_1) \delta(\omega_2 + \tilde{\omega}_2) \delta(\omega_4 + \tilde{\omega}_3) \delta(\omega'_2 + \omega_3) \\ &\quad \cdot \delta(\tilde{\omega}_1 + \tilde{\omega}_2 + \tilde{\omega}_3 - \omega'_3) \delta(\omega'_1 + \omega'_2 + \omega'_3 - \omega_1) \\ &\quad \cdot \prod_{i=1}^4 G^R(\omega_i) \prod_{i=1}^3 G^R(\omega'_i) \prod_{i=1}^3 G^R(\tilde{\omega}_i) \\ &= 36 \cdot 3 \left( \frac{\lambda}{18 H_0 \hbar} \right)^2 \left( \frac{H_0^3 \hbar}{4\pi^2} \right)^4 \int \frac{\prod_{i=1}^4 d\omega_i}{(2\pi)^4} e^{i(\Sigma\omega_i t_i)} \frac{1}{2\eta\hbar} \frac{\eta\hbar - i\omega_1}{(2\eta\hbar + i(\omega_2 + \omega_4))} \\ &\quad \cdot G^R(\omega_2) G^R(-\omega_2) G^R(\omega_3) G^R(-\omega_3) G^R(\omega_4) G^R(-\omega_4) \delta(\Sigma\omega_i). \end{aligned} \quad (2.138)$$

The other three diagrams are obtained by performing the following permutations:

$$\begin{aligned} \mathbb{B} &= \mathbb{A}, (1 \leftrightarrow 3) \\ \mathbb{C} &= \mathbb{A}, (1 \leftrightarrow 2, 3 \leftrightarrow 4) \\ \mathbb{D} &= \mathbb{A}, (1 \leftrightarrow 4, 2 \leftrightarrow 3) \end{aligned} \quad (2.139)$$

Then, the sum of the four diagrams, as expected from (2.101), is:

$$\begin{aligned} \mathbb{F} &= \mathbb{A} + \mathbb{B} + \mathbb{C} + \mathbb{D} \\ &= 36 \cdot \frac{3}{2\eta\hbar} \left( \frac{\lambda}{18 H_0 \hbar} \right)^2 \left( \frac{H_0^3 \hbar}{4\pi^2} \right)^4 \int \frac{\prod_i d\omega_i}{(2\pi)^4} e^{i(\Sigma\omega_i t_i)} \prod_i F(\omega_i) \\ &\quad \cdot \left[ \frac{\eta\hbar - i\omega_1}{(2\eta\hbar + i(\omega_2 + \omega_4))} + \frac{\eta\hbar - i\omega_3}{(2\eta\hbar + i(\omega_2 + \omega_4))} + \frac{\eta\hbar - i\omega_2}{(2\eta\hbar + i(\omega_1 + \omega_3))} + \frac{\eta\hbar - i\omega_4}{(2\eta\hbar + i(\omega_1 + \omega_3))} \right] \\ &= \frac{3}{\eta\hbar} \left[ \frac{\lambda}{3\hbar H_0} \right]^2 \int \frac{\prod_i d\omega_i}{(2\pi)^4} e^{i(\Sigma\omega_i t_i)} \prod_i F(\omega_i) \delta(\Sigma\omega_i). \end{aligned} \quad (2.140)$$

Here, the multiplicative factor of 36 is due to the Wick contractions as follows: There are 3  $\tilde{\omega}_i$  prongs that can form the  $G^R$ -loop with one of the two  $\omega'_i$  prongs, giving rise to a factor of 6. The two left over of the  $\tilde{\omega}_i$  are interchangeable (resulting in a factor of 2) and lastly, there is a single way to connect the remaining  $\omega'_i$  prong with any one of  $\omega_2, \omega_3$  or  $\omega_4$ , giving a horizontal, vertical or knotted G-candy, respectively (another factor of 3). Hence, the total one-loop correction to the 4-point vertex is:

$$\mathcal{Z} = \frac{9}{2\eta\hbar} \left( \frac{\lambda}{3\hbar H_0} \right)^2 \int \frac{d\omega_1 d\omega_2 d\omega_3 d\omega_4}{(2\pi)^4} \cdot \delta(\Sigma\omega_i) e^{i(\Sigma\omega_i t_i)} \prod F(\omega_i), \quad (2.141)$$

as previously found in (2.103).

## 2.7 Backreaction Contributions to the Two-Point Correlators

In this section, we compute corrections stemming from the  $\phi$  dependence of the multiplicative noise amplitude,  $\mathcal{A} \propto H^3(\phi)$ . We note that we neglect any new vertices that are further suppressed by  $\frac{m^2}{H_0^2}$  or  $\lambda$ . Furthermore, we have not computed corrections to the noise amplitude due to the modified behaviour of the scalar modes as they exit the horizon, which are presumably suppressed by similar factors. This computation, therefore, serves as an illustration of the new types of vertices that arise due to the gravitational backreaction of the field  $\phi$ , but should also contain the leading order result. The new contributions are easy to compute in the path integral formalism where a new set of vertices appears, see section 2.5. These new vertices alter the two-point function, to leading order, are given as follows:

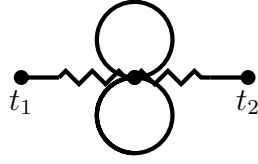
$$\begin{aligned} \mathcal{I}(t_1, t_2) &= \frac{3\eta\hbar^2 \hbar H_0^3 \chi}{4\pi^2} \int \frac{d\omega}{2\pi} \frac{e^{i\omega(t_2-t_1)}}{(\eta\hbar^2 + \omega^2)^2} \\ &= \frac{3\hbar H_0^3 \chi}{4\pi^2 \eta\hbar} \int \frac{d\sigma}{2\pi} \frac{e^{i\eta\sigma(t_2-t_1)}}{(1 + \sigma^2)^2} \\ &= \frac{3}{4} \chi \left[ \frac{\hbar \mathcal{A}_0^2}{\eta\hbar} \right] (1 + \eta\hbar|\Delta(t)|) e^{-\eta\hbar|\Delta t|} \end{aligned} \quad (2.142)$$

$$\begin{aligned} \mathcal{J}(t_1, t_2) &= \frac{\lambda \hbar H_0^5 \chi}{(8\pi^2)^2} \int \frac{d\omega}{2\pi} \frac{e^{i\omega(t_2-t_1)}}{(\eta\hbar^2 + \omega^2)^2} \\ &= \frac{\lambda \hbar H_0^5 \chi}{(8\pi^2)^2 \eta\hbar^3} \int \frac{d\sigma}{2\pi} \frac{e^{i\eta\sigma(t_2-t_1)}}{(1 + \sigma^2)^2} \\ &= -\frac{3}{8} \chi \left[ -\frac{\lambda}{3\hbar H_0} \right] \left[ \frac{\hbar \mathcal{A}_0^2}{\eta\hbar} \right] \left[ \frac{\hbar \mathcal{A}_0^2}{2\eta\hbar^2} \right] \\ &\quad \times (1 + \eta\hbar|\Delta(t)|) e^{-\eta\hbar|\Delta t|} \end{aligned} \quad (2.143)$$



$$\begin{aligned}
 \mathcal{L}(t_1, t_2) &= \frac{3\chi}{2} \frac{\hbar H_0^3}{(4\pi^2)} \int \frac{d\omega}{2\pi} \frac{e^{i\omega(t_2-t_1)}}{(\eta\hbar^2 + \omega^2)} \\
 &= \frac{3\chi}{(4\pi^2)} \frac{\hbar H_0^3}{2\eta\hbar} \int \frac{d\sigma}{2\pi} \frac{e^{i\eta\sigma(t_2-t_1)}}{(1 + \sigma^2)} \\
 &= \frac{3}{4} \chi \left[ \frac{\hbar \mathcal{A}_0^2}{\eta\hbar} \right] e^{-\eta|\Delta t|}
 \end{aligned} \tag{2.144}$$

The symmetry factor of the last two sets of diagrams is  $1/2$ . Lastly, there is a single diagram with two scalar loops:



$$\begin{aligned}
 \mathcal{K}(t_1, t_2) &= \frac{\lambda \hbar H_0^5 \chi}{(8\pi^2)^2 4\eta\hbar^2} \int \frac{d\omega}{2\pi} \frac{e^{i\omega(t_2-t_1)}}{(\eta\hbar^2 + \omega^2)} \\
 &= \frac{1}{4} \frac{\lambda \hbar H_0^5 \chi}{(8\pi^2)^2 \eta\hbar^3} \int \frac{d\sigma}{2\pi} \frac{e^{i\eta\sigma(t_2-t_1)}}{(1 + \sigma^2)} \\
 &= -\frac{3}{16} \chi \left[ -\frac{\lambda}{3\hbar H_0} \right] \left[ \frac{\hbar \mathcal{A}_0^2}{\eta\hbar} \right] \left[ \frac{\hbar \mathcal{A}_0^2}{2\eta\hbar^2} \right] e^{-\eta|\Delta t|},
 \end{aligned} \tag{2.145}$$

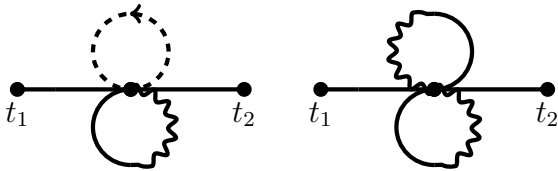
with symmetry factor  $1/8$  and noting that  $\mathcal{A}_0^2 \equiv \frac{H_0^3}{4\pi^2}$ , throughout.

Summing the aforementioned contributions, leads to the first order (in the interaction vertices described in Table 2.3) correction to the two-point function

$$\text{B.R.}_{\text{total}}^{\mathcal{O}(1)} = \frac{3\chi}{2} \left[ \frac{\hbar \mathcal{A}_0^2}{\eta\hbar} \right] e^{-\eta|\Delta t|} \left[ 1 + \frac{1}{2} \eta|\Delta t| \left( 1 - \frac{1}{2} Q \right) - \frac{3}{8} Q \right] \tag{2.146}$$

where  $\Delta t = t_1 - t_2$  and  $Q$  is the expansion parameter associated with self-interaction in de Sitter, as in (2.90).

We observe that, in this case, ghost loops do not, always, cancel closed  $G$  loops due to non-matching numerical factors in the new vertices. We comment on this feature in the final section. It is important to note that the above comment does not apply to the bubble diagrams in the partition function; they still cancel as described in (2.70). This is also true for the following diagram



$$\begin{aligned}
 \mathcal{O}(t_1, t_2) &= \int \frac{d\omega_2}{2\pi} \left[ \frac{\hbar \mathcal{A}_0^2}{(\eta\hbar^2 + \omega_1^2)} \right]^2 \Theta(0)^2 \\
 &\quad \times \left[ i \left( \frac{i\chi\lambda}{\hbar H_0} \right) + \frac{i^2}{2} \left( \frac{-2\chi\lambda}{\hbar H_0} \right) \right],
 \end{aligned} \tag{2.147}$$

as was expected from observing that the symmetry factor ( $1/2$ ) of the second diagram above cancels the factor of two which differentiates the two vertices. Similar cancellations are expected to occur at higher orders and caution is necessary. This computation serves as a correction and addition to the work originally presented in [1].



## 2.8 Conclusion and Motivation for Further Work

In this work, we elaborated on the path integral representation of the Langevin equation describing the infrared behaviour of a spectator scalar field, in de Sitter. Elaborating on this methodology, we obtained simple Feynman rules that allow for the straightforward computation of arbitrary unequal-time correlators of the field. Such quantities can also be computed via a perturbative expansion applied directly to the Langevin equation. As we demonstrated, the two approaches are equivalent but the former offers a more streamlined and efficient way to the final result, circumventing a lot of the steps necessitated by the latter that involve (a) breaking down the solution for  $\phi$  in different orders, represented by the ‘tree’-like graphs of section 2.6 and (b) computing expectation values of their products by glueing the “trees” in all possible ways across their crossed tips. These steps become increasingly complex with the number of fields in the desired correlator, and with perturbative order. On the contrary, the Feynman rules directly build any correlator out of two propagators and a small, fixed number of vertices. We expect that their utility will become even clearer when more than one field is involved. Our results agree with and generalise existing computations in literature [48] that follow similar methods.

Additionally, in the small perturbative parameter limit  $|Q| \ll 1$ , our work accurately reproduces the first non-vanishing eigenvalues of the spectral expansion approach [55] beyond the zeroth-order in  $|Q|$ , as well as the zeroth-order coefficients (2.71) exactly. Further investigation is required to establish the correspondence between the two methodologies, to higher order in the expansion parameter, motivating an intriguing potential research pursuit.

Furthermore, we briefly considered backreaction by including the dependence of the noise amplitude on  $\phi$ , making the noise multiplicative, and calculated new contributions to the two-point functions. In this case, the direct Langevin equation approach would have proven substantially more involved.

Our Feynman rules necessitated the introduction of ghost fields that contribute closed loops in the diagrams. In the case of additive noise,  $H = H_0$ , ghost loops act to cancel closed  $G$  loops. Such loops do not appear in the perturbative solution of the Langevin equation, indicating that ghosts are essential in ensuring that the Feynman diagrams give the correct result. In the case of backreaction, with  $H = H(\phi)$ , the contributions from ghost loops and closed  $G$  loops do not always add up to zero and hence may contribute to the final result. This is a manifestation of the well known fact that when the noise is multiplicative, results depend on the discretization prescription of the Langevin equation which, in a continuum description, translates to the choice of the value of  $\Theta(0)$  [63]. Our formalism naturally picks the midpoint value  $\Theta(0) = \frac{1}{2}$ , corresponding to the Stratonovich prescription. Other prescriptions would also be possible to implement in a simple manner by adding appropriate “spurious force” terms to the potential.

Here, we made the ansatz that the inclusion of backreaction in the original Quantum Field Theory introduces a minimal effect in the form of the equation of motion, (2.19),

solely modifying the noise from additive to a state-dependent multiplicative one. Remembering that this equation was obtained by adopting a window function in order to perform the split between the "long" and "short" wavelength modes, we observe that this window will depend on the field value, when we let  $H = H(\phi)$ . This will, consequently, result in a state-dependent window function, which will lead to further modification in the obtained equation of motion. Further investigation of these effects is necessary for the proper treatment of scalar fields in realistic spacetimes.

For the time being, it is unclear which prescription would be appropriate when gravity is consistently included, with different prescriptions leading to different results for the correlators - albeit suppressed by powers of  $\chi \equiv \hbar G H_0^2 / 2\pi$ . It is remarked in [68] that this theoretical uncertainty should be commensurable to corrections to the leading stochastic picture. However, such corrections are now accessible and the uncertainty becomes relevant for investigations beyond the leading stochastic description. As stressed in [69], the correct prescription for modelling dynamics via a stochastic differential equation can only be decided by either a first principles computation or other external physical considerations - mathematically all prescriptions ( $\Theta(0) \in [0, 1]$  in a continuum description) are equally admissible. In our case, the stochastic action entering the path integral must be a truncated version of the full underlying QFT action in the Schwinger-Keldysh formulation (see [46] for the spectator field case) and therefore, a particular prescription must be chosen from the underlying dynamics. Since no determinants appear in the QFT path integral, the Ito prescription seems favoured, but this will need to be verified via a concrete computation. A similar reduction to that described in [46], including gravitational degrees of freedom, for which a QFT path integral has been derived [70], as well as its comparison to the stochastic  $\Delta N$  formalism [68, 71–73] would also be an interesting future research pursuit.

## Chapter 3. Covariant One-Loop Gravitational Corrections to the Effective Higgs Potential in de Sitter

### 3.1 Overview of the Chapter

In this chapter, we are motivated by the meta-stability of the Higgs vacuum at high energies, but still below the Planck mass  $M_p$ , during inflation. We begin by outlining the motivation for the computation presented here and by providing some general introductory clarifications for manipulating quantum fields in curved field space. Furthermore, we introduce the field-space covariant one-loop correction to the effective action for the Higgs-Gravity sector, treating General Relativity as an Effective Field Theory of gravity and obtain the relevant operators in de Sitter spacetime. Utilising heat kernel methods on the  $S_4$  sphere, we find the zeta-function-regularised contributions to the beta functions and consequently obtain new and improved results for the running couplings of the one-loop effective potential.

### 3.2 Introduction

Extrapolation of the Standard Model of particle physics to high energies leads to the remarkable conclusion that our vacuum may be a long-lived metastable state, in which the Higgs field sits at a local minimum of the Higgs potential surrounded by a potential barrier of width somewhere in the range  $10^{10} - 10^{14}$  GeV [74–76]. This raises an interesting question about initial conditions, because if the Standard Model is correct at these energies, then somehow the Higgs field had to evolve into this metastable vacuum state during the early stages of the universe [77].

The Higgs potential barrier depends strongly on the effective Higgs mass at high energies, and it is quite possible that gravitational corrections may be important. In the relevant energy range, there is no reason to abandon General Relativity as an ‘Effective Field Theory’ description of gravity [78]. There are two contributions to the effective Higgs mass, the ordinary mass and the one due to the coupling  $\xi R \mathcal{H}^\dagger \mathcal{H}$ , between the Higgs field  $\mathcal{H}$  and the space-time curvature  $R$  [79, 80]. We will assume that inflation is driven by an inflaton field, not the Higgs field, which is assumed weakly interacting and makes no contribution to the Higgs potential. The curvature coupling increases the height of the potential barrier around the metastable minimum if  $\xi R$  is positive, and has the opposite effect when  $\xi R$  is negative, making Higgs stability sensitive to the value of  $\xi$  [77, 81, 82].

Placing the Higgs decay into a cosmological context [83], introduces an ambiguity in how we define the spacetime geometry. In particular, we can perform a conformal re-scaling of the metric which removes the curvature-coupling term, transforming the theory from the original Jordan frame to the Einstein frame. It has been noted that quantum calculations can sometimes lead to different results when done in the Jordan or the Einstein frame [84, 85]. This is a puzzle, because we want to avoid a situation in which the physical properties of the Higgs field (for example the stability of its vacuum) are frame-dependent. The contradiction would be best resolved by having an approach to quantisation that is consistent irrespective of the choice of the spacetime metric [86–89]. We here present a covariant quantisation scheme, through which the inflationary regime properties of the Higgs vacuum can be addressed unambiguously.

The basic tool we use is an effective action, which is covariant under field transformations [90–94]. This is a stronger requirement than general covariance or covariance under spacetime coordinate transformations. The idea of a field-space covariant Quantum Field Theory (hereafter called covariant) is illustrated by the diagram in Eq.(3.1). Quantisation followed by a field redefinition should give the same result as starting with a field redefinition and then quantising, i.e. the diagram should commute.

$$\begin{array}{ccc}
 \varphi & \rightarrow & \varphi' \\
 \downarrow & & \downarrow \\
 \Gamma[\varphi] & \rightarrow & \Gamma[\varphi']
 \end{array} \tag{3.1}$$

Demanding covariance of the effective action guarantees covariance of the effective field equations. Without covariance, there is a different quantum field theory for each choice of field variables. Imposing covariance has another virtue. In the standard QFT approach, the solutions of the effective field equations depend on the choice of the gauge-fixing terms, that are added to the classical Lagrangian to fix the gauge freedom. However, in the covariant approach, the solutions to the covariant effective field equations are independent of these gauge-fixing terms.

Covariant approaches are widely used to quantise non-linear sigma models [95, 96], but they are very rarely used for gauge theories. One reason they are not widely used is that the gauge-fixing dependence of the usual effective action is not considered problematic, since the dependence goes away ‘on-shell’, i.e. the action takes the same value at solutions to the effective field equations [97–100]. Furthermore, it is easy to show that the Jordan and Einstein frame Higgs theories have equivalent perturbative expansions when the background fields are on-shell and the Higgs field is small [101].

Using a covariant approach retains the gauge-fixing and frame independence *off-shell*, for any value of the Higgs field. On the other hand, covariant approaches are not totally unambiguous, because there are two versions of the covariant effective action:  $\Gamma[\varphi^*, \varphi]$  which generates the 1-particle-irreducible (1PI) diagrams but depends on an extra field  $\varphi^*$  [102], and the DeWitt effective action  $\Gamma[\varphi]$  which does not generate 1PI diagrams

[103]. Fortunately, both generate the same effective field equations, and they agree on-shell. They are therefore equivalent for determining the effective potential, so we will use the simpler DeWitt effective action.

Higgs vacuum decay is an example of a situation where the effective action and the classical action lead to very different qualitative behaviour [104–107]. Another example is Coleman-Weinberg theory of massless electrodynamics, where quantum corrections to the effective action lead to symmetry breaking. In these situations, we use the solutions of the renormalisation group (RG) corrected field equations with running coupling constants to determine the vacuum state or to calculate tunnelling amplitudes [108]. Note that we use ‘on shell’ to refer to fields that satisfy the *effective* field equations rather than the classical field equations.

We will investigate whether covariant and non-covariant approaches to the effective action give different physical results by doing specific calculations of the running couplings in the Higgs effective potential.

The renormalisation group corrected potential used here is constructed as follows. The DeWitt effective action for the modulus of the Higgs field  $\phi$  is written as a functional  $\Gamma(g_i, \phi, g_{\mu\nu}, \mu_R)$ , where  $g_i$  are running couplings depending on  $\mu_R$ , the renormalisation scale. At one-loop order, the explicit dependence on the renormalisation scale has contributions from all types of fields in the standard model. These contributions are determined by perturbation theory and depend on a set of second order differential operators  $\Delta^n(\phi)$  [109]. Following Coleman and Weinberg [108], the  $\beta$  functions ( $\beta_{g_i} = dg_i/d\ln(\mu_R)$ ) can be obtained by comparing coefficients in the renormalisation group equation for the Lagrangian,

$$\sum_i \beta_i \frac{\partial \mathcal{L}}{\partial g_i} - \gamma_\phi \phi \frac{\partial \mathcal{L}}{\partial \phi} - \gamma_g g_{\mu\nu} \frac{\partial \mathcal{L}}{\partial g_{\mu\nu}} = -\frac{1}{16\pi^2} \sum_n (\pm) b_2(\Delta^n), \quad (3.2)$$

where the sign is positive for bosons and negative for fermions and ghosts. Renormalisation of the fields is responsible for the anomalous dimensions  $\gamma_\phi = d \ln \sqrt{Z_\phi}/d\ln(\mu_R)$  and  $\gamma_g = d \ln \sqrt{Z_g}/d\ln(\mu_R)$ , where we are using the sign conventions of [107]. The functions  $b_2$  are polynomial combinations of coefficients in the operators  $\Delta^n$ . General expressions for  $b_2$  are known for many types of operators on arbitrary spacetime backgrounds (e.g. [110, 111]). Since the theory we are dealing with is not renormalisable, the Lagrangian, which has an infinite series of terms, has to be truncated at some inverse power of the cut-off scale of the theory, which we naturally take to be the Planck mass. At one-loop, the  $b_2$  coefficient gives us terms up to order  $M_p^{-4}$ .

A change of variable from  $\mu_R$  to  $t = \ln(\phi/\mu_R)$  changes the functional form of the couplings in the effective action from  $g_i(\mu_R)$  to  $g'_i(t)$ ,

$$\Gamma'(g'_i(t), \phi'(t), g'_{\mu\nu}(t), t) = \Gamma(g_i(\mu_R), \phi(\mu_R), g_{\mu\nu}(\mu_R), \mu_R). \quad (3.3)$$

The RG corrected Lagrangian is defined by the leading term,  $\mathcal{L}'(g'_i(t), \phi'(t), g'_{\mu\nu}(t))$ . The dependence of the parameters on the Higgs field modulus  $\phi$  is determined by the renor-

malisation group, which implies

$$\frac{dg'_i}{dt} = \frac{\beta_i(g'_j)}{1 + \gamma_\phi(g'_j)}, \quad (3.4)$$

subject to boundary conditions fixed at a given (low energy) mass scale  $M$ .

The first thing to note about the Coleman-Weinberg method for calculating the  $\beta$ -functions is that it relies on the functional form of the effective action. Therefore a knowledge of the effective action, which is only valid for solutions to the background field equations, is not sufficient. The covariant effective action gives us an unambiguous off-shell formulation and a unique set of beta functions. In order to construct this covariant effective action we make use of the non-trivial geometry of the space of metrics and fields. In the general case of a gauge theory with fields  $\varphi^I$  and action  $S[\varphi]$ , the covariant operator  $\Delta_{IJ}$  for the field fluctuations is given by [90, 91]

$$\Delta_{IJ} = -\frac{\delta^2 S}{\delta\varphi^I \delta\varphi^J} + \Gamma^K{}_{IJ} \frac{\delta S}{\delta\varphi^K} + \lambda_g \mathcal{R}_I{}^\alpha[\varphi] \mathcal{R}_{J\alpha}[\varphi], \quad (3.5)$$

where  $\mathcal{R}^I{}_a$  are the gauge group generator vector ( $\mathcal{R}_a \equiv \mathcal{R}^I{}_a \partial_I$ ) components.

The innovation of Vilkovisky and DeWitt was to put the second functional derivatives into covariant form by introducing a field-space connection  $\nabla_I$  with connection coefficients  $\Gamma^K{}_{IJ}$ . The connection ensures that the effective action is covariant under field redefinitions. In the Landau gauge limit,  $\lambda_g \rightarrow \infty$ , the connection coefficients reduce to the Levi-Civita connection coefficients, for the local metric, on the space of fields. The final term in (3.5) is a gauge-fixing term. Details of the covariant approach are given in section 3.3.

The connection term vanishes when the background field satisfies the classical field equations i.e.  $\delta S/\delta\varphi^I = 0$ , and then non-covariant and covariant effective actions agree. However, we might expect differing results when the background satisfies the *quantum corrected* field equations. The beta-functions and the renormalisation group corrected effective Lagrangians defined using non-covariant and covariant approaches need not be the same.

In sections 3.5 and 3.6 we will calculate the beta-functions for the Higgs potential parameters, in both covariant and non-covariant form, and present the differences between the beta-functions obtained in the Einstein, Jordan and covariant frames. As is well known, from standard scalar-gravity theory, the beta-function for the curvature coupling  $\beta_\xi \propto 6\xi - 1$  in the Jordan frame. This result cannot hold in a covariant approach, because  $\xi$  vanishes in the Einstein frame, and consequently the covariant  $\beta_\xi$  cannot depend on  $\xi$ <sup>1</sup>. As expected, when we do the calculation, the non-covariant results are frame dependent whilst the covariant results are frame independent. However, the combination  $\mu^2 + \xi R$ , which acts as an effective Higgs mass, and the Higgs self-coupling  $\lambda$  have the same scale

---

<sup>1</sup>In fact,  $\xi$  appears as a correction to the mass in the Einstein frame, and contributes to  $\beta_{\mu^2}$ .

behaviour in the non-covariant and covariant approaches. The leading behaviour of the renormalisation group effective potential is therefore frame independent, and differences arise only in terms that are suppressed by factors of  $M_p^{-4}$ . Our results for the properties of the Higgs vacuum, using the renormalisation group corrected potential, hence, are similar to those found previously [79].

In section 3.5 we will explore some of the consequences of the covariant approach. One of these is that field redefinitions mix some of the parameters of the theory, and respecting covariance leads to a set of relations between the beta functions for these parameters. These relations can be used, for example, to completely determine the dependence of the beta-functions on the curvature coupling  $\xi$ . Another consequence of using a covariant approach is that the path integral is independent of the gauge-fixing terms in the Lagrangian. Therefore, physical observables that depend on the quantum field action (for example, the quantum tunnelling rates) will be computed unambiguously. In non-covariant approaches, this issue is non-trivial, and independence has only been demonstrated explicitly when the true vacuum is not radiatively generated [112, 113].

This chapter focuses on the UV behaviour of the quantum theory and how it affects the Higgs potential in de Sitter space. In many ways, though, the IR behaviour of Higgs fields in de Sitter space is a more interesting subject. It has become apparent, initially from stochastic theory [47, 52, 114, 115] and also from infrared expansions [116, 117], that a self-coupled massless scalar field in a de Sitter invariant state acquires a mass squared of order  $\lambda^{1/2}H^2$ , where  $H$  is the expansion rate. This limits the applicability of our results for small curvature coupling. It also means that, when integrating the renormalisation group equations for the effective mass in de Sitter space, we start with this IR mass, rather than the low energy Higgs mass.

### 3.3 Covariant Effective Actions

In this section, after a concise introduction to the geometrical interpretation of a curved field space and some fundamentals on the effective action, we give an exposition to the field-space covariant effective action, following DeWitt [118], and present two methods for evaluating its one-loop contribution. Furthermore, we show specifically, that the Landau gauge-fixing limit and the decomposition into gauge-fixed and pure gauge modes lead to equivalent results for the one-loop effective potential.

#### 3.3.1 Field Space Generalities

In field space, the background fields define coordinates, the components of which are denoted here by capital Latin indices  $I, J, \dots$  (the interested reader is directed to Appendix B). The gauge sub-space parameters will be specified by using Greek indices  $\alpha, \beta, \dots$ . DeWitt condensed notation [91] is used throughout, with the indices  $I, J, \dots$  and  $\alpha, \beta, \dots$  representing all field variables associated with the field in question (for ex-

ample  $\Phi^I \rightarrow \Phi^{\mathcal{I}}(x)$ ) and contractions over  $I, J, \dots, \alpha, \beta \dots$  incorporating the Einstein convention (summation over repeated tensor indices), but also integration over spacetime. Hence, the inner product, for example, becomes

$$V^I D_I = V^I \mathcal{G}_{IJ} D^J \equiv \int d^n x d^n x' V^{\mathcal{I}}(x) \mathcal{G}_{\mathcal{I}\mathcal{J}}(x, x') D^{\mathcal{I}}(x'), \quad (3.6)$$

where in the last equation, we write the integration over spacetime explicitly and employ only the Einstein summation over the indices  $\mathcal{I}, \mathcal{J} \dots$ . For clarity, we present in Table 3.1 a comprehensive list of all the different types of indices used in this chapter, along with their implicit summations.

Index Type	Component Type	Summation Convention
$\mu, \nu, \dots$	Spacetime Coordinate	Einstein
$i, j, \dots$	Higgs (Scalar) Field	Einstein
$\mathcal{I}, \mathcal{J}, \dots$	Field Space Coordinate	Einstein
$I, J, \dots$	Field Space Coordinate	Einstein & Spacetime Integration
$\alpha, \beta, \dots$	Gauge Group Indices	Einstein & Spacetime Summation

Table 3.1: Tensor component indices, the type of tensor they refer to and their respective implicit summation conventions.

In this context, any tensor field  $\phi^I$ , depending on some spacetime coordinate  $x^\mu$  defined on a curved spacetime background with integral measure  $d\mu = d^n x |g|^{1/2}$ , can be represented with the aid of the biscalar Dirac  $\delta$ -distribution, as

$$\phi^I \equiv \phi^{\mathcal{I}}(x) = \int d\mu(y) \delta(x, y) \delta^{\mathcal{I}}_{\mathcal{J}} \phi^{\mathcal{J}}(y). \quad (3.7)$$

The partial variation of a functional of  $\phi$ ,  $F[\phi]$ , with respect to  $\phi$  follows by expanding it in powers of the variation of  $\phi$ . To first order, one obtains

$$\delta F[\phi] = \int d\mu(y) \delta(x, y) \frac{\delta F[\phi]}{\delta \phi^{\mathcal{J}}(x)} \delta \phi^{\mathcal{J}}(y) = \frac{\delta F[\phi]}{\delta \phi^{\mathcal{J}}} \delta \phi^{\mathcal{J}}, \quad (3.8)$$

which leads, identically, to the definition of the field-space Dirac  $\delta$ -distribution.

$$\frac{\delta \phi^I}{\delta \phi^{\mathcal{J}}} = \frac{\delta \phi^{\mathcal{I}}(x)}{\delta \phi^{\mathcal{J}}(y)} \equiv |g(y)|^{1/2} \delta^{\mathcal{I}}_{\mathcal{J}} \delta(x, y) \equiv \delta^I_{\mathcal{J}}. \quad (3.9)$$

A field-covariant effective action can be constructed whenever there exists a covariant notion of the distance between two field configurations. Formally, this means that we have a Riemannian geometry on the space of fields  $\varphi^I$  and geodesics can be defined [90, 91, 93]. This approach allows us to interpret geometrically the ordinary field displacement  $\varphi^I - \phi^I$ , which is sensible in a flat field-space with Cartesian coordinates, as a vector and generalise



this notion. The geodesic interval  $\sigma[\phi, \varphi]$  is defined as

$$\sigma[\phi, \varphi] = \frac{1}{2} [\text{length of geodesic from } \phi \text{ to } \varphi]^2, \quad (3.10)$$

hence, the covariant tangent vector to the geodesic from  $\phi^I$  to  $\varphi^I$  is given by  $-\sigma^I(\phi, \varphi)$ , with

$$\sigma^I[\phi, \varphi] = \mathcal{G}^{IJ}[\phi] \frac{\delta}{\delta \phi^J} \sigma[\phi, \varphi], \quad (3.11)$$

and can be regarded as the natural extension of the flat-space coordinate difference in general geometries. The local field-space metric  $\mathcal{G}_{IJ}$  can also be used to define a field-space invariant volume measure  $D\varphi$  for functional integration.

### 3.3.2 Effective Action Generalities

The effective action is a fascinating tool for the computation of the quantum properties of interacting fields theories, especially when attention is paid to the intrinsic properties of fields - like correlation functions, potential minima, etc - rather than their particle states. We briefly review some basic notions on the subject for the sake of completeness and refer the interested reader to excellent expositions of the topic [93, 102, 107, 119].

Starting from the classical Lagrangian,  $\mathcal{L}(\phi)$  and adding a source term  $J_{\mathcal{I}}(x)$  with linear dependence to the classical field, on a curved space-time background with volume element  $d\mu = |g|^{1/2} d^4x$  (focusing on situations where both the initial and final states of the system are approximate vacuum states and ignoring particle production), results in the definition of the ground state amplitude

$$Z[g, J] = e^{iW[g, J]} = \int \mathcal{D}\phi e^{iS_J[g, \phi]}. \quad (3.12)$$

The generating function, here, apart from being a function of the external source  $J$ , is also a function of the metric  $g_{\mu\nu}$ ,

$$S_J[g, \phi] = S[g, \phi] + \int d\mu(x) J_{\mathcal{I}}(x) \phi^{\mathcal{I}}(x). \quad (3.13)$$

Let us define the effective field  $\varphi^{\mathcal{I}}$ ,

$$\varphi^{\mathcal{I}}(x) \equiv \frac{\delta W[J]}{\delta J_{\mathcal{I}}(x)} = \langle \phi^{\mathcal{I}}(x) \rangle_J, \quad (3.14)$$

as the expectation value of  $\phi^{\mathcal{I}}(x)$ , which is, manifestly, a functional of  $J_{\mathcal{I}}$ . The effective action can, then, be defined as

$$\Gamma[g, \phi] = W[J] - \int d\mu(x) J_{\mathcal{I}}(x) \varphi^{\mathcal{I}}(x) \equiv W[J] - J_{\mathcal{I}} \varphi^{\mathcal{I}}, \quad (3.15)$$

resulting in

$$\begin{aligned} e^{i\Gamma[g,\varphi]} &= \int \mathcal{D}\phi e^{iS[g,\phi]+i\int d\mu(x)J_{\mathcal{I}}(x)(\phi^{\mathcal{I}}(x)-\varphi^{\mathcal{I}}(x))} \\ &= \int D[\delta\varphi] e^{iS[\varphi+\delta\varphi]+iJ_I\delta\varphi^I}, \end{aligned} \quad (3.16)$$

with the source term given by

$$J_{\mathcal{I}}(x) = -\frac{\delta\Gamma[g,\varphi]}{\delta\varphi^{\mathcal{I}}(x)}. \quad (3.17)$$

This is the implicit definition of the effective action.

An alternative method for obtaining the effective action revolves around the expansion of the classical action about the background field  $\varphi^I \rightarrow \varphi^I + \delta\varphi^I$ ,

$$S_J[g,\varphi + \delta\varphi] = S[g,\varphi] + S_{,I}[g,\varphi]\delta\varphi^I + \frac{1}{2}\delta\varphi^I\Delta_{IJ}\delta\varphi^J, \quad (3.18)$$

with  $\Delta_{IJ}$  being the second variation operator. In this context,  $\Gamma[g,\varphi] = S[g,\varphi] + \mathcal{O}(1)$  and the source current (3.17) is obtained perturbatively by

$$J_I(x) = -S_{,I}[g,\varphi] + \mathcal{O}(1). \quad (3.19)$$

Therefore, the linear to the variation  $\delta\varphi$  term in (3.16), can also be treated perturbatively; its effect is such that, taking (3.17) into account, one obtains  $\langle\delta\varphi^I\rangle_{J=0}$ , resulting in the effective action acting as the generator of 1PI irreducible diagrams [102].

In the attempt to construct a field theory that is independent of field redefinitions, a property demanded for any physical theory, one stumbles across the term in (3.16)  $\delta\varphi^{\mathcal{I}} = \phi^{\mathcal{I}} - \varphi^{\mathcal{I}}$  which is not a covariant quantity. What is more, the effective theory obtained for gauge theories using the Faddeev-Popov method renders the aforementioned approach not only background, but also, gauge condition dependent.

The resolution to this is the introduction of a field-reparametrisation covariant function of the background field  $\phi$ . Choosing  $\delta\phi^{\mathcal{I}} \rightarrow \sigma^{\mathcal{I}}$  as in (3.11), leads to the Vilkovisky-DeWitt effective action, which does not suffer from the aforementioned constraints and will be our starting point in calculating the running of the parameters of the gravity-Higgs effective potential.

### 3.3.3 Construction of the Effective Action

Our starting point is the covariant action of Burgess and Kunstatter [93, 102], defined implicitly by,

$$e^{i\Gamma[\varphi,\varphi_*]} = \int D\phi e^{iS[\phi]-i(\delta\Gamma/\delta\sigma^J)(\sigma^J[\varphi_*,\phi]-\sigma^J[\varphi_*,\varphi])}. \quad (3.20)$$

This expression depends on the effective field  $\varphi^I$  and an arbitrary expansion point  $\varphi_*^I$ .

The effective action generates effective field equations for  $\varphi^I$ , in the sense that

$$\partial_I \Gamma[\varphi, \varphi_*] = 0 \implies \langle \sigma[\varphi, \hat{\phi}] \rangle = 0, \quad (3.21)$$

where  $\sigma[\varphi, \hat{\phi}]$  is the geodesic distance and  $\hat{\phi}^I$  is the field operator. In the covariant approach, unlike (3.14), the effective field does not coincide with the expectation value of the field operator  $\varphi^I \neq \langle \hat{\phi}^I \rangle$ , but instead  $\varphi^I$  is the classical field with minimal invariant distance to the quantum field. Making use of the fact that the effective field equations do not depend on the expansion point  $\varphi_*$ , we choose  $\varphi_*^I = \varphi^I$ , which defines the DeWitt effective action [93, 103],

$$\Gamma[\varphi] = \Gamma[\varphi, \varphi]. \quad (3.22)$$

Just as in the introduction, this implicit definition of the effective action is not really illuminating for the purpose of doing explicit calculations. It has been elaborately manifested that there is an equivalent to (3.18), in the covariant sense, which can be obtained by expanding the classical action in powers of the operator  $\zeta^J = (\sigma^J[\varphi_*, \phi] - \sigma^J[\varphi_*, \varphi])$  covariantly. The Vilkovisky-Dewitt choice results in  $\zeta^I \equiv \sigma^I[\varphi, \phi]$ , so utilising the background field expansion for the classical action, naively, is identical to the covariant variation of the action, as expected from drawing similarities to Non-Linear Sigma Models (see Appendix B). The DeWitt effective action generates the effective field equations using  $\partial_I \Gamma[\varphi] = 0$ .

Finally, and in similarity to (3.18), the covariant effective action can be expanded as:

$$S[\varphi, \zeta^I] = S[\varphi] + \zeta^I \partial_I S[\varphi] + \frac{1}{2} \zeta^I \Delta_{;IJ} \zeta^J + \dots, \quad (3.23)$$

where now the second variation operator will include not only the covariant variation of the classical action, but also contributions stemming from the quantum treatment of any gauge symmetries of the classical Lagrangian, with condensed notation used throughout.

The proper treatment of gravity as an effective quantum theory, demands that the gauge symmetry of the classical Lagrangian needs to be taken into account. The group in question, here, is invariance under general coordinate transformations (group indices  $\alpha, \beta \dots$  and spacetime coordinate indices  $\mu, \nu, \dots$  both refer to gauge group tensor components; the difference being that the former include the implicit integration over spacetime, whereas the latter do not). Let  $x^\mu \rightarrow x^\mu + \delta\epsilon^\mu$ , where  $\delta\epsilon^\mu$  are the infinitesimal group parameters. Then, under the group operation, the fields transform as

$$\delta_{||} g_{\mu\nu} = 2\nabla_{(\mu} \delta\epsilon_{\nu)} \quad \text{and} \quad \delta_{||} \phi^i = \delta\epsilon^\mu \phi^i_{,\mu}. \quad (3.24)$$

Geometrically, in the field-space spanned by field variations, there will be a subspace defined by infinitesimal gauge transformations of the field  $\varphi^I$  of the form

$$\delta_{||} \varphi^I = \varphi^I_\epsilon - \varphi^I \equiv \mathcal{R}^I_\alpha \delta\epsilon^\alpha = \int dx' \mathcal{R}^I_{\mu}(x, x') \delta\epsilon^\mu(x'), \quad (3.25)$$

where, as before,  $\delta\epsilon^\alpha$  represent the gauge group parameters, and  $\mathcal{R}^I_a$  are the group generator vector ( $\mathcal{R}_a \equiv \mathcal{R}^I_a \partial_I$ ) components which leave the action invariant, i.e.  $\mathcal{R}^I_a \partial_I S = 0$ . The gauge is fixed using a gauge-fixing functional  $\chi^\alpha[\phi, \varphi]$ , and then the path integral is modified as,

$$S[\varphi] \rightarrow S[\varphi] + \frac{1}{2} \gamma_{\alpha\beta} \chi^\alpha \chi^\beta + \frac{\hbar}{i} \text{tr} \ln Q^\alpha_\beta. \quad (3.26)$$

This introduces a metric  $\gamma_{\alpha\beta}$  on the space of gauge parameters and a ghost operator

$$Q^\alpha_\beta = (\partial_I \chi^\alpha) \mathcal{R}^I_\beta. \quad (3.27)$$

Next, the procedure developed by Vilkovisky and DeWitt [90] generates the geometry in field space, which guarantees that the effective action is:

1. Covariant under field redefinitions of  $\varphi^I$ ;
2. Independent of the choice of gauge fixing functional  $\chi^\alpha$ ;
3. Independent of the metric  $\gamma_{\alpha\beta}$ .

The field-space geometry includes a local field-space metric  $\mathcal{G}_{IJ}$  and a non-local field space connection  $\nabla_I$ . The metric allows an orthogonal decomposition of field variations into pure gauge and gauge-fixed directions. Projection in the pure-gauge direction can be done using

$$\bar{\Pi}^I_J = \mathcal{R}^I_\alpha \mathcal{N}^{\alpha\beta} \mathcal{R}_{J\beta}, \quad (3.28)$$

where indices are lowered using the metric tensor in the usual way and the normalisation factor appearing here is

$$\mathcal{N}^{\alpha\beta} = (\mathcal{R}^I_\alpha \mathcal{R}_{I\beta})^{-1}. \quad (3.29)$$

This projection operator acts trivially on pure-gauge variations,  $\bar{\Pi}^I_J \delta_{\parallel} \varphi^J = \delta_{\parallel} \varphi^I$ . The orthogonal projection, in the gauge-fixed direction, is the DeWitt projection  $\Pi = \mathbb{I} - \bar{\Pi}$ .

The local metric also generates a Levi-Civita connection in field space, denoted by  $\mathcal{D}_I$ , for example

$$\mathcal{D}_I \mathcal{D}_J S = \partial_I \partial_J S - \Gamma^K_{IJ} \partial_K S. \quad (3.30)$$

In a gauge theory, the Vilkovisky-DeWitt connection  $\nabla_I$  is *not* equal to the Levi-Civita connection, but it is related to it by the fixed-gauge (physical) sub-space projection operator,

$$\nabla^I \nabla_J S = \Pi^I_K (\mathcal{D}^K \mathcal{D}_L S) \Pi^L_J. \quad (3.31)$$

The one-loop correction to the covariant effective action obtained from a geodesic expansion of the fields in the path integral, with the inclusion of the gauge-fixing and ghost Lagrangians, is

$$\Gamma^{(1)} = \frac{\hbar}{2i} \text{tr} \ln \{ \Pi (\mathcal{D}^I \mathcal{D}_J S) \Pi + (\partial^I \chi^\alpha) (\partial_J \chi_\alpha) \} - \frac{\hbar}{i} \text{tr} \ln Q^\alpha_\beta. \quad (3.32)$$

### 3.3.4 Fixing the Gauge

The non-locality of (3.32), which stems from the non-locality of the connection in the covariant variation of the classical action, is one of the disadvantages of the covariant approach. Nevertheless, it can be dealt with, to one-loop accuracy.

For an actual calculation, we can reduce the amount of work by choosing a convenient gauge-fixing functional, in particular the  $\mathcal{R}_\xi$  gauges in which  $\partial_I \chi^\alpha = \lambda_g^{1/2} \mathcal{R}_I^\alpha$ , where  $\lambda_g$  is a constant gauge-fixing parameter. The one-loop effective action is then

$$\Gamma^{(1)} = \frac{\hbar}{2i} \text{tr} \ln \{ \Pi(\mathcal{D}^I \mathcal{D}_J S) \Pi + \lambda_g \mathcal{R}^{\mathcal{I}\alpha} \mathcal{R}_{\mathcal{J}\alpha} \} - \frac{\hbar}{i} \text{tr} \ln \{ \lambda_g^{1/2} \mathcal{R}^{\mathcal{I}\alpha} \mathcal{R}_{\mathcal{I}\beta} \}. \quad (3.33)$$

If the covariant derivatives in (3.30) are replaced by ordinary functional derivatives, and the projections are dropped, then the result is a non-covariant effective action contribution  $\Gamma_{\text{nc}}^{(1)}$ ,

$$\Gamma_{\text{nc}}^{(1)} = \frac{\hbar}{2i} \text{tr} \ln \{ \partial^I \partial_J S + \lambda_g \mathcal{R}^{I\alpha} \mathcal{R}_{J\alpha} \} - \frac{\hbar}{i} \text{tr} \ln \{ \lambda_g^{1/2} \mathcal{R}^{I\alpha} \mathcal{R}_{I\beta} \}. \quad (3.34)$$

If the background fields are ‘on shell’, specifically when  $\partial_I S = 0$ , then the connection  $\nabla_I \rightarrow \partial_I$ , and the covariant and non-covariant results coincide,  $\Gamma^{(1)} = \Gamma_{\text{nc}}^{(1)}$ . Most calculations are done on shell, and Eq. (3.34) is the traditional route to the evaluation of the effective action.

The off-shell result (3.33) can be simplified in two equivalent ways. Firstly, it will be shown, by interpreting the logarithms in a particular way, described below, that

$$\Gamma^{(1)} = \frac{\hbar}{2i} \text{tr} \ln \{ \Pi(\mathcal{D}^I \mathcal{D}_J S) \Pi \} - \frac{\hbar}{2i} \text{tr} \ln \{ \mathcal{R}^{I\alpha} \mathcal{R}_{I\beta} \}. \quad (3.35)$$

If we have  $n$  fields and  $m$  gauge variations, then there are  $n - m$  non-gauge fields but there are  $n - 2m$  degrees of freedom. The ghost contribution accounts for the difference between these two. Secondly, using the Landau gauge,  $\lambda_g \rightarrow \infty$ ,

$$\Gamma^{(1)} = \lim_{\lambda_g \rightarrow \infty} \frac{\hbar}{2i} \text{tr} \ln \{ \mathcal{D}^I \mathcal{D}_J S + \lambda_g \mathcal{R}^{I\alpha} \mathcal{R}_{J\alpha} \} - \frac{\hbar}{i} \text{tr} \ln \{ \lambda_g^{1/2} \mathcal{R}^{I\alpha} \mathcal{R}_{I\beta} \}. \quad (3.36)$$

This appears to be more complicated, but the advantage of this method is that removing the projection operators, leaves an operator that is explicitly local in spacetime, making it suitable for adiabatic expansion techniques.

For simplicity, we define the functional traces using Euclidean methods (see Appendix C ) with

$$\text{tr} \ln A_L = -i\zeta'(0, A) - i\zeta(0, A) \ln \mu_R^2, \quad (3.37)$$

where  $A$  is a positive definite operator obtained from the Lorentzian operator  $A_L$  by analytic continuation of the time-like coordinate. This limits us to metrics with a valid analytic continuation. The generalised zeta-function is defined by  $\zeta(s, A) = \text{tr} A^{-s}$  and  $\mu_R$  is the renormalisation scale. We can read off the scaling of the Euclidean effective action

$\Gamma_E$  from (3.36):

$$\mu_R \frac{d\Gamma_E^{(1)}}{d\mu_R} = \hbar \lim_{\lambda_g \rightarrow \infty} \left\{ -\zeta(0, \mathcal{D}^I \mathcal{D}_J S + \lambda_g \mathcal{R}^{I\alpha} \mathcal{R}_{J\alpha}) + 2\zeta(0, \lambda_g^{1/2} \mathcal{R}^{I\alpha} \mathcal{R}_{I\beta}) \right\}. \quad (3.38)$$

In Landau gauge, the operators are local, and it is possible to prove that  $\zeta(0, A)$  can be expressed in terms of a local adiabatic expansion coefficient  $b_2(A)$ ,

$$\zeta(0, A) = \frac{1}{16\pi^2} \int b_2(A) |g|^{1/2} d^4x. \quad (3.39)$$

Eq. (3.38) is the origin of the renormalisation group equation (3.2) we gave in the introduction. For Laplace type operators  $A = -\nabla^2 + E$ , the expansion coefficient  $b_2(A)$  is an invariant polynomial combination of the spacetime curvature and derivatives of  $E$ . In Ref. [120], it was shown that the expansion coefficients remain polynomial for some classes of non-Laplacian operators relevant to the covariant effective action. In these cases, we can use  $b_2(A)$  to read off the rescaling behaviour of the terms in the effective potential or the effective Lagrangian using the renormalisation group equation (3.2).

To obtain the two representations of the covariant effective action given earlier, we first split  $\varphi^I \rightarrow (\xi^I, \theta^I)$  into non-gauge and pure-gauge directions. We decompose the operator  $\mathcal{D}^I \mathcal{D}_J S$  as

$$\mathcal{D}^I \mathcal{D}_J S = A = \begin{pmatrix} a & c \\ c^\dagger & d \end{pmatrix}. \quad (3.40)$$

Similarly,

$$R^{I\alpha} R_{J\alpha} = B = \begin{pmatrix} 0 & 0 \\ 0 & b \end{pmatrix}. \quad (3.41)$$

Eq.(3.35) follows from this decomposition when we set  $\lambda_g = 1$ , in the one-loop result (3.33). Noting (as will manifestly be shown later after the decomposition of the operators in a harmonic basis) that the non-zero eigenvalues of  $\mathcal{R}^{I\alpha} \mathcal{R}_{J\alpha}$  and  $\mathcal{R}^{I\alpha} \mathcal{R}_{I\beta}$  are identical,

$$\Gamma^{(1)} = \frac{\hbar}{2i} \text{tr} \ln a + \frac{\hbar}{2i} \text{tr} \ln b - \frac{\hbar}{i} \text{tr} \ln b = \frac{\hbar}{2i} \text{tr} \ln a - \frac{\hbar}{2i} \text{tr} \ln b. \quad (3.42)$$

This recovers Eq. (3.35).

In order to obtain the Landau gauge representation, eq.(3.36), we start with the generalised zeta-function  $\zeta(s, A)$ ,

$$\zeta(s, A + \lambda_g B) = \frac{1}{\Gamma(s)} \int_0^\infty dt t^{s-1} \text{tr} \left( e^{-(A + \lambda_g B)t} \right). \quad (3.43)$$

If we rescale  $\lambda_g t \rightarrow t$ ,

$$\zeta(s, A + \lambda_g B) = \frac{\lambda_g^{-s}}{\Gamma(s)} \int_0^\infty dt t^{s-1} \text{tr} \left( e^{-(B + \lambda_g^{-1} A)t} \right) \quad (3.44)$$

and separate the diagonal and non-diagonal parts,

$$\mathrm{tr} \left( e^{-(B+\lambda_g^{-1}A)t} \right) = \mathrm{tr} \left( \exp \left[ - \begin{pmatrix} \lambda_g^{-1}a & 0 \\ 0 & b + \lambda_g^{-1}d \end{pmatrix} t \right] \exp \left[ - \begin{pmatrix} 0 & \lambda_g^{-1}c \\ \lambda_g^{-1}c^\dagger & 0 \end{pmatrix} t \right] \right), \quad (3.45)$$

it is clear that only the even powers of  $\lambda_g^{-1}$  survive in the second exponential due to the trace. Of these, only the leading term survives in the large  $\lambda_g$  limit, and after rescaling  $t$  back, we are left with

$$\zeta(s, A + \lambda_g B) = \zeta(s, a) + \lambda_g^{-s} \zeta(s, b + \lambda_g^{-1}d) + O(\lambda_g^{-s-2}). \quad (3.46)$$

We use analytic continuation to  $s = 0$  and then, in the limit  $\lambda_g \rightarrow \infty$ ,

$$\zeta(0, A + \lambda_g B) \sim \zeta(0, a) + \zeta(0, b) \quad (3.47)$$

$$\zeta'(0, A + \lambda_g B) \sim \zeta'(0, a) + \zeta'(0, b) - \zeta(0, b) \ln \lambda_g. \quad (3.48)$$

Hence, the terms on the right hand side of (3.36) are

$$\lim_{\lambda_g \rightarrow \infty} \frac{\hbar}{2i} \mathrm{tr} \ln \{A + \lambda_g B\} - \frac{\hbar}{i} \mathrm{tr} \ln \{\lambda_g^{1/2} b\} = \frac{\hbar}{2i} \mathrm{tr} \ln a - \frac{\hbar}{2i} \mathrm{tr} \ln b. \quad (3.49)$$

Therefore the Landau gauge result (3.36) is equal to (3.42), which is equal to the gauge decomposition (3.35).

### 3.4 The Gravity-Higgs Effective Field Theory

Having established that the object of interest, namely the first order correction to the effective action, is well-described, despite the non-locality of the action, we return to (3.23) and obtain the operators that contribute to it, specifically, the covariant second variation of the action, the gauge-fixing and ghost operators.

#### 3.4.1 Jordan Frame Lagrangian

We take the point of view that the gravity-Higgs sector is a low-energy Effective Field Theory for the spacetime metric  $g_{\mu\nu}$  and the Higgs doublet field  $\mathcal{H}$ , in which non-renormalisable terms are assumed to be suppressed by inverse powers of the reduced Planck mass,  $\kappa = M_p^{-1} = (8\pi G)^{1/2}$  [78]. For questions relative to this energy regime (for example in the case of Higgs instability, which sets in at a scale below the Planck mass), the renormalisable couplings will be expected to play the most important role. During inflation, we suppose that the vacuum energy is dominated by an inflaton field and takes some fixed value  $V_0$ , and then the expansion rate in the Higgs vacuum is determined by the Friedmann equation  $H^2 = \kappa^2 V_0/3$ .

For convenience, we replace the Higgs doublet by a set of four real scalars  $\phi^i$ , denoting

the gauge invariant magnitude of the field by  $\phi$  and the projection along the pure-gauge direction by  $\delta_{ij}^\perp$ . The Lagrangian density for the gravity-Higgs sector  $\mathcal{L}_g$  with non-minimal coupling is

$$\mathcal{L}_g(g, \phi) = -\frac{1}{2\kappa^2}U(\phi)R(g)|g|^{1/2} + \frac{1}{2}G_{ij}(\phi)g^{\mu\nu}\partial_\mu\phi^i\partial_\nu\phi^j|g|^{1/2} + V(\phi)|g|^{1/2}, \quad (3.50)$$

where  $\partial_\mu$  denotes an ordinary spacetime derivative. The non-minimal coupling terms are contained in the function  $U(\phi)$  multiplying the Ricci scalar  $R$ .

Each one of the scalar functions in the Lagrangian has an expansion in powers of  $\kappa$ ,

$$V(\phi) = V_0 + \frac{1}{2}\mu^2\phi^2 + \frac{1}{4}\lambda\phi^4 + \frac{1}{6}\lambda_6\kappa^2\phi^6 + \dots \quad (3.51)$$

$$G_{ij}(\phi) = \delta_{ij} + \alpha\kappa^2\delta_{ik}\delta_{jl}\phi^k\phi^l + \beta\kappa^2\delta_{ij}^\perp\phi^2 + \dots \quad (3.52)$$

$$U(\phi) = 1 - \xi\kappa^2\phi^2 + \dots \quad (3.53)$$

Most of the results we obtain have been truncated to  $O(\kappa^2\phi^2)$ . We will use a wave function renormalisation to keep the leading order behaviour in  $R$  and  $G_{ij}$  fixed. The anomalous dimensions will be denoted by  $\gamma_g$  and  $\gamma_\phi$  respectively. This keeps the effective Planck scale fixed. Note that it is not possible to eliminate both coefficients  $\alpha$  and  $\beta$  by redefinitions of  $\phi$  if  $G_{ij}$  has a non-vanishing curvature tensor.

### 3.4.2 Conformal Transformation to the Einstein Frame

One of the questions we address is the effect of conformal rescaling of the metric from the original Jordan Frame to the Einstein frame to remove the  $\xi$  term in the original Lagrangian. We transform the metric as  $g_{\mu\nu}^E = U(\phi)g_{\mu\nu}^J$ . Then, the Lagrangian density in the Einstein frame becomes

$$\mathcal{L}_g(g_E, \phi) = -\frac{1}{2\kappa^2}R(g_E)|g_E|^{1/2} + \frac{1}{2}G_{Eij}(\phi)g_E^{\mu\nu}\partial_\mu\phi^i\partial_\nu\phi^j|g_E|^{1/2} + V_E(\phi)|g_E|^{1/2}, \quad (3.54)$$

where

$$V_E(\phi) = U^{-2}V(\phi) \quad (3.55)$$

$$G_{Eij}(\phi) = U^{-1}G_{ij} + \frac{3}{2}\kappa^{-2}U^{-2}\frac{\partial U}{\partial\phi^i}\frac{\partial U}{\partial\phi^j}. \quad (3.56)$$

In a covariant theory it should be possible to calculate the beta functions by transforming to the Einstein frame, rescale the effective action, and transforming back to the Jordan frame.

If we expand the Einstein frame theory in powers of  $\kappa$ , we have relationships between



the sets of Einstein frame and Jordan frame parameters,

$$\mu_E^2 = \mu^2 + 4\xi'\kappa^2 V_0 \quad (3.57)$$

$$\lambda_E = \lambda + 4\xi'\kappa^2 \mu^2 \quad (3.58)$$

$$\xi_E = \xi - \xi'. \quad (3.59)$$

Note that we have used a different  $\xi'$  for the conformal transformation. Since we have adopted a covariant quantisation approach, these relations also hold for the running couplings up to field renormalisation factors. We differentiate the relations with respect to the renormalisation scale keeping  $\xi'$  fixed, and then set  $\xi' = \xi$  at the end,

$$\tilde{\beta}_{\mu^2}(0, \lambda_E, \mu_E^2, \dots) = \tilde{\beta}_{\mu^2}(\xi, \lambda, \mu^2, \dots) + 4\xi\kappa^2 \tilde{\beta}_{V_0}(\xi, \lambda, \mu^2, \dots) \quad (3.60)$$

$$\tilde{\beta}_{\lambda}(0, \lambda_E, \mu_E^2, \dots) = \tilde{\beta}_{\lambda}(\xi, \lambda, \mu^2, \dots) + 4\xi\kappa^2 \tilde{\beta}_{\mu^2}(\xi, \lambda, \mu^2, \dots) \quad (3.61)$$

$$\tilde{\beta}_{\xi}(0, \lambda_E, \mu_E^2, \dots) = \tilde{\beta}_{\xi}(\xi, \lambda, \mu^2, \dots). \quad (3.62)$$

The beta functions  $\tilde{\beta}$  include anomalous dimension factors, for example

$$\tilde{\beta}_{\xi} = \beta_{\xi} - 2\gamma_{\phi}\xi - \gamma_g\xi, \quad (3.63)$$

and similarly for the rest of the coupling coefficients. These relations can be used to evaluate covariant beta functions for non-trivial curvature coupling if we have results for minimal coupling. We note that for the scalar-gravity theory, the anomalous dimensions  $\gamma$  vanish to one loop order  $\gamma = O(\lambda^2)$ , [121].

Already, an unexpected result follows from (3.62), namely that the one-loop  $\beta_{\xi}$  for gravity-Higgs theory is independent of  $\xi$  at order  $\kappa^0$ , see Table 3.2. We remark that this is due to the fact that the wave function renormalisation is order  $\kappa^2$  in this theory. This is unlike the result obtained from the quantum theory of scalar fields on a curved background gives  $\beta_{\xi} \propto 6\xi - 1$  [122]. The  $\xi$  dependence must cancel when we include quantum gravity and require field-covariance of the gravity-Higgs effective action [89]. Subsequent results will confirm this using explicit calculations.

### 3.5 Expansions of the Gravity-Higgs Action

From the previous section, it is clear that in order to obtain the beta functions for the gravity-Higgs effective action, one needs to compute the contributions to the heat kernel coefficients from the covariant second-variation operator appearing in (3.32). This is achieved by obtaining the (non-covariant) second order variations of the action, adding the contribution of the Vilkovisky-DeWitt corrections (3.30), as well as the contribution of the gauge-fixing Lagrangian. Hence, one reads off the field-space metric  $\mathcal{G}_{IJ}$  (as the coefficient of the highest order derivative term in the action, following Vilkovisky [123]), the projection operator  $\mathcal{P}^{\alpha\beta}_{IJ}$  (as the coefficient of the non-minimal part of the operator),

and a potential term  $V_{IJ}$  (involving no derivatives). Subsequently, these operators can be projected onto a harmonic basis on  $S_4$ , and diagonalised. Lastly, the ghost action needs to also be taken into account, similarly, so that we are only left with the physical degrees of freedom in the zeta-function calculation. Most of the details have been left out because these are already covered in the literature, particularly in the work of Barvinsky [124–126], however, we attempt to make appropriate clarifications wherever necessary. We use the Jordan frame Lagrangian and then the covariant formulation can be checked by verifying the relations between the beta functions given in Eqs. (3.60)-(3.62).

The easiest, and most intuitive, method for obtaining the aforementioned operators is to expand the action using the background field method  $\phi^I \rightarrow \phi^I + \eta^I$  and subsequently vary with respect to the field perturbations  $\eta^I$ , which define the coordinates of the field-space. Hence, we combine the metric and scalar directions, rescaled so as to have the same dimensions, as

$$\eta^I \equiv \begin{pmatrix} \frac{1}{2\kappa} \delta g_{\mu\nu} \\ \delta \phi^i \end{pmatrix}. \quad (3.64)$$

Variations of functionals in field space, then, are taken as

$$\partial_I S = \frac{\delta S}{\delta \eta^I} = \left( 2\kappa \frac{\delta S}{\delta (\delta g_{\mu\nu})}, \frac{\delta S}{\delta (\delta \phi^i)} \right). \quad (3.65)$$

The second-order variation of the sum of the gravity-Higgs and gauge-fixing actions,  $S = S_g + S_{gf}$ , will be decomposed as a generic second order, self-adjoint differential operator,

$$\begin{aligned} -\mathcal{D}_I \mathcal{D}_J S &= -\partial_I \partial_J S + \Gamma^K_{IJ} \partial_K S \\ &= -\mathcal{G}_{IJ} \nabla^2 - \zeta \mathcal{P}^{\alpha\beta}_{IJ} \nabla_\alpha \nabla_\beta - (\mathcal{A}^\mu_{IJ} \nabla_\mu + \nabla_\mu \mathcal{A}^\mu_{IJ}) + E_{IJ}. \end{aligned} \quad (3.66)$$

Here,  $\mathcal{G}_{IJ}$  is the field space metric,  $\mathcal{P}^{\alpha\beta}_{IJ}$  combines non-minimal derivative terms and projects out the gauge-fixed directions,  $\mathcal{A}^\mu_{IJ} \propto \nabla_\nu \phi^j$  combines first order terms (and will vanish when the background fields are taken to be constant),  $E_{IJ}$  is an effective mass term and  $\zeta$  is a gauge-fixing parameter. The metric is used to construct the Levi-Civita connection by the usual expression,

$$\Gamma^I_{JK} = \frac{1}{2} \mathcal{G}^{IL} (\partial_K \mathcal{G}_{LJ} + \partial_J \mathcal{G}_{LK} - \partial_L \mathcal{G}_{JK}). \quad (3.67)$$

When writing down local operators like  $\mathcal{G}_{IJ}$  we usually omit delta function terms.

### 3.5.1 First Order Variations

The first order variation of the action defines the background field equations for the gravitational and Higgs fields, which will be denoted by  $F^{\mu\nu}$  and  $F_i$ ,

$$F^{\mu\nu} = -\frac{1}{2} \frac{2\kappa}{\sqrt{g}} \frac{\delta S}{\delta(\delta g_{\mu\nu})} = UG^{\mu\nu} - U^{;\mu\nu} + g^{\mu\nu}U^{;\rho}{}_{\rho} - \kappa^2 T^{\mu\nu}, \quad (3.68)$$

$$F_i = -\frac{1}{\sqrt{g}} \frac{\delta S}{\delta(\delta\phi^i)} = -\frac{1}{2\kappa^2} RU_{,i} - D_{\mu}(G_{ij}\nabla^{\mu}\phi^i) + V_{,i}, \quad (3.69)$$

where  $D_{\mu}$  is a covariant derivative for the Higgs-field-space metric  $G_{ij}$ ,

$$D_{\mu}\delta\phi^i = \nabla_{\mu}\delta\phi^i + \Gamma^i{}_{jk}(\partial_{\mu}\phi^j)\delta\phi^k, \quad (3.70)$$

and  $T^{\mu\nu}$  is the scalar field stress-energy tensor,

$$T^{\mu\nu} = G_{ij}\nabla^{\mu}\phi^i\nabla^{\nu}\phi^j - g^{\mu\nu}\left(\frac{1}{2}G_{ij}\nabla^{\mu}\phi^i\nabla_{\mu}\phi^j + V\right). \quad (3.71)$$

Here,  $F^{\mu\nu}$  has been scaled so that  $F^{\mu\nu} = 0$  resembles the usual Einstein equation in the minimal coupling limit  $U \rightarrow 1$ .

### 3.5.2 Second Order Variations

In the rest of this chapter the background scalar field will be assumed constant, for simplicity. Here, we follow and generalise the work of Barvinsky [125] in order to obtain the (non-covariant) second order variation of the action,  $-\partial_I\partial_J S_g$ , by taking functional derivatives of the first order variations:

$$-\partial_I\partial_J S_g = -\frac{1}{\sqrt{g}} \frac{\delta^2 S}{\delta\eta^I\delta\eta^J} = \frac{1}{\kappa^2|g|^{1/2}} \begin{pmatrix} \frac{2\kappa\delta(F_{\mu\nu}|g|^{1/2})}{\delta(\delta g_{\rho\sigma})} & \frac{\delta(F^{\mu\nu}|g|^{1/2})}{\delta(\delta\phi^i)} \\ \frac{2\kappa\delta(F_i|g|^{1/2})}{\delta(\delta g_{\rho\sigma})} & \frac{\delta(F_i|g|^{1/2})}{\delta(\delta\phi^j)} \end{pmatrix}. \quad (3.72)$$

Then, after performing the computation, we observe that (3.72) is shown to have derivative terms,

$$\begin{pmatrix} -Ug^{(\mu\nu)(\rho\sigma)}\nabla^2 + UP^{\alpha\beta(\mu\nu)(\rho\sigma)}\nabla_{\alpha}\nabla_{\beta} & -\kappa^{-1}U_{,j}(\nabla^{\mu}\nabla^{\nu} - g^{\mu\nu}\nabla^2) \\ -\kappa^{-1}U_{,i}(\nabla^{\rho}\nabla^{\sigma} - g^{\rho\sigma}\nabla^2) & -G_{ij}\nabla^2 \end{pmatrix} |g|^{1/2}, \quad (3.73)$$

and a potential term,

$$E_{gIJ} = \begin{pmatrix} E_g^{(\mu\nu)(\rho\sigma)} & \kappa g^{\mu\nu}V_{,j} \\ \kappa g^{\rho\sigma}V_{,i} & V_{,ij} - \frac{1}{2}R\kappa^{-2}U_{,ij} \end{pmatrix} |g|^{1/2}. \quad (3.74)$$

Two important tensors in the kinetic terms (3.73) are the DeWitt metric,

$$g^{(\mu\nu)(\rho\sigma)} = \frac{1}{2}(g^{\mu\rho}g^{\nu\sigma} + g^{\mu\sigma}g^{\nu\rho} - g^{\mu\nu}g^{\rho\sigma}), \quad (3.75)$$

and another tensor, which will also appear in the gauge-fixing terms below,

$$P^{\alpha\beta(\mu\nu)(\rho\sigma)} = 2g_{\gamma\delta}g^{(\alpha\gamma)(\mu\nu)}g^{(\beta\delta)(\rho\sigma)}. \quad (3.76)$$

The mass-like gravity terms are

$$E_g^{(\mu\nu)(\rho\sigma)} = -2UR^{\dot{\mu}\rho\dot{\nu}\sigma} + 2UR^{\dot{\mu}\rho}g^{\dot{\nu}\sigma} + UR_T^{\mu\nu}g^{\rho\sigma} + Ug^{\mu\nu}R_T^{\rho\sigma} - 4UR_T^{\dot{\mu}\rho}g^{\dot{\nu}\sigma} - 2\kappa^2Vg^{(\mu\nu)(\rho\sigma)}, \quad (3.77)$$

with overdots over indices indicating symmetrisation in those indices, and a subscript  $T$  denotes the trace-free part of the tensor. The terms have been organised this way to isolate those that vanish when the differential operator is applied to transverse traceless perturbations, and those which remain.

Since we want the effective action to respect the original symmetry of the classical action under general coordinate redefinitions,  $x^\mu \rightarrow x^\mu + \epsilon^\mu$ , a gauge-fixing method needs to be implemented. Hence, following Barvinski [124], we take

$$\mathcal{L}_{\text{gf}} = -\lambda_g U g_{\alpha\beta} \chi^\alpha \chi^\beta, \quad (3.78)$$

where the generators of the gauge-group are taken as

$$\chi^\alpha = \mathcal{R}^\alpha_I \eta^I = \frac{1}{2\kappa}(g^{(\alpha\beta)(\gamma\delta)}\nabla_\beta \delta g_{\gamma\delta} - U^{-1}U_{,i}\nabla^\alpha \delta\phi^i). \quad (3.79)$$

The addition of the gauge-fixing Lagrangian, results in a contribution to the second variation,

$$-\partial_I \partial_J S_{gf} = -\lambda_g \left( \begin{array}{cc} UP^{\alpha\beta(\mu\nu)(\rho\sigma)}\nabla_\alpha \nabla_\beta & -\kappa^{-1}U_{,j}g^{(\mu\nu)(\alpha\beta)}\nabla_\alpha \nabla_\beta \\ -\kappa^{-1}U_{,i}g^{(\rho\sigma)(\alpha\beta)}\nabla_\alpha \nabla_\beta & \frac{1}{2}\kappa^{-2}U^{-1}U_{,i}U_{,j}\nabla^2 \end{array} \right) |g|^{1/2}. \quad (3.80)$$

We have enough information now to obtain the field-space metric  $\mathcal{G}_{IJ}$ . We will do this by requiring the operator to have Laplacian form in the gauge-fixed directions, i.e.

$$-(\partial_I \partial_J S_g) \eta_\perp^I = -\mathcal{G}_{IJ} \nabla^2 \eta_\perp^J + E_{IJ} \eta_\perp^J, \quad (3.81)$$

when  $\chi^\mu(\eta_\perp^I) = 0$ . It is important to note that we are only interested in the action of the second variation operator on the gauge-fixed directions due to the projection operators acting in (3.35). Hence, since variations of the gauge-fixing term vanish when applied to the gauge-fixed directions, an arbitrary amount of  $\partial_I \partial_J S_{gf}$  can be added to the differential operator. However,  $(\partial_I \partial_J S_g) + \lambda_g^{-1}(\partial_I \partial_J S_{gf})$ , which results in  $\zeta = 0$  in (3.66), is the unique combination of the second order variations that results in a Laplacian form. The coefficient

of  $-\nabla^2$  in this combination is therefore the field-space metric, and this gives

$$\mathcal{G}_{IJ} = \begin{pmatrix} U g^{(\mu\nu)(\rho\sigma)} & -\frac{1}{2}\kappa^{-1}U_{,j}g^{\mu\nu} \\ -\frac{1}{2}\kappa^{-1}U_{,i}g^{\rho\sigma} & G_{ij} + \frac{1}{2}\kappa^{-2}U^{-1}U_{,i}U_{,j} \end{pmatrix} |g|^{1/2}. \quad (3.82)$$

We also obtain exactly the same result using  $\partial_I \chi^\alpha = \lambda_g^{1/2} \mathcal{R}_I^\alpha$  for the  $R_\xi$  gauges as in section 3.3. This is a special feature of the gauge fixing term (3.79), and for other choices it becomes necessary to combine information from both gauge-fixed and pure gauge directions to obtain the metric. For future reference, the inverse metric is given by

$$\mathcal{G}^{IJ} = \begin{pmatrix} U^{-1}g_{(\mu\nu)(\rho\sigma)} + \frac{1}{4}\kappa^{-2}U^{-1}U_{,k}U^{,k}W^{-1}g_{\mu\nu}g_{\rho\sigma} & -\frac{1}{2}\kappa^{-1}W^{-1}U^{,j}g_{\mu\nu} \\ -\frac{1}{2}\kappa^{-1}W^{-1}U^{,i}g_{\rho\sigma} & G^{ij} - \frac{3}{2}W^{-1}\kappa^{-2}U^{,i}U^{,j} \end{pmatrix} |g|^{-1/2}, \quad (3.83)$$

where  $W = U + \frac{3}{2}\kappa^{-2}U^{-1}U_{,i}U^{,i}$ .

Finally, comparing to the expression (3.66), we can also read off the tensor  $\mathcal{P}^{\alpha\beta}_{IJ}$ ,

$$\mathcal{P}^{\alpha\beta}_{IJ} = \begin{pmatrix} U P^{\alpha\beta(\mu\nu)(\rho\sigma)} & -\kappa^{-1}U_{,j}g^{(\mu\nu)(\alpha\beta)} \\ -\kappa^{-1}U_{,i}g^{(\rho\sigma)(\alpha\beta)} & \frac{1}{2}\kappa^{-2}U^{-1}U_{,i}U_{,j} \end{pmatrix} |g|^{1/2}. \quad (3.84)$$

The variations are considerably simpler in the Einstein frame  $U \equiv 1$ . Indeed, one of the motivations for considering covariant approaches is to ensure that the Einstein frame result can always be used reliably.

### 3.5.3 *Vilkovisky-DeWitt Corrections*

The Levi-Civita connection is given by the usual expression (3.67). The connection converts the scalar derivatives  $V_{,ij}$  into covariant derivatives  $V_{;ij}$ , and adds extra terms to the differential operator (3.66). For simplicity, we just quote the terms in the matrix components that contribute up to  $O(\kappa^2)$ , and take the spacetime curvature  $R$  to be of order  $\kappa^2$  and the scalar derivatives  $V_{,i}$  of order  $\kappa$ . The contributing non-trivial Christoffel symbols are

$$\Gamma^1_{11} = \Gamma_{(ef)}^{(ab)(cd)} = \frac{1}{4}U \left[ 2g_{ef}g^{ab}g^{cd} + \delta_e^{(a}\delta_f^{c)}g^{bd} + \delta_e^{(a}\delta_f^{d)}g^{bc} + \delta_e^{(b}\delta_f^{c)}g^{ad} + \delta_e^{(b}\delta_f^{d)}g^{ac} \right], \quad (3.85)$$

$$\Gamma^1_{22} = \Gamma_{(ef)ij} = \frac{1}{2}\kappa g_{ef}(G_{ij} + \kappa^{-2}U_{,ij}) \quad \text{and} \quad \Gamma^2_{12} = \Gamma^i_{(ef)j} = \frac{1}{2}\kappa g_{ef}G^{ik}G_{kj}. \quad (3.86)$$

Then, the VdW contribution to the effective action becomes,

$$\Gamma^K_{IJ}\partial_K S_g = \begin{pmatrix} E_\Gamma^{(\mu\nu)(\mu\nu)} & -\frac{1}{4}\kappa(2V_{,j} - \kappa^{-2}RU_{,j})g^{\mu\nu} \\ -\frac{1}{4}\kappa(2V_{,i} - \kappa^{-2}RU_{,i})g^{\rho\sigma} & \frac{1}{2}(G_{ij} + \kappa^{-2}U_{,ij})(R - 4\kappa^2V) \end{pmatrix}, \quad (3.87)$$

where

$$E_{\Gamma}^{(\mu\nu)(\rho\sigma)} = 2Ug^{\mu\rho}R_T^{\nu\sigma} - \frac{1}{2}UR_T^{\mu\nu}g^{\rho\sigma} - \frac{1}{2}Ug^{\rho\sigma}R_T^{\mu\nu}. \quad (3.88)$$

Eq. (3.87) is exact in the minimally coupled case  $U = 1$ .

In the non-minimally coupled case, when the Levi-Civita connection term (3.87) is combined with the mass terms from the second variation of the action (3.74), we see that the curvature coupling terms  $U_{;ij}R$  cancel. In particular, the  $2\xi\kappa^2R$  term, which would contribute the  $\xi$  dependence to the beta-function  $\beta_\xi$  has been cancelled off by the Vilkovisky-DeWitt corrections, verifying the claim made at the end of (3.4.2), explicitly.

### 3.6 Gravity-Higgs Mode Expansions

We have obtained the operators for the gravity-Higgs action in a completely field-covariant formalism. Therefore, we can reduce the dimensionality of the scalar field-space from four to one, so long as the non-trivial nature of the scalar field-space metric  $G_{ij}$  is taken into account, appropriately. Transforming the action to its Euclidean counterpart, the spacetime background becomes  $S_4$ . Through this simplification we can compute the coefficients of the heat kernel coefficient  $\beta_2$  for the simpler system of a single scalar field non-minimally coupled to gravity on the sphere by expanding the fields in a basis of  $S_4$  harmonics.

#### 3.6.1 Covariant Gravity-Scalar Model

We argued in section 3.3 that the scaling behaviour of the gravity-scalar effective action (3.38) can be expressed in terms of spacetime invariant tensor combinations. General expressions for these combinations are known from heat kernel methods for a wide range of second order operators [110, 120], but there are some non-Laplace type operators where the general results are not yet available. Furthermore, it can be very cumbersome applying these general results. A more practical approach, and one permitted by the field-space covariant approach followed in this work, is to use a direct evaluation of the generalised zeta function on a simple manifold for a simple operator, for example gravity with a single scalar field on the sphere [109, 127], and read off the relevant coefficients (see Appendix C and in particular (C.21)-(C.24)).

On the sphere  $S_4$ , the curvature is given in terms of the Ricci scalar,

$$R_{\mu\nu\rho\sigma} = \frac{1}{12}R(g_{\mu\rho}g_{\nu\sigma} - g_{\mu\sigma}g_{\nu\rho}), \quad (3.89)$$

and the radius of the sphere is  $\sqrt{12/R}$ . The Euclidean Lagrangian of a single constant scalar background field  $\phi$  with non-minimal coupling to gravity is given by

$$\mathcal{L}_E = \frac{1}{2}K(\phi)(\nabla\phi)^2 + V(\phi) - \frac{1}{2\kappa^2}U(\phi)R. \quad (3.90)$$

The second variation operator for the Euclidean theory (including the gauge-fixing term  $\lambda_g \mathcal{R}^{I\alpha} \mathcal{R}_{J\alpha}$ ), is

$$\mathcal{D}^I \mathcal{D}_J (S_E + S_{gf}) = -\delta^I_J \nabla^2 + (\lambda_g - 1) \mathcal{R}^{I\alpha} \mathcal{R}_{J\alpha} + E^I_J, \quad (3.91)$$

where the general expressions for  $\mathcal{R}^{I\alpha} \mathcal{R}_{J\alpha}$  and  $E^I_J$  were given in section 3.5. Then, the heat-kernel coefficient is given as [88]

$$b_2(\Delta) = \alpha_1 V_{;ij} V^{;ij} + \alpha_2 \kappa^2 V_{;i} V^{;i} + \alpha_3 \kappa^2 V V_{;i}^i + \alpha_4 \kappa^4 V^2 + \alpha_5 R V_{;i}^i + \alpha_6 \kappa^2 R V + \mathcal{O}(R^2). \quad (3.92)$$

For a single field, we replace  $V_i$  by  $V'$  and  $V_{;ij}$  by the covariant derivative associated with the scalar field space metric  $K(\phi)$ ,

$$V'' = K^{1/2} (K^{-1/2} V')'. \quad (3.93)$$

### 3.6.2 Orthonormal Harmonic Basis Expansion

The differential operators can be diagonalised by expanding the fields in a basis of  $S_4$  orthonormal harmonics: scalar modes  $h^S$ , transverse vector modes  $h^V_\mu$  and transverse-traceless tensor modes  $h^T_{\mu\nu}$ . Transverse modes are divergence free,  $\nabla^\mu h^V_\mu = 0$  and  $\nabla^\mu h^T_{\mu\nu} = 0$ . The eigenvalues of  $-\nabla^2$  for the respective modes are  $\lambda_S$ ,  $\lambda_V$  and  $\lambda_T$ . Modes can be traded up into higher rank tensors by applying derivatives to the basic set of harmonics. The general decomposition of the metric plus scalar field into the basis of harmonic functions and their derivatives is given by mode sums with coefficients  $x^I$ ,

$$\begin{aligned} \delta g_{\mu\nu} &= 2\kappa \sum_{\text{modes}} \{x^1 h^T_{\mu\nu} + 2x^2 \nabla_{(\mu} h^V_{\nu)} + x^3 \nabla_{\mu\nu} h^S + x^4 g_{\mu\nu} h^S\} \\ \delta\phi^i &= \sum_{\text{modes}} x^5 h^S, \end{aligned} \quad (3.94)$$

where  $\nabla_{\mu\nu} = \nabla_\mu \nabla_\nu - \frac{1}{4} g_{\mu\nu} \nabla^2$ . In the ghost and gauge sector, there is a similar decomposition,

$$c_\mu = \sum_{\text{modes}} \{y^1 h^V_\mu + y^2 \nabla_\mu h^S\}. \quad (3.95)$$

The eigenvalues of the derived modes change due to non-commutation of the covariant derivatives, for example

$$-\nabla^2 (\nabla_{(\mu} h^V_{\nu)}) = (\lambda_V - \frac{5}{12} R) \nabla_{(\mu} h^V_{\nu)} \quad (3.96)$$

The derived modes are not normalised, but their normalisation can be deduced from the original harmonic, for example

$$4 \int \nabla_{(\mu} h^V_{\nu)} \nabla^{(\mu} h^V_{\nu)} |g|^{1/2} d^4x = 2 (\lambda_V - \frac{1}{4} R). \quad (3.97)$$

The action of the operators and products in the harmonic basis, for a given set of eigenvalues, can be represented now by  $5 \times 5$  matrices, for the full field space, and  $2 \times 2$  matrices for the induced gauge-subspace metric, as defined in (3.26).

The eigenvalues of the matrix  $\Delta = \Pi(-\nabla^2 + E)\Pi$  and the ghost matrix  $Q$  are used to obtain the zeta functions needed for the heat kernel methods in the next section and, consequently, the beta functions. These matrices are given explicitly, albeit with the inclusion of only those terms from the expansion of the non-minimally coupling that are relevant in our approximation, as in (3.87).

The Laplacian,

$$(-\nabla^2)^{IJ} = \begin{pmatrix} \lambda_T & 0 & 0 & 0 & 0 \\ 0 & \lambda_V - \frac{5}{12}R & 0 & 0 & 0 \\ 0 & 0 & \lambda_S - \frac{2}{3}R & 0 & 0 \\ 0 & 0 & 0 & \lambda_S & 0 \\ 0 & 0 & 0 & 0 & \lambda_S \end{pmatrix}. \quad (3.98)$$

The field-space metric (3.82),

$$\mathcal{G}_{IJ} = \begin{pmatrix} U & 0 & 0 & 0 & 0 \\ 0 & 2U(\lambda_V - \frac{1}{4}R) & 0 & 0 & 0 \\ 0 & 0 & \frac{3}{4}U\lambda_S(\lambda_S - \frac{1}{3}R) & 0 & 0 \\ 0 & 0 & 0 & -4U & -2\kappa U' \\ 0 & 0 & 0 & -2\kappa U' & K + \frac{1}{2}\kappa^2 U'^2/U \end{pmatrix}. \quad (3.99)$$

The non-covariant mass matrix (3.74), writing  $m_T^2 = \frac{2}{3}UR - 2\kappa^2V$ ,

$$E_{gIJ} = \begin{pmatrix} m_T^2 & 0 & 0 & 0 & 0 \\ 0 & 2m_T^2(\lambda_V - \frac{1}{4}R) & 0 & 0 & 0 \\ 0 & 0 & \frac{3}{4}m_T^2\lambda_S(\lambda_S - \frac{1}{3}R) & 0 & 0 \\ 0 & 0 & 0 & 8\kappa^2V & 4\kappa V' \\ 0 & 0 & 0 & 4\kappa V' & V'' - \frac{1}{2\kappa^2}RU'' \end{pmatrix}. \quad (3.100)$$

The covariant mass matrix including the connection terms (3.87),

$$E_{IJ} = \begin{pmatrix} m_T^2 & 0 & 0 & 0 & 0 \\ 0 & 2m_T^2(\lambda_V - \frac{1}{4}R) & 0 & 0 & 0 \\ 0 & 0 & \frac{3}{4}m_T^2\lambda_S(\lambda_S - \frac{1}{3}R) & 0 & 0 \\ 0 & 0 & 0 & 8\kappa^2V & 2\kappa V' + \kappa^{-1}RU' \\ 0 & 0 & 0 & 2\kappa V' + \kappa^{-1}RU' & M^2 \end{pmatrix}, \quad (3.101)$$

where  $M^2 = V'' - 2\kappa^2KV + \frac{1}{2}KUR - 2VU''$ .



The gauge transformation matrix

$$\mathcal{R}^I{}_\alpha = \begin{pmatrix} 0 & 0 \\ 1 & 0 \\ 0 & 2 \\ 0 & -\frac{1}{2}\lambda_S \\ 0 & 0 \end{pmatrix}. \quad (3.102)$$

The (unnormalised) pure-gauge projector (3.76),  $P^I{}_J = \mathcal{G}^{IK} P^{\alpha\beta}{}_{KJ} \nabla_\alpha \nabla_\beta$ ,

$$P^I{}_J = \mathcal{R}^I{}_\alpha \mathcal{R}^{\alpha}{}_J = \begin{pmatrix} 0 & 0 & 0 & 0 & 0 \\ 0 & \lambda_V - \frac{R}{4} & 0 & 0 & 0 \\ 0 & 0 & \frac{3}{2}(\lambda_S - \frac{R}{3}) & 2 & 0 \\ 0 & 0 & -\frac{3}{8}\lambda_S(\lambda_S - \frac{R}{3}) & -\frac{\lambda_S}{2} & 0 \\ 0 & 0 & 0 & 0 & 0 \end{pmatrix}. \quad (3.103)$$

The diagonalisation of which, is

$${}_D P^I{}_J = \begin{pmatrix} 0 & 0 & 0 & 0 & 0 \\ 0 & \lambda_V - \frac{R}{4} & 0 & 0 & 0 \\ 0 & 0 & \lambda_S - \frac{R}{2} & 0 & 0 \\ 0 & 0 & 0 & 0 & 0 \\ 0 & 0 & 0 & 0 & 0 \end{pmatrix}. \quad (3.104)$$

The gauge-fixed direction projection matrix,  $\Pi^I{}_J = \delta^I{}_J - \mathcal{R}^I{}_\alpha \mathcal{N}^{\alpha\beta} \mathcal{R}_{J\beta} = \delta^I{}_J - [{}_D P^{-1}]^I{}_K P^K{}_J$ ,

$$\Pi^I{}_J = \frac{1}{\lambda_S - \frac{1}{2}R} \begin{pmatrix} \lambda_S - \frac{1}{2}R & 0 & 0 & 0 & 0 \\ 0 & 0 & 0 & 0 & 0 \\ 0 & 0 & -\frac{1}{2}\lambda_S & -2 & 0 \\ 0 & 0 & \frac{3}{8}\lambda_S(\lambda_S - \frac{1}{3}R) & \frac{3}{2}(\lambda_S - \frac{1}{3}R) & 0 \\ 0 & 0 & 0 & 0 & \lambda_S - \frac{1}{2}R \end{pmatrix}. \quad (3.105)$$

The ghost operator,

$$Q^\alpha{}_\beta = \mathcal{R}^{I\alpha} \mathcal{R}_{I\beta} = \begin{pmatrix} \lambda_V - \frac{1}{4}R & 0 \\ 0 & \lambda_S - \frac{1}{2}R \end{pmatrix}. \quad (3.106)$$

The ghost metric as defined in (3.35) is obtained, following [92], as the coefficient of the highest derivative term in the ghost Lagrangian,

$$\gamma_{\alpha\beta} = \begin{pmatrix} 2U & 0 \\ 0 & 2U\lambda_S \end{pmatrix}. \quad (3.107)$$

Hence, it is shown that the non-trivial eigenvalues of (3.104) and those of the ghost

operator (3.106) are identical. This property was used in (3.3.4) in order to establish the equivalence of the two expressions of the one-loop effective action (3.35) and (3.36).

Here, we would like to stress an important point. The matrices  $\mathcal{D}_I \mathcal{D}_J (S_E + S_{gf})$  are not positive definite, since the field-space metric  $G_{IJ}$  is not, so there are directions which decrease the Euclidean action and invalidate the path integral approach. This is the famous conformal mode problem of Euclidean quantum gravity. However, the matrices representing  $\Pi \mathcal{D}_I \mathcal{D}_J S_E \Pi$ , and  $\mathcal{D}_I \mathcal{D}_J (S_E + S_{gf})$  for sufficiently large  $\lambda_g$ , are both positive definite and the path integral can be defined. This is the solution to the conformal mode problem of Euclidean quantum gravity referred to in Ref. [120].

### 3.7 Gravity-Higgs $\beta$ -functions

The renormalisation scale dependence of the one-loop effective action (C.9) can be calculated in two different ways, and the comparison gives a check on the accuracy of the result. The first way is by gauge decomposition,

$$\mu_R \frac{d\Gamma_E^{(1)}}{d\mu_R} = -\zeta(0, \Pi(\mathcal{D}^I \mathcal{D}_J S)\Pi) + \zeta(0, \mathcal{R}^{I\alpha} \mathcal{R}_{I\beta}). \quad (3.108)$$

The second version is in Landau gauge (3.38),

$$\mu_R \frac{d\Gamma_E^{(1)}}{d\mu_R} = \lim_{\lambda_g \rightarrow \infty} \left\{ -\zeta(0, \mathcal{D}^I \mathcal{D}_J S + \lambda_g R^{I\alpha} R_{J\alpha}) + 2\zeta(0, \lambda_g^{1/2} \mathcal{R}^{I\alpha} \mathcal{R}_{I\beta}) \right\}. \quad (3.109)$$

In each case, the eigenvalues, which are the same for either method, are evaluated by diagonalising the matrices and can be associated (see Appendix C) with the generalised zeta functions, which are defined for  $s > 2$  by the series,

$$\zeta(s, A) = \sum_{\lambda} \lambda^{-s}. \quad (3.110)$$

Spherical harmonic eigenvalues are all quadratic polynomials in a single ‘angular momentum’ index  $n$ . After diagonalisation, the operator eigenvalues are algebraic functions of the spherical harmonic eigenvalues, but standard zeta-function methods can be modified to analytically continue and evaluate  $\zeta(0, A)$  [128].

We will use the transverse-traceless tensor sector  $I = J = 1$  as an example to showcase the methodology followed and obtain  $\zeta(0, \Pi D^I{}_J \Pi)$ , for each component of the gravity-scalar and ghost Lagrangians. Hence, the first eigenvalue of the operator  $\Delta = \Pi(-\nabla^2 + E)\Pi$ , which involves the transverse-traceless tensor term in the Laplacian (3.98), using the inverse of the field-space metric (3.99) to raise the indices of the covariant mass matrix (3.101), is given as

$$\lambda_1 = \lambda_T + U^{-1} m_T^2. \quad (3.111)$$

The tensor eigenvalues are given in appendix C, and after analytic continuation using

(C.19), we find

$$\zeta(0, (\mathcal{D}^2 S)^1_1) = -\frac{1}{18} + 20 \frac{m_T^2}{UR} + 60 \frac{m_T^4}{U^2 R^2}. \quad (3.112)$$

Contributions to the beta-functions from the transverse-traceless tensors can be obtained, following (3.2), using (3.91) from (C.10),

$$\mu_R \frac{d\mathcal{L}_E^{(1)}}{d\mu_R} = -\frac{b_2}{16\pi^2}, \quad (3.113)$$

where the contribution to the adiabatic expansion coefficient  $b_2$  from the transverse-traceless modes can be extracted from (3.39)

$$b_2^T = \frac{16\pi^2}{\text{Volume } S_4} \zeta(0, (\mathcal{D}^2 S)^1_1) = \frac{R^2}{24} \zeta(0, (\mathcal{D}^2 S)^1_1). \quad (3.114)$$

After substituting for  $m_T^2$ , see above (3.100), the tensor mode contribution to  $b_2$  becomes

$$b_2^T = \frac{719}{432} R^2 - \frac{25}{3} \frac{\kappa^2 R V}{U} + 10 \frac{\kappa^4 V^2}{U^2}. \quad (3.115)$$

Similarly, one computes the adiabatic expansion coefficient contributions for the rest of the vector and scalar modes and ghosts and, using (3.2), obtains the associated  $\beta$ -functions.

For example, with  $U = 1 - \xi \kappa^2 \phi^2$ , we have a contribution to  $\beta_\xi$  from expanding the second term of (3.115) in powers of  $\kappa$ ,

$$\beta_\xi - 2\gamma_\phi \xi - \gamma_g \xi = 2 \text{coeff}(b_2, R\phi^2) = \frac{50}{3} \kappa^4 V_0 + O(\kappa^6). \quad (3.116)$$

Other contributions to the beta functions can be obtained in a similar way from the matrices given in (3.6) and the interested reader is directed to Appendix C.

We will, now, give results for the contributions to the beta functions from the Higgs background direction, and the gravitational sector with which it mixes.

	Jordan frame	Einstein frame
$16\pi^2 \beta_\xi$	$(6\xi - 1)\lambda$	$-\lambda$
$16\pi^2 \beta_{\mu^2}$	$6\mu^2 \lambda$	$6(\mu^2 + 4\xi \kappa^2 V_0)\lambda$
$16\pi^2 (\beta_{\mu^2} + 4\kappa^2 V_0 \beta_\xi)$	$6(\mu^2 + 4\xi \kappa^2 V_0)\lambda - 4\lambda \kappa^2 V_0$	$6(\mu^2 + 4\xi \kappa^2 V_0)\lambda - 4\lambda \kappa^2 V_0$
Covariant		
$16\pi^2 \beta_\xi$	$2\lambda$	
$16\pi^2 \beta_{\mu^2}$	$6(\mu^2 + 4\xi \kappa^2 V_0)\lambda - 12\lambda \kappa^2 V_0$	
$16\pi^2 (\beta_{\mu^2} + 4\kappa^2 V_0 \beta_\xi)$	$6(\mu^2 + 4\xi \kappa^2 V_0)\lambda - 4\lambda \kappa^2 V_0$	

Table 3.2:  $\beta$ -functions for the curvature coupling and the mass of a gravity coupled scalar field at leading order for small  $\kappa^4 V_0$ . The Jordan frame result has been calculated directly from the original action. The Einstein frame result is obtained by transforming the action to the Einstein frame. The covariant result uses a geodesic expansion in field space and is independent of the frame used. The renormalisation group flow of the effective mass,  $\mu^2 + 4\kappa^2 V_0 \xi$ , is the same for each of these approaches.

	Jordan frame	Covariant
$16\pi^2\beta_\lambda$	$18\lambda^2$	$18\lambda^2$
$16\pi^2\beta_6$	$90\lambda\lambda_6 - 18\lambda^2(2 - 8\xi + 18\xi^2)$	$90\lambda\lambda_6 - 18\lambda^2(1 - 7\xi + 24\xi^2)$
$16\pi^2\gamma_g$	$-\frac{1}{3}\kappa^2\mu^2 + 2\kappa^2(\mu^2\xi - 4\kappa^2V_0)$	$\frac{2}{3}(\mu^2 + 4\xi\kappa^2V_0)\kappa^2 - \frac{52}{3}\kappa^4V_0$

Table 3.3:  $\beta$ -functions for the quartic scalar self-coupling  $\lambda$  and the sixth order scalar self-coupling  $\lambda_6$  of a gravity coupled scalar field at leading order for small  $\kappa^4V_0$ . The wave function renormalisation of the metric,  $\gamma_g$ , is given at order  $\kappa^4V_0$ . The Jordan frame results have been calculated directly from the original action. The Einstein frame results are obtained by transforming the action to the Einstein frame. The covariant result uses a geodesic expansion in field space and is independent of the frame used.

A few comments are in order. Tables 3.2 and 3.3 show results at leading order for small  $\kappa^4V_0$ , assuming that the curvature  $R$  and the mass squared  $\mu^2$  are of order  $\kappa^2V_0$ . These choices are well-motivated in inflationary energy scales, considering the curvature of the -de Sitter- universe,  $R \approx 4\kappa^2V_0$ , and where the Higgs mass is negligible. Contributions to the beta functions from the gravitational perturbations, like the transverse traceless tensor modes discussed above, enter only at order  $\kappa^4V_0$ , in agreement with the conclusion of Ref. [101]. However, quantum gravitational corrections do have an effect at leading order through the Vilkovisky-DeWitt connection terms, in the operators.

The first thing to notice in Table 3.2 is the absence of  $\xi$  terms for  $\beta_\xi$  in the Einstein frame and the covariant results. The reason for this, in the Einstein frame, is obvious since the  $\xi R\phi^2$  term has been eliminated by the conformal transformation, and  $\xi$  appears in the Einstein frame scalar potential  $V_J/U^2$  instead. The absence of  $\xi$ , in the covariant results, follows from the beta-function relations (3.60)-(3.62). In the explicit calculation, the leading order contribution to  $\beta_\xi$  from  $RU''$ , in the mass matrix (3.101), cancels with the Vilkovisky-DeWitt correction.

In Table 3.2 we see that the renormalisation group flow of  $\mu^2 + 4\kappa^2V_0\xi$ , is the same in all the different approaches. In the relevant energy range, in de Sitter,  $R \approx 4\kappa^2V_0$ , and the effective square mass of the Higgs field  $\mu^2 + \xi R \approx \mu^2 + 4\kappa^2V_0\xi$ . This is the crucial combination, with a covariant meaning, for addressing questions regarding physical observables.

The non-covariant formulation in the Jordan or the Einstein frame therefore gives the same outcome for the effective mass renormalisation group flow, as the covariant formalism, at least for small values of  $\kappa^4V_0$ .

### 3.8 Gauge Bosons, Goldstone Modes and Fermions

Having obtained the one-loop effective potential contributions from the Gravity-Higgs sector of the action, we proceed with the inclusion of results for the gauge boson, Goldstone mode and fermion contributions to the effective action for the scalar field on a curved spacetime background. These computations go beyond the topic of this thesis (the inter-

ested reader is advised to review the relevant section of [2] and references therein). This subsection is included for completeness and the results are quoted from existing literature [121, 129]. In this case, there are no background gauge fields and the gauge modes decouple from the graviton and scalar modes of the previous section. Quantum gravity still has an effect via the Vilkovisky-DeWitt connection term. Irrespective of the computation frame, the beta function results can be translated between the Jordan and the Einstein frame using the beta-function relations (3.60)-(3.62).

The gauge-Goldstone mode Lagrangian, which we use is

$$\mathcal{L}_g = -\frac{1}{4}F_{a\mu\nu}F^{a\mu\nu}|g|^{1/2} - \frac{1}{2}\delta_{ij}^\perp(D_\mu\phi)^i(D^\mu\phi)^j|g|^{1/2} - V(\phi)|g|^{1/2}, \quad (3.117)$$

where  $D_\mu\phi = \nabla_\mu\phi - gA_{a\mu}T^a\phi$  is the spacetime-gauge group covariant derivative [121], with  $T^a = \sigma^a/2$  the SU(2) symmetry generators involving the Pauli matrices  $\sigma^a$ , and  $\delta_{ij}^\perp$  is orthogonal to the background Higgs direction used in the previous section, as in (3.52).

In the covariant approach, there are connection terms in the differential operator  $\mathcal{D}_I\mathcal{D}_J S$  because the field-space metric  $\mathcal{G}_{IJ}$  depends on the spacetime metric, leading to a connection coefficient  $\Gamma^K_{IJ}$ , with  $K$  in the metric direction. The contribution to the operator is  $E_{\Gamma IJ} = \Gamma^K_{IJ}\partial_K S$ ,

$$E_{\Gamma IJ} = \begin{pmatrix} -G_{\mu\nu} - \kappa^2 V g_{\mu\nu} & 0 \\ 0 & \frac{1}{2}(R - 4\kappa^2 V) \end{pmatrix} |g|^{1/2}, \quad (3.118)$$

where  $G_{\mu\nu} + \kappa^2 V g_{\mu\nu} = 0$  is the Einstein equation when  $\phi$  is constant.

The scaling behaviour of the one-loop action can be found as before by taking the spacetime background to be the Euclidean four-sphere. An important new consideration, for the gauge boson beta-functions, is the Higgs field wave function renormalisation at one-loop,

$$16\pi^2\gamma_\phi = -\frac{3}{4}g_{\text{tot}}^2 + O(\kappa^4 V_0), \quad (3.119)$$

where  $g_{\text{tot}}^2 = 3g^2 + g'^2$ . We note that the inclusion of the wave function renormalisation which, unlike the Gravity-Higgs case, here enters at order  $\mathcal{O}(\kappa^0)$  resulting in the  $\xi$  dependence in  $\beta_\xi$  in Table 3.3. The leading term is simply the flat space result in Landau gauge.

Results are given in Tables 3.4 and 3.5. The covariant  $\beta$ -functions are independent of frame, and differ from the non-covariant expressions. As before, the two approaches agree for the effective square mass,  $\mu^2 + 4\kappa^2 V_0 \xi$ . There are differences in the sixth order coupling  $\lambda_6$ , but this only enters the Higgs field equations at  $O(\kappa^4 V_0)$ . Therefore, we conclude that the covariant 1-loop effective Higgs potential, at leading order and for small  $\kappa^4 V_0$ , and its non-covariantly computed counterpart lead to the same physical observables.

Jordan frame	
$16\pi^2\beta_\xi$	$-\frac{1}{4}(6\xi - 1)g_{\text{tot}}^2 + (6\xi - 1)\lambda$
$16\pi^2\beta_{\mu^2}$	$-\frac{1}{2}\mu^2 g_{\text{tot}}^2 + 6\lambda\mu^2$
$16\pi^2(\beta_{\mu^2} + 4\kappa^2 V_0\beta_\xi)$	$[6\mu_E^2 - 4\kappa^2 V_0]\lambda - \frac{1}{2}[\mu_E^2 - 2\kappa^2 V_0]g_{\text{tot}}^2$
Covariant	
$16\pi^2\beta_\xi$	$-\frac{1}{4}(6\xi - 4)g_{\text{tot}}^2 + 2\lambda$
$16\pi^2\beta_{\mu^2}$	$-\frac{1}{2}[\mu^2 - (8\xi - 6)\kappa^2 V_0]g_{\text{tot}}^2 + 6[\mu^2 + (4\xi - 2)\kappa^2 V_0]\lambda$
$16\pi^2(\beta_{\mu^2} + 4\kappa^2 V_0\beta_\xi)$	$[6\mu_E^2 - 4\kappa^2 V_0]\lambda - \frac{1}{2}[\mu_E^2 - 2\kappa^2 V_0]g_{\text{tot}}^2$

Table 3.4: W and Z vector boson contributions to the  $\beta$ -functions for the curvature coupling and the mass of a gravity-coupled scalar field at leading order in  $\kappa^4 V_0$ . The Jordan frame result has been calculated directly from the original action. The covariant result uses a geodesic expansion in field space and is independent of the frame used. The renormalisation group flow of  $\mu_E^2 = \mu^2 + 4\kappa^2 V_0 \xi$  is the same for each of these approaches.

	Jordan frame	Covariant
$16\pi^2\beta_\lambda$	$6\lambda^2 - \lambda g_{\text{tot}}^2 + \frac{3}{8}\sum g^4$	$6\lambda^2 - \lambda g_{\text{tot}}^2 + \frac{3}{8}\sum g^4$
$16\pi^2\beta_6$	$18\lambda\lambda_6 - \frac{3}{2}\lambda_6 g_{\text{tot}}^2$	$18\lambda\lambda_6 - \frac{3}{2}\lambda_6 g_{\text{tot}}^2 + 3\xi\lambda g_{\text{tot}}^2 - \frac{9}{4}\lambda g_{\text{tot}}^2 + 9(2\xi - 1)\lambda^2$
$16\pi^2\gamma_g$	$(6\xi - 1)\kappa^2\mu^2$	$2\kappa^2\mu_E^2 - \frac{23}{2}\kappa^4 V_0$

Table 3.5: W and Z vector boson contributions to the  $\beta$ -functions for the quartic scalar self-coupling,  $\lambda$ , and the sixth order scalar self-coupling,  $\lambda_6$ , of a gravity-coupled scalar field at leading order in  $\kappa^4 V_0$ . The metric wave function anomalous dimension is given to order  $\kappa^4 V_0$ . The covariant result uses a geodesic expansion in field space and is independent of the frame used.

The core of the covariant formalism lies in the treatment of the fields that describe the system in question as coordinates on a manifold. Hence, the requirement of symmetry under field redefinitions is translated to diffeomorphism invariance of the field space and differential geometry provides the technology that permits the formulation of theories with actions that are manifestly reparametrization invariant. This is possible when only bosonic degrees of freedom are included, as in the case of the gravity-scalar action. The generalisation of the covariant approach to fermion fields, however, is highly non-trivial due to mathematical description of fermionic fields, namely their anticommutativity and their equations of motion. The former property requires that the field manifold must be generalised to a supermanifold, namely one in which (some of) the coordinates are Grassmanian. The latter relates to the fact that the equations of motion for fermionic fields are first order - in contrast with the Klein-Gordon equation of the scalar fields. Furthermore, as shown in Appendix B, the equation of motion of free bosonic degrees of freedom constitutes the geodesic deviation equation of the induced space. Hence, one is motivated to introduce a different definition for the metric of a space that includes fermionic fields and a radically different treatment is, therefore, necessary. The interested

reader is referred to [121] for a detailed exposition of the treatment of fermion fields in curved spacetime and to [130] and references therein, for a frame-covariant approach and details on the supermanifold structure. Here, we take the minimalist approach and leave off any extra contributions to the effective action that originate from the inclusion of fermionic degrees of freedom. The results are then checked for consistency against the covariant beta function relations (3.60)-(3.62).

The wave-function renormalisation at one-loop is  $16\pi^2\gamma_\phi = 3y^2$ . The beta functions are quoted from pre-existing literature [131], but we repeat them here for completeness. Using the renormalisation group equation (3.2) we obtain,

$$16\pi^2\beta_\xi = (6\xi - 1)y^2, \quad 16\pi^2\beta_{\mu^2} = 6y^2\mu^2, \quad 16\pi^2\beta_\lambda = -6y^4 + 12\lambda y^2. \quad (3.120)$$

There is no contribution to  $\beta_6$  and  $\gamma_g$  at one-loop order.

### 3.9 The Gravity-Scalar Running Couplings

We return to (3.51) and (3.53) and truncate them to  $O(\kappa^2)$ , remembering that the sixth order coupling enters the Higgs field equations at  $O(\kappa^4)$ . In particular, we take

$$V_{\text{eff}}^{O(\kappa^2)} = \frac{1}{2}\mu_{\text{eff}}^2(\phi)\phi^2 + \frac{1}{4}\lambda_{\text{eff}}(\phi)\phi^4, \quad (3.121)$$

where the effective mass is given by the combination  $\mu_{\text{eff}}^2 = \mu^2 + 12\xi H^2$ . The effective couplings are obtained by solving the renormalisation group equations (3.3). It is worth noting that despite the fact that the effective potential is independent of the renormalisation group scaling parameter  $\mu_R$ , the 1-loop approximation is not. This leads to the need to establish a criterion for the appropriate definition of the renormalisation scale [132] and one such criterion has been suggested in [133], and further implemented in [121]. It defines  $\mu_R$  implicitly, such that the one-loop correction to the *Renormalisation Group Improved* effective potential vanishes. Furthermore, it has been proposed (see [79] and references therein) that a simple definition that takes into account the non-trivial space-time curvature,

$$\mu_R = a\phi^2 + bR \quad (3.122)$$

with  $a, b$  constants, despite not leading to the cancellation of the one-loop logarithms in the RGI, offers computational advantages. In this work, in order to retain familiarity with standard renormalisation group methods [93], we have simply chosen  $\mu_R = \phi$  and not included these recent results. In a completely covariant treatment, one should treat the renormalised field as a non-linear mapping into field space  $\phi_R = \phi_R(\phi, \mu_R)$  taking into account the appropriate, for a curved space-time background, definition for  $\mu_R$ .

Initial conditions for the running couplings are set at some chosen point. We take this point to be  $\phi = 170\text{GeV}$ , close to the top quark mass. Combining the results from the tables of beta functions and replacing the vacuum energy by the expansion rate,  $H$ , gives

$$16\pi^2 \frac{d\mu_{\text{eff}}^2}{dt} = 12 (\mu_{\text{eff}}^2 - 2H^2) \lambda - \frac{1}{2} (\mu_{\text{eff}}^2 - 6H^2) g_{\text{tot}}^2 + 6 (\mu_{\text{eff}}^2 - 2H^2) y^2. \quad (3.123)$$

The value of the Gravity-Higgs coupling is known from experiments at energies less than 1TeV. The best available values of the Higgs and top quark masses imply that  $\lambda(170\text{GeV}) = 0.12577$  [74]. These experiments are, essentially, at zero vacuum energy  $V_0 \approx 0$ , but since there is no dependence on the vacuum energy  $V_0$  in  $\beta_\lambda$ , we can take the experimental values over to the early universe where  $V_0$  is large.

The value of  $\mu^2$  for the Higgs field, as determined in the laboratory, is negligible compared to the value of  $\xi R$  in the inflationary universe, but here we have to take care because of subtleties in the properties of light fields in de Sitter space [134]. We already see a hint of this in the covariant beta-function, which is large, of order  $H^2/3$ . In the Euclidean approach to quantum field theory, the infrared problems lead to a breakdown of perturbation theory (as shown in (1.58)) for  $\mu_{\text{eff}}^2 \lesssim \lambda^{1/2} H^2$  [117], so our treatment will only be valid above this bound. Stochastic approximations imply that the light Higgs field develops a mass  $\mu_{\text{eff}}^2 \approx 0.3534 \lambda^{1/2} H^2$  [47, 46, 52, 117]. If we assume  $\mu^2(170\text{GeV}) \ll H^2$ , then a lower limit for de Sitter space of  $\xi(170\text{GeV}) > 0.029 \lambda^{1/2}$  is set. We can say nothing about curvature couplings smaller than this, because the techniques required for dealing with loop corrections with smaller effective mass scales are quite different from the ones we use here [134, 135].

The effective couplings, using (3.123), are plotted in Figure 3.1. The standard model couplings  $\lambda$ ,  $g$ ,  $g'$  and  $y$  have been evolved simultaneously using the two-loop flat space  $\beta$ -functions given in [77]. The value of the top quark mass,  $m_t$ , sets the scale of the Yukawa coupling  $y$  and this has a significant effect on the running of the Higgs self-coupling,  $\lambda$ , and the value of the field where it vanishes. The location of the point  $\lambda = 0$  is not fixed very accurately by the renormalisation group corrected potential; including other two-loop effects results in raising  $\lambda(170\text{GeV})$  by 0.2%.

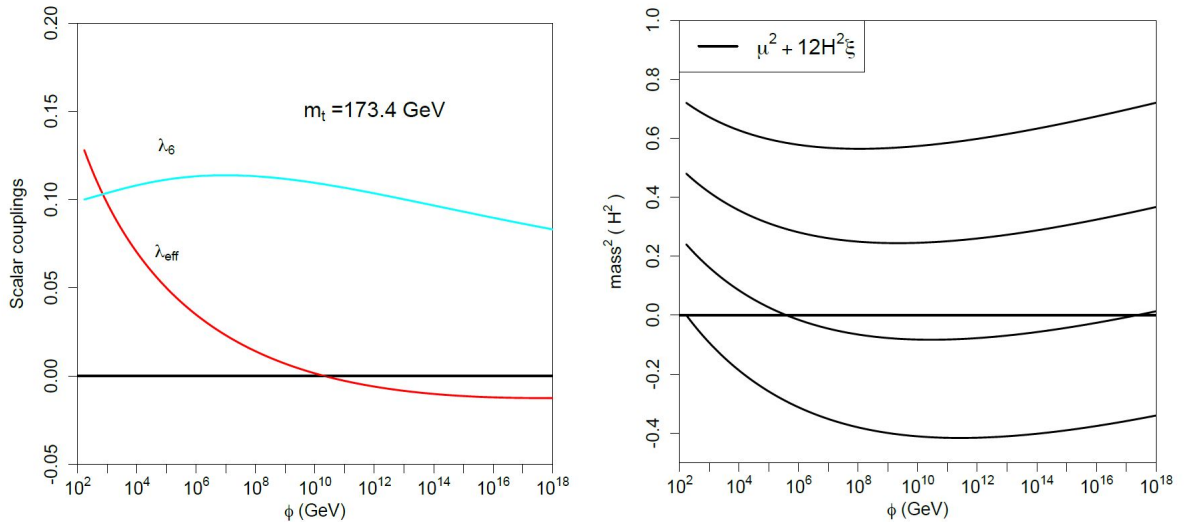


Figure 3.1: On the left, running couplings  $\lambda$  and  $\lambda_6$  (which appears as an  $O(\kappa^4)$  correction in  $V_{\text{eff}}$ ), with  $m_t = 173.4\text{GeV}$ . On the right, the effective mass squared  $\mu_{\text{eff}}^2 = \mu^2 + 12H^2\xi$ . The initial conditions are  $\lambda(170\text{GeV}) = 0.128$ ,  $\lambda_6(170\text{GeV}) = 0.1$  and  $\mu^2(170\text{GeV}) = 0$ .



The determination of the running couplings permits the description of the dependence of the one-loop effective potential on the Higgs field value  $\phi$ . Depending on the value of the curvature coupling parameter,  $\xi$ , the potential exhibits a substantially different field dependence, manifested in Figure 3.2.

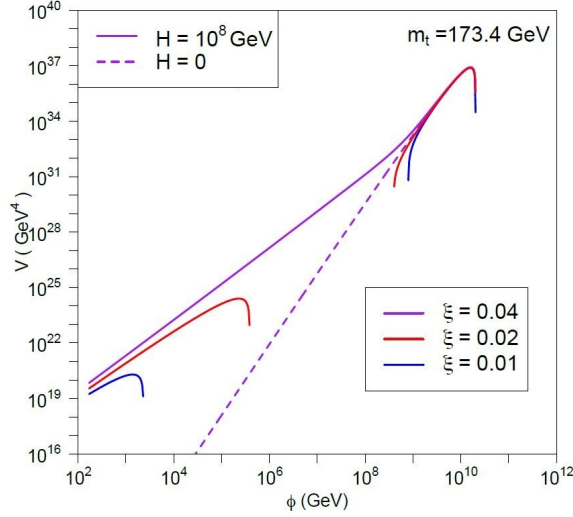


Figure 3.2: The effective Higgs potential plotted as a function of the Higgs field for  $\mu^2 = 0$  and a range of curvature coupling,  $\xi$ , values at  $170\text{GeV}$ . There is a single maximum for large expansion rate,  $H$ , or curvature coupling,  $\xi$ , but new maxima and minima appear for small values of  $H$  and  $\xi$ .

Note that for small initial values, the effective mass becomes negative at Higgs field values below the Planck scale. This can further alter the shape of the Higgs potential and can even give rise to a second maximum. This is illustrated by the potential plots in Figure 3.2. A combination of small initial  $\mu_{\text{eff}}^2$  and small expansion rate  $H$  leads to twin maxima. It is sometimes possible for the Higgs field to tunnel to the lower maximum, roll down the potential, and then tunnel up to the larger maximum. This combination is less likely than the single tunnelling event, however, for small curvature coupling, the field could become trapped between the two maxima during inflation, and return to the present vacuum state after inflation.

The determination of physical observables, depending on the effective potential (e.g. the stability of Higgs vacuum) is independent of the conformal frame. This is the main result of this work.

### 3.10 Conclusion and Motivation for Further Work

The Gravity-Higgs action provides an exciting laboratory for trying out ideas in (effective) quantum gravity. One of the issues quantum gravity raises is how to define the spacetime geometry when scalar and metric backgrounds are allowed to mix freely. We presented a methodology that is fully covariant under such field redefinitions (and has, subsequently, been explored further in [136]) and remarked its applicability. This description allows a complete physical equivalence between the different conformal frames. On the other hand, non-covariant approaches can still lead to correct results, on scales below the Planck mass, as long as appropriate care is taken. Our analysis has led us to advocate the use of the effective mass  $\mu^2 + \xi R$ , since it is a combination that has a covariant meaning, and then the simpler Einstein frame can always be used.

In particular, we have found that it is always possible to work consistently in a frame in which the curvature coupling vanishes. The dependence on the curvature coupling in other frames can be recovered from relations like those given, for the beta function, in section 3.4.2.

In one respect, the approach adopted, here, has not been as general as it could, and maybe should, be. The covariant effective action has been used, but field redefinitions have not been fully integrated with the renormalisation group. In a fully general treatment, the renormalised field  $\phi_R = Z(\mu_R)\phi$  should become a non-linear mapping into field space,  $\phi_R = \phi_R(\phi, \mu_R)$ , with  $\mu_R$  taken appropriately for a curved background consideration. We have not attempted this, in order to retain as much familiarity with conventional renormalisation group methods as possible.

Furthermore, at the end of (3.4.1) we commented on the couplings  $\alpha$  and  $\beta$  in the kinetic terms. Those proved to not contribute in the approach followed here, which focused on the treatment of the effective potential. Their contribution to the heat kernel coefficients is expected to shift the numerical results, when the entirety of the one-loop effective action is taken into account.

Finally, we should point out that we have used existing non-covariant results for the standard model beta functions, which are not associated with the spacetime curvature. This could cause problems if the running couplings depend on gauge parameters. In fact, the ‘ $g^2\lambda$ ’ terms in  $\beta_\lambda$  are dependent on gauge parameters [137]. The field value at which the quartic Higgs coupling becomes negative is not protected by any Nielsen identities and may well be gauge parameter dependent. We leave such investigations as a potential future research project.

## Chapter 4. Observational Constraints on Hyperinflation

### 4.1 Overview of the Chapter

In this chapter, we turn our attention to a topical variant of multifield inflation, namely Hyperinflation, and investigate the constraints on the model's parameters placed by observations.

We draw inspiration from the numerous multifield inflation models and thoroughly examine the background field evolution and the linearised perturbations of a model with a two-dimensional hyperbolic field-space and an exponential potential that admits a scaling solution. We start by reviewing the background dynamics and manifestly showcase the parameter values for which the gradient and hyperbolic solutions are stable and unstable. We then obtain the evolution for the linear perturbations of the fields and numerically evaluate the power spectrum and the spectral index for a range of values of the geometrically normalised Killing direction velocity,  $y$ , of the hyperbolic solution. We find that observational results place tight bounds on its permissible values within the narrow region of  $0.74 \times 10^{-2} \leq y \leq 0.94 \times 10^{-2}$  and  $0.1603 \leq y \leq 0.1774$ , corresponding to a very narrow range of admissible potential slopes  $0.54 \times 10^{-4} \leq p - 3 \leq 0.88 \times 10^{-4}$  and  $0.025 \leq p - 3 \leq 0.031$ . Ultimately, working in the small  $\epsilon_H$  regime we find that there is a maximal value for the slow-roll parameter allowed by observations.

We close by motivating the use of the obtained potential bounds in order to obtain the stochastic Langevin equation for both field-space directions, which will permit the computation of arbitrary N-point functions in the large-wavelength limit and any potentially emerging non-Gaussianities (preliminary work for which has been included in Appendix D).

### 4.2 The Motivation for Multifield Inflation

Since its inception, Inflation [11–13] has been extensively tested both theoretically and observationally. The model's striking successes, but also its shortcomings, have resulted in a multitude of subsequent developments in model building, starting from single-field slow-roll chaotic inflation [138] (for an excellent review, see [17]) to more complex multifield models [139–142].

On physical grounds, extended research on multifield inflation models was motivated in the late '90s and early '00s [25, 143–145], due to the expectation that advanced observational probes [23, 28, 146] would detect signals indicating the existence of isocurvature

perturbations and non-Gaussianity in the primordial universe.

On theoretical grounds, one of the most sought-after objectives, recently, has been the embedding of the inflationary scenario, as an effective low energy limit, in a more fundamental high energy theory - such as String Theory [19, 147]. Recent investigations have resulted in de Sitter space being excluded as a String Theory vacuum [148], placing single-field slow-roll inflationary models in the Swampland [149–151], with the subsequent introduction of the corresponding Conjectures [37, 148]. These considerations indicated that the Swampland constraints would favour multifield inflationary models with potentially non-trivial kinetic terms [38, 39].

#### 4.2.1 *Hyperinflation*

A model dubbed Hyperinflation [152] has become topical in recent years due to its capacity to evade the Swampland while making predictions in agreement with observations. In its introduction, Brown presents the model and its connection to Spinflation [139], showcasing how Hyperinflation can produce a large number of e-folds, even for steep potentials, therefore relaxing the constraint for a slow-roll regime. Furthermore, the model is demonstrated to have the ability to seed the observed Large Scale structure through adiabatic perturbations, all the while motivating the existence of Hyperinflation signatures, in the form equilateral non-Gaussianity. These qualitative statements were detailed quantitatively in [153], and both the background and perturbation dynamics of the fields were studied, resulting in analytical expressions for cosmological parameters being presented in the slow-varying approximation. More recently, Hyperinflation was generalised to models with an arbitrary number of fields and for various potentials, even non-rotationally symmetric ones [154], and was established as being able to lay the groundwork for observationally viable models that satisfy the Swampland Conjectures [155]. Lastly, the original statement by Brown in [152] that Hyperinflation is an attractor in the regime that slow-roll is a repeller [156–158] was extensively studied in the context of dynamical attractors [159].

### 4.3 Model Description and Background Field Considerations

#### 4.3.1 *Fundamentals*

The model we consider involves a scalar doublet with a hyperbolic  $\mathbb{H}^2$  field-space geometry, minimally coupled to gravity and normalised by the field-space scale,  $M_H$ ,  $\varphi^a = \phi^a/M_H$ . The action is given by:

$$S = \frac{1}{2} \int d^D x \sqrt{-g} [M_p^2 R - M_H^2 \mathcal{G}_{ab}(\varphi) \partial_\mu \varphi^a \partial_\nu \varphi^b g^{\mu\nu} - 2M_H^2 V(\varphi^a)], \quad (4.1)$$

where  $V(\varphi^a)$  is the scalar field potential. Here, we adopt the notation that latin indices  $\{a, b, ..\} = \{1, 2\}$  correspond to directions in field-space with metric  $\mathcal{G}_{ab}$ , while greek

letters  $\{\mu, \nu, \dots\} = \{0, \dots, 3\}$  correspond to spacetime indices and are associated with a Friedman-Lemaître-Robertson-Walker spacetime metric, with line element

$$ds^2 = g^{\mu\nu} dx^\mu dx^\nu = -dt^2 + a(t)\delta_{ij}dx^i dx^j, \quad (4.2)$$

describing a homogeneous and isotropic universe. As usual, the Hubble parameter is defined as  $H = \dot{a}/a$ .

Varying the action with respect to the doublet and the metric leads to the field equations of motion and the Einstein equation,

$$\begin{aligned} \mathcal{D}^\mu \mathcal{D}_\mu \varphi^a - \mathcal{G}^{ab} V_{,b} &= 0 \\ M_p^2 G_{\rho\sigma} + M_H^2 \left( \frac{1}{2} g_{\rho\sigma} \mathcal{G}_{ab} \varphi^a_{, \mu} \varphi^b_{, \mu} + g_{\rho\sigma} V - \mathcal{G}_{ab} \varphi^a_{, \rho} \varphi^b_{, \sigma} \right) &= 0, \end{aligned} \quad (4.3)$$

where  $G_{\rho\sigma}$  is the Einstein tensor. Here, we have introduced the covariant derivative

$$\mathcal{D}_\mu V^a = \partial_\mu V^a + \Gamma_{bc}^a \partial_\mu \varphi^b V^c, \quad (4.4)$$

associated with the spacetime metric  $g_{\mu\nu}$ , acting on a field-space vector  $V^a [\varphi^b(x^\mu)]$  through the pushforward operator  $[\mathcal{O}_*]_\mu^a = \varphi^a_{, \mu}$ , which relates spacetime-tensors with those defined on the field-space manifold,  $D^a = \varphi^a_{, \mu} \mathcal{D}^\mu$ .

When homogeneity and isotropy are imposed, equations (4.3) reduce to:

$$\mathcal{D}_t \partial_t \varphi^a + 3H \partial_t \varphi^a + \mathcal{G}^{ab} V_{,b} = 0, \quad (4.5)$$

$$3H^2 = \kappa^2 \left( \frac{1}{2} \mathcal{G}_{ab} \partial_t \varphi^a \partial_t \varphi^b + V \right), \quad (4.6)$$

$$\partial_t H = -\frac{1}{2} \kappa^2 \mathcal{G}_{ab} \partial_t \varphi^a \partial_t \varphi^b \quad (4.7)$$

where we have defined the hierarchy parameter  $\kappa^2 = M_H^2/M_p^2$ , given by the ratio of the hyperbolic field space scale to the Planck mass.

Despite the fact that higher dimensionality ( $d > 2$ ) field spaces can give rise to a plethora of interesting realisations, and have been argued to even take inflation out of the Swampland [154], we choose to restrict ourselves to a two-dimensional manifold, as it provides a sufficiently illustrative stage for showcasing the intriguing effects that result from non-trivial geometry. Focusing on the hyperbolic inflation scenario [152, 153, 159], in which the field-space, with canonical coordinates  $\varphi^1 \equiv \rho$  and  $\varphi^2 \equiv \varphi$ , has a transitive isometry, in the sense of shifts in the  $\varphi^2$  direction, leads to a metric of the form

$$\mathcal{G}_{ab} = \begin{bmatrix} 1 & 0 \\ 0 & f^2(\rho) \end{bmatrix}. \quad (4.8)$$

One parametrisation of the hyperbolic field space is the Poincaré half-plane defined by  $f(\rho) = \sinh(\rho)$ . For large radial-direction field values,  $\rho \gg 1$ , the field-space metric

function becomes  $f(\rho) = \sinh(\rho) \approx e^\rho$ .

For the metric (4.8), the Ricci scalar and the non-vanishing Christoffel symbols, prove to be

$$\Gamma_{\phi\phi}^\rho = -f^2(\rho), \quad \Gamma_{\rho\phi}^\phi = 1, \quad \mathcal{R} = -2 \frac{\partial_\rho^2 f(\rho)}{f(\rho)}. \quad (4.9)$$

We choose an exponential potential that respects the isometry of the field space and depends only on the ‘‘radial’’ direction,

$$V(\rho) \approx V_0 e^{\kappa^2 p \rho}, \quad (4.10)$$

where  $p$  is a positive constant. The potential gradient in the  $a$  direction is denoted by  $p_a$ ,

$$p_a = \kappa^{-2} \frac{\partial(\ln V)}{\partial \phi^a}. \quad (4.11)$$

Following the work of [159], the Klein-Gordon equations (4.5) can take the form of an autonomous system for the normalised field-space coordinates  $\varphi^a$  and their velocities  $v^a$ ,

$$\begin{aligned} \varphi^{a'} &= v^a \\ v^{a'} &= -(3 - \epsilon_H)(v^a + p^a) - \Gamma_{bc}^a v^b v^c, \end{aligned} \quad (4.12)$$

where the velocities  $v^a = d\varphi^a/dN \equiv \varphi^{a'}$  are obtained with respect to the e-fold number  $dN = H dt$ . Here,  $\epsilon_H = -\dot{H}/H^2$  is the rate of change of the Hubble parameter, which can be written, using (4.7), as

$$\epsilon_H = \frac{1}{2} \kappa^2 v_a v^a, \quad (4.13)$$

and its evolution equation is given by

$$\epsilon_H' = -(3 - \epsilon_H)(2\kappa^2 \epsilon_H - p_a v^a). \quad (4.14)$$

It is useful, here, to define the coordinates  $(x, y) \equiv (v^\rho, f(\rho) v^\phi)$ , namely the projections of the field-space velocity orthogonal to and along the Killing direction  $k_a = (0, f(\rho))$ . In these coordinates, the autonomous system (4.12) becomes:

$$\begin{aligned} x' &= -(3 - \epsilon_H)(x + p_\rho) + y^2 \\ y' &= -(3 - \epsilon_H + x)y, \end{aligned} \quad (4.15)$$

and (4.13) takes the useful form

$$\epsilon_H = \frac{1}{2} \kappa^2 (x^2 + y^2). \quad (4.16)$$

### 4.3.2 Background Field and Linear Stability in de Sitter

Scaling solutions, by definition, satisfy  $\epsilon'_H = 0$ . Therefore, from (4.14) we observe that

$$\epsilon_H = -\frac{1}{2}\kappa^2 p_a v^a. \quad (4.17)$$

Hence, the system (4.12) admits two types of scaling solutions:

- The gradient solution: In this case,  $(x, y) = (-p_\rho, 0)$ . To examine the stability of this solution we obtain the local Lyapunov exponents (the eigenvalues of the matrix  $J$  for the linearised system  $(x^a)' = J^a_b x^b$ ), as  $(\lambda_1, \lambda_2) = (-3, p - 3)$ . Solving the linearised system, one obtains

$$\begin{aligned} \rho &= \rho(0) - \frac{1}{3}u_\rho(0) e^{-3N} - p_\rho N \\ \phi &= \phi(0) + \frac{1}{p_\rho - 3}u_\phi(0) e^{(p_\rho - 3)N}. \end{aligned} \quad (4.18)$$

For  $p < 3$ , the angular velocity vanishes exponentially fast, irrespective of any initial value, while the radial velocity approaches the critical point value,  $x = -p_\rho$ . Thus, this solution is stable. This can be explicitly seen from the phase space diagram Figure 4.1(left). For steeper potentials,  $p > 3$ , the gradient solution, depicted as dashed black, red and purple lines in Figure 4.1(right), are unstable and for any non-trivial initial value of  $y$ , the system diverges from the gradient solution critical point  $(x, y) = (-p_\rho, 0)$  and evolves exponentially fast towards the hyperbolic solution critical point.

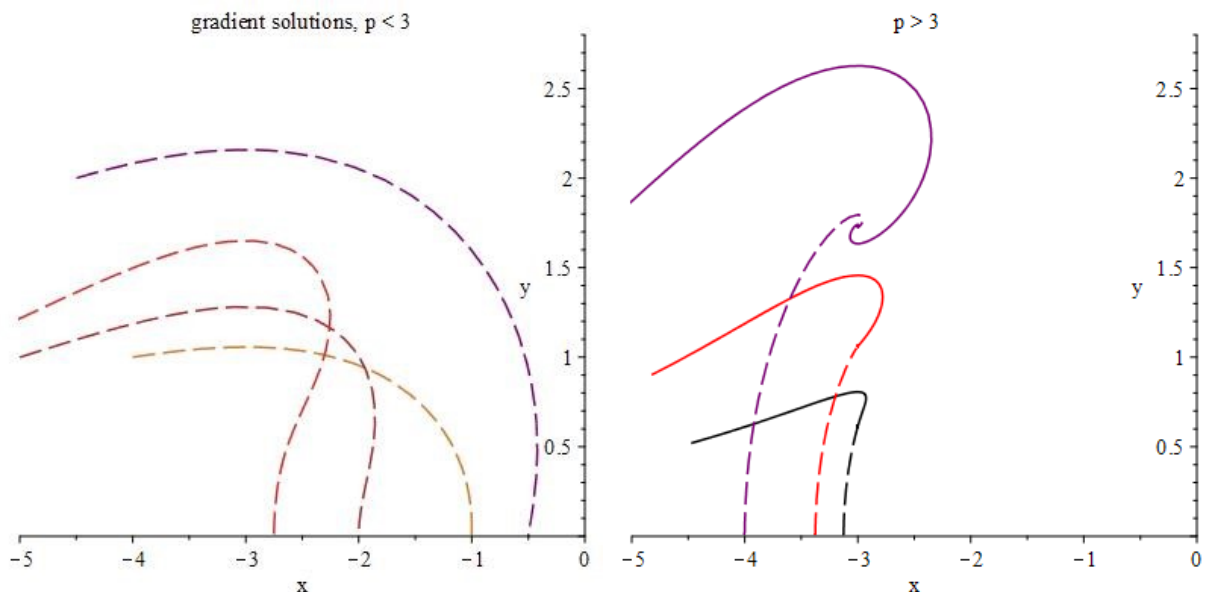


Figure 4.1: Phase diagram of  $[x(t), y(t)]$ , with initial conditions away from the critical point, for various values of the potential gradient  $p$ . For  $p < 3$ , the system evolves to the gradient solution, while for  $p \geq 3$  the system will evolve towards the hyperbolic solution, irrespective of the initial conditions. On the right panel, dashed lines commence with zero angular velocity,  $y = 0$ , and evolve to the Hyperbolic solution. The red solid line corresponds to a potential with  $p = 3$ .

- The hyperbolic solution: Here, the system is allowed to assume velocity in both directions and consequently, evolves towards the critical point

$$(x, y)_{Hyper} = \left(-3, \pm\sqrt{3p-9}\right). \quad (4.19)$$

This solution is only admissible if  $p \geq 3$ , to ensure positivity of the argument of the square root. The local Lyapunov exponents, in this case, are

$$(\lambda_1, \lambda_2) = \left(-\frac{3}{2} + \frac{3}{2}\sqrt{1 - \frac{8}{9}y^2}, -\frac{3}{2} - \frac{3}{2}\sqrt{1 - \frac{8}{9}y^2}\right) \quad (4.20)$$

and depending on the value of  $p$ , the critical point falls under one of the following categories:

- For  $3 < p < 3.375$  or  $0 < y < \frac{3\sqrt{2}}{4}$ , the eigenvalues are real and  $\lambda_1 \neq \lambda_2 < 0$ , so the system evolution, represented as the solid black line of Figure 4.1, leads towards the critical point, that is a stable node Figure 4.2a.
- For  $p > 3.375$  or  $y > \frac{3\sqrt{2}}{4}$ , the eigenvalues are complex conjugates with negative real part and therefore the system, which is represented by the solid purple line in Figure 4.1, when perturbed, will spiral towards this stable focus, as portrayed in Figure 4.2c.

Shifting the hyperbolic field-space curvature function argument by a constant, does not alter the dynamics. Hence, after redefining  $f(\rho) \equiv e^{[\rho-\rho(0)]}$ , and using the linearised expression for  $\rho - \rho(0) \approx -3N$  we see that in both the aforementioned cases the solutions evolve towards the hyperbolic solution as:

$$\begin{aligned} \rho &= \rho(0) - 3N - \frac{c_1}{y} e^{\lambda_1 N} - \frac{c_2}{y} e^{\lambda_2 N} \\ \phi &= \phi(0) + \frac{c_1}{\mu_1} e^{\mu_1 N} + \frac{c_2}{\mu_2} e^{\mu_2 N} \pm y e^{3N}, \end{aligned} \quad (4.21)$$

with  $(\mu_1, \mu_2) = (3 + \lambda_1, 3 + \lambda_2)$ .

- For  $p = 3.375$  or  $y = \frac{3\sqrt{2}}{4}$ , there is a single eigenvalue,  $\lambda = -\frac{3}{2}$ . Using the linearised solution for  $\rho - \rho(0)$ , again, we observe that the field follows the trajectory represented as the solid red line in Figure 4.1, towards the critical point, that is an improper stable node, depicted in Figure 4.2b and the hyperbolic solution takes the form

$$\begin{aligned} \rho &= \rho(0) - 3N - \frac{2}{3} [c_1 N + c_2] e^{-\frac{3}{2}N} \\ \phi &= \phi(0) + \frac{1}{y} \left[ \left( \frac{3}{2}N - 1 \right) c_1 + \frac{3}{2}c_2 \right] e^{\frac{3}{2}N} \pm \frac{y}{3} e^{3N}. \end{aligned} \quad (4.22)$$



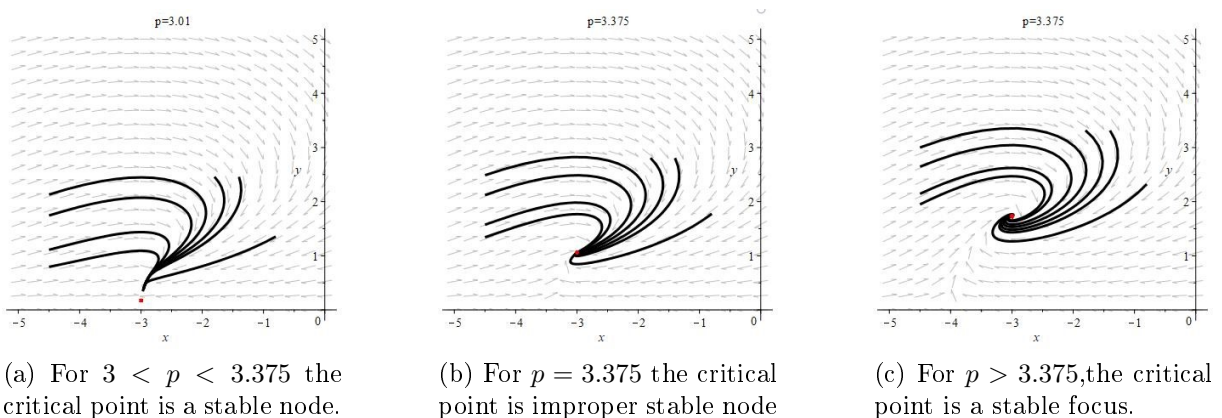


Figure 4.2: Phase diagrams for the hyperbolic solution for various values of the potential gradient,  $p$ .

Finally, as is manifest from the linearised equations, the system close to the critical points evolves towards the minimum of the potential  $\rho = 0$ , until the condition  $\rho > 1$  ceases to hold, that is when the approximation  $f(\rho) = \sinh(\rho) \simeq e^\rho$  stops being valid.

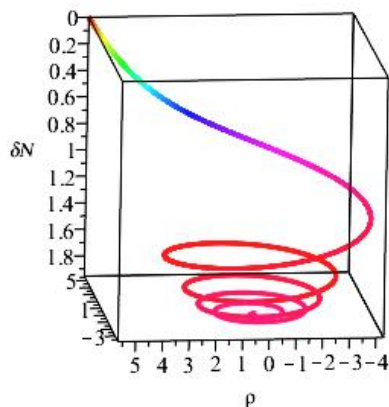


Figure 4.3: Evolution into the homogeneous hyperbolic solution for  $p = 3.01$ , with the vertical axis denoting the elapsed number of e-folds from the beginning of the trajectory.

#### 4.4 Linear Perturbations

Having thoroughly explored the dynamics of homogeneous field configurations and their attractor scaling solutions, we now turn to the study of small amplitude inhomogeneities around the background described by the hyperbolic solution. Since it is well motivated that  $\kappa^2 = M_H^2/M_p^2 \ll 1$  [152], we will be dropping  $\mathcal{O}(\epsilon_H)$  terms in the linearised perturbation equations - see (4.13). Hence, for the rest of the chapter, we will be ignoring spacetime metric fluctuations and their effect on the dynamics of the perturbations of the scalar fields.

#### 4.4.1 Linear Perturbation Analysis

Assuming a general coordinatisation of the field manifold, we can always split the field coordinates as

$$\varphi^a(t, \mathbf{x}) = \bar{\varphi}^a(t) + q^a(t, \mathbf{x}), \quad (4.23)$$

where the background field,  $\bar{\varphi}^a(t)$ , will be taken to follow the hyperbolic solution discussed above. The equations of motion for the perturbations  $q^a$ , then, read [137]

$$D_\mu D^\mu q^a + \mathcal{G}^{ab} q^d D_d V_{,b} + \mathcal{R}_{bcd}^a q^d \partial_\mu \phi^b \partial^\mu \phi^c = 0. \quad (4.24)$$

Projecting these equations along and orthogonal to the Killing (angular) direction, and using the results from (4.9), leads to the following equations of motion for the geometrically normalised field perturbations  $(r, q) = (q^1, f(\rho) q^2)$ ,

$$\ddot{r} + 3H\dot{r} - a^{-2}\nabla_{\mathbf{x}}^2 r - 2H^2 y^2 r - 2Hy\dot{q} + 2H^2 xyq = 0 \quad (4.25)$$

$$\ddot{q} + 3H\dot{q} - a^{-2}\nabla_{\mathbf{x}}^2 q + 2Hy\dot{r} + 3H^2 qp - H^2(x^2 + y^2)q = 0. \quad (4.26)$$

The fluctuations of the field multiplet can be expressed as a mode expansion in Fourier space

$$q^a(\mathbf{x}, t) = \int \frac{d^3k}{(2\pi)^3} \left[ U^a{}_I(k, t) a_{\mathbf{k}}^I e^{i\mathbf{k}\cdot\mathbf{x}} + U^{\star a}{}_I(k, t) a_{\mathbf{k}}^{\dagger I} e^{-i\mathbf{k}\cdot\mathbf{x}} \right], \quad (4.27)$$

noting that each multiplet member receives contributions from all creation/annihilation operators via the mode matrix  $U^a{}_I(k, t)$ . The normalisation is chosen such that the creation/annihilation operators satisfy

$$\left[ a_{\mathbf{k}}^I, a_{\mathbf{k}'}^{J\dagger} \right] = (2\pi)^3 \delta^{IJ} \delta(\mathbf{k} - \mathbf{k}'). \quad (4.28)$$

The mode matrix involves four complex entries (obviously  $N^2$  for an  $N$ -dimensional multiplet), but since the different fields are initially uncorrelated and evolve independently on small scales, there are only two independent modes corresponding to an initial condition where  $U^a{}_I \propto \delta^a{}_I$ . Later evolution, around and after horizon exit, mixes all the components of the matrix  $U$ . Below we will use two sets of modes, denoted by the index  $I$ . We choose these depending on whether the field initially fluctuates along the adiabatic or isocurvature direction, which we now describe.

#### 4.4.2 Local Orthogonal Basis

In the case of multiple fields, the assumption that the fluctuations will be purely *adiabatic*, i.e. expressible as a time-shift in the background scalar field  $\delta\phi = \dot{\phi}\delta t(t, \mathbf{x})$ , as is the case in single-field inflation, is not well-motivated. Geometrically, the fields can fluctuate in the direction orthogonal to the direction of the background field evolution. Physically, the adiabatic heritage of the inflationary modes will be bequeathed by the

radiation era density perturbations of the photons ( $\gamma$ ), neutrinos ( $\nu$ ), baryons (b) and cold dark matter particles (c) after the field decays [25], resulting in

$$\delta t = \frac{\delta\rho_\gamma}{\dot{\rho}_\gamma} = \frac{\delta\rho_\nu}{\dot{\rho}_\nu} = \frac{\delta\rho_b}{\dot{\rho}_b} = \frac{\delta\rho_c}{\dot{\rho}_c}, \quad (4.29)$$

or, using the continuity equation (1.9),

$$\frac{3}{4} \frac{\delta\rho_\gamma}{\rho_\gamma} = \frac{3}{4} \frac{\delta\rho_\nu}{\rho_\nu} = \frac{\delta\rho_c}{\rho_c} = \frac{\delta\rho_b}{\rho_b}. \quad (4.30)$$

Deviation from this behaviour, e.g.  $\frac{3}{4} \frac{\delta\rho_\nu}{\rho_\nu} - \frac{\delta\rho_c}{\rho_c} \neq 0$ , can indicate the existence of *isocurvature* perturbations.

Therefore, it is useful to introduce the adiabatic direction along the background field trajectory and the isocurvature direction that is normal to the former [25, 160]. These are defined by unit vectors  $\hat{e}_\sigma$  and  $\hat{e}_s$ , with components

$$(\hat{e}_\sigma)^a = \frac{\dot{\varphi}^a}{\dot{\sigma}} \quad \text{and} \quad (\hat{e}_s)^a = \frac{1}{\sqrt{\mathcal{G}}} \epsilon^{ac} \hat{e}_\sigma^b \mathcal{G}_{bc}, \quad (4.31)$$

where  $\dot{\sigma} = \sqrt{G_{ab}\dot{\varphi}^a\dot{\varphi}^b}$  is the background field velocity. This introduces a local orthogonal basis, related to the original coordinate basis, through the zweibeins

$$\begin{bmatrix} \hat{e}_\sigma \\ \hat{e}_s \end{bmatrix} = \begin{bmatrix} \frac{\dot{\rho}}{\dot{\sigma}} & \frac{\dot{\varphi}}{f\dot{\sigma}} \\ \frac{\dot{\varphi}}{\dot{\sigma}} & -\frac{\dot{\rho}}{f\dot{\sigma}} \end{bmatrix} \cdot \begin{bmatrix} \hat{e}_\rho \\ \hat{e}_\phi \end{bmatrix} = \begin{bmatrix} \frac{x}{\sigma'} & \frac{y}{f\sigma'} \\ \frac{y}{\sigma'} & -\frac{x}{f\sigma'} \end{bmatrix} \cdot \begin{bmatrix} \hat{e}_\rho \\ \hat{e}_\phi \end{bmatrix}, \quad (4.32)$$

with  $\sigma' = \sqrt{x^2 + y^2} = \dot{\sigma}/H$ .

In this basis, the covariant derivative is given by

$$\mathcal{D}_a V^b = \partial_a V^b + \mathcal{V}_{ca}^b V^c, \quad (4.33)$$

with  $\mathcal{V}$  being the - non-symmetric in the lower two indices - zweibein basis connection. The analytic form of this connection can be obtained in relation to the Christoffel connection associated with the original coordinate basis,  $\Gamma_{JK}^I$ , via

$$\mathcal{V}_{bc}^a = \hat{e}_b^K \hat{e}_c^I \hat{e}_J^a \Gamma_{IK}^J - \hat{e}_b^K \hat{e}_c^I \partial_I (\hat{e}_K^a), \quad (4.34)$$

where the capital indices are related to the coordinate basis and the lower-case ones to the zweibein, and  $\hat{e}_a^I$  are components of the transformation matrix (4.32). In this basis, the only non-vanishing connection components are:

$$\mathcal{V}_{21}^1 = \frac{y}{\sigma'} \quad \text{and} \quad \mathcal{V}_{12}^2 = \frac{x}{\sigma'}. \quad (4.35)$$

Having established the relation between the two bases, we can obtain equations (4.25) and (4.26) in the zweibein basis, as

$$\begin{aligned} \ddot{q}^\sigma + 3H\dot{q}^\sigma + \left(\frac{k}{a}\right)^2 q^\sigma + 6H^2 y q^s + 2Hy\dot{q}^s &= 0 \\ \ddot{q}^s + 3H\dot{q}^s + \left(\frac{k}{a}\right)^2 q^s - 2H^2 y^2 q^s - 2Hy\dot{q}^\sigma &= 0, \end{aligned} \quad (4.36)$$

where we used (4.27),  $q^\sigma(\mathbf{k}, t) = \int \frac{d^3k}{2\pi^3} U^\sigma_I(k, t) a_{\mathbf{k}}^I e^{i\mathbf{k}\cdot\mathbf{x}} + c.c.$  and similarly for  $q^s$ . Introducing the time variable  $z = Ht + \ln(H/k)$ , the equation of motion for the modes becomes:

$$\begin{aligned} \partial_z^2 q^\sigma + 3\partial_z q^\sigma + e^{-2z} q^\sigma + 6y q^s + 2y\partial_z q^s &= 0 \\ \partial_z^2 q^s + 3\partial_z q^s + e^{-2z} q^s - 2y^2 q^s - 2y\partial_z q^\sigma &= 0. \end{aligned} \quad (4.37)$$

Note that our time variable  $z$  is simply the number of e-folds up to a  $k$ -dependent shift and that all modes experience the same time evolution, only shifted in time, with  $z = 0$  denoting horizon exit for each mode. In the limit of radial motion,  $y \rightarrow 0$ , the effect of the field-space curvature vanishes and the fields decouple. In this limit, we obtain the one-dimensional equations of motion, the solution of which are the positive frequency  $k$ -modes for a massless, minimally coupled scalar field in de Sitter, which define the Bunch–Davies vacuum state [62] and assume a set of normalised solutions, in four spacetime dimensions [29], given in (1.53),

$$u_k = \frac{H}{\sqrt{k^3}} \frac{\sqrt{\pi}}{2} (-\eta)^{\frac{3}{2}} H_{3/2}(k\eta), \quad (4.38)$$

where  $\eta = -e^{-z}$ .

#### 4.4.3 Adiabatic and Isocurvature Perturbation Power Spectra

Deep inside the horizon, where the spatial gradient term of equations (4.37) dominates, the modes decouple and evolve independently, unaffected by the mixing induced by the field space curvature. As discussed above, we take our two sets of modes to be defined, as  $z \rightarrow -\infty$ , by

$$U^a_I \rightarrow u_k \delta^a_I, \quad (4.39)$$

where now  $a = (\sigma, s)$  denotes the adiabatic and isocurvature directions. We define the rescaled modes  $\mathcal{U}^a_I$  as

$$U^a_I \equiv \frac{H}{\sqrt{k^3}} \mathcal{U}^a_I. \quad (4.40)$$

The field perturbation power spectra can, then, be written as

$$\begin{aligned} \mathcal{P}^{ab}(k, t) &= \frac{k^3}{2\pi^2} \int d^3x e^{-i\mathbf{k}\cdot\mathbf{x}} \langle q^a(t, \mathbf{0}) q^b(t, \mathbf{x}) \rangle \\ &= \frac{H^2}{2\pi^2} \left( \sum_I \mathcal{U}_I^{a*} \mathcal{U}_I^b \right). \end{aligned} \quad (4.41)$$

To obtain the modes, we solve equations (4.37) twice, once with  $q^a = U^{a_1}$  and initial conditions ( $U^{\sigma_1} \rightarrow u_k, U^s_1 \rightarrow 0$ ), and once with  $q^a = U^{a_2}$  and initial conditions ( $U^{\sigma_2} \rightarrow 0, U^s_1 \rightarrow u_k$ ). In practice, the calculation starts at a sufficiently large, negative  $z$  such that the two equations are effectively decoupled. Subsequently, we solve them for  $z = 60$  e-folds after horizon exit, defining the longest mode of interest. The evolution of the modes can be seen in figure 4.4.

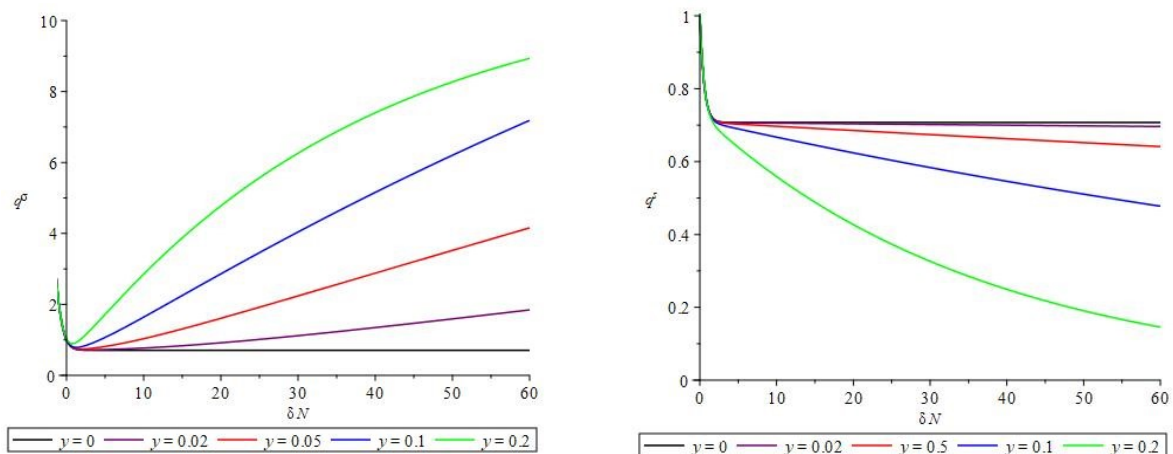


Figure 4.4: Time evolution of the adiabatic (left) and entropic (right) modes, for various values of  $y$ . The horizontal semi-axes' origin corresponds to the time of horizon exit for a mode with wavenumber  $k$  that is followed for further 60 e-folds. Increasing values  $y$ , or the potential slope  $p$ , lead to a faster increase of the adiabatic perturbation and decrease of the isocurvature one.

To corroborate the superhorizon behaviour of the linearised field perturbations, as obtained by the numerical solution presented above, we have also followed the evolution of two “separate universes” that start off at slightly displaced points in field-space. Figure 4.5 shows one such configuration, where two solutions of the background equations with neighbouring initial conditions are allowed to evolve, while depicting their difference in field-space, at equal times. In this particular example, we see that an initially dominant entropic perturbation feeds into an initially subdominant adiabatic one and decays while the adiabatic perturbation, corresponding to a time shift of a single background solution, eventually evolves towards a small, constant value. It is noteworthy, however, to remark that this only occurs after an observationally inaccessible number of e-folds.

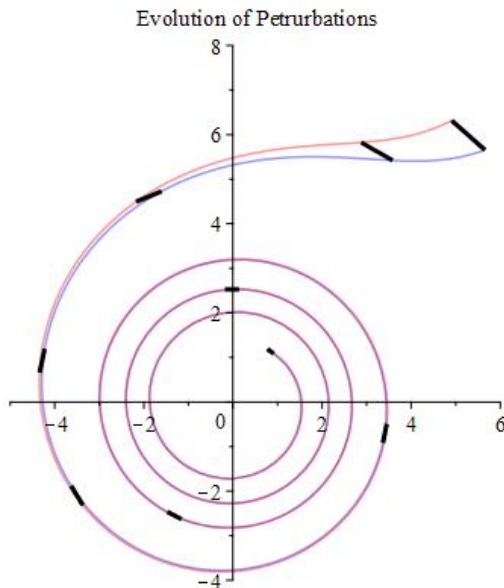


Figure 4.5: Evolution of the linearised field perturbations with parameter  $p = 3.01$  or  $y \approx 0.17$ . The adiabatic (tangent to the trajectory) perturbation approaches a small constant value. It is worth noting that the apparent shrinkage is due to the choice of coordinates.

The power spectra are easy to obtain as a function of the wavenumber,  $k$ , since all  $k$ -modes follow the same evolution, only time-shifted by  $t \rightarrow t + H^{-1} \ln(H/k)$ . This is, of course, a consequence of the hierarchy of the energy scale of the scalar field background  $M_H \ll M_P$ , which leads to the Hubble parameter  $H$  being treated as a constant. In general, for a time-dependent value of  $H$ , each mode would cross the horizon at a different amplitude and their subsequent temporal evolution, after horizon crossing, would vary. This would render this identification inaccurate. We plot the power spectra for hyperbolic scaling attractors, characterised by different values of  $y$ , in Figure 4.6.

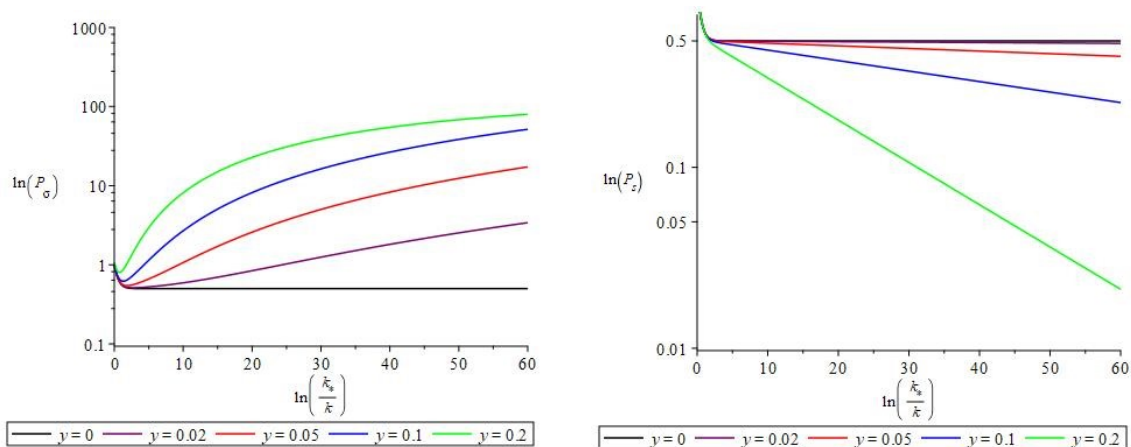


Figure 4.6: The adiabatic  $\mathcal{P}_\sigma$  and entropic  $\mathcal{P}_s$  power spectra at time  $t$  for various values of  $y$ , where  $k^*$  is the wavenumber of the mode exiting the horizon at that time and  $\ln(k^*/k) = 60$  represents the wavenumber corresponding to the scale of the universe today.

We utilise the numerically evaluated adiabatic power spectrum matrix component  $P^{\sigma\sigma}$  and plot the adiabatic spectral index,

$$n_s^{ad} = 1 + \frac{d \ln [P^{\sigma\sigma}]}{d(\ln k)}, \quad (4.42)$$

along with the 68% confidence range for its value from the Planck collaboration [28] (green band  $n_s = 0.9649 \pm 0.0042$ ) in Figure 4.7. Hence, it is manifest that the observationally obtained range places very tight bounds to the permissible values for  $y$ , restricting them to  $0.74 \times 10^{-2} \leq y \leq 0.94 \times 10^{-2}$  and  $0.1603 \leq y \leq 0.1774$ , severely constraining this family of hyperinflation models to those with exponential potential parameters in the ranges  $0.54 \times 10^4 \leq p - 3 \leq 0.88 \times 10^{-4}$  and  $0.025 \leq p - 3 \leq 0.031$ .

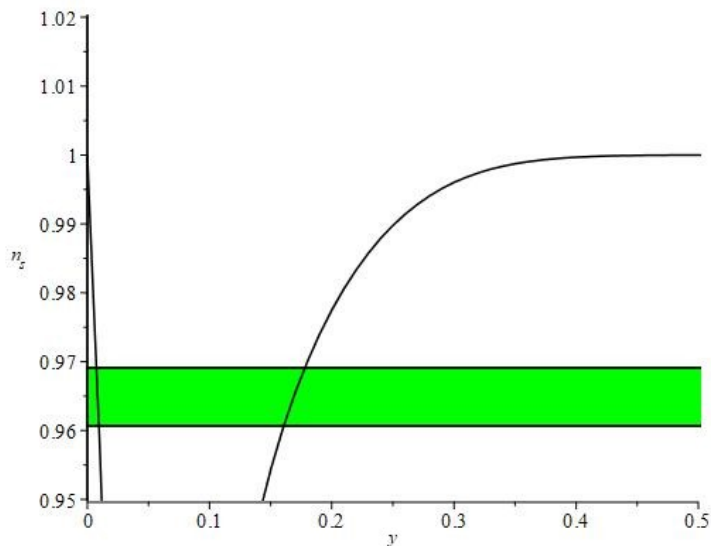


Figure 4.7: The adiabatic spectral index,  $n_s$  as a function on  $y$ . The green band corresponds to observationally permitted values.

Finally, we look at the tensor-to-scalar ratio. We have, at horizon crossing,

$$r = \frac{\mathcal{P}_t(k)}{\mathcal{P}_s(k)} = \frac{4\kappa^2 \dot{\varphi}^a \dot{\varphi}_a}{U^2 H^2} = \frac{8\epsilon_H}{U^2} = \frac{4\kappa^2}{U^2} [9 + y^2], \quad (4.43)$$

where  $U^2 = \sum_I \mathcal{U}_I^{\sigma*} \mathcal{U}_I^\sigma$  and we have only taken the adiabatic perturbations into account, as the contribution of the isocurvature ones is negligible. The Planck collaboration [28] set the observational bound for the tensor-to-scalar ratio to  $r < 0.10$ . Hence, taking into account that in the first few e-folds after horizon crossing  $U^2 \lesssim 1$  and using (4.19), we obtain bounds for the parameter of the exponential potential,

$$\kappa^2 p \lesssim 0.01. \quad (4.44)$$

This, in turn, results in limits for the permitted values for the Hubble parameter  $\epsilon_H$ :

$$\begin{aligned}\epsilon_H &= \frac{1}{2}\kappa^2 [x^2 + y^2] \\ &= \frac{3}{2}\kappa^2 p \\ &\lesssim 0.015,\end{aligned}\tag{4.45}$$

in close agreement with [153]. Furthermore, the tight observational bounds on the value of the exponential parameter (see above Table 4.7) provide a numerical estimate for the hierarchy parameter  $\kappa^2 \approx 0.2/9$  improving the condition set in [153] that  $\kappa^2 \ll 2/9$ . Equation (4.45) shows that our original ansatz of small  $\epsilon_H$  is observationally consistent.

We remark that the definitions of the Hubble slow-roll parameter  $\epsilon_H \equiv -\dot{H}/H^2$ , given by (4.13), and that of the potential slow-roll parameter

$$\epsilon_V \equiv \frac{1}{2}\kappa^{-2} \frac{V^{,a} V_{,a}}{V^2} = \frac{1}{2}\kappa^2 p^a \mathcal{G}_{ab} p^b,\tag{4.46}$$

are inequivalent in multifield models and can differ substantially [39]. Equation (4.46) is covariant. Therefore, using (4.32) to transform from the convenient local orthogonal basis  $(\sigma, s)$  to  $(\rho, \varphi)$ , one readily obtains

$$\epsilon_V = \frac{1}{2}\kappa^2 p^2 \frac{x^2}{x^2 + y^2}.\tag{4.47}$$

Due to the characteristics of our particular model, namely that we consider scaling solutions and use a potential that respects the field-space isometries (and subsequently resulting in (4.47) receiving contributions only from the radial direction), it is evident that the two slow-roll parameters coincide,

$$\epsilon_V = \frac{1}{2}\kappa^2 p^2 \frac{9}{3p} = \epsilon_H < 0.015.\tag{4.48}$$

Finally, this indicates that this type of exponential potential hyperinflation models, which is the simplest type of those that are not observationally excluded (as opposed to those with a power-law potential [153]), cannot elevate (hyper)inflation out of the Swampland unless the requirement of the conjecture is relaxed beyond  $\epsilon_V \approx \mathcal{O}(10^{-1})$  as originally argued in [154]. This conclusion can be made more robust by extending our analysis beyond the small  $\epsilon_H$  regime.



## 4.5 Conclusion and Motivation for Further Work

In this work, we have reviewed Hyperinflation with an exponential potential and used observational results to constrain the model's parameter space. Adopting a hierarchy of scales,  $M_H < \phi < M_P$ , results in the slow-roll parameter  $\epsilon_H$  being negligible, while its time derivative vanishes in the hyperbolic attractor solution. This results in the equations of motion for the background field taking the form of an autonomous system. After solving the linearised equations, we have manifestly shown the dynamical patterns that describe the behaviour of the system for various values of the exponential parameter  $p$ . Additionally, the linear stability of the background has been manifestly demonstrated and two different regimes have been distinguished: For  $p < 3$ , the gradient solution is a stable attractor and for  $p > 3$ , where the gradient solution is a repeller, the hyperbolic solution dominates.

Furthermore, by introducing a local orthogonal basis, we obtained the equations of motion of the adiabatic and isocurvature perturbations and noted their highly coupled behaviour that is due to the field-space curvature. We proceeded to solve these numerically and described the dynamics of the perturbations, noting their behaviour after horizon crossing: The adiabatic perturbations grow with the parameter  $y$ , which is associated with the field-space curvature, and the entropic ones rapidly decay.

Finally, after producing the adiabatic and entropic power spectra, we compared the resulting adiabatic spectral index and tensor-to-scalar ratio with recent observations, placing tight bounds to the permissible values of the exponential potential parameter  $p$ , also setting an upper limit for the slow-roll parameter,  $\epsilon \approx \mathcal{O}(10^{-2})$ . Our results are shown to agree with, and improve on, similar results in the literature [152],[153].

Hyperinflation is a regime that could shine light on intriguing aspects of inflationary cosmology. It has been shown in [161] that this model is a specific case of side-tracked inflation, namely the attractor phase emerging from geometrical destabilisation [156]. Brown [152], in his original paper, notes that the model can give rise to equilateral non-Gaussianities and substantial work has been carried out for the computation of such quantities in a general class of multifield models with a curved field-space [162–166]. We leave the derivation of the relevant stochastic equations and the computation of the arising non-Gaussianity, utilising the stochastic formalism for future work.

**Part III**

**Conclusion**

## Chapter 5. Summary & Motivation for Future Work

In this closing chapter, we summarise the results of the presented research works. We start by reviewing each of the covered topics and after commenting on relevant past and contemporary projects, we motivate their potential future extensions.

In Chapter 2, we elaborated on the path integral representation for the Langevin equation describing the infrared behaviour of a spectator scalar in de Sitter. The simple Feynman rules derived, allow for the straightforward computation of arbitrary unequal-time correlators of the field. These quantities can also be obtained from the perturbative expansion of the Langevin equation. As demonstrated, the two approaches are equivalent, but the former offers computational advantages and increased efficiency, as opposed to the latter that involves a separation of the Langevin equation solution in different orders, represented by the ‘tree’ graphs of section 2.6 and the evaluation of expectation values of their products. This last step becomes increasingly complex with the number of fields in the desired correlator and with perturbative order, as all possible ‘tree’ configurations need to be taken into account. The proposed Feynman rules, on the other hand, directly build any correlator out of two propagators and a small, fixed number of vertices resulting in a conjectured form for the arbitrary N-point function, to the m-order.

Furthermore, the case of minimal backreaction was studied. We included the dependence of the noise amplitude on  $\phi$ , making the noise multiplicative, and new contributions to the two-point functions were calculated. Hence, we demonstrated the comparative superiority of the Feynman rule method, in an example in which the perturbative solution of the Langevin equation would have proven substantially more involved.

Increased attention was paid to the role of the functional Jacobian determinant in the path integral, in the form of a ghost Lagrangian. The ghost fields introduced, contribute closed loops in the diagrams. In the case of additive noise  $H = H_0$ , ghost loops act to cancel the ill-defined closed  $G$  loops. The perturbative Langevin solution is free from such structures, so ghosts are essential in ensuring that Feynman diagrams lead to the correct result. In the case of multiplicative noise  $H = H(\phi)$ , the contributions from the ghost and closed  $G$  loops do not vanish and hence, contribute to the final correlator. This was expected, as it constitutes the manifestation of the dependence of N-point correlators on the discretisation prescription of the Langevin equation, when the noise is multiplicative. In a continuum description, this property translates to the choice of the value of  $\Theta(0)$  [63]. The methodology followed results in our formalism naturally picking the midpoint value  $\Theta(0) = \frac{1}{2}$ , corresponding to the Stratonovich prescription.

It is manifest, when gravitational backreaction is included, that different discretisation

prescriptions lead to different results for the correlators, albeit suppressed by powers of the backreaction coupling. This theoretical uncertainty has been noted [68] to be proportional to corrections to the leading stochastic picture. From a purely mathematical perspective, all prescriptions ( $\Theta(0) \in [0, 1]$  in a continuum description) are equally admissible, therefore the "correct" - in the sense that it reproduces results in agreement with the full QFT - prescription for modelling inflationary scalar field dynamics via a stochastic differential equation, requires either a first principles computation or other external to the model justifications, as stressed in [69]. In our approach, the underlying dynamics dictate the choice for the discretisation prescription, since the path integral derived from the stochastic equation must be a truncated version of the full underlying action, in the Schwinger-Keldysh formulation. The lack of functional determinants in the QFT path integral, indicates that the Ito prescription seems favoured, but a concrete computation is necessary for the verification of this expected result.

In Chapter 3 we shifted our focus to the UV limit of scalar fields in de Sitter. The gravity-Higgs sector has been shown to be fertile soil for testing out ideas in (effective) quantum gravity. The quantisation procedure of gravity, raises intriguing concerns on how spacetime geometry is to be defined when scalar and metric backgrounds are allowed to mix freely. The ambiguity stemming from the use of different conformal frames, Einstein or Jordan, and the different results obtained with each approach, has resulted in controversy in literature. Our treatment indicates that applying a methodology, which is fully covariant under field redefinitions is perfectly feasible and leads to unambiguous results about physical observables, manifesting a complete physical equivalence between the different conformal frames. On the other hand, on scales below the Planck mass, where quantum gravitational effects are suppressed, non-covariant approaches can still lead to correct results. Our analysis has led us to advocate the use of the frame-independent effective mass  $\mu^2 + \xi R$ , and - provided appropriate attention is paid to the intricacies associated with the conformal transformation - the simpler Einstein frame, in which the curvature coupling vanishes, can always be used. The curvature coupling dependence in the Jordan frame can be recovered from relations similar to the beta function ones given in section 3.4.

The methodology followed is not as general as it could. The covariant effective action has been used, but field redefinitions were limited to the form  $\phi_R = Z(\mu_R)\phi$ , whereas in a fully general treatment, the renormalised field transformation should, *a priori* take the form of a non-linear mapping into field space,  $\phi_R = \phi_R(\phi, \mu_R)$ . Furthermore, at the end of subsection 3.4.1, we commented on the importance of the couplings in the kinetic terms, which despite not contributing to our approach, are expected to affect results when the entirety of the one-loop effective action, rather than simply the one-loop effective potential, is taken into account. Nevertheless, our approach can provide a strong basis for a potential future research endeavour.

Additionally, we remarked the use of existing non-covariant results for the standard

model beta-functions, which are not associated with the spacetime curvature. The dependence of the running couplings on gauge parameters, as noted in [137], can prove to be problematic, motivating the need for further research in gauge-parameter dependence for Higgs instability in flat space.

Lastly, in Chapter 4 we reviewed and extended the topical ‘‘Hyperinflation’’ model with an exponential potential, explored its dynamics and, imposing physical observational bounds, constrained its parameter space. We adopted a scale hierarchy  $M_H \ll \phi \ll M_P$  which resulted in the slow-roll parameter  $\epsilon_H$  being negligible, while its time derivative vanishes in the hyperbolic attractor solution. After linearising the autonomous system of background field equations of motion, we studied in detail the dynamical patterns that describe the evolution of the fields for various values of the exponential parameter  $p$ . Furthermore, the linear stability of the background has been, manifestly, demonstrated and two different regimes have been distinguished. The introduction of a local orthogonal basis leads to distinctly different equations of motion for the adiabatic and isocurvature perturbations, while their highly coupled behaviour, due to the field space curvature, requires non-analytical manipulations. Our numerical solutions lead to a clear description of the dynamics of the perturbations, distinguishing their behaviour after horizon crossing: The adiabatic perturbations grow with the field-space curvature parameter  $y$  while the entropic ones, rapidly, decay. Finally, after producing the adiabatic and entropic power spectra, the resulting adiabatic spectral index and tensor-to-scalar ratio were contrasted against contemporary observational values, highlighting the narrow permissible range of the exponential potential parameter  $p$ , and consequently, restricting the upper limit for the slow-roll parameter  $\epsilon_H$  to  $\mathcal{O}(10^{-2})$ .

The investigation of the theoretical and phenomenological implications of inflationary models with elaborate field-space structure is a fascinating contemporary topic. The introduction of non-minimal coupling has been shown to raise questions regarding the proper conformal frame, in which the action should be expressed, demanding the development of descriptions that respect covariance under field redefinitions. The dynamics of the low-energy sector of inflationary models, which is more significantly affected by the existence of the underlying spacetime curvature, can be described by application of the stochastic formalism. Furthermore, the consistent inclusion of gravity has been hindered by the uncertainty that pertains to the appropriate choice of descritisation prescription. Eventually, these obstacles can be surpassed by constructing a prescription-independent, fully field-space covariant methodology and steps towards that direction have, very recently, been made [42]. It would be of particular interest to investigate and elaborate on this formalism and use it to study observationally relevant quantities and even discover, potentially, qualitatively new phenomena.

## Bibliography

- [1] M. Bounakis and G. Rigopoulos (2020), 2002.03402.
- [2] M. Bounakis and I. G. Moss, JHEP **04**, 071 (2018), 1710.02987.
- [3] M. Bounakis, I. G. Moss, and G. Rigopoulos (2020), 2010.06461.
- [4] P. W. Higgs, Phys. Rev. **145**, 1156 (1966), URL <https://link.aps.org/doi/10.1103/PhysRev.145.1156>.
- [5] T. W. B. Kibble, Phys. Rev. **155**, 1554 (1967), URL <https://link.aps.org/doi/10.1103/PhysRev.155.1554>.
- [6] P. Higgs, Physics Letters **12**, 132 (1964), ISSN 0031-9163, URL <http://www.sciencedirect.com/science/article/pii/0031916364911369>.
- [7] P. W. Higgs, Phys. Rev. Lett. **13**, 508 (1964), URL <https://link.aps.org/doi/10.1103/PhysRevLett.13.508>.
- [8] F. Englert and R. Brout, Phys. Rev. Lett. **13**, 321 (1964), URL <https://link.aps.org/doi/10.1103/PhysRevLett.13.321>.
- [9] G. Aad et al. (ATLAS), Phys. Lett. B **716**, 1 (2012), 1207.7214.
- [10] S. Chatrchyan et al. (CMS), Phys. Lett. B **716**, 30 (2012), 1207.7235.
- [11] A. H. Guth, Adv. Ser. Astrophys. Cosmol. **3**, 139 (1987).
- [12] A. A. Starobinsky, Adv. Ser. Astrophys. Cosmol. **3**, 130 (1987).
- [13] A. D. Linde, Adv. Ser. Astrophys. Cosmol. **3**, 149 (1987).
- [14] S. Dodelson, *Modern Cosmology* (Academic Press, Amsterdam, 2003), ISBN 978-0-12-219141-1.
- [15] V. Mukhanov, *Physical Foundations of Cosmology* (Cambridge University Press, Oxford, 2005), ISBN 978-0-521-56398-7.
- [16] S. Weinberg, *Cosmology* (2008), ISBN 978-0-19-852682-7.
- [17] D. Baumann, in *Theoretical Advanced Study Institute in Elementary Particle Physics: Physics of the Large and the Small* (2011), pp. 523–686, 0907.5424.

- 
- [18] D. Baumann and L. McAllister, *Inflation and String Theory*, Cambridge Monographs on Mathematical Physics (Cambridge University Press, 2015).
- [19] A. D. Linde, Prog. Theor. Phys. Suppl. **163**, 295 (2006), hep-th/0503195.
- [20] S. M. Carroll, *Spacetime and Geometry* (Cambridge University Press, 2019), ISBN 978-0-8053-8732-2, 978-1-108-48839-6, 978-1-108-77555-7.
- [21] C. L. Bennett, A. Banday, K. M. Gorski, G. Hinshaw, P. Jackson, P. Keegstra, A. Kogut, G. F. Smoot, D. T. Wilkinson, and E. L. Wright, Astrophys. J. Lett. **464**, L1 (1996), astro-ph/9601067.
- [22] W. R. Stoeger, S. J., R. Maartens, and G. F. R. Ellis, Astrophys. J. **443**, 1 (1995).
- [23] E. Komatsu et al. (WMAP), Astrophys. J. Suppl. **180**, 330 (2009), 0803.0547.
- [24] N. Aghanim et al. (Planck), Astron. Astrophys. **641**, A1 (2020), 1807.06205.
- [25] C. Gordon, D. Wands, B. A. Bassett, and R. Maartens, Phys. Rev. D **63**, 023506 (2000), astro-ph/0009131.
- [26] K. A. Malik and D. Wands, Phys. Rept. **475**, 1 (2009), 0809.4944.
- [27] V. F. Mukhanov, Sov. Phys. JETP **67**, 1297 (1988).
- [28] Y. Akrami et al. (Planck), Astron. Astrophys. **641**, A10 (2020), 1807.06211.
- [29] S. Miao, P. Mora, N. Tsamis, and R. Woodard, Phys. Rev. D **89**, 104004 (2014), 1306.5410.
- [30] B.-L. B. Hu and E. Verdaguer, *Semiclassical and Stochastic Gravity: Quantum Field Effects on Curved Spacetime*, Cambridge Monographs on Mathematical Physics (Cambridge University Press, Cambridge, 2020), ISBN 978-0-511-66749-7.
- [31] V. Gorbenko and L. Senatore (2019), 1911.00022.
- [32] J. Rubio, Front. Astron. Space Sci. **5**, 50 (2019), 1807.02376.
- [33] G. 't Hooft and M. J. G. Veltman, Ann. Inst. H. Poincare Phys. Theor. A **20**, 69 (1974).
- [34] A. Shomer (2007), 0709.3555.
- [35] S. Deser, H.-S. Tsao, and P. van Nieuwenhuizen, Phys. Rev. D **10**, 3337 (1974), URL <https://link.aps.org/doi/10.1103/PhysRevD.10.3337>.
- [36] Y. Akrami et al. (Planck), Astron. Astrophys. **641**, A9 (2020), 1905.05697.
- [37] P. Agrawal, G. Obied, P. J. Steinhardt, and C. Vafa, Phys. Lett. B **784**, 271 (2018), 1806.09718.

- 
- [38] P. Berglund and G. Ren (2009), 0912.1397.
- [39] A. Achúcarro and G. A. Palma, JCAP **02**, 041 (2019), 1807.04390.
- [40] D. Wands, Lect. Notes Phys. **738**, 275 (2008), astro-ph/0702187.
- [41] J.-O. Gong, Int. J. Mod. Phys. D **26**, 1740003 (2016), 1606.06971.
- [42] L. Pinol, S. Renaux-Petel, and Y. Tada (2020), 2008.07497.
- [43] V. F. Mukhanov and G. V. Chibisov, JETP Lett. **33**, 532 (1981).
- [44] B. L. Hu and D. J. O'Connor, Phys. Rev. Lett. **56**, 1613 (1986), URL <https://link.aps.org/doi/10.1103/PhysRevLett.56.1613>.
- [45] D. Seery, Class. Quant. Grav. **27**, 124005 (2010), 1005.1649.
- [46] I. Moss and G. Rigopoulos, JCAP **1705**, 009 (2017), 1611.07589.
- [47] B. Garbrecht and G. Rigopoulos, Phys. Rev. **D84**, 063516 (2011), 1105.0418.
- [48] B. Garbrecht, G. Rigopoulos, and Y. Zhu, Phys. Rev. D **89**, 063506 (2014), 1310.0367.
- [49] B. Garbrecht, F. Gautier, G. Rigopoulos, and Y. Zhu, Phys. Rev. D **91**, 063520 (2015), 1412.4893.
- [50] N. Tsamis and R. Woodard, Nuclear Physics B **724**, 295–328 (2005), ISSN 0550-3213, URL <http://dx.doi.org/10.1016/j.nuclphysb.2005.06.031>.
- [51] A. A. Starobinsky, Lect. Notes Phys. **246**, 107 (1986).
- [52] A. A. Starobinsky and J. Yokoyama, Physical Review D **50**, 6357–6368 (1994), ISSN 0556-2821, URL <http://dx.doi.org/10.1103/PhysRevD.50.6357>.
- [53] F. Gautier and J. Serreau, Phys. Rev. D **92**, 105035 (2015), 1509.05546.
- [54] D. López Nacir, F. D. Mazzitelli, and L. G. Trombetta, JHEP **08**, 052 (2019), 1905.03665.
- [55] T. Markkanen, A. Rajantie, S. Stopyra, and T. Tenkanen, JCAP **08**, 001 (2019), 1904.11917.
- [56] A. Cable and A. Rajantie (2020), 2011.00907.
- [57] G. Moreau and J. Serreau, Phys. Rev. D **101**, 045015 (2020), 1912.05358.
- [58] G. Moreau, J. Serreau, and C. Noûs, Phys. Rev. D **102**, 125015 (2020), 2004.09157.
- [59] M. Mirbabayi (2020), 2010.06604.



- 
- [60] M. Mirbabayi, JCAP **12**, 006 (2020), 1911.00564.
- [61] H. E. Kandrup, Phys. Rev. D **39**, 2245 (1989), URL <https://link.aps.org/doi/10.1103/PhysRevD.39.2245>.
- [62] T. Bunch and P. Davies, Proc. Roy. Soc. Lond. A **360**, 117 (1978).
- [63] A. W. C. Lau and T. C. Lubensky, Physical Review E **76** (2007), ISSN 1550-2376, URL <http://dx.doi.org/10.1103/PhysRevE.76.011123>.
- [64] P. H. Damgaard and H. Huffel, Phys. Rept. **152**, 227 (1987).
- [65] T. Prokopec and G. Rigopoulos, JCAP **08**, 013 (2018), 1710.07333.
- [66] C. Burgess, R. Holman, L. Leblond, and S. Shandera, JCAP **10**, 017 (2010), 1005.3551.
- [67] T. Markkanen and A. Rajantie, JCAP **03**, 049 (2020), 2001.04494.
- [68] V. Vennin and A. A. Starobinsky, Eur. Phys. J. C **75**, 413 (2015), 1506.04732.
- [69] U. Felderhof and H. van Beijeren, Journal of Statistical Physics **154** (2013).
- [70] T. Prokopec and G. Rigopoulos, Phys. Rev. D **82**, 023529 (2010), 1004.0882.
- [71] K. Enqvist, S. Nurmi, D. Podolsky, and G. Rigopoulos, JCAP **04**, 025 (2008), 0802.0395.
- [72] T. Fujita, M. Kawasaki, Y. Tada, and T. Takesako, JCAP **12**, 036 (2013), 1308.4754.
- [73] T. Fujita, M. Kawasaki, and Y. Tada, JCAP **10**, 030 (2014), 1405.2187.
- [74] G. Degrassi, S. Di Vita, J. Elias-Miro, J. R. Espinosa, G. F. Giudice, et al., JHEP **1208**, 098 (2012), 1205.6497.
- [75] D. Buttazzo, G. Degrassi, P. P. Giardino, G. F. Giudice, F. Sala, A. Salvio, and A. Strumia, JHEP **12**, 089 (2013), 1307.3536.
- [76] K. Blum, R. T. D'Agnolo, and J. Fan, JHEP **03**, 166 (2015), 1502.01045.
- [77] J. R. Espinosa, G. F. Giudice, and A. Riotto, JCAP **0805**, 002 (2008), 0710.2484.
- [78] C. P. Burgess, Living Rev. Rel. **7**, 5 (2004), [gr-qc/0311082](https://arxiv.org/abs/gr-qc/0311082).
- [79] M. Herranen, T. Markkanen, S. Nurmi, and A. Rajantie, Phys. Rev. Lett. **113**, 211102 (2014), 1407.3141.
- [80] M. Herranen, T. Markkanen, S. Nurmi, and A. Rajantie (2015), 1506.04065.

- 
- [81] A. Joti, A. Katsis, D. Loupas, A. Salvio, A. Strumia, N. Tetradis, and A. Urbano, *JHEP* **07**, 058 (2017), 1706.00792.
- [82] D. G. Figueroa, A. Rajantie, and F. Torrenti, *Phys. Rev. D* **98**, 023532 (2018), 1709.00398.
- [83] T. Markkanen, A. Rajantie, and S. Stopyra, *Front. Astron. Space Sci.* **5**, 40 (2018), 1809.06923.
- [84] D. P. George, S. Mooij, and M. Postma, *JCAP* **1402**, 024 (2014), 1310.2157.
- [85] C. F. Steinwachs and A. Y. Kamenshchik, *AIP Conf.Proc.* **1514**, 161 (2012), 1301.5543.
- [86] A. Yu. Kamenshchik and C. F. Steinwachs, *Phys. Rev.* **D91**, 084033 (2015), 1408.5769.
- [87] D. P. George, S. Mooij, and M. Postma, *JCAP* **1604**, 006 (2016), 1508.04660.
- [88] I. G. Moss (2014), 1409.2108.
- [89] I. G. Moss (2015), 1509.03554.
- [90] G. A. Vilkovisky, in *Quantum Theory of Gravity* (Adam Hilger, 1984), p. 169.
- [91] B. S. DeWitt, *Dynamical Theory of Groups and Fields* (Gordon and Breach, 1965).
- [92] A. O. Barvinsky and G. A. Vilkovisky, *Physics Reports* **119**, 1 (1985).
- [93] L. E. Parker and D. J. Toms, *Quantum Field Theory in Curved Spacetime* (Cambridge University Press, 2009), ISBN 978-0-521-87787-9.
- [94] S. R. Huggins, G. Kunstatter, H. P. Leivo, and D. J. Toms, *Nuclear Physics B* **301**, 627 (1987).
- [95] L. Alvarez-Gaumé, D. Z. Freedman, and S. Mukhi, *Annals of Physics* **134**, 85 (1981), ISSN 0003-4916, URL <http://www.sciencedirect.com/science/article/pii/0003491681900063>.
- [96] P. S. Howe, G. Papadopoulos, and K. S. Stelle, *Nucl. Phys.* **B296**, 26 (1988).
- [97] N. Nielsen, *Nucl. Phys.* **B101**, 173 (1975).
- [98] R. Fukuda and T. Kugo, *Phys. Rev. D* **13**, 3469 (1976).
- [99] R. Kobes, G. Kunstatter, and A. Rebhan, *Nuclear Physics B* **355**, 1 (1991), ISSN 0550-3213, URL <http://www.sciencedirect.com/science/article/pii/055032139190300M>.

- 
- [100] C. Contreras and L. Vergara, Phys. Rev. **D55**, 5241 (1997), [Erratum: Phys. Rev.D56,6714(1997)], [hep-th/9610109](#).
- [101] T. Markkanen, S. Nurmi, and A. Rajantie (2017), [1707.00866](#).
- [102] C. P. Burgess and G. Kunstatter, Mod. Phys. Lett. **A2**, 875 (1987), [Erratum: Mod. Phys. Lett.A2,1003(1987)].
- [103] B. S. DeWitt, in *Quantum Field Theory and Quantum Statistics, Volume 1* (Adam Hilger, 1987), p. 191.
- [104] I. Krive and A.D.Linde, Nucl. Phys. **B432**, 265 (1976).
- [105] H. D. Politzer and S. Wolfram, Physics Letters B **82**, 242 (1979), ISSN 0370-2693, URL <http://www.sciencedirect.com/science/article/pii/0370269379907469>.
- [106] N. Cabibbo, L. Maiani, G. Parisi, and R. Petronzio, Nucl. Phys. **B158**, 295 (1979).
- [107] M. Sher, Phys. Rept. **179**, 273 (1989).
- [108] S. Coleman and E. Weinberg, Phys. Rev. D **7**, 1888 (1973).
- [109] G. Cognola, E. Elizalde, S. Nojiri, S. D. Odintsov, and S. Zerbini, JCAP **0502**, 010 (2005), [hep-th/0501096](#).
- [110] D. V. Vassilevich, Phys. Rept. **388**, 279 (2003), [hep-th/0306138](#).
- [111] I. G. Avramidi, *Heat kernel and quantum gravity*, vol. 64 (Springer, 2000).
- [112] A. D. Plascencia and C. Tamarit, JHEP **10**, 099 (2016), [1510.07613](#).
- [113] M. Endo, T. Moroi, M. M. Nojiri, and Y. Shoji, Phys. Lett. **B771**, 281 (2017), [1703.09304](#).
- [114] C. P. Burgess, L. Leblond, R. Holman, and S. Shandera, JCAP **1003**, 033 (2010), [0912.1608](#).
- [115] J. Serreau, Phys. Rev. Lett. **107**, 191103 (2011), [1105.4539](#).
- [116] A. Rajaraman, Phys. Rev. **D82**, 123522 (2010), [1008.1271](#).
- [117] M. Beneke and P. Moch, Phys. Rev. **D87**, 064018 (2013), [1212.3058](#).
- [118] B. S. DeWitt, Phys.Rev. **162**, 1195 (1967).
- [119] S. Davidson, P. Gambino, M. Laine, M. Neubert, and C. Salomon, eds., *Proceedings, Les Houches summer school: EFT in Particle Physics and Cosmology: Les Houches (Chamonix Valley), France, July 3-28, 2017*, vol. 108 of *Lecture Notes of the Les Houches Summer School* (Oxford University Press, Oxford, 2020), ISBN 978-0-19-885574-3.

- 
- [120] I. G. Moss and D. J. Toms, J.Phys. **A47**, 215401 (2014), 1311.5445.
- [121] T. Markkanen, S. Nurmi, A. Rajantie, and S. Stopyra, JHEP **06**, 040 (2018), 1804.02020.
- [122] I. L. Buchbinder and S. D. Odintsov, Yad. Fiz. **42**, 1268 (1985), [Class. Quant. Grav.2,721(1985)].
- [123] G. Vilkovisky, Nucl. Phys. B **234**, 125 (1984).
- [124] A. Barvinsky, A. Y. Kamenshchik, C. Kiefer, A. Starobinsky, and C. Steinwachs, Eur.Phys.J. **C72**, 2219 (2012), 0910.1041.
- [125] A. Barvinsky, A. Y. Kamenshchik, C. Kiefer, A. Starobinsky, and C. Steinwachs, JCAP **0912**, 003 (2009), 0904.1698.
- [126] A. O. Barvinsky, Prog.Theor.Phys.Suppl. **190**, 1 (2011), 1012.4523.
- [127] J. S. Dowker, Commun. Math. Phys. **162**, 633 (1994), hep-th/9306154.
- [128] E. Elizalde, S. D. Odintsov, A. Romeo, A. A. Bytsenko, and S. Zerbini, *Zeta regularization techniques with applications* (World Scientific, Singapore, 1994).
- [129] A. Mantziris, T. Markkanen, and A. Rajantie (2020), 2011.03763.
- [130] K. Finn, S. Karamitsos, and A. Pilaftsis (2020), 2006.05831.
- [131] A. Rajantie and S. Stopyra (2017), 1707.09175.
- [132] J. A. Casas, J. R. Espinosa, and M. Quiros, Phys. Lett. B **342**, 171 (1995), hep-ph/9409458.
- [133] L. Chataignier, T. Prokopec, M. G. Schmidt, and B. Swiezewska, JHEP **03**, 014 (2018), 1801.05258.
- [134] S. Weinberg, Phys. Rev. **D72**, 043514 (2005), hep-th/0506236.
- [135] E. O. Kahya and R. P. Woodard, Phys. Rev. **D76**, 124005 (2007), 0709.0536.
- [136] K. Finn, S. Karamitsos, and A. Pilaftsis, Phys. Rev. D **102**, 045014 (2020), 1910.06661.
- [137] L. E. Parker and D. Toms, *Quantum Field Theory in Curved Spacetime: Quantized Field and Gravity*, Cambridge Monographs on Mathematical Physics (Cambridge University Press, 2009), ISBN 978-0-521-87787-9, 978-0-521-87787-9, 978-0-511-60155-2.
- [138] A. D. Linde, Phys. Lett. B **129**, 177 (1983).

- 
- [139] D. A. Easson, R. Gregory, D. F. Mota, G. Tasinato, and I. Zavala, JCAP **02**, 010 (2008), 0709.2666.
- [140] S. Cremonini, Z. Lalak, and K. Turzynski, JCAP **03**, 016 (2011), 1010.3021.
- [141] A. Achúcarro, V. Atal, C. Germani, and G. A. Palma, JCAP **02**, 013 (2017), 1607.08609.
- [142] A. Achúcarro, V. Atal, and Y. Welling, JCAP **07**, 008 (2015), 1503.07486.
- [143] A. R. Liddle, A. Mazumdar, and F. E. Schunck, Phys. Rev. D **58**, 061301 (1998), astro-ph/9804177.
- [144] G. Rigopoulos, JCAP **07**, 035 (2016), 1604.04313.
- [145] G. I. Rigopoulos, E. P. S. Shellard, and B. J. W. van Tent, Phys. Rev. D **73**, 083522 (2006), URL <https://link.aps.org/doi/10.1103/PhysRevD.73.083522>.
- [146] Y. Akrami et al. (Planck), Astron. Astrophys. **641**, A7 (2020), 1906.02552.
- [147] D. Baumann and L. McAllister, *Inflation and String Theory*, Cambridge Monographs on Mathematical Physics (Cambridge University Press, 2015), ISBN 978-1-107-08969-3, 978-1-316-23718-2, 1404.2601.
- [148] G. Obied, H. Ooguri, L. Spodyneiko, and C. Vafa (2018), 1806.08362.
- [149] S. K. Garg and C. Krishnan, JHEP **11**, 075 (2019), 1807.05193.
- [150] C. Vafa (2005), hep-th/0509212.
- [151] H. Ooguri and C. Vafa, Nucl. Phys. B **766**, 21 (2007), hep-th/0605264.
- [152] A. R. Brown, Phys. Rev. Lett. **121**, 251601 (2018), 1705.03023.
- [153] S. Mizuno and S. Mukohyama, Phys. Rev. D **96**, 103533 (2017), 1707.05125.
- [154] T. Bjorkmo and M. D. Marsh, JHEP **04**, 172 (2019), 1901.08603.
- [155] M. Cicoli, G. Dibitetto, and F. G. Pedro, Phys. Rev. D **101**, 103524 (2020), 2002.02695.
- [156] S. Renaux-Petel and K. Turzyński, Phys. Rev. Lett. **117**, 141301 (2016), 1510.01281.
- [157] M. Cicoli, V. Guidetti, F. G. Pedro, and G. P. Vacca, JCAP **12**, 037 (2018), 1807.03818.
- [158] M. Cicoli, V. Guidetti, and F. G. Pedro, JCAP **05**, 046 (2019), 1903.01497.

- [159] P. Christodoulidis, D. Roest, and E. I. Sfakianakis, JCAP **12**, 059 (2019), 1903.06116.
- [160] S. Groot Nibbelink and B. van Tent, Class. Quant. Grav. **19**, 613 (2002), hep-ph/0107272.
- [161] P. Christodoulidis, D. Roest, and E. I. Sfakianakis, JCAP **08**, 006 (2020), 1903.03513.
- [162] S. Garcia-Saenz, L. Pinol, and S. Renaux-Petel, JHEP **01**, 073 (2020), 1907.10403.
- [163] S. Garcia-Saenz and S. Renaux-Petel, JCAP **11**, 005 (2018), 1805.12563.
- [164] J. Fumagalli, S. Garcia-Saenz, L. Pinol, S. Renaux-Petel, and J. Ronayne, Phys. Rev. Lett. **123**, 201302 (2019), 1902.03221.
- [165] T. Bjorkmo, R. Z. Ferreira, and M. D. Marsh, JCAP **12**, 036 (2019), 1908.11316.
- [166] R. Z. Ferreira, JCAP **08**, 034 (2020), 2003.13410.
- [167] T. David, *Lectures on Kinetic Theory: Chapter 3; Stochastic Processes* (2012).

Part IV  
Appendix

## Appendix A. Schrödinger-like Probability Equation

This appendix aims to manifestly demonstrate the comparative advantages of the auxiliary field action used in subsection 2.4, as opposed to the Euclidean action obtained from the Schrödinger-like equation associated with the original the Fokker-Planck equation.

Expanding (2.28) and applying the redefinition (2.40), leads to

$$\begin{aligned} f(\phi) \dot{\tilde{P}}(\phi, t) &= [f(\phi) \mathcal{C}_1(\phi) + f'(\phi) \mathcal{C}_2(\phi) + f''(\phi) \mathcal{C}_3(\phi)] \tilde{P}(\phi, t) \\ &\quad + [f(\phi) \mathcal{C}_2(\phi) + 2f'(\phi) \mathcal{C}_3(\phi)] \tilde{P}'(\phi, t) + f(\phi) \mathcal{C}_3(\phi) \tilde{P}''(\phi, t), \end{aligned} \quad (\text{A.1})$$

where, we have defined the parameters

$$\begin{aligned} \mathcal{C}_1 &= \left[ \frac{V'}{3H} \right]' + [1 - \Theta(0)] \hbar (\mathcal{A}')^2 + [1 - \Theta(0)] \hbar \mathcal{A} \mathcal{A}'' \\ \mathcal{C}_2 &= \frac{V'}{3H} + \frac{1}{2} [2 - \Theta(0)] \hbar (\mathcal{A}^2)' \\ \mathcal{C}_3 &= \frac{1}{2} \hbar \mathcal{A}^2. \end{aligned} \quad (\text{A.2})$$

Using the relations for the first and second derivative of the transformation function,

$$f'(\phi) = f(\phi) \left[ -\frac{3H'}{2H} (2 - \Theta(0)) - \frac{V'}{3\hbar H \mathcal{A}^2} \right] \quad (\text{A.3})$$

and

$$\begin{aligned} f''(\phi) = f(\phi) \left\{ \left[ \frac{3H'}{2H} (2 - \Theta(0)) + \frac{V'}{3\hbar H \mathcal{A}^2} \right]^2 - \frac{3}{2} (2 - \Theta(0)) \left[ \frac{H''}{H} - \left( \frac{H'}{H} \right)^2 \right] \right. \\ \left. - \left( \frac{V''}{3\hbar H \mathcal{A}^2} - \frac{4V' H'}{3\hbar H^2 \mathcal{A}^2} \right) \right\} \end{aligned} \quad (\text{A.4})$$

one, readily, observes that the coefficient of  $\tilde{P}'$  vanishes, resulting in a Wick-rotated ( $t \rightarrow -it$ ) Schrödinger-like equation,

$$\begin{aligned} \dot{\tilde{P}}(\phi, t) &= \left[ \mathcal{C}_1 + \mathcal{C}_2 \frac{f'(\phi)}{f\phi} + \mathcal{C}_3 \frac{f''(\phi)}{f(\phi)} \right] \tilde{P}(\phi, t) + \mathcal{C}_3 \tilde{P}'' \\ \dot{\tilde{P}}(\phi, t) &= \hat{\mathcal{H}} \tilde{P}, \end{aligned} \quad (\text{A.5})$$



with Hamiltonian,

$$\begin{aligned}\hat{\mathcal{H}} &= \left[ \mathcal{C}_1 + \mathcal{C}_2 \frac{f'(\phi)}{f\phi} + \mathcal{C}_3 \frac{f''(\phi)}{f(\phi)} \right] + \mathcal{C}_3 \partial_\phi^2 \\ &\equiv U(\phi) + \mathcal{C}_3 \partial_\phi^2,\end{aligned}\tag{A.6}$$

where the potential  $U(\phi)$  is given by

$$\begin{aligned}U(\phi) &= \frac{1}{2} \left[ \frac{V'}{3H} \right]' - \frac{1}{2\hbar\mathcal{A}^2} \left( \frac{V'}{3H} \right)^2 - \frac{1}{2} (1 - \Theta(0)) \frac{V'}{3H} \frac{H'}{H} \\ &\quad + \frac{1}{2} \left( 1 - \frac{\Theta(0)}{2} \right)^2 \left( \frac{3H'}{H} \right)^2 \hbar\mathcal{A}^2 - \left( 1 - \frac{\Theta(0)}{2} \right) \hbar\mathcal{A}^2 \left( \frac{3H'}{H} \right)'.\end{aligned}\tag{A.7}$$

To verify the accuracy of the correspondence between the path integral approach of the Schrödinger and the Fokker-Planck equations, we write the one-dimensional Euclidean action associated with the former:

$$\begin{aligned}-S_{Schr}^{Eucl} &= - \int dt \left[ p\dot{q} - \hat{\mathcal{H}} \right] \\ &= - \int dt \left[ \frac{\dot{\phi}^2}{4\mathcal{C}_3} - U(\phi) \right].\end{aligned}\tag{A.8}$$

For the case of additive noise, when the Hubble parameter  $H$  is constant, all derivatives of  $H(\phi)$  and  $\mathcal{A}$ , in (A.7) vanish, resulting in

$$-U(\phi) = -\frac{1}{2} \frac{V''}{3H} + \frac{1}{2} \left( \frac{V'}{3H} \right)^2 \frac{1}{\hbar\mathcal{A}^2},\tag{A.9}$$

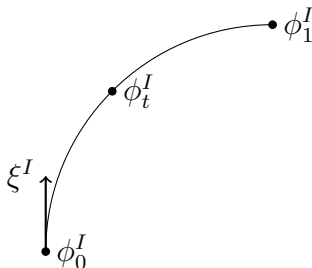
in direct agreement with [167], in which the same action has been obtained from the Fokker-Planck equation associated with the original Langevin.

The corresponding action, including the entirety of (2.56), despite *a priori* being expected to give the correct results, is computationally, a lot more complicated than its auxiliary field method counterpart (2.52).

## Appendix B. Field space Geometry

In this appendix, we provide a visual aid to the treatment of fields in a curved field space and showcase the equivalence between the covariant background field expansion and the addition of the DeWitt term, for the simple case of a Non-Linear Sigma Model, as an example of the methodology used in chapter 3. We proceed to obtain the equations of motion for the perturbations, which were used in chapter 4. These subjects are well-documented in the literature in a mathematically rigorous manner, however, a more intuitive exposition may be useful and instructive.

### B.1 Covariant Background Field Expansion



Let  $\phi^I$  denote the coordinates of a point in a  $D$ -dimensional Riemannian manifold  $\mathcal{M}$  and  $\phi_{t=0}^I$  a point around which we choose to expand. Define a geodesic  $s^I(t)$  depending on the affine parameter  $t$ , extending from this point to another point in its neighborhood (such that they are connected by a single geodesic)  $\phi_{t=1}^I = \phi_{t=0}^I + \delta\phi^I(t)$ . For any point  $s^I(t)$ , the geodesic equation demands that

$$\ddot{s}^I(t) + \Gamma_{JK}^I(s) \dot{s}^J(t) \dot{s}^K(t) = 0 \quad (\text{B.1})$$

be true, with the overdot representing differentiation with respect to the affine parameter. Expanding the geodesic around  $\phi_0^I$ , one obtains:

$$s^I(t) = \sum_{n=0}^{\infty} \frac{1}{n!} [s^I]_{|t=0}^n t^n, \quad (\text{B.2})$$

with  $[s^I]_{|t=0}^n$  denoting the  $n$ -th derivative of the geodesic components evaluated at the origin  $t = 0$ . With  $\xi^I \equiv \dot{s}^I|_{t=0}$  being the tangent to the geodesic vector, at the origin, the geodesic expansion can be obtained recursively to any order using (B.1), as

$$[s^I]^n(t) = C_{J_1 \dots J_N}^I(s) \dot{s}^{J_1}(t) \dots \dot{s}^{J_N}(t), \quad (\text{B.3})$$

where the coefficients  $C_{J_1 \dots J_N}^I$  are obtained by varying (B.1) with respect to the affine parameter  $t$ . For example, the first two terms are

$$\begin{aligned} C_{JK}^I(s) &= -\Gamma_{JK}^I \\ C_{JKL}^I(s) &= -\Gamma_{JK,L}^I - \frac{1}{2}\Gamma_{JM}^I \Gamma_{KL}^M - \frac{1}{2}\Gamma_{KM}^I \Gamma_{LJ}^M, \end{aligned} \quad (\text{B.4})$$

where  $\Gamma_{JK}^I$  is the Christoffel connection associated with the metric  $\mathcal{G}_{IJ}$  of the field space manifold  $\mathcal{M}$ . After computing the coefficients in (B.2), we can expand the coordinates of the end-point of the geodesic interval  $\phi|_{t=1} = s|_{t=1} = \phi|_{t=0} + \delta\phi^I(t)$ , or

$$\delta\phi^I = \xi^I - \frac{1}{2}\Gamma_{JK}^I \xi^J \xi^K + \dots, \quad (\text{B.5})$$

where dots signify higher order corrections in the, appropriately small for the ansatz of vicinity to the origin to be satisfied, vector  $\xi^I$ .

## B.2 The NLSM Perturbation Equation of Motion

The classical action of a Non-Linear Sigma Model, is given by

$$S = \frac{1}{2} \int d^D x \sqrt{-g} G_{IJ}(\phi) g^{\mu\nu} \partial_\mu \phi^I \partial_\nu \phi^J \quad (\text{B.6})$$

with  $g^{\mu\nu}$  being the  $D$ -dimensional spacetime metric and  $G_{IJ}$  being the field space metric. Expanding the action in orders of  $\delta\phi^I$ , up to the second order, we obtain:

$$S = S|_{\delta\phi^I=0} + \frac{\delta S}{\delta[\delta\phi^I]}|_{\delta\phi^I=0} \delta\phi^I + \frac{1}{2} \frac{\delta^2 S}{\delta[\delta\phi^I] \delta[\delta\phi^J]}|_{\delta\phi^I=0} \delta\phi^I \delta\phi^J. \quad (\text{B.7})$$

Substituting (B.5) in the first order variation of the action, leads to

$$\begin{aligned} \delta_1 S &= \int d^D x \sqrt{-g} \left\{ \frac{1}{2} \mathcal{G}_{IJ,K} \delta\phi^K \partial_\mu \phi^I \partial_\nu \phi^J g^{\mu\nu} + \mathcal{G}_{IJ} \partial_\mu \delta\phi^I \partial_\nu \phi^J g^{\mu\nu} \right\} \\ &= \delta_1 S^{\xi^1} + \delta_1 S^{\xi^2}, \end{aligned} \quad (\text{B.8})$$

which includes terms of both first and second order in  $\xi$ . Furthermore, the second variation of the action becomes

$$\begin{aligned} \delta_2 S &= \int \sqrt{-g} g^{\mu\nu} d^D x \left[ \frac{1}{2} \mathcal{G}_{IJ,KL} \xi^K \xi^L \partial_\mu \phi^I \partial_\nu \phi^J + \frac{1}{2} \mathcal{G}_{IJ,K} \xi^K \partial_\mu \xi^I \partial_\nu \phi^J \right. \\ &\quad \left. + \frac{1}{2} \mathcal{G}_{IJ,K} \xi^K \partial_\mu \phi^I \partial_\nu \xi^J + \mathcal{G}_{IJ,K} \xi^K \partial_\mu \xi^I \partial_\nu \phi^J + \mathcal{G}_{IJ} \partial_\mu \xi^I \partial_\nu \xi^J \right]. \end{aligned} \quad (\text{B.9})$$

Grouping these contributions in powers of  $\xi$  we obtain

$$S(\xi)|_{\xi=0} = S_{(\xi=0)} + \Delta_1 S^{\xi^1} + \Delta_2 S^{\xi^2}, \quad (\text{B.10})$$

where  $\Delta_1 S^{\xi^1} = \delta_1 S^{\xi^1}$  and

$$\begin{aligned} \Delta_2 S^{\xi^2} &\equiv \frac{1}{2} \left[ \delta_2 S + 2\delta_1 S^{\xi^2} \right] \\ &= \frac{1}{2} \int d^D x \sqrt{-g} \left[ \left( -\mathcal{R}_{bcad} \right) \partial_\mu \phi^a \partial^\mu \phi^b \xi^c \xi^d + \mathcal{G}_{ab} D_\nu \xi^a D^\nu \xi^b \right], \end{aligned} \quad (\text{B.11})$$

where we have introduced the action of the covariant, with respect to the spacetime metric  $g_{\mu\nu}$ , derivative on the tangent to the field space manifold vector  $\xi^a [\phi(x^\mu)]$ , as

$$D_\mu \xi^a = \nabla_\mu \xi^a + \phi^d{}_{,\mu} \Gamma_{dc}^a \xi^c. \quad (\text{B.12})$$

### B.2.1 The *Vilkovisky-deWitt Term*

Returning to the background field expansion, from (B.8) one can take the  $\delta_1 S^{\xi^2}$ , namely the terms of the first order variation of the action that are second order in  $\xi$ . These prove to be:

$$\begin{aligned} \delta_1 S^{\xi^2} &= \int \sqrt{-g} d^D x \left\{ \frac{1}{2} \mathcal{G}_{ab,c} \delta \phi^c (\partial^\mu \phi^a \partial_\mu \phi^b) + \mathcal{G}_{ab} \partial^\mu \phi^a \partial_\mu \delta \phi^b \right\} \\ &= \int \sqrt{-g} d^D x \xi^e \xi^f \left\{ \frac{1}{2} \mathcal{G}_{ab} D^\mu [\partial_\mu \phi^a] \Gamma_{ef}^b \right\}. \end{aligned} \quad (\text{B.13})$$

Similarly, expanding the first order variation (B.8) and keeping the terms linear in  $\xi$  we obtain

$$\begin{aligned} \delta_1 S^{\xi^1} &= \int d^D x \sqrt{-g} \left\{ \frac{1}{2} G_{ab,c} \delta \phi^c \partial_\mu \phi^a \partial_\nu \phi^b g^{\mu\nu} + G_{ab} \partial_\mu \delta \phi^a \partial_\nu \phi^b g^{\mu\nu} \right\} \\ &= \int d^D x \sqrt{-g} \left\{ -G_{ab} D^\mu (\partial_\mu \phi^a) \xi^b \right\}. \end{aligned} \quad (\text{B.14})$$

Hence, we conclude, using the background expansion method, that the covariant second order in  $\xi$  variation of the action is given by the naive second order variation, corrected by the Vilkovisky-deWitt term

$$\Delta_I \Delta_J S^{\xi^2} = \delta_I \delta_J S^{\xi^2} - \Gamma_{IJ}^K \frac{\delta_1 S^{\xi^1}}{\delta \xi^K}. \quad (\text{B.15})$$

### B.2.2 *Perturbation Equation of Motion*

Integrating (B.11) by parts, it is straightforward, to obtain the equation of motion for the perturbation  $\xi^d$ ,

$$\left( \mathcal{R}_{bcad} \right) \partial_\mu \phi^a \partial^\mu \phi^b \xi^c + \mathcal{G}_{cd} D^\nu D_\nu \xi^c = 0, \quad (\text{B.16})$$

which was used in (4.24).

This result can also be obtained from purely geometrical considerations. Treating  $\phi^a$  as coordinates of a point in field space, the fiducial geodesic for the tangent vector  $\nabla^\mu \phi^a$  is:

$$\nabla_\mu \nabla^\mu \phi^a + \Gamma_{bc}^a \partial_\mu \phi^b \partial^\mu \phi^c = 0. \quad (\text{B.17})$$

Performing a parallel transport of the coordinate  $\phi^a$  along the vector  $\xi^a$  as  $\phi'^a \rightarrow \phi^a + \xi^a$  results in a perturbation of the fiducial geodesic

$$\nabla_\mu \nabla^\mu \phi^a + \nabla_\mu \nabla^\mu \xi^a + \Gamma_{bc}^a [\phi + \xi] [2\partial_\mu \phi^b \nabla^\mu \xi^c + \partial_\mu \phi^b \partial^\mu \phi^c + O(\xi^2)] = 0. \quad (\text{B.18})$$

Expanding the connection around  $\phi^a$

$$\Gamma_{bc}^a(\phi + \xi) = \Gamma_{bc}^a(\phi) + \Gamma_{bc,d}^a \xi^d, \quad (\text{B.19})$$

and using (B.17), (B.18) becomes

$$\nabla_\mu (\nabla^\mu \xi^a) + 2\Gamma_{bc}^a \partial_\mu \phi^b \nabla_\mu \xi^c + \Gamma_{bc,d}^a \xi^d \partial_\mu \phi^b \partial^\mu \phi^c = 0. \quad (\text{B.20})$$

In order to determine the second spacetime-covariant derivative of the field space vector  $\xi^a$ , we start by expanding the action of the total covariant derivative, which acts on both field space and spacetime indices, on a vector  $[V^\nu]^a$ ,

$$D_\mu [V^\nu]^a = \partial_\mu [V^\nu]^a + \Gamma_{\mu\rho}^\nu [V^\rho]^a + \Gamma_{bc}^a [V^\nu]^b \partial_\mu \phi^c. \quad (\text{B.21})$$

Hence, for the field space vector  $\xi^a$ , utilising (B.17), we have

$$\begin{aligned} D_\mu D^\mu \xi^a &= \nabla_\mu (D^\mu \xi^a) + \Gamma_{bc}^a D^\mu \xi^b \partial_\mu \phi^c \\ &= \nabla_\mu (\nabla^\mu \xi^a) + \Gamma_{bc,d}^a \xi^b \partial_\mu \phi^d \partial^\mu \phi^c + 2\Gamma_{bc}^a \nabla_\mu \xi^b \partial^\mu \phi^c \\ &\quad + \Gamma_{bc}^a \xi^b [-\Gamma_{gh}^c \partial^\mu \phi^g \partial_\mu \phi^h] + \Gamma_{bc}^a \Gamma_{ed}^b \xi^d \partial_\mu \phi^e \partial^\mu \phi^c, \end{aligned} \quad (\text{B.22})$$

and using (B.20) we, finally, obtain the expected result (B.16),

$$D_\mu D^\mu \xi^a = \mathcal{R}_{cbd}^a \xi^d \partial_\mu \phi^b \partial^\mu \phi^c. \quad (\text{B.23})$$

## Appendix C. Zeta-function Evaluation

We review and extend the basic tools of heat kernel methods needed for the evaluation of the zeta function, and subsequently, using the renormalisation group equation (3.2), the beta functions for the Gravity-scalar model (3.6).

We may start by showcasing the basic concepts of functional Gaussian integration. Let  $A_{ij}$  be a diagonalisable, non-degenerate matrix with real eigenvalues. Then, the Gaussian integral can be defined throughout the space with volume element  $d\mu$  described by coordinates  $x^i$ , as

$$\begin{aligned} \mathcal{P}(A) &= \int d\mu e^{\left(\frac{i}{2} x^i A_{ij} x^j\right)} \\ &= \prod_i \int d\mu e^{\left(\frac{i}{2} \lambda_i x^2\right)} \\ &= (2\pi i)^{n/2} \det(A)^{-1/2}. \end{aligned} \tag{C.1}$$

Where, in the first line, a coordinate transformation permits the diagonalisation of the matrix  $A_{ij}$ , resulting in a set of real eigenvalues the product of which leads to the determinant in the last line.

We now return to (3.12) and utilise (3.13) and the definition of the functional integral. Hence, the effective action (3.16) is straightforwardly obtained [93] as

$$\Gamma[g, \varphi] = S[\varphi] + \frac{i\hbar}{2} \ln \det \left( \frac{\Delta}{\mu_R^2} \right), \tag{C.2}$$

leading to (3.33),

$$\Gamma^{(1)} = \frac{\hbar}{2i} \text{tr} \ln \frac{\Delta}{\mu_R^2}, \tag{C.3}$$

or, alternatively, using a Wick-rotation to imaginary time, transforming the spacetime background to a Euclidean space with positive signature, the one-loop correction to the Euclidean effective action becomes

$$\Gamma_E^{(1)} = \frac{\hbar}{2} \text{tr} \ln \frac{\Delta}{\mu_R^2}. \tag{C.4}$$

This analytic continuation results in the invariant volume element becoming imaginary, but this can be resolved by defining the one-loop correction to the effective action as

$\Gamma_E^{(1)} = i\Gamma^{(1)}$ . Using a gradient expansion of the effective action,

$$\Gamma_E[\phi] = \int d\mu \left[ \frac{1}{2} Z(\phi) (\nabla\phi)^2 + V(\phi) \right] + \dots, \quad (\text{C.5})$$

or, to one-loop accuracy and for constant background fields,

$$\Gamma_E^{(1)}[\phi] = V^{(1)}(\phi) \times \text{spacetime volume}. \quad (\text{C.6})$$

At this point, we introduce the Riemann  $\zeta$ -function. For an operator  $\Delta$  with a discrete set of eigenvalues,  $\lambda_n$ ,

$$\zeta(s, \Delta) = \sum_{n=0}^{\infty} \lambda_n^{-s}. \quad (\text{C.7})$$

Extending this definition to operators with an infinite number of eigenvalues is well motivated, as we describe below. We define, in general

$$\zeta(s, \Delta) = \text{tr} (\Delta^{-s}). \quad (\text{C.8})$$

It must be noted that, this sum only converges when  $2s > D$ , where  $D$  is the number of spacetime dimensions, however, this limitation can be removed through the process of analytic continuation in the complex  $s$ -plane. It is crucial for this type of regularisation that the  $\zeta$ -function is analytic at the point  $s = 0$ .

With these in mind, one can define the one-loop correction to the effective action,

$$2\Gamma_E^{(1)} = \ln \det \frac{\Delta}{\mu_R^2} = -\zeta'(0, \Delta) - \zeta(0, \Delta) \log \mu_R^2. \quad (\text{C.9})$$

It is easy to see, that in the case of finite eigenvalues, this formula would be an identity resulting from trivial algebraic calculations following from (C.3) and (C.8). In the case of infinite eigenvalues, the regularisation procedure defined by (C.9) allows one to obtain finite results.

Varying (C.9) with respect to the renormalisation scale  $\mu_R$  and using (C.6) in  $S_4$ , it is clear that

$$\mu_R \frac{dV^{(1)}}{d\mu_R} = -\frac{\zeta(0, \Delta) R^2}{16\pi^2} \frac{R^2}{24}. \quad (\text{C.10})$$

Having obtained the eigenvalues for the operator  $\Delta_{IJ}$ , given in (3.91), in the harmonic basis, we proceed to evaluate  $\zeta(0, \Delta)$ . Generalised zeta-functions for the operator eigenvalues on a four-sphere can be evaluated by using a standard binomial expansion method [127, 128]. Eigenvalues of the Laplacian are quadratic in  $n$ , but after diagonalisation of our operators some of the eigenvalues are non-polynomial, and a modification of the usual techniques is required.

The operators obtained in section 3.6.2 act on scalar, vector and tensor fields on a four-dimensional de Sitter space. Their eigenvalues and degeneracies can be related to

the Laplacian eigenvalues,  $\hat{\lambda}_n = (n + \nu)^2$  through:

$$\lambda_n = \frac{R}{12} (\hat{\lambda}_n - a), \quad g_n = b(n + \nu)^3 + c(n + \nu), \quad (\text{C.11})$$

where  $n = 0, 1, 2, \dots$ , and the parameters  $\nu, a, b$  and  $c$  depend on the type of tensor according to Table C.1.

	$\nu$	$a$	$b$	$c$
Scalar	$\frac{3}{2}$	$\frac{9}{4} + q$	$\frac{1}{3}$	$-\frac{1}{12}$
Vector	$\frac{5}{2}$	$\frac{13}{4} + q$	1	$-\frac{9}{4}$
Tensor	$\frac{7}{2}$	$\frac{17}{4} + q$	$\frac{5}{3}$	$-\frac{125}{12}$

Table C.1: Numerical values of Laplace-like operator eigenvalue parameters. Here,  $q$  are dimensionless parameters of the model and are functions of the background field and the Ricci scalar  $R$ .

The eigenvalues  $\lambda_n$  obtained after diagonalisation of the - projected to the physical subspace - operator  $\Pi^I_K G^{KM} \Delta_{ML} \Pi^L_J$  are algebraic functions of the Laplacian eigenvalues  $\hat{\lambda}_n$  and can be expanded for large  $n$  as power series

$$\lambda_n = \frac{1}{12} R [(n + \nu)^2 + A + B(n + \nu)^{-2} + \dots]. \quad (\text{C.12})$$

We proceed by replacing  $\lambda_n^{-s}$  in the zeta-function with its binomial expansion,

$$\begin{aligned} \zeta(s) &= \sum_{n=0}^{\infty} g_n \lambda_n^{-s} \\ &= \sum_{n=0}^{\infty} \left( \frac{R}{12} \right)^{-s} \left\{ c \left[ (n + \nu)^{(1-2s)} - s A (n + \nu)^{-(1+2s)} + \dots \right] \right. \\ &\quad \left. + b \left[ (n + \nu)^{(3-2s)} - s A (n + \nu)^{(1-2s)} - (n + \nu)^{-(1+2s)} B s \right. \right. \\ &\quad \left. \left. + \frac{s(s+1) A^2}{2} (n + \nu)^{-(2s+1)} + \dots \right] \right\}, \end{aligned} \quad (\text{C.13})$$

and then the sums of powers of  $n + \nu$  can be replaced by the Hurwitz zeta-function  $\zeta_H(s, \nu)$ ,

$$\zeta_H(s, \nu) = \sum_{n=0}^{\infty} (n + \nu)^{-s}. \quad (\text{C.14})$$

The Hurwitz zeta-function has an analytic extension with a pole at  $s = 0$  with residue 1, a Laurent series expansion,

$$\zeta_H(s, \nu) = \frac{1}{s-1} + \Psi(A) + \mathcal{O}(s), \quad (\text{C.15})$$



where  $\Psi(A)$  is the digamma function, and for values  $s = -1$  and  $s = -3$  takes the form of Bernoulli polynomials,

$$\zeta_H(-1, \nu) = -\frac{1}{2}B_2(\nu), \quad \zeta_H(-3, \nu) = -\frac{1}{4}B_4(\nu). \quad (\text{C.16})$$

After rearranging the summations, we arrive at an expression for the zeta function,

$$\zeta(s) = \left(\frac{R}{12}\right)^{-s} \{bf(s) + cg(s)\}, \quad (\text{C.17})$$

where

$$\begin{aligned} f(s) &= \zeta_H(2s-3, \nu) - sA\zeta_H(2s+1, \nu) - sB\zeta_H(2s+1, \nu) + \frac{1}{2}s(s+1)A^2\zeta_H(2s+1, \nu) + \dots \\ g(s) &= \zeta_H(2s-1, \nu) - sA\zeta_H(2s+1, \nu) + \dots \end{aligned} \quad (\text{C.18})$$

All of the terms denoted by  $\dots$  vanish at  $s = 0$  and we are left with

$$\zeta(0) = -\frac{1}{2}cB_2(\nu) - \frac{1}{4}bB_4(\nu) - \frac{c}{2}A - \frac{b}{4}(2B - A^2). \quad (\text{C.19})$$

The zeta-function sum is always taken from  $n = 0$ , but some of the derived modes are identically zero for some  $n$ . These exceptions are handled by subtracting the contributions of the  $N(h)$  non-existent modes,

$$\zeta(0) = \lim_{s \rightarrow 0} \left( \sum_{n=0}^{\infty} g_n \lambda_n^{-s} \right) - N(h). \quad (\text{C.20})$$

For example, the gradient of a constant scalar mode does not give a valid vector mode, resulting in  $N(\nabla_\mu h^S) = 1$ . Furthermore, for the vector case, there is a zero-eigenvalue mode with multiplicity  $N(\nabla_{(\mu} h_{\nu)}^V) = 10$ , that needs to be excluded [109], as well as  $N(\nabla_{\mu\nu} h^S) = 6$ , vanishing tensor modes.

Hence, we obtain the  $\zeta(0)$  contribution of the scalar, tensor, and ghost eigenvalues for the simple scalar-gravity operator (3.91) as a function of the parameters in Table C.1 and the functions  $A$  and  $B$  (which are dependent on the scalar potential and its derivatives),

$$\begin{aligned} \zeta(0)_{\text{total}} &= \zeta_{\text{scalar}}(0) + \zeta_{\text{tensor}}(0) - 2\zeta_{\text{ghost}}(0) \\ &= \frac{1}{R^2} [336\kappa^4 V^2 - 48\kappa^2 V V_{;i}{}^i + 12V_{;ij} V^{;ij} - 36\kappa^2 V_{;i} V^{;i}] \\ &\quad + \frac{1}{R} (8V_{;i}{}^i - 208\kappa^2 V) + O(R^2). \end{aligned} \quad (\text{C.21})$$

Then, we obtain the heat kernel coefficient on  $S_4$ , from (3.39)

$$\frac{1}{16\pi^2} b_2(\Delta) = \zeta(0) \text{Volume}_{S_4} = \zeta(0) \frac{1}{16\pi^2} \frac{R^2}{24} \quad (\text{C.22})$$

and comparing with the general expression (3.92) we find, for the single scalar case  $N=1$ ,

$$a_1 = \frac{1}{2} \qquad a_2 = -\frac{3}{2} \qquad a_3 = -2 \qquad (C.23)$$

$$a_4 = 2N + 12 \qquad a_5 = \frac{1}{3} \qquad a_6 = -\frac{1}{3}(24 - 2N), \qquad (C.24)$$

in agreement with [88].

Finally, expanding the heat kernel coefficient  $b_2(\Delta)$  in powers of  $\phi$  and truncating up to order  $\kappa^2$ , we find the coefficients

$$\begin{aligned} b_2(\Delta)|_{\phi^2} &= \frac{1}{16\pi^2} \frac{R^2}{24} \left[ \frac{12}{R^2} V_{;ij} V^{;ij}|_{\phi^2} - \frac{48}{R^2} \kappa^2 V V_{;i}{}^i|_{\phi^2} \right] \phi^2 \\ &= \frac{1}{16\pi^2} [3\mu^2\lambda + 3\kappa^2\lambda(4\xi V_0) - 2\kappa^2 \times 3\lambda V_0 + O(\kappa^4)] \phi^2 \end{aligned} \qquad (C.25)$$

$$b_2(\Delta)|_{R\phi^2} = \frac{1}{16\pi^2} \frac{R^2}{24} \frac{8}{R} V_{;i}{}^i|_{\phi^2} = \frac{1}{16\pi^2} \lambda R \phi^2 \qquad (C.26)$$

$$b_2(\Delta)|_{\phi^4} = \frac{1}{16\pi^2} \frac{1}{2} 12 V_{;ij} V^{;ij}|_{\phi^4} = \frac{1}{16\pi^2} \frac{9}{2} \lambda \phi^4 \qquad (C.27)$$

$$\begin{aligned} b_2(\Delta)|_{\phi^6} &= \frac{1}{16\pi^2} \frac{R^2}{24} \left[ \frac{12}{R^2} V_{;ij} V^{;ij}|_{\phi^6} - \frac{36\kappa^2}{R^2} V_{;i} V^{;i}|_{\phi^6} - 48\kappa^2 V V_{;i}{}^i|_{\phi^6} \right. \\ &\qquad \qquad \qquad \qquad \qquad \qquad \qquad \qquad \qquad \qquad \qquad \qquad \qquad \qquad \qquad \left. + \frac{8}{R} V_{;i}{}^i|_{\phi^6} \right] \\ &= \frac{1}{16\pi^2} [15\lambda \lambda_6 - 3\lambda^2 + 21\lambda^2\xi - 72\lambda^2\xi^2] \kappa^2 \phi^6. \end{aligned} \qquad (C.28)$$

Expanding (3.2) as in the example, (3.116) and remembering that the anomalous dimensions vanish to one loop order  $\gamma = O(\lambda^2)$  [121], the covariant  $\beta$ -functions of Tables 3.2 and 3.3 follow trivially.

## Appendix D. Stochastic Noise Kernel for Hyperinflation

Utilising the modes obtained numerically in section 4.4.3, we obtain the noise kernel of the covariant second-order Langevin equation associated with the two-dimensional hyperbolic field space of section 4.3. We pay attention to two cases of coarse-graining window functions, namely the Heaviside and a new type, which we name ‘chintz’. We close by demonstrating the temporal evolution of the noise kernel for observationally permitted values of the field-space curvature parameter  $y$ . This preliminary work is part of a follow-up paper to [3]. The interested reader is directed to the detailed publication [42] and references therein.

### D.1 Noise Kernel for the Heaviside Coarse-Graining Window

It was covered in Chapter 2 that a scalar field  $\Phi^a$  can be split into a quasi-classical long-wavelength field  $\varphi$ , coarse-grained over scales of the order of the Hubble length  $\Delta r \approx 1/H$  with a window function  $W_k$ , and a short-wavelength quantum perturbation  $q^a$  that satisfies the perturbed de Sitter Klein-Gordon equation. The mode expansion for the short-wavelength field, which includes only modes of wavenumber larger than the Hubble wavenumber  $k_0$ , in Fourier space is given by

$$\begin{aligned} q^a(\underline{x}, t) &= \int \frac{d^3k}{(2\pi)^3} W_k(t) \xi^a(\underline{x}, t) \\ q^a(\underline{x}, t) &= \int \frac{d^3k}{(2\pi)^3} W_k(t) \left[ U^a{}_I(k, t) a_k^I e^{i\mathbf{k}\cdot\mathbf{x}} + U^{\dagger a}{}_I(k, t) a_k^{\dagger I} e^{-i\mathbf{k}\cdot\mathbf{x}} \right], \end{aligned} \quad (\text{D.1})$$

with  $[a_k^I, a_{k'}^{J\dagger}] = \delta^{IJ} \delta(k - k')$ . The split between long- and short-wavelength modes (2.4) results in the perturbed equations of motion

$$\partial_\mu \partial^\mu \phi^a + \Gamma_{\mu\nu}^\mu \partial^\nu \phi^a + \Gamma_{bc}^a \partial_\mu \phi^b \partial^\mu \phi^c + V_{,a} = - \left[ D_\mu D^\mu q^a + \mathcal{R}_{cbd}^a q^b \partial_\mu \phi^d \partial^\mu \phi^c + q^d D_d V_{,b} \mathcal{G}^{ab} \right]. \quad (\text{D.2})$$

Using (4.24) and the fact that  $\xi^a$  annihilates the perturbed Klein-Gordon equation, one obtains the covariant form of the second-order Langevin equation for the long-wavelength field,  $\phi$ , as

$$\begin{aligned}
 D_\mu D^\mu \phi^a + V_{,b} \mathcal{G}^{ab} &= \left[ \partial_t^2 + 3 \frac{\dot{\alpha}}{\alpha} \partial_t - \alpha^{-2} \nabla^2 \right] \phi^a + \Gamma_{bc}^a \partial_\mu \phi^b \partial^\mu \phi^c + V_{,b} \mathcal{G}^{ab} \\
 &= - \left[ D_\mu D^\mu q^a + \mathcal{R}_{cbd}^a q^b \partial_\mu \phi^d \partial^\mu \phi^c + q^d D_d V_{,b} \mathcal{G}^{ab} \right] \\
 &= - \int \frac{d^3 k}{(2\pi)^3} \left\{ \xi^a D_\mu D^\mu [W_k(t) (|k| - \epsilon/\eta)] \right. \\
 &\qquad\qquad\qquad \left. + 2 D_\mu W_k(t) D^\mu \xi^a \right\} \\
 &\equiv \Xi^a(x, t).
 \end{aligned} \tag{D.3}$$

Had we known the analytic expression for the perturbation doublet mode functions  $U_I^a$ , this equation would result in a Langevin equation that could be solved, either perturbatively or by exponentiation into a path integral, as in section 2. Nevertheless, we can still produce some general expressions before resorting to numerics.

The most straightforward and widely used [48, 50, 52] choice for a coarse graining window is the Heaviside function,  $\Theta(|k| - \epsilon a H)$ . Then, one needs to compute the covariant derivatives appearing in (D.3) acting on the Heaviside

$$D_\mu \Theta(|\mathbf{k}| - \epsilon a H) = \partial_\mu \Theta(|\mathbf{k}| - \epsilon a H) \tag{D.4}$$

$$\begin{aligned}
 D_\mu D^\mu \Theta(|\mathbf{k}| - \epsilon a H) &= \partial_t^2 \Theta(|\mathbf{k}| - \epsilon a H) + 3 \frac{\dot{\alpha}}{\alpha} \partial_t \Theta(|\mathbf{k}| - \epsilon a H) - \alpha^{-2} \nabla^2 \Theta(|\mathbf{k}| - \epsilon a H) \\
 &= \partial_t^2 \Theta(|\mathbf{k}| - \epsilon a H) + 3 \frac{\dot{\alpha}}{\alpha} \partial_t \Theta(|\mathbf{k}| - \epsilon a H).
 \end{aligned} \tag{D.5}$$

Here, all spatial derivatives vanish, since  $\Theta(|\mathbf{k}| - \epsilon a H)$  is only time-dependent.

With these considerations, we obtain a covariant definition for the noise kernel vector,

$$\Xi^a(x, t) = \int \frac{d^3 k}{(2\pi)^3} \delta(|k| - \epsilon/\eta) \left[ a_{\mathbf{k}}^I Z^a_I(|\mathbf{k}|) e^{-i\mathbf{k}\cdot\mathbf{x}} + a_{\mathbf{k}}^{\dagger I} Z^{a*}_I(|\mathbf{k}|) e^{i\mathbf{k}\cdot\mathbf{x}} \right], \tag{D.6}$$

where

$$Z^a_I(\mathbf{k}, \eta, \mathbf{x}) = \frac{-2\epsilon}{\eta^2 \alpha^2} D_\eta U_I^a + \frac{2\epsilon}{\alpha^2 \eta^3} \left[ 1 - \frac{\eta}{\alpha} \frac{d\alpha}{d\eta} \right] U_I^a + e^{i\mathbf{k}\cdot\mathbf{x}} \frac{\epsilon^2}{\alpha^2 \eta^4} \partial_{k^b} \left( \frac{k^b}{|k|} e^{-i\mathbf{k}\cdot\mathbf{x}} U_I^a \right), \tag{D.7}$$

$\eta = -\frac{1}{a(t)H}$  is the conformal time and  $U_I^a(k)$  are the mode functions that satisfy (4.24).

Having obtained the covariant expression for the noise kernel vector  $\Xi^a$ , the last step is expressing the noise amplitude with respect to the Fourier space projection operators (D.7),

$$\begin{aligned}
 \langle \Xi^a(x_1, t_1), \Xi^b(x_2, t_2) \rangle &= \frac{\eta^2 \alpha}{\epsilon} \int \frac{d^3 k}{(2\pi)^3} \delta(|k| - \epsilon/\eta) \delta(t - t') \\
 &\qquad\qquad\qquad \left\{ Z_I^{*a} Z^{Ib} e^{-i\mathbf{k}\cdot(\mathbf{x}-\mathbf{x}')} + n(|k|) \left[ Z_I^a Z^{*bI} + Z_I^a Z^{Ib} \right] e^{-i\mathbf{k}\cdot(\mathbf{x}-\mathbf{x}')} \right\},
 \end{aligned} \tag{D.8}$$

where  $\langle a_k^{I\dagger} a_{k'}^J \rangle = (2\pi)^3 \delta^{IJ} \delta^{(3)}(k-k') n(|k|)$ . For a Bunch-Davies Vacuum [62],  $n(|k|) = 0$ ,

$$\begin{aligned} \langle \Xi^a(x_1, t_1), \Xi^b(x_2, t_2) \rangle &= \frac{\eta^2 \alpha}{\epsilon} \int \frac{d^3 k}{(2\pi)^3} \delta(|k| - \epsilon/\eta) \left[ Z_I^{*a} Z^{Ib} e^{-i\mathbf{k}\cdot(\mathbf{x}-\mathbf{x}')} \right] \delta(t-t') \\ &= D^{ab}(x, x', \eta) \delta(t-t'). \end{aligned} \quad (\text{D.9})$$

## D.2 Noise Kernel for the Chintz Coarse-Graining Window

Having obtained numerically the linearised perturbation functions  $U_I^a$  in (4.4.3) we could plug them into the results for the Fourier-space projection operators (D.7), from which the noise kernel components (D.9) follow. Here, we decide to choose a smarter coarse-graining window function, drawing inspiration from [144], which results in more manageable Fourier space projection operators.

We introduce the coarse-graining window function ‘chintz’ as

$$\begin{aligned} W(t, t', \mathbf{x}, \mathbf{y}) &= \delta(t-t') \int \frac{d^3 k}{(2\pi)^3} W_k(t) e^{i\mathbf{k}\cdot(\mathbf{x}-\mathbf{y})} \\ W_k(t) &= \left( 1 - \frac{|\mathbf{k}|^3}{(\epsilon \alpha H)^3} \right) \Theta \left[ \ln \left( \frac{|\mathbf{k}|}{\epsilon \alpha H} \right) \right] \end{aligned} \quad (\text{D.10})$$

and return to the equation of motion for the short wavelength mode (D.3). Hence, we obtain

$$\begin{aligned} D_\mu D^\mu \phi^a + V_{,b} \mathcal{G}^{ab} &= \left[ \partial_t^2 + 3 \frac{\dot{\alpha}}{\alpha} \partial_t - \alpha^{-2} \nabla^2 \right] \phi^a + \Gamma_{bc}^a \partial_\mu \phi^b \partial^\mu \phi^c + V_{,b} \mathcal{G}^{ab} \\ &= H^2 \int \frac{d^3 k}{(2\pi)^3} \delta \left( \ln \left[ \frac{|\mathbf{k}|}{\epsilon \alpha H} \right] \right) \left[ a_{\mathbf{k}}^I Z_I^a e^{-i\mathbf{k}\cdot\mathbf{x}} + a_{\mathbf{k}}^{I\dagger} Z_I^{*a} e^{i\mathbf{k}\cdot\mathbf{x}} \right] \\ &\equiv \Xi^a(\mathbf{x}, t). \end{aligned} \quad (\text{D.11})$$

This  $\delta$ -function is somewhat ugly, but it can be massaged into something a lot more reasonable

$$\delta \left( \ln \left[ \frac{|\mathbf{k}|}{\epsilon \alpha H} \right] \right) = |\mathbf{k}| \delta(|\mathbf{k}| - \alpha \epsilon H), \quad (\text{D.12})$$

resulting in the corresponding noise correlation function

$$\begin{aligned} \langle \Xi^a(\mathbf{x}, t), \Xi^b(\mathbf{x}', t') \rangle &= H^3 \int \frac{d^3 |\mathbf{k}|}{(2\pi)^3} |\mathbf{k}| \delta(|\mathbf{k}| - \epsilon \alpha H) \delta(t-t') \\ &\quad \left\{ Z_I^a Z^{*Ib} e^{-i|\mathbf{k}|\cdot(\mathbf{x}-\mathbf{x}')} + n(|k|) \left[ Z_I^a Z^{*bI} + Z_I^{*a} Z^{Ib} \right] e^{-i|\mathbf{k}|\cdot(\mathbf{x}-\mathbf{x}')} \right\} \\ &= D^{ab}(\mathbf{x}, \mathbf{x}', t) \delta(t-t'), \end{aligned} \quad (\text{D.13})$$

where the Fourier space projection operators are given, for this window function, as

$$Z_I^a = 2 D_z q_I^a + 3 q_I^a, \quad (\text{D.14})$$

an expression far more appealing and easily manageable than the one associated with the sharp Heaviside window (D.7).

Remembering the normalisation (4.40), we obtain the expression that relates the projection operators to the perturbation mode functions

$$Z_I^a = \left[ \frac{H}{\sqrt{k^3}} \right] (2 D_z U_I^a + 3 U_I^a) \equiv \left[ \frac{H}{\sqrt{k^3}} \right] \Omega_I^a. \quad (\text{D.15})$$

The rescaled projection operators  $\Omega_I^a$  are here given analytically with respect to their associated partial derivatives in the original  $(\phi^1, \phi^2)$  coordinate system. It is evident that in the zweibein basis there is no field-geometrical contribution in the entropic direction as the background field velocity in that direction vanishes. Therefore, the rescaled Fourier operators read

$$\Omega_I^\sigma = 2 \partial_z U_I^1 + 2y U_I^2 + 3 U_I^1 \quad (\text{D.16})$$

$$\Omega_I^s = 2 \partial_z U_I^2 + 3 U_I^2. \quad (\text{D.17})$$

Making the assumption of a Bunch-Davies vacuum,  $n(|k|) = 0$ , the stochastic noise kernel (D.13) becomes

$$\begin{aligned} D^{ab}(x, x', t) &= H^3 \int \frac{|\mathbf{k}|^2 d|\mathbf{k}|}{(2\pi)^2} |\mathbf{k}| \delta(|\mathbf{k}| - \epsilon \alpha H) \frac{2 \sin(|\mathbf{k}|r)}{|\mathbf{k}|r} [Z_I^a Z_I^{*b}], \\ &= \frac{H^5 \sin(\epsilon \alpha H r)}{2\pi^2 \epsilon \alpha H r} [K^{ab}] \end{aligned} \quad (\text{D.18})$$

where  $K^{ab} \equiv \Omega_I^a \Omega_I^{*b}$  is obtained from the numerical evaluation of  $U_I^a$  and the definition of  $\Omega_I^a$  (D.15).

A direct verification of the validity of this approach can be obtained in the  $y \rightarrow 0$  limit, in which the fields decouple, evolving independently just as in the single-field case. Then, the noise kernel for both the adiabatic and entropic directions should reproduce the well-known single-field result [61]

$$\langle \Xi^a(x, t), \Xi^a(x', t') \rangle |_{a=(\sigma,s)} = \frac{9H^5}{4\pi^2} \frac{\sin(\epsilon \alpha H r)}{\epsilon \alpha H r} \delta(t - t'). \quad (\text{D.19})$$

Substituting the numerically obtained value for the noise kernel,  $K^{\sigma\sigma}$  and  $K^{ss}$ , in (D.18), in the flat field-space limit, produces a result in agreement to the theoretically predicted value to the fourth decimal place, even as early as a few e-folds after horizon crossing, for each mode (depicted as the black line in Figure D.1). Hence, this serves as an adequate indication that this approach is a good starting point for the numerical computation of solutions of the second order Langevin equation and, subsequently, arbitrary stochastic N-point functions in curved field-space.

We close by demonstrating explicitly the temporal evolution of the noise kernel  $K^{ab}$  components for various observationally permitted, as per section 4.4.3, values of the field-

space curvature parameter  $y$ .

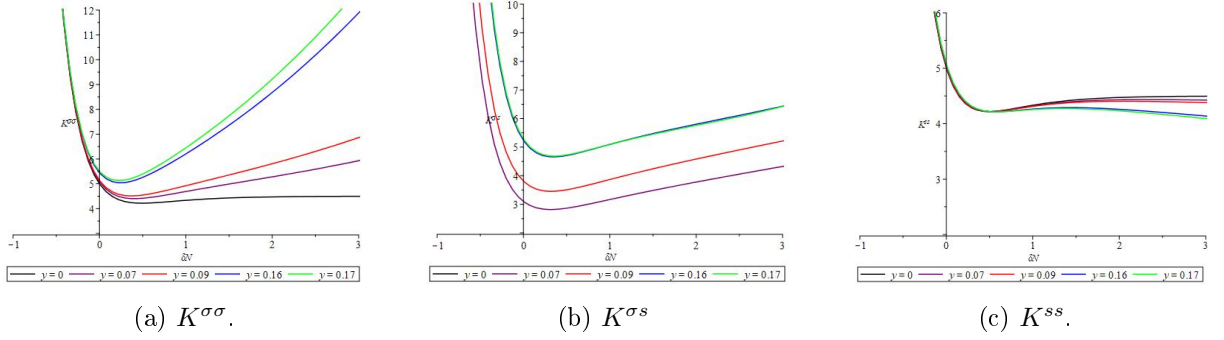


Figure D.1: Temporal evolution of the noise kernel components, in the first few e-folds after horizon exit for various observationally permitted values of  $y$ . In the flat field-space limit, the adiabatic and entropic directions appear to evolve independently, assuming the single-field value just a few e-folds after horizon crossing. For non-trivial field-space curvature, the modes mix resulting in amplification of the adiabatic mode.